



Chiral Macrocycles based on the morphine scaffold

Ewa Kowalska M.Eng.Sc

A thesis presented for the degree of Doctor Philosophy in
Organic and Medicinal Chemistry at Dublin City University,
School of Chemical Sciences



National Institute for Cellular Biotechnology

November 2008

Declarations

I hereby certify that this material, which I now submit for assessment on the programme of study leading to the award of PhD in organic chemistry is entirely my own work, that I have exercised reasonable care to ensure that the work is original, and does not to the best of my knowledge breach any law of copyright, and has not been taken from the work of others save and to the extent that such work has been cited and acknowledged within the text of my work.

Signed: _____

(Candidate) ID No.: 55143164

Date: _____

Acknowledgments

First would like to thank to my supervisor Dr. Nick Gathergood for his help, encouragement and support.

Would like to express my gratitude to:

The National Institute for Cellular Biotechnology and Dublin City University for funding my research to date.

Dr. Robert O'Connor and Aoife Devery in The National Institute for Cellular Biotechnology for the cytotoxicity and synergistic studies carried out.

Dr. Kieran Nolan for support and advice in several fields.

Dr. Helge Müller-Bunz in University College Dublin for excellent X-ray crystallography work.

The entire technical staff of the School of Chemical Sciences and the National Institute of Cellular Biotechnology, especially Damien ☺, Ambrose ☺☺, John, Mick, Veronica, Vinny and Mary.

Many thanks and appreciation to Dr. Ian Beadham for incredible help with correcting this thesis.

A special thanks and big hug to all postgraduate researchers for their friendship and support, Saibh, Dan, Brian D., Brian M., Shelly, Alan, Neil, Monika, Martin, Thomas, Debbie, Haibo, Áine, Rohit, Mukund, Emma, Brian Murphy, Will, Andy, Mette and Bruce. Thank You from the bottom of my heart ☺.

Very special thanks to my family, my parents Teresa and Edward and my sister Anna for all their support and encouragement.

Abstract

The preparation of a variety of novel macrocyclic model systems based on 2-(2-hydroxyethoxy) phenol and both aliphatic and aromatic linkers has been achieved. Optimization of the alkylation and ring closure step conditions has given a robust and reliable protocol for cyclizing the precursors of dimeric morphine macrocycles.

Herein we disclose the synthetic methodology, structural characterization and biological evaluation of a series of morphine macrocycles and their precursors. These macrocyclic chiral species varying in terms of cavity size, were synthesized by a concise synthetic route exploiting the two hydroxyl groups in the morphine moiety.

18 model macrocycles varying in ring sizes (23-28 atoms), number of aromatic rings (2-4), and number of donor atoms (6-10 including oxygen and nitrogen) were characterized by a range of spectroscopic techniques including ^1H , ^{13}C NMR, HRMS and IR. Both the macrocycles and their precursors were screened for therapeutic activity as part of our cancer research program. Binding affinities were also assessed by extraction studies against a series of metal picrates.

A small library of analogues of adrenaline was synthesised by a novel environmentally benign Friedel-Crafts reaction. In this thesis we have developed Friedel-Crafts reactions using this green methodology by reacting a glyoxamide with aromatic nucleophiles in the presence of a Lewis acid catalyst in organic solvents. Furthermore, the reactions proved to work smoothly using an aqueous environment in which novel compounds of interest as pharmaceutical intermediates containing heterocyclic rings were synthesised avoiding formation of hydrochloric acid as a byproduct.

Abbreviation

ATP	Adenosine triphosphate
b.p.	Boiling point
<i>t</i> -BuOK	Potassium tertiary butoxide
Cat.	Catalyst
CSPs	Chiral stationary phases
DCC	Dicyclohexylcarbodiimide
DCE	Dichloroethane
DCM	Dichloromethane
DMAP	4-Dimethylaminopyridine
DMF	<i>N,N</i> -Dimethylformamide
DMSO- <i>d</i> ₆	Deuterated dimethyl sulfoxide
ee	Enantiomeric excess
eq	Equivalent
IR	Infrared
NIS	<i>N</i> -iodosuccinimide
NMR	Nuclear magnetic resonance
M	Molarity
min	Minutes
mol	Mole
m.p.	Melting point
P-gp	P-glycoprotein
RCM	Ring closure metathesis
RT	Room temperature
S.A.R.	Structure-Activity-Relationship
TfOH	Triflic acid
THF	Tetrahydrofuran
TLC	Thin layer chromatography
$[\alpha]_{\text{D}}^{20}$	Specific rotation
δ	Chemical shift
ν	Frequency
<i>J</i>	Coupling constant

List of content

1	Introduction	1
1.1	Naturally occurring relatives of crown ethers	2
1.2	Preparation of crown ethers	4
1.3	Chiral crown ethers	7
1.4	Chiral macrocycles based on sugar moiety.....	12
1.5	Chiral aza-macrocycles.....	16
1.6	Application of crown ethers.....	20
1.6.1	Crown ethers in chromatography.....	20
1.6.2	Crown ethers in organic synthesis	22
1.7	Catalytic Friedel-Crafts Reactions	30
1.8	P- glycoprotein efflux pump	33
1.8.1	P- glycoprotein efflux pump inhibitors	33
1.9	Conclusion	38
2	Friedel-Crafts Chemistry	39
2.1	Preparation of L-tartramides	39
2.2	Oxidative cleavage of L-tartramides	40
2.3	Friedel-Crafts reactions	40
2.3.1	Catalytic Friedel-Crafts reaction of <i>N,N</i> -dimethyl glyoxamides.....	40
2.3.2	Catalytic Friedel-Crafts reaction of 2-oxo-2-(pyrrolidin-1-yl)acet- aldehyde.....	42
2.3.3	Catalytic Friedel-Crafts reactions of ethyl glyoxylate	44
2.3.4	Catalytic Friedel-Crafts reactions of ethyl 3,3,3-trifluoropyruvate ...	44
2.3.5	Catalytic Friedel-Crafts reactions of ethyl pyruvate	46
2.3.6	Catalytic Friedel-Crafts reaction of ethyl 3,3,3-trifluoropyruvate with indoles	47
2.3.7	Friedel-Crafts reaction of glyoxamides in aqueous solution.....	48
2.3.8	Catalytic Friedel-Crafts reaction in ionic liquids.....	51
2.4	Conclusion	53
3	Model Macrocycles and their Precursors	56
3.1	Preparation of phenoxy-linked open structures	58
3.2	Preparation of macrocycles from their phenoxy-linked precursors	60
3.3	Preparation of macrocycles by one pot synthesis	71
3.4	Spectroscopic discussion on model macrocycles.....	73
3.4.1	NMR study of 173 and 182	73
3.4.2	NMR study of 174	78
3.4.3	NMR study of 181	80
3.4.4	The ¹ H NMR studies of 171 and 172.....	83
3.5	Conclusion	85
4	Morphine compounds.....	88
4.1	Preparation of morphine macrocycle precursors.....	91
4.2	Modifications on 6-hydroxyl group of morphine.....	97
4.3	Preparation of morphine macrocycles.....	99
4.4	Spectroscopic discussion on morphine macrocycles.....	107
4.4.1	NMR study of 194 and its macrocycles 217 and 218	107
4.5	Conclusion	113
5	Crystallographic studies	115
5.1	Structural studies of macrocycle 179	115
5.2	Structural studies of macrocycle 184	118
5.3	Structural studies of macrocyclic precursor 160.....	122

5.4	Structural studies of macrocyclic precursor 161.....	123
5.5	Structural studies of macrocyclic precursor 163.....	125
5.6	Structural studies of macrocyclic precursor 164.....	127
5.7	Structural studies of macrocyclic precursor 165.....	130
5.8	Structural studies of macrocyclic precursor 166.....	133
5.9	Conclusion	135
6	Metal binding studies	137
6.1	Introduction.....	137
6.2	Results and discussion.....	138
6.3	Conclusion	159
6.4	Experimental.....	160
7	Biological activity of model macrocycles and their precursors.....	162
7.1	Lung cell carcinoma assay.....	162
7.2	MultiDrug Resistance Proteins	163
7.3	Biological results.....	164
7.3.1	Biological activity of macrocyclic precursors.....	164
7.3.2	Biological activity of compounds with ester groups.....	171
7.3.3	Summary of carcinoma assay for ester compounds.....	175
7.3.4	Biological activity of commercially available compounds.....	175
7.3.5	Biological activity of macrocycles.....	177
7.4	Conclusion	182
8	Experimental.....	185
8.1	Friedel-Crafts chemistry	186
8.2	Model macrocycles and their precursors.....	200
8.3	Morphine macrocycles and their precursors.....	222
	Bibliography.....	239
9	Appendix	247
9.1	Appendix A.....	247
9.2	Appendix B.....	288
9.3	List of Figures	292
9.4	List of Tables	296
9.5	List of Graphs.....	298

1 Introduction

Molecular recognition lies at the heart of virtually all biological phenomena and model studies of molecular recognition in biomimetic settings are necessary to provide important insight into the mechanisms of life processes. One of the essential processes occurring in living systems is the specific recognition of a particular chiral molecule by receptor “host” which specifically recognizes a stereoisomer “guest”. In living organisms the chemical or biological activity of a compound often depends upon its stereochemistry. For this reason crown ethers have been the subject of intensive study for over forty years. The serendipitous discovery of macrocyclic polyethers and their selective complexation of alkali metal cations is regarded as the beginning of supramolecular chemistry. This discovery is generally also associated with the pioneering work of Charles Pedersen on macrocyclic polyethers, published in 1967, which opened up the new field of supramolecular chemistry¹. For the past 40 years this branch of chemistry has been considered to be one of the most dynamic interdisciplinary sciences, combining elements of chemistry, physics and biology. At the heart of supramolecular chemistry are non-covalent bonds, including electrostatic, hydrogen bonding, Van der Waals and hydrophobic interactions. The great diversity of synthetic possibilities and immense number of molecular interactions place supramolecular chemistry at a distinctive position in the history of science. The major contributions to the development of supramolecular chemistry were made by C. Pedersen, D. J. Cram and J.-M. Lehn who were awarded the Nobel Prize in Chemistry in 1987. Impressive numbers of synthetic, as well as many natural macrocyclic species have been studied since then, and frequently unexpected ligand properties have emerged. Cellular studies have established that macrocyclic ligand complexes play a significant role in many fundamental biological systems, such as photosynthesis and the transport of oxygen in mammalian and other respiratory systems. These discoveries using synthetic macrocycles as models for the biological systems occurring macrocyclic ligand complexes has provided an impetus for much of this research. Aspects of macrocyclic chemistry are also of relevance to a number of other areas such as organic synthesis, metal-ion catalysis, metal-ion discrimination, and analytical techniques, as well as a variety of potential medical and industrial applications.

1.1 Naturally occurring relatives of crown ethers

Nature has found ways to complex cations using substances such as valinomycin, nonactin or monesin using not only simple ethers but carbonyl groups, ketones and other residues^{2,3}. The compounds that have thus far inspired the greatest interest to chemists working in the macrocycle area are those capable of binding cations. Compounds that can bind and transport cations are referred to as ionophores and the antibacterial nature of those compounds arises from their interference with cellular content and membrane function thus interfering with the normal working of the cell. Valinomycin **1** is a depsipeptide that exhibits antibiotic activity and is produced by microorganisms *Streptomyces fulvissimus* strains, however, Merrifield and coworkers have also prepared this cyclic peptide synthetically⁴.

Structurally valinomycin is a cyclic compound composed of alternating α -amino acids and α -hydroxy acids and has been found to form especially stable complex with potassium resulting in formation of a lipophilic outer shell which envelopes the metal ion thus facilitating ion transfer through cell membranes.

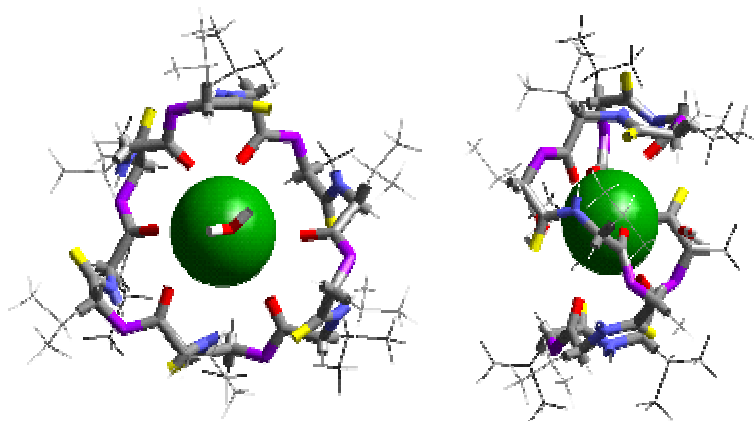


Fig. 1.1 Valinomycin 1

Nonactin **2** incorporates four ether and four ester groups and while complexing potassium the cyclic molecule twists until it resembles the seam of a tennis ball⁵. An important feature of these macrocycles is that on metal coordination the inside of the complex is hydrophilic while the outside is hydrophobic. Complexation is consequently favoured by non polar conditions.

Nonactin is a member of the macrotetrolide antibiotics, isolated from *Streptomyces* cultures⁶. Nonactin is biologically important because of its ability to bind alkali metal cations. Potassium is bound selectively in the presence of sodium making nonactin an effective ionophore against *Gram* positive bacteria, mycobacteria and fungi⁷.

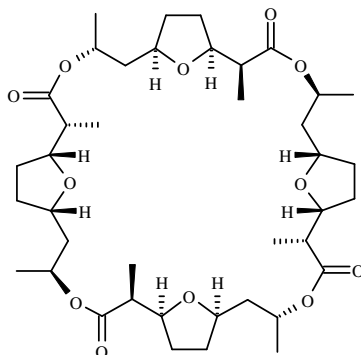


Fig. 1.2 Nonactin 2

From a synthetic point of view the total synthesis of nonactin was a challenging goal, completed first by Gerlach⁸, then by Schmidt⁹, Bartlett¹⁰, Fleming¹¹ and Lee¹². However, availability of this complex natural product is still limited by a low overall yield.

Monensin **3** is an acyclic carboxylic acid ionophore obtained from the soil bacterium *Streptomyces cinnamonensis*. It is known to be an anticoccidial agent, and a growth-promoting feed additive in agriculture¹³. Monensin forms a cyclic complex with metal cations using both the carboxyl group at one end of the structure and a hydroxyl at the other.

This results in the formation of a pseudo-macrocyclic complex with mono and divalent cations and allows them to be transported across cellular membranes.

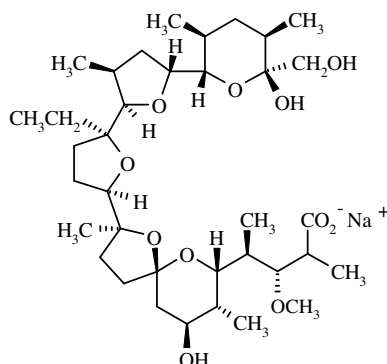


Fig. 1.3 Monensin 3

The most important discovery was that monensin proved to be highly selective for Pb²⁺ compared with other divalent cations, moreover it accelerates the excretion of this cation that has previously accumulated, without depleting the organs of zinc or copper¹⁴. This feature of monensin, used alone or in combination with other agents could be useful for the treatment of Pb²⁺ poisoning.

1.2 Preparation of crown ethers

Pedersen's pioneering work revealed a major new development in the study of the metal-ion chemistry of macrocyclic ligands¹. It became clear that crowns exhibit a number of unusual properties such as the ability to form complexes with alkali metal ions which, in certain cases, are stable in aqueous solution. Furthermore, they can also form stable complexes of a range of non-transition metal ions but tend to bind less strongly. If some of the oxygen atoms in a cyclic polyether are replaced with nitrogen or sulfur atoms, it is possible to change the selectivity of such a macrocycle towards metal cations. According to Pearson's HSAB ("hard and soft acid and bases") theory that "hard" acids prefer to bind to "hard" or nonpolarizable bases, and "soft" acids favor "soft" polarizable acids¹⁵. If one oxygen atom in 18-crown-6 **4** is replaced with a nitrogen atom, it has been observed that the selectivity of the new

aza-analog between potassium and silver is similar. However, if a second nitrogen atom is introduced **5** the selectivity between silver and lead cations increases significantly. In the case of sulfur derivatives it has been discovered that the selectivity between Ag^+ and Pb^{2+} depends strongly on the position of nitrogen in the ring, however, thio-crown **6** binds stronger to the transition metal cations over the potassium cation (Table 1.1)¹⁶.

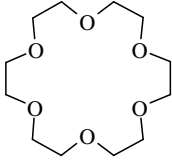
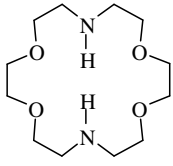
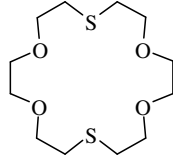
Cation (solvent)			
	Equilibrium constants log K		
K^+ (methanol)	6.10	2.04	1.15
Ag^+ (water)	1.60	7.80	4.34
Pb^{2+} (water)	4.27	7.01	3.30

Table 1.1 Stability constants for 1:1 18-crown-6 and its aza- and thio- analogs

Crown ethers are relatively easy to prepare from inexpensive commercially available precursors and are both easy to modify and chemically stable. It is also possible to create macrocyclic species which are tailor-made for complexation. Most crown ethers have been built around the ethyleneoxy unit, which is a readily available substrate. The first macrocycle dibenzo-18-crown-6 **9** was synthesized by Pedersen¹. He reacted catechol (1,2-dihydroxybenzene) **7** with 2,2'-dichlorodiethyl ether **8** in the presence of sodium hydroxide in *n*-butanol at 117 °C. The final product was isolated by recrystallization to give fluffy needles in 40 % yield (Fig. 1.4).

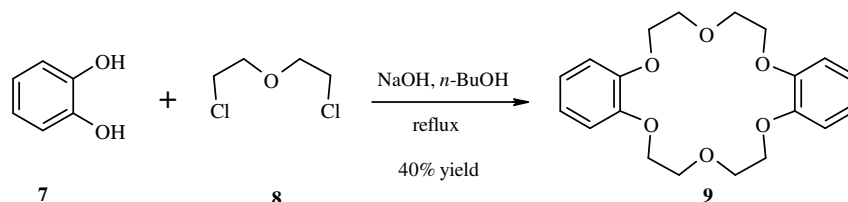


Fig. 1.4 Synthesis of dibenzo-18-crown-6 **9**

This early preparation of dibenzo-18-crown-6 has been used as a model for many subsequent crown preparations. One of the main obstacles in the preparation of

macrocyclic rings is the formation of polymeric side products. To minimize this problem many preparations of the polyether class of macrocycles have been carried out using high dilution techniques¹⁷. A typical direct synthetic procedure involves combining equimolar concentrations of two reagents incorporating the required fragments for the target macrocycle such that a 1:1 condensation occurs. By employing high dilution conditions it is more likely to favour 'head-to-tail' cyclization, rather than an intermolecular condensation leading to oligomeric or polymeric products. Another very important factor in the synthesis of macrocyclic structures is the effect of metal ions in promoting cyclization reactions. It has been recognized and defined by Bush and Thomson¹⁸, however, the first real evidence for the template effect came from Greene's work¹⁹. Pedersen had previously synthesized 18-crown-6 by reacting hexaethylene glycol monochloride in the presence of potassium *tert*-butoxide. Obtained yield for the cyclization step was only 1.8 %. However, Greene demonstrated the applicability of the template idea to macrocyclic polyether synthesis by reaction of triethylene glycol and triethylene ditosylate in the presence of potassium cations as matrices. Under those reaction conditions the yields increased dramatically and 18-crown-6 was formed in 93 % yields (Fig. 1.5).

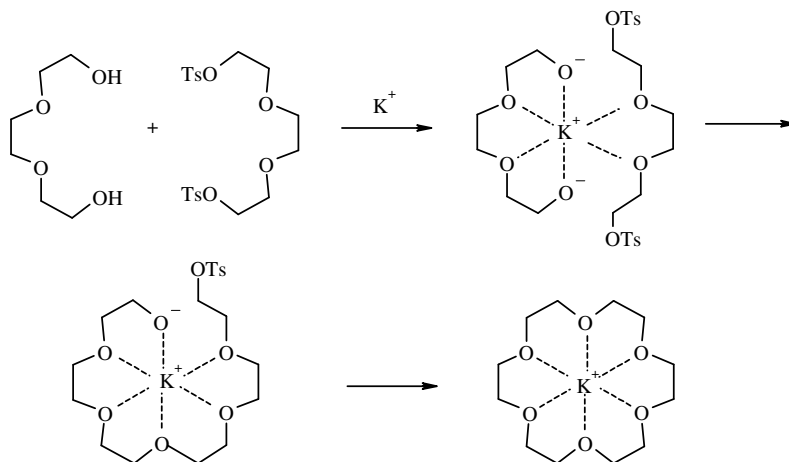


Fig. 1.5 Synthesis of 18-crown-6 employing potassium cations as a templating agent

Mandolini who investigated the template effect of alkali metal cations on the intramolecular cyclization reaction of *o*-HO-C₆H₄(OCH₂CH₂)₄Br in the presence of Et₄NOH as a base^{20,21}. Mandolini further demonstrated that the most suitable templates for preparation of benzo-15-crown-5, benzo-18-crown-6 and benzo-21-crown-7 would be metal cations in the following order: Na⁺, K⁺, Cs⁺²².

1.3 Chiral crown ethers

The design and synthesis of crown ethers possessing chiral recognition ability has been extensively explored over the past 40 years. Optically active crown ethers that have great potential for the separation of enantiomers and for analytical purposes have become a very important and attractive discipline of host-guest chemistry. One of the advantages of crown ethers containing chiral building blocks is that for the majority of them it is rather easy to modify the chiral cavity in order to improve enantiomer selectivity. Cram and co workers made the first advancement towards the preparation of chiral polycyclic ethers by incorporating binaphthyl subunits in the macrocyclic ring^{23,24,25}.

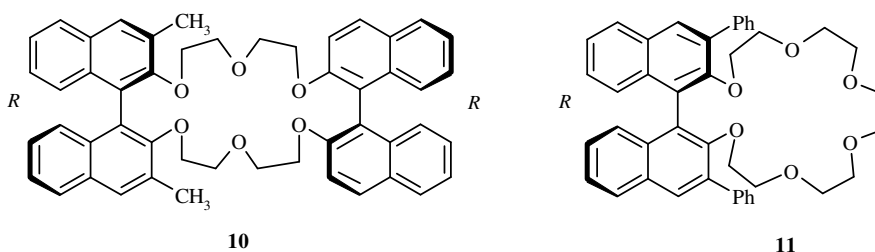


Fig. 1.6 Structures of chiral crown ethers with binaphthyl units

Macrocycle **10** shows high chiral discrimination on interaction with racemic amine salts. Such subtle behavior mimics the discrimination that is characteristic of interactions between a wide range of optically active biological molecules. Chiral recognition of this type also provides a molecular basis for the design of new hosts for the practical resolution of amino acids and their esters²⁶. For example, crown ether **11** which was also investigated by Cram has shown very high chiral recognition towards the phenylalanine methyl ester perchlorate salt²⁷.

Chiral crowns have been employed for optical resolutions *via* both liquid-liquid and solid-liquid chromatography, where crowns were immobilized on solid substrates such as silica gel or polystyrene²⁸. Chiral crown ethers with chiral biphenanthryls as a part of the macrocyclic cavity have been synthesized and described by Yamamoto (Fig. 1.7)²⁹.

The synthesis of two reported macrocyclic structures (-)-(*S*)-**12** and (-)-(*R,R*)-**13** began with the preparation of 10,10'-dihydroxy-9,9'-biphenanthryl, which was obtained as a racemic mixture then purified into the constituent (*R*) and (*S*) enantiomers. The (*S*) enantiomer underwent a condensation reaction with pentaethyleneglycol ditosylate to give crown ether (-)-(*S*)-**12** in 22% overall yield. The (*R*) enantiomer was reacted with diethyleneglycol ditosylate to give the crown ether (-)-(*R,R*)-**13** in 12.5% overall yield. These two crown ethers have been tested for chiral recognition towards chiral guest molecules. Crown ether (-)-(*S*)-**12** was shown to have better enantiomeric selectivity toward 1,2-diphenylethylamine.

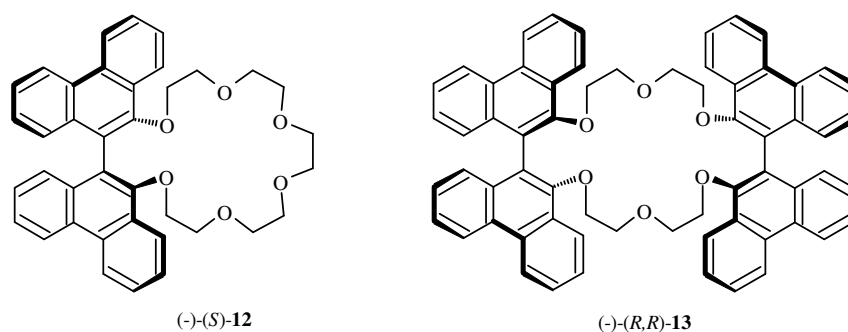


Fig. 1.7 Structures of chiral crown ethers incorporating biphenanthryl unit

Chirality also has been introduced into crown hosts using optically active functional groups other than *bis-β*-naphthol. For example the crown **14** derived from the optically active sugar D-mannitol exhibits varying degrees of chiral recognition towards a range of optically active hosts³⁰.

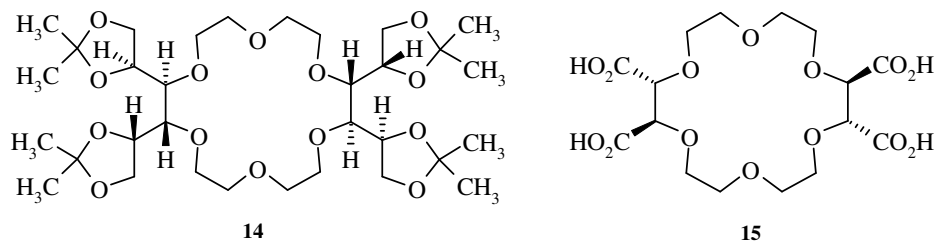


Fig. 1.8 Structures of macrocycles derived from D-mannitol and L-tartaric acid

Another example is the crown **15** which incorporates an L-tartaric acid moiety and in this case the chiral host has shown much less distortion of the periphery of the crown than in crowns incorporating binaphthyl or biphenanthryl units^{31,32}.

Hirose *et al* reported the synthesis of phenolic chiral crown ethers using (*S*)-(+)-mandelic acid derivatives as the source of the chiral unit³³. Chiral recognition of secondary amines by these compounds has been investigated.

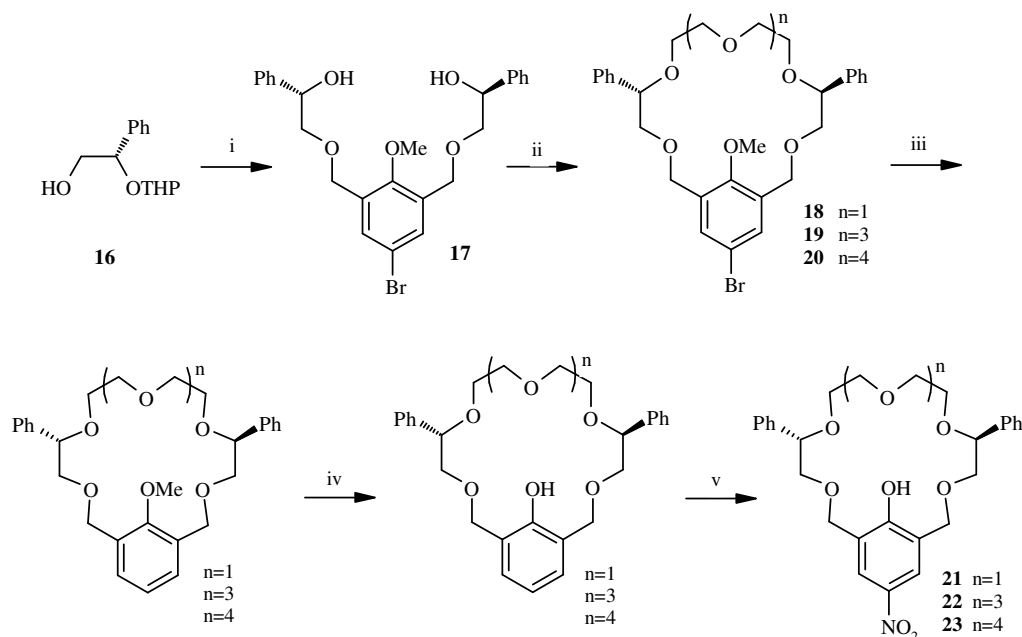


Fig. 1.9 Synthesis of chiral macrocycles based on (*S*)-(+)-mandelic acid derivatives

Reagents and conditions: (i) a. 5-Bromo-1,3-bis(bromomethyl)-2-methoxybenzene, NaH, b. pyridinium *p*-toluenesulfonate, ethanol, 95%; (ii) NaH, glycol ditosylate ($n=1$), 44%; ($n=3$) 36%; ($n=4$), 25%; (iii) *n*-BuLi, hexane; H₂O, ($n=1$), 62 %; ($n=3$) 62 %; ($n=4$), 68 %; (iv) EtSNa, DMF, ($n=1$), 91 %; ($n=3$) 86 %; ($n=4$), 30 %; (v) HNO₃, NaNO₂.

The synthesis started with condensation of 2 equivalents of mandelic acid derivative **16** with 5-bromo-1,3-bis(bromomethyl)-2-methoxybenzene in the presence of NaH then deprotection of THP groups with pyridinium *p*-toluenesulfonate in ethanol to give **17** in 95 % overall yield. Podand **17** was then reacted with different di(*p*-toluenesulfonate) ethylene glycols under high dilution conditions in the presence of NaH as a base, to form *p*-methoxy aryl bromide crown ethers **18-20** in up to 25 % yields. The further steps were to remove bromine substituting *para*-position on the aromatic ring by reaction with *n*-BuLi then selective cleavage of the methyl ether with sodium ethanethiolate in DMF. As a final step nitration reaction was performed

using a $\text{HNO}_3/\text{NaNO}_2$ mixture to introduce a nitro group in the *para* position to the phenolic hydroxyl group. These macrocycles incorporating a chiral moiety with varied cavity sizes **21-23** were capable of binding primary and secondary amines and also recognizing their chirality. Since pseudo-18-crown-6 exhibits excellent enantioselectivity toward primary ethanolamine derivatives, analogues of 24-crown-8 were expected to possess a larger binding site and therefore bind selectively to secondary amines. Among all the macrocyclic compounds reported *p*-nitro phenolic crown ethers showed the most promising results as chiral hosts for secondary amines. Crown ether **22** showed the best selectivity, with crown ether **21** being too small to accommodate a secondary amine and crown ether **23** being too large to efficiently inhibit binding of the unwanted enantiomer.

Pedersen synthesized the first series of chiral crown ethers containing cyclohexyl units by hydrogenation of dibenzo-18-crown-6¹. This method afforded a mixture of the *cis,syn,cis*- and *cis,anti,cis*-isomers, however, since then various synthetic approaches have been used to selectively prepare the *cis,anti*- isomer^{34,35}. One approach employed (+)-(*1S,2S*)-*trans*-cyclohexane-1,2-diol which was alkylated with allyl bromide, then the product was submitted to ozonolysis followed by a reductive work-up³⁶. The resulting diol was then transformed into a ditosylate derivative and reacted with a series of different diols to yield the corresponding chiral macrocyclic structures **24-26**. It is worth mentioning that **26** has also been synthesized *via* an enzymatic reaction³⁷.

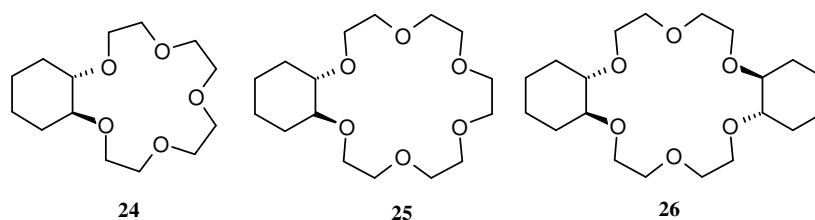


Fig. 1.10 Chiral crown ethers containing cyclohexyl units

Another group of optically active macrocycles based on either *cis*-1-phenylcyclohexane-1,2-diol, *trans*-1-phenylcyclohexane-1,2-diol³⁸ or *trans*-1-diphenylcyclohexane-1,2-diol, as chiral subunits, have been reported by Naemura and co-workers³⁹. Naemura's preparation of optically active 18-crown-6 macrocycles of this type involved performing enantioselective hydrolysis on ester precursors of

the required diols using pig liver esterase. The reason for this was that the enzymatic method of obtaining chiral cyclohexane-1,2-diol derivatives gave higher optical purity and was more straightforward than chemical methods.

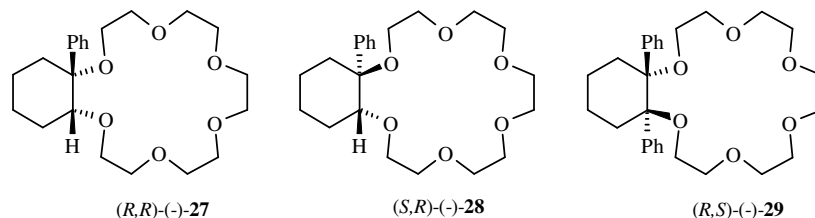


Fig. 1.11 Optically active 18-crown-6 macrocycles with chiral cyclohexane unit

Further synthesis of macrocycles containing one cyclohexane-1,2-diol unit was attempted by refluxing the corresponding chiral diol in THF with pentaethyleneglycol *bis*(toluene-*p*-sulphonate) in the presence of NaH and KBF_4 . Isolated yields for the corresponding macrocyclic products varied from 15 to 62%. These chiral crown ethers have been tested for transport of enantiomeric molecules through bulk liquid membranes, using two guest species, (\pm)-1,2-diphenylethylamine hydrochloride and methyl (\pm)-phenylglycinate hydrochloride. In particular crown ether (*R,S*)-(-)-**29** exhibited high enantiomer selectivity for (\pm)-1,2-diphenylethylamine, suggesting that at least two phenyl units are required on these macrocycles to act as a significant steric barrier for the guest species tested. Attachment of additional benzyl, ester and amide groups to 14-crown-4 has been performed by the condensation reaction of (*S*)-1,4-benzyloxymethylbutane-2,3-diol and 1,10-dichloro-4,7-dioxadecane in the presence of ${}^t\text{BuOLi}$ in ${}^t\text{BuOH}$ ⁴⁰.

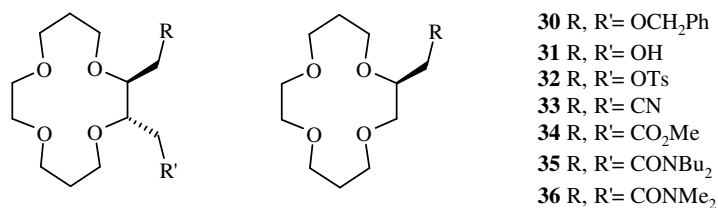


Fig. 1.12 Chiral 14-crown-4 ether

Mono- and di-substituted macrocycles **30** have been modified by first removing the benzyl groups *via* hydrogenation then bonding the alcohol groups of the products by

tosylation **32**. The tosylates were then substituted by treatment with sodium cyanide to give nitriles **33**, then methanolysed in the presence of HCl to yield methyl esters **34**. Hydrolysis with $\text{Me}_4\text{NOH}/\text{MeOH}-\text{H}_2\text{O}$ gave carboxylic acids which were converted to acid chloride with PCl_5 . In the final step acid chlorides of the mono- and disubstituted 14-crown-4 ether were reacted with *N,N*-dibutylamine or *N,N*-dimethylamine to form the corresponding amide products **35**, **36**.

Macrocycles **35**, **36** were then tested for Li^+ selectivity in a solution mimicking blood serum and the disubstituted *bis-N,N*-dibutylamide crown ether proved to be the best and was superior to previously reported systems^{41,42}.

α -Amino acids such as L-valine, L-leucine, L-isoleucine and L-phenylalanine have been used to create crown ethers incorporating chiral units in the structure^{43,44}. First the α -amino acids **37** were converted into the corresponding chiral glycols **38** then reacted with pentaethylene glycol ditosylate **39** in the presence of a template sodium ion. All macrocycles **40-43** were synthesized in yields varying between 28-45 % for the final macrocyclization step.

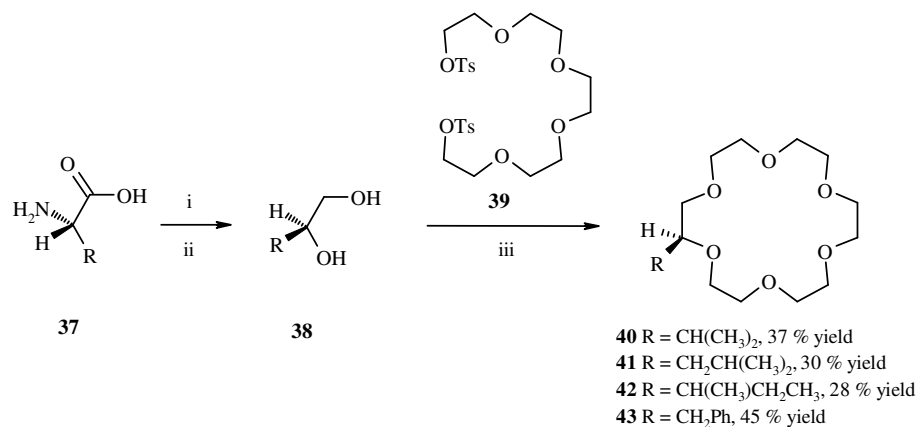


Fig. 1.13 Synthesis of chiral 18-crown-6 from α -amino acids

Reaction conditions: i) NaNO_2 , CH_3COOH ; ii) LiAlH_4 , THF; iii) NaOH , dioxane/water

1.4 Chiral macrocycles based on sugar moiety

The disaccharide sucrose presents a useful source of chirality for chemical synthesis, however, the eight hydroxyl groups in its structure pose a considerable synthetic challenge in terms of selectivity. Differentiation between individual hydroxyl groups is difficult and the glycosidic bond is highly sensitive in acidic media. In spite of

these difficulties sucrose had been applied to the synthesis of bio-degradable polymers and surfactants, using a biocatalytic approach to ensure regioselectivity⁴⁵.

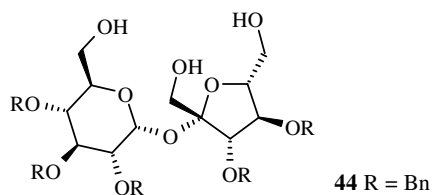


Fig. 1.14 Sucrose unit

Sucrose has also been used to prepare sucroses modified at the terminal positions, so connection of the C-6 and C-6' positions opened a route to the crown ether type analogs with sugar incorporated into the macrocyclic backbone⁴⁶. Jarosz *et al* selected 2,3,3',4,4'-penta-*O*-benzylsucrose **44** for the preparation of macrocyclic derivatives containing the sucrose unit (Fig 1.15)^{47 48}.

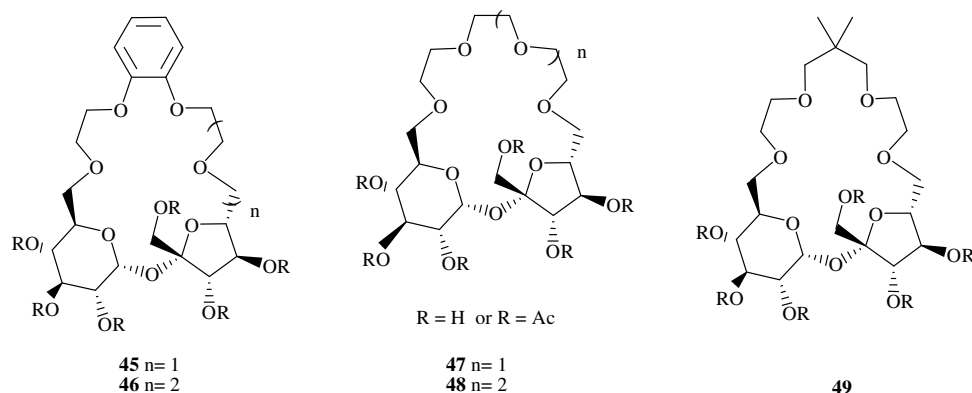


Fig. 1.15 Chiral macrocycles with sucrose unit

Crown ether analogues of varying macrocyclic ring size with sucrose units incorporated were prepared by reaction of **44** with the corresponding polyethylene ditosylates. Reactions were carried out in DMF at RT in the presence of NaH giving the corresponding macrocycles in up to 52 % yield. Subsequently, simple hydrogenolysis with hydrogen gas and 10 % Pd/C in an ethanol/ethyl acetate mixture removed the benzyl protecting groups and allowed isolation of the free macrocycles. However, for chromatographic purposes these were further acetylated and isolated as peracetates.

A series of crown ether derivatives containing D-glucose and polyethylene glycol units where the sugar moiety is introduced into the crown ether periphery *via* 1,4-hydroxy groups has been synthesized from allyl- α -D-glucopyranoside and the corresponding polyether ditosylates⁴⁹. Macrocycles **51**, **52** and **55** were prepared by reaction of 2-hydroxy ethyl 2,3,6-tri-O-benzyl-4-O-(2-hydroxyethyl)- α -D-glucopyranoside **50** with the appropriate polyethylene glycol ditosyl esters under anhydrous conditions in THF, at 70 °C in the presence of NaH in yields of 30-34 %.

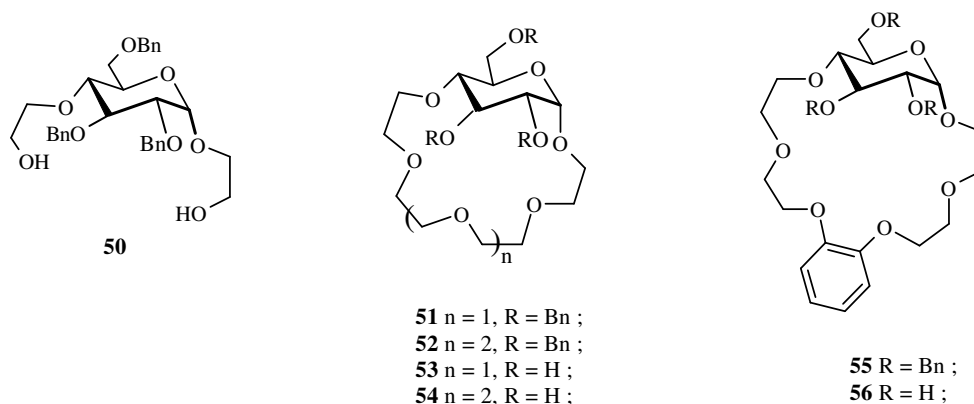
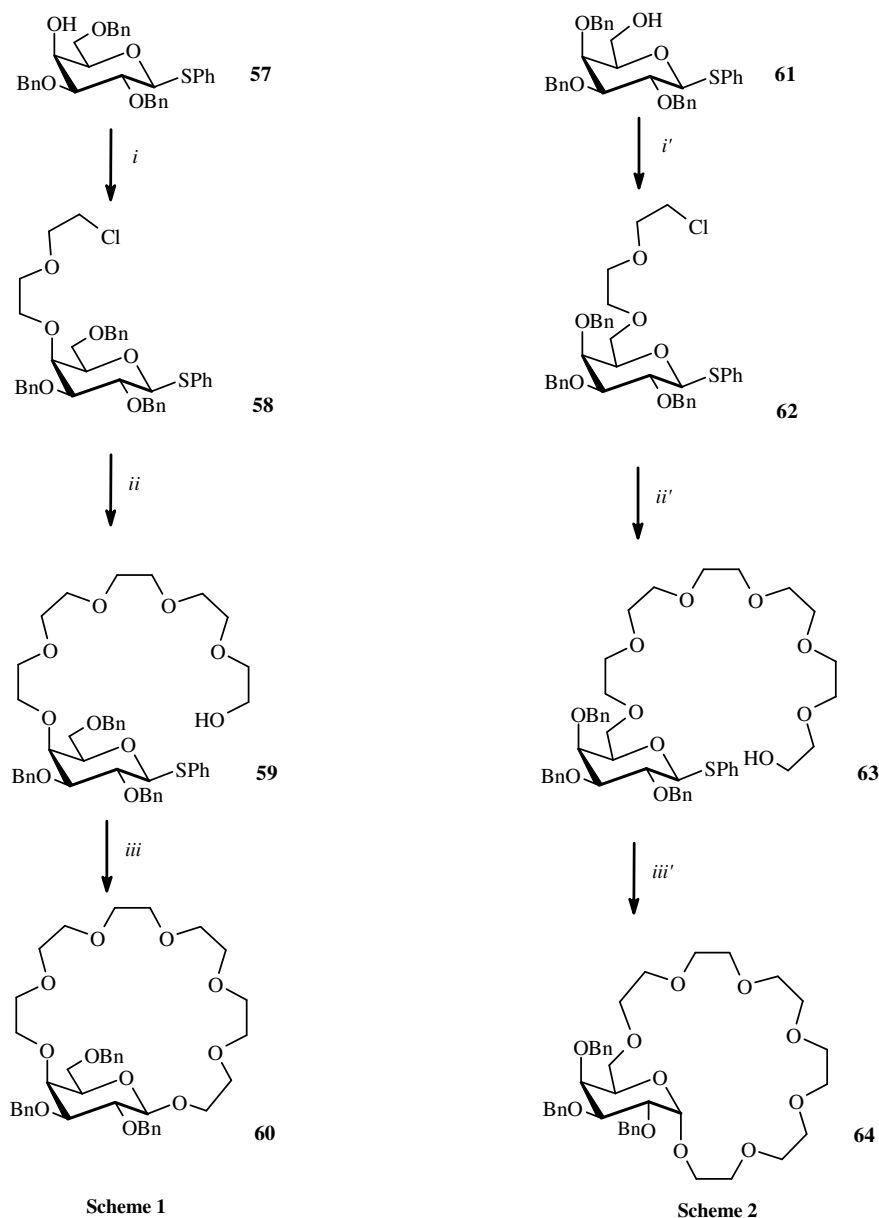


Fig. 1.16 Chiral crown ethers with D-glucose unit

Further hydrogenolysis to remove the benzyl groups in compounds **51**, **52**, **55** was carried out in methanol/ethyl acetate (9:1) solution in the presence of 10 % Pd/C to give unprotected chiral mono-*gluco*-crowns **53**, **54**, **56**.

Faltin *et al* reported a synthesis of chiral crown ethers based on gluco- and galactopyranoside moieties 1,4- and 1,6-bridged with ethylene glycol units^{50,51}. The synthesis of chiral *galacto*-crown ethers based on galactopyranosides is presented in Fig. 1.17. Polyethylene glycol side chains in the 4- and 6-positions of the 1-thio-D-galactopyranoside derivatives **57** and **61** were incorporated under phase transfer conditions to give phenyl 2,3,6-tri-O-benzyl-4-[2-(2-chloroethoxy)ethyl]-1-thio- β -D-galactopyranoside **58** in 90 % yield and phenyl 2,3,6-tri-O-benzyl-6-[2-(2-chloroethoxy)ethyl]-1-thio- β -D-galactopyranoside **62** in 80 % isolated yields, respectively. Subsequent side chain elongations were realized by alkoxylation with tetraethylene glycol in the presence of potassium hydroxide and the final intramolecular transglycosidation steps of compounds **59** and **63**, were carried out using *N*-iodosuccinimide (NIS) and catalytic amounts of triflic acid (TfOH) in

anhydrous acetonitrile or dichloromethane in the presence of a template salt, potassium borofluoride.



$i = (\text{ClC}_2\text{H}_4)_2\text{O} / \text{THF} / \text{KOH} / \text{H}_2\text{O} / \text{TBAHSO}_4 / \text{R.T.} / 3\text{-}5 \text{ d};$
 $ii = \text{HO}(\text{C}_2\text{H}_4\text{O})_3\text{C}_2\text{H}_4\text{OH} / \text{KOH} / 70 \text{ }^\circ\text{C} / 30 \text{ h};$
 $iii = \text{NIS} / \text{TfOH} / \text{KBF}_4 / \text{MeCN} / 3 \text{ h};$

$i' = (\text{ClC}_2\text{H}_4)_2\text{O} / \text{THF} / \text{KOH} / \text{H}_2\text{O} / \text{TBAHSO}_4 / \text{R.T.} / 20 \text{ h};$
 $ii' = \text{HO}(\text{C}_2\text{H}_4\text{O})_3\text{C}_2\text{H}_4\text{OH} / \text{KOH} / 5 \text{ h} / 60\text{-}70 \text{ }^\circ\text{C};$
 $iii' = \text{NIS} / \text{TfOH} / \text{KBF}_4 / \text{MeCN} / \text{R.T.} / 20 \text{ h};$

Fig. 1.17 Synthesis of *galacto*-crown ethers

According to Scheme 1 product **60** was prepared in 61 % yield and turned out to be exclusively the β -linked *galacto*-crown ether although the reagent NIS/TfOH does not normally lead to formation of a specific anomer⁵³. Moreover, the high

β -selectivity seems to be independent of both the solvent and addition of a template salt. The last step of the synthesis of *galacto*-crown ether **64** proceeds in 38 % yield and only the α -configured macrocyclic product was identified. The high α -stereoselectivity of the intramolecular transglycosidation which generated a 23-membered 1,6-*ansa*-galactoside was unexpected because the polyethylene glycol chain seems to be flexible enough to allow an intramolecular nucleophilic attack on the glycosidic centre from either the β - or the α -face. Complexes containing chiral ligands based on carbohydrates are of interest in asymmetric catalysis⁵¹. A rhodium (I)-chelate of a D-pyranoside 2,3-*O*-bisphosphinite was even used in an industrial process for L-DOPA⁵³.

1.5 Chiral aza-macrocycles

L-Valine has been used as a precursor to prepare two chiral monoaza-15-crown-5 ethers^{54,55}. The synthesis began with the reduction of L-valine to L-valinol which was then benzylated to form the *N*-benzyl amino alcohol. Subsequent reaction with ethylene oxide to form a diol was followed by nucleophilic substitution of triethylene glycol ditosylate to form aza-crown **65** or 1,2-*bis*(2-tosylethoxy)benzene to yield product **66** respectively.

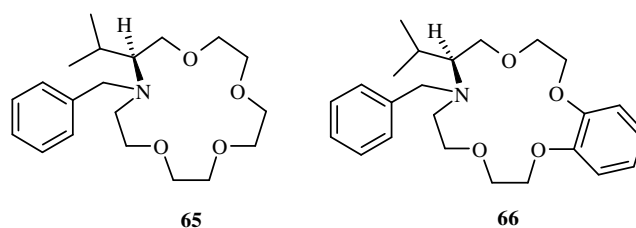


Fig. 1.18 Chiral monoaza-15-crown-5 ethers

65 and **66** were tested for molecular recognition towards (*R,S*)- α -phenylethylamine and (*R,S*)- α -(1-naphthyl)ethylamine and their protonated perchlorate salts.

Another example of a chiral macrocycle derived from an amino acid is the chiral aza crown ether **67** synthesized from L-threonine⁵⁶.

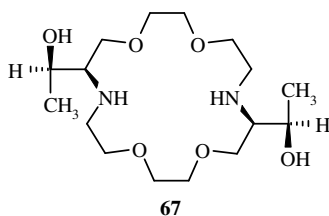


Fig. 1.19 Chiral aza crown ether **67** synthesized from L-threonine

The first step of the synthesis was benzylation of the amino and carboxyl groups, followed by reduction of the carbonyl group with LiAlH_4 to give an alcohol. *O*-alkylation of the primary alcohol with diethylene glycol dichloride has been accomplished in 50 % aq. NaOH and NBu_4HSO_4 . The two final steps were to deprotect the *N*-benzyl groups by hydrogenation using Pearlman's catalyst, then the two molecules of unprotected amine underwent a cyclization reaction to yield crown ether **67** in 42 % yield.

Zhao and Hua synthesized new chiral macrocyclic compounds containing pyridine moieties and chiral L-amino acids as a part of the macrocyclic ring⁵⁷. The procedure was initiated by condensation of 2,6-bis(hydroxymethyl)pyridine **68** and the corresponding L-amino acid **69** in the presence of DMAP and DCC. Final acylation of the chiral diamine **70** was performed by employing high dilution techniques. This step yielded two macrocyclic products **71** and **72** in 15 % and 13 % yield, respectively.

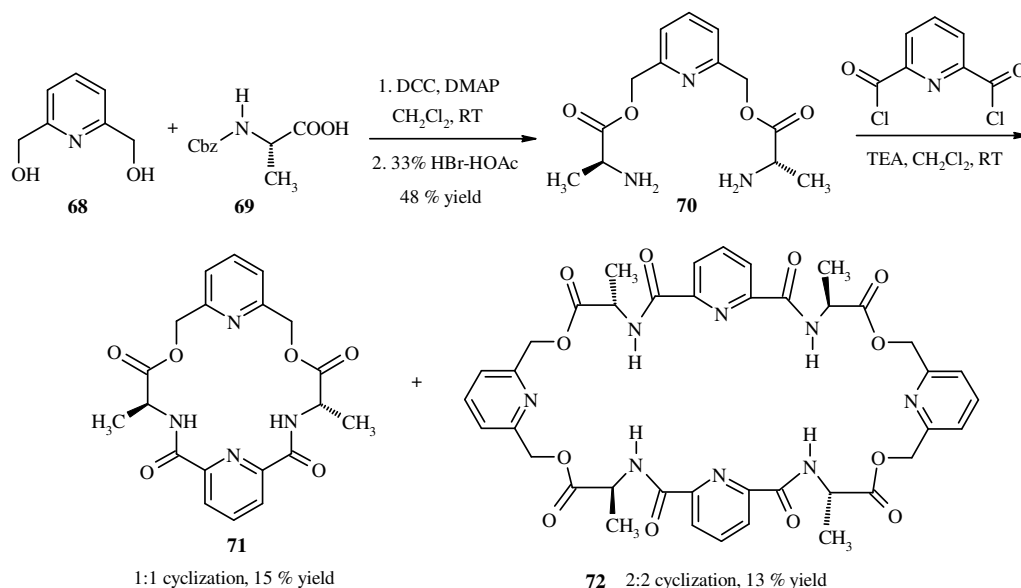


Fig. 1.20 Synthesis of chiral macrocycles containing pyridine moieties and chiral L-amino acids

These new macrocyclic receptors have been tested towards different D- and L-amino acid methyl ester hydrochlorides to measure whether they exhibit enantiomeric recognition.

A chiral diaza 18-crown-6 derived from (*R*)-(+)-1-phenylethylamine has been synthesized by Demirel and Bulut⁵⁸. The synthesis of podand **73** started with one pot reaction of catechol and ethylene oxide in the presence of piperidine hydrochloride in methanol. Conversion of the hydroxy groups into tosylates was achieved by treating the diol with *para*-toluenesulfonyl chloride in pyridine. Amination was accomplished by heating 1,2-bis(2-*p*-tolylsulphonylethoxy)-benzene with (*R*)-(+)-1-phenylethylamine in xylene at 120 °C. Podand **73** was then used for subsequent macrocyclization steps with 1,2-bis(2-*p*-tolylsulphonyl-ethoxy)benzene and triethylene glycol ditosylate, respectively in the presence of tripropylamine. Finally macrocycles **74**, **75** were isolated in 45 % and 54 % yields, respectively.

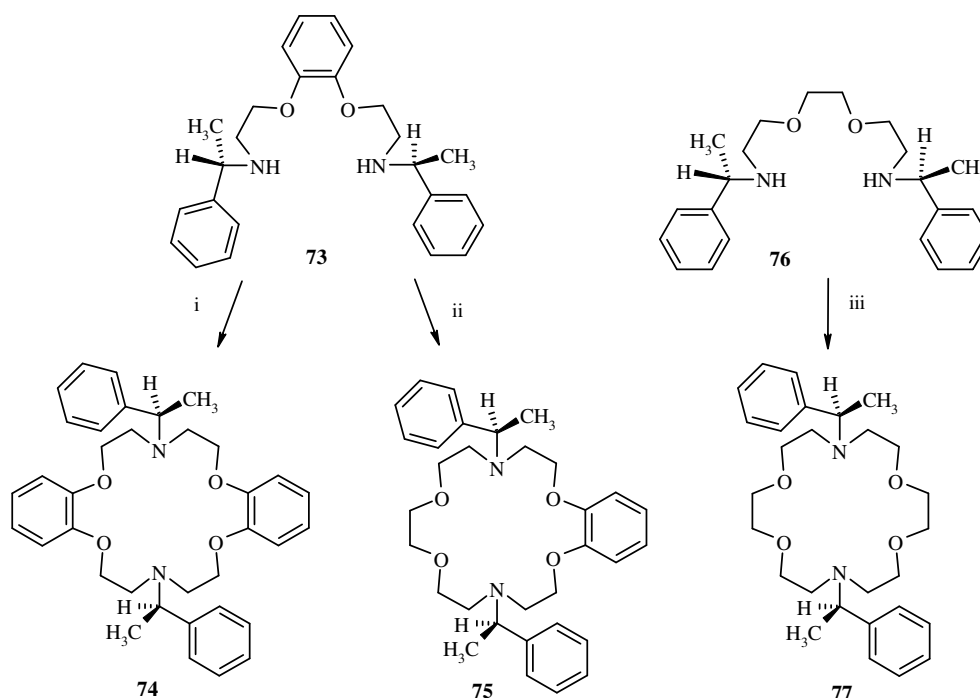


Fig. 1.21 Chiral diaza 18-crown-6 derived from (*R*)-(+)-1-phenylethylamine

Reaction conditions: i) tripropylamine (10 eq), xylene, 120 °C, 48h; ii) tripropylamine (10 eq); xylene, 120 °C, 48h; iii) tripropylamine (10 eq), triethylene glycol ditosylate, xylene, 120 °C, 48h;

Synthetic routes for preparation of macrocycle **77** were based on the same procedures as products **74** and **75**. The routes started with alkylation of (*R*)-(+)-1-

phenylethylamine with triethylene glycol ditosylate then finally macrocyclization with another equivalent of triethylene glycol ditosylate yielded product **77** in 48 % isolated yield.

1.6 Application of crown ethers

1.6.1 Crown ethers in chromatography

The selective binding properties of crown ethers have allowed them to be applied widely in chromatographic techniques.

Immobilized polyether systems are generally synthesized by either copolymerization of suitably functionalized macrocycles in the presence of cross-linking agents or by appending functionalized macrocycles to existing polymeric species⁵⁹. Structures **78-80** presented below exhibit different polymer types and have been employed in ion-selective membranes, as chromatographic stationary phases in HPLC and even for trace enrichment of radionuclides. Polymer **79** has been found to capture selectively K^+ and Cs^+ from methanol or methanol/water system while immobilized crown ether system **80** attached to silica has been employed to separate F^- , Cl^- , Br^- and I^- from each other as well as SO_4^{2-} from Cl^- using Na^+ as a counter ion. Utilization of immobilized benzo-18-crown-6 on a polystyrene matrix as the solid phase for HPLC has made a clean resolution of alkali metal halides and also divalent alkaline earth metal salts possible⁶⁰.

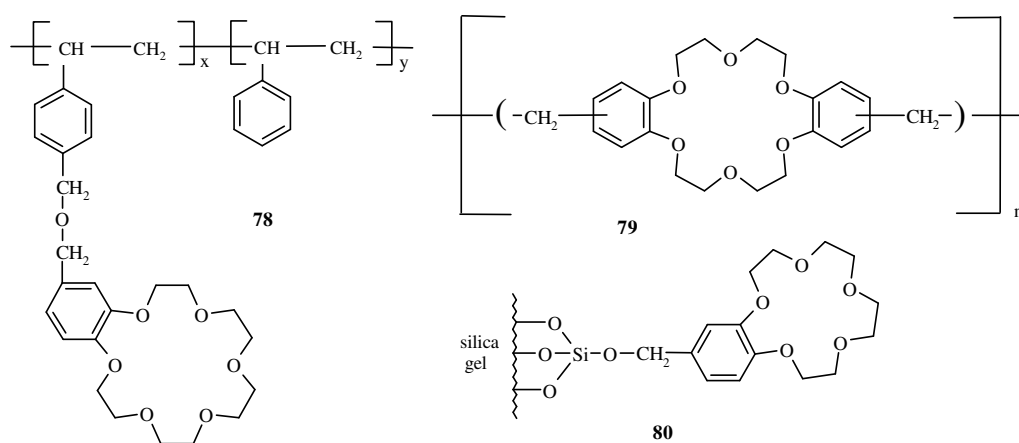


Fig. 1.22 Crown ethers incorporated on polystyrene and silica gel

In most cases only one enantiomer of chiral drugs has the desired bioactivity while the other may be inactive or even display undesirable side effects like toxicity⁶¹. It is

therefore crucial that the drug be properly analyzed for enantiomeric purity. One of the great problems faced by the pharmaceutical industry is the quantitation of undesired enantiomers in drug raw material. In order to determine enantiomeric purity, it has become advantageous to create a specific host molecule which would act as a molecular sensor, with the capability to differentiate enantiomers. Such molecular sensors would afford rapid and effective analysis for enantiomeric materials and also play an essential role in developing the techniques of enantiomer separation and assays for exact enantiomeric composition. For this purpose the liquid chromatography of enantiomers on chiral stationary phases (CSPs) incorporating binaphthyl units **81** have been developed to perform separation of such species like biologically important chiral primary amines⁶², chiral cyclic amines⁶³, amino alcohols⁶⁴ and α - and β -amino acids^{65,66}. Chiral drugs such as baclofen (muscle relaxant), primaquine (antimalarial) and gemifloxacin mesylate, a new fluoroquinolone antibacterial agent have also been efficiently resolved using 1,1'-binaphthyl units⁶⁷.

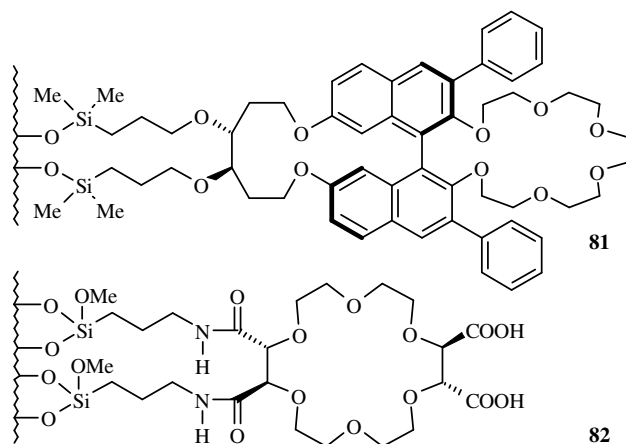


Fig. 1.23 Structures of CSPs based on chiral crown ethers incorporating 1, 1'-binaphthyl and tartaric acid units

Incorporation of (+)-(18-crown-6) 2,3,11,12-tetracarboxylic acid on the stationary phase **82** was used to resolve of α -amino acids, α -amino amides and α -amino esters⁶⁸ including afloqualone (muscle relaxant), and also primaquine⁶⁹. Crown ether-based chiral stationary phases have also been used to resolve racemic primary amines⁷⁰.

1.6.2 Crown ethers in organic synthesis

One obstacle to the development of new reagents for organic synthesis is that the majority of inorganic salts are insoluble or sparingly soluble in organic solvents. This problem can often be eliminated by employing crown ethers which improve the solubility of polar species in non-polar environments by forming complexes with metal cations. A variety of organic reactions use polyether macrocycles in this way, including saponification, esterification, redox reactions, nucleophilic substitution (fluorination, alkoxylation, cyanation, nitration), elimination, (carbene and nitrene formation, decarboxylation) and condensation reaction (alkylation, arylation).

1. Solid/liquid and liquid/liquid phase transfer catalysis

The presence of 18-crown-6 in a solution of KF and acetonitrile generates 'naked' fluoride ion. The considerable nucleophilicity of this anion under these conditions is demonstrated by the fact that it is capable of displacing leaving groups from both sp^2 and sp^3 hybridized carbons in various structural environments^{71,72,73,74,75,76}.

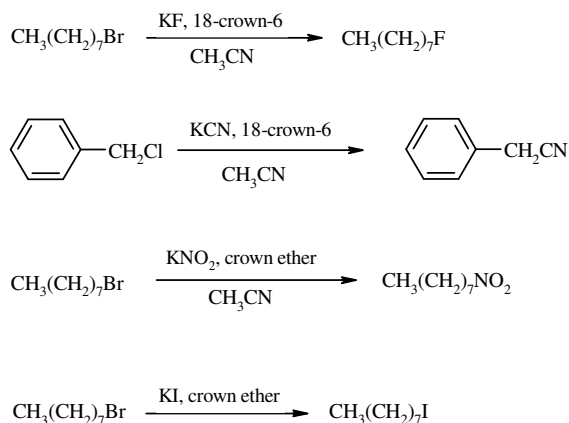


Fig. 1.24 18-crown-6 in organic synthesis

2. Saponification of sterically hindered esters

Pedersen recognized that by using hydrophobic dicyclohexano-18-crown-6 **83** it is possible to dissolve potassium hydroxide in hydrocarbon media such as toluene and benzene¹. The resulting “free” OH⁻ anion has been shown to be an excellent reagent to hydrolyze sterically hindered esters under such conditions.

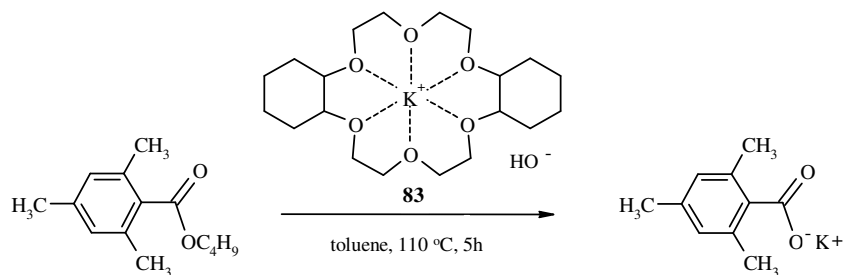


Fig. 1.25 Dicyclohexano-18-crown-6 in ester hydrolysis

3. Nucleophilic substitution reactions

Simmons also recognized the great potential for crown ethers in synthetic applications and realized that nucleophilic substitution reactions might take place in systems which had previously proved resistant. When 1,2-dichlorobenzene **84** and potassium methoxide were heated at 90 °C in the absence of solvent the reaction yielded 2-chloroanisole **85** as the only product. However, formation of the *meta*-isomer was not observed, suggesting that nucleophilic aromatic substitution had occurred, but not by formation of aryne as an intermediate, the mechanism normally invoked for such a reaction⁷⁷.

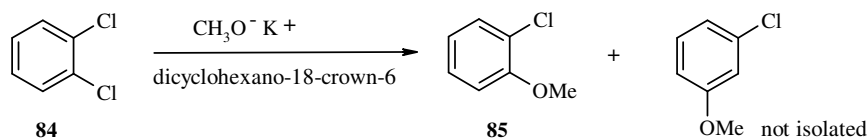


Fig. 1.26 Dicyclohexano-18-crown-6 in nucleophilic substitution reaction

4. Reduction reactions of ketones to secondary alcohols

Use of dibenzo-18-crown-6 **9** together with sodium borohydride also improves the reducing power of this reagent when reacting with a number of ketones to give the corresponding alcohols in quantitative yields⁷⁸.

Cyclohexanol **87** has been prepared from cyclohexanone **86** using mild reaction conditions in 92 % yield. The increased yield in this reaction probably stems from the high reactivity of a “naked” BH_4^- anion.

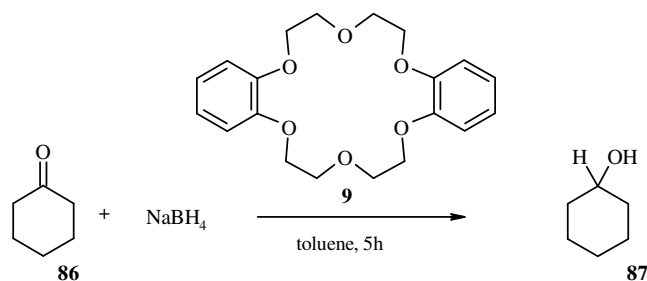


Fig. 1.27 Dibenzo-18-crown-6 in reduction reaction

5. Base-catalyzed elimination reactions

Bartsch investigated the behaviour of potassium *tert*-butoxide in elimination reactions in the presence and in the absence of crown ether. Addition of dicyclohexano-18-crown-6 into the reaction mixture significantly increased reactivity and also influenced the geometry of the product⁷⁹.

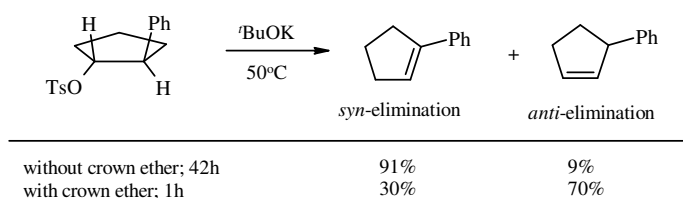


Fig. 1.28 Dicyclohexano-18-crown-6 in elimination reaction

6. Oxidation reaction with potassium permanganate

Potassium permanganate is a powerful oxidizing agent, however, its general utility is limited by its solubility properties. It is a crystalline purple compound that fails to

dissolve in anhydrous benzene. However, when used in the presence of crown ethers and a little water ‘purple benzene’ is generated, enabling oxidations to be performed in benzene⁸⁰. Sam and Simmons showed that ‘purple benzene’ can oxidize a range of alkenes, alcohols, aldehydes and alkylbenzenes to the corresponding carboxylic acids under mild conditions in near quantitative yields⁸¹. An interesting example is the reaction of β -pinene **88** in the presence of ‘purple benzene’ where the double bond of the terpene system is cleanly cleaved forming *cis*-pinonic acid **89** in 90 % yield.

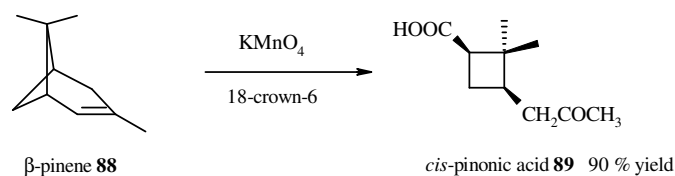


Fig. 1.29 18-crown-6 in oxidation reaction

7. Catalysis of asymmetric aldol condensation

Gao and Martell investigated the catalytic properties of chiral polyaza macrocyclic ligand and its zinc(II) complexes **90** in the direct enantioselective aldol reaction of 4-nitrobenzaldehyde **91** and acetone **92** in DMSO at RT⁸². Chiral complex **90** catalyzed the aldol reaction at a concentration of 5 mol% and 4-hydroxy-4-(4-nitrophenyl)butan-2-one **93** of configuration (*R*) was isolated in up to 95 % yield with enantiomeric excess of 57 %.

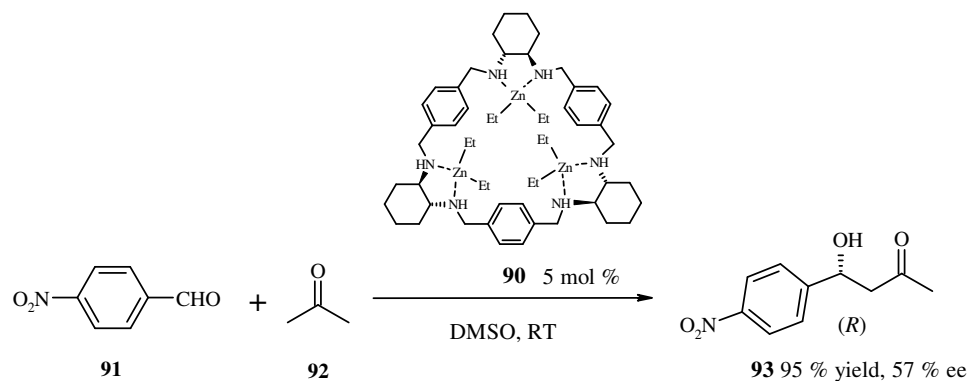


Fig. 1.30 Enantioselective aldol reaction catalysed by a chiral macrocycle **90** complexed to diethyl zinc

8. Alkyne addition to aldehydes

The 1,1'-binaphthyl macrocycle **94** has been employed as a ligand to form a Lewis acidic complex for asymmetric catalysis⁸³. Asymmetric addition of alkynes to linear or branched aliphatic aldehydes was investigated in the presence of chiral macrocycle **94** (20 mol%), complexed with Me₂Zn (2 eq) as the catalyst. The reactions were carried out in THF or CH₂Cl₂ at RT and the results demonstrated that chiral **94** and its Me₂Zn complex is an excellent catalyst for the synthesis of chiral propargyl alcohols and the ee of the products varied from 89-96 %.

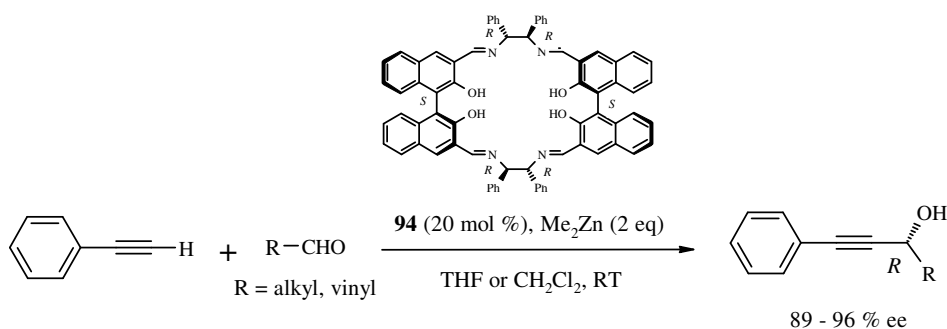


Fig. 1.31 Synthesis of propargylic alcohols catalysed by a chiral macrocyclic catalyst of **94** with Me₂Zn

9. Asymmetric epoxidation of alkenes

Optically active metallosalens are widely used catalysts for asymmetric synthesis⁸⁴. This is mainly due to their facile preparation which gives rise to a highly asymmetric coordination sphere, and their versatile catalytic activity that depends on the nature of the metal chelated by the salen ligands⁸⁵. Synthesis of chiral macrocycles and their manganese(III) salen complexes has been reported by Martinez *et al*⁸⁶.

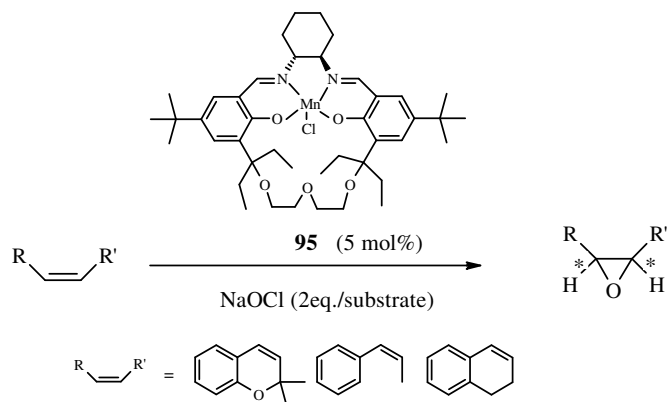


Fig. 1.32 Asymmetric epoxidation of alkenes with macrocyclic catalyst **95**

The catalytic properties of **95** were investigated in the asymmetric epoxidation of various alkenes with NaOCl or H₂O₂ as an oxygen atom donor. Depending on the features and the stability of the complex enantiomeric excesses up to 96 % have been obtained in the asymmetric epoxidation, together with a quantitative conversion of the olefin.

10. Enantioselective Michael addition

Cram first reported the use of chiral crown ethers incorporating a 1,1-binaphthyl moiety as chiral phase transfer catalysts for the classical Michael addition⁸⁷.

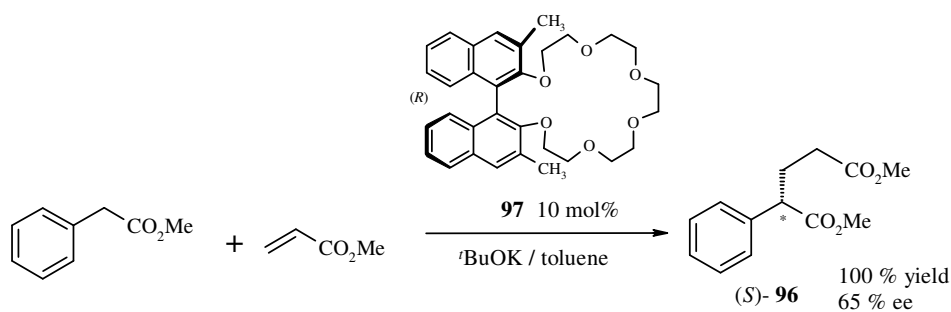


Fig. 1.33 Michael addition catalyzed by a chiral crown complex of **97** with ^tBuOK

Cram's new approach afforded Michael addition product (*S*)-**96** with high yields (up to 100 %) and satisfactory ee (up to 65 %) catalysed by a complex formed between potassium *tert*-butoxide and the chiral host **97**.

More recently Boyle *et al* developed a new class of chiral cage annulated macrocycles and investigated their use as catalysts for enantioselective Michael addition⁸⁸.

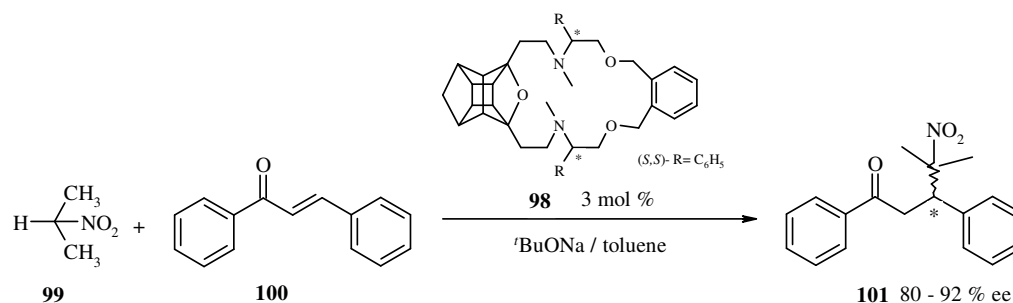


Fig. 1.34 Michael addition catalyzed by a chiral crown complex of **98** with *t*BuONa

The catalytic activity of the cage macrocycle **98** in the Michael addition of 2-nitropropane **99** to chalcone **100** was investigated using stoichiometric *t*BuONa with respect to macrocycle 1:1. Firstly, reaction in the absence of the macrocycle was attempted but failed to give the Michael adduct and starting material was recovered. 18-Crown-6 as a control host catalyzed the reaction with 54 % yield and 0 % ee (as expected racemic product was obtained), whereas the cage macrocycle **98** gave product **101** in low yield (20 %) but with an impressive enantiomeric excess of 92 %.

11. Enantioselective Friedel-Crafts reaction

Zhu *et al* synthesised a new macrocyclic salen ligand from 2,6-bis-hydroxy-methyl-4-*tert*-butyl phenol in a five-step synthesis⁸⁹.

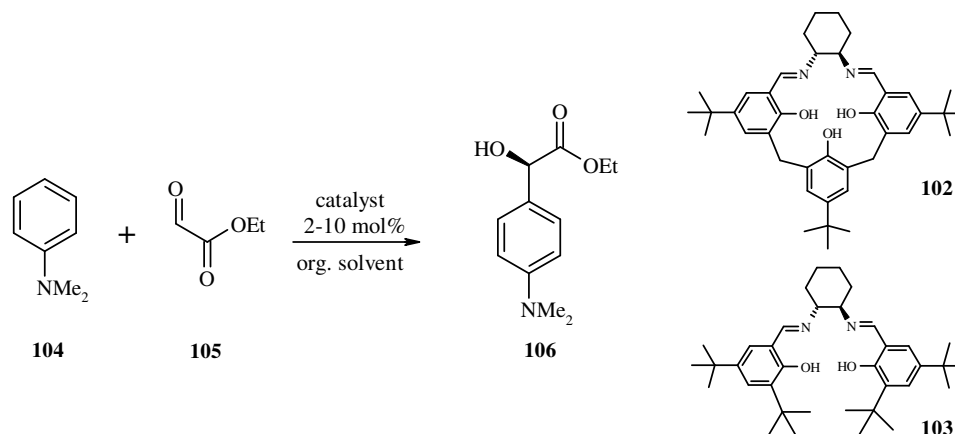


Fig. 1.35 Enantioselective Friedel-Crafts reaction catalyzed by chiral macrocycle complex of **102** with Ti(O^{*i*}Pr)₄

Macrocycle **102** was then employed as a chiral ligand with Ti(O^{*i*}Pr)₄ (1:1) to investigate the enantioselective Friedel-Crafts reaction of *N,N*-dimethylaniline **104** with ethyl glyoxylate **105**. Reactions carried out in the presence of 10 mol% of the Ti macrocycle catalyst in Et₂O at 0 °C, gave 85 % isolated yield of **106** and an excellent enantioselectivity of 98 %. Very similar results were observed using 5 mol% of catalyst, whereas further decreasing the amount of catalyst (to 2 mol%) resulted in lower chemical yields, although a high enantiomeric excess of 95 % was maintained. For comparison Friedel-Crafts reactions were carried out employing titanium complexes with chiral ligand **103**. Use of these catalysts gave good yields of the expected 2-(4-dimethylaminophenyl)-2-hydroxyacetic acid ethyl ester **106**, but with a significant drop in enantioselectivity.

1.7 Catalytic Friedel-Crafts Reactions

Electrophilic substitution of aromatic rings with carbonyl compounds *via* the Friedel-Crafts reaction is one of the most fundamental C-C bond-forming reactions in organic chemistry⁹⁰. The Friedel-Crafts reaction, which typically requires a Lewis acid catalyst provides access to a range of biologically active compounds with applications in the pharmaceutical, agrochemical and material science areas. Conventional Friedel-Crafts reactions between acid chlorides and aromatic compounds normally require one equivalent of a strong Lewis acid, such as AlCl₃, and anhydrous reaction conditions. 1 equivalent of HCl is generated as a by product, which requires disposal^{91,92}. However, if an aldehyde is used as the electrophile instead of an acyl chloride, a clean reaction to give a benzylic alcohol takes place. If a substoichiometric Lewis acid can be used to promote the reaction then it may be classified as 100 % atom efficient.

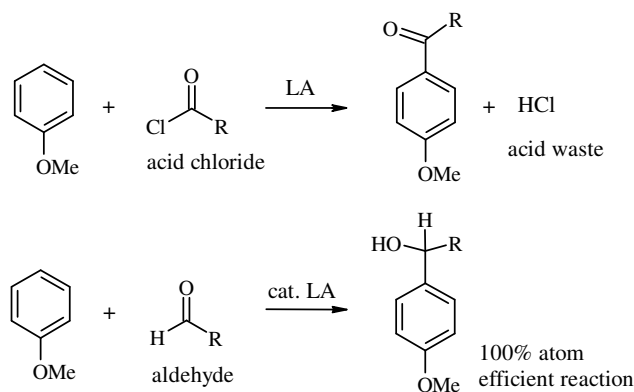


Fig. 1.36 Friedel-Crafts reaction

This project focuses on the developing synthetic methodology of facile and direct preparation of compounds based on the phenylethanolamine core, by reaction of activated glyoxamides with electron-rich aromatic nucleophiles in Lewis acid catalysed Friedel-Crafts reactions.

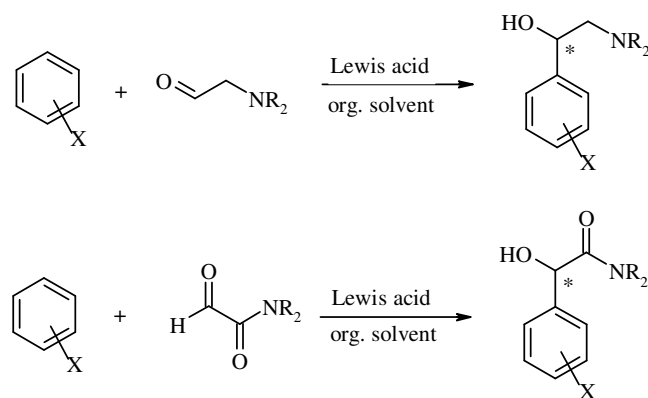


Fig. 1.37 Direct preparation of phenylethanolamine library

The advantage of the Friedel-Crafts approach is that Friedel-Crafts products can be synthesized in high yields often with catalytic Lewis acids like Cu(I), Cu(II), Zn(II), Sc(III), Yb(III) in substoichiometric amounts. Furthermore, by introducing chiral ligands, chiral Lewis acid catalysts can be formed in order to control the enantioselectivity of Friedel-Crafts reactions with activated aldehydes and ketones^{93,94}. This aspect is crucial considering the importance of enantiopure compounds as pharmaceuticals and cosmetics. An example of a chiral product from the enantioselective Friedel-Crafts reaction is provided by substituted mandelic acid derivatives including *p*-aminomandelic acid derivatives and mandelic amide compounds which have dual activities as antibacterial and anti-ageing agents⁹⁵. Mandelic acid **107** has bacteriostatic properties and is used as an antiseptic in urinary tract infections. Furthermore, mandelic acid and its derivatives are useful as intermediates in the synthesis of target molecules for other applications⁹⁶.

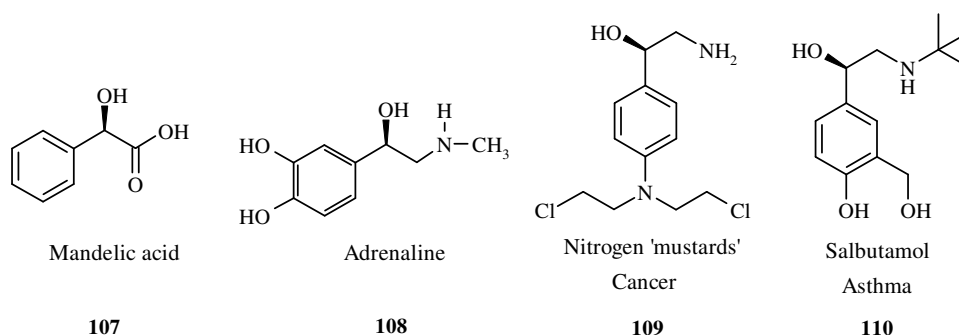


Fig. 1.38 Target compounds of interest

The target scaffold of phenylethanolamine can also be found in such pharmacologically active compounds as adrenaline **108**, nitrogen mustards **109** and salbutamol **110**. Adrenaline is a neurotransmitter and plays a central role in the short-term stress reaction in the human body⁹⁷. The nitrogen mustards include cytotoxic chemotherapy agents, as well as mustard gas a chemical warfare agent⁹⁸. Salbutamol is a short-acting β_2 -adrenergic receptor agonist used for the relief of bronchospasm in conditions such as asthma and chronic obstructive pulmonary disease (COPD), and is usually given by the inhaled route for direct effect on bronchial smooth muscle⁹⁹

1.8 P- glycoprotein efflux pump

P-glycoprotein (P-gp) is a multidrug efflux pump. It is one of the membrane bound glycoproteins that allow cancer cells to develop a resistance not only to a single drug but towards other structural and mechanistically unrelated drugs, a phenomenon called multidrug resistance (MDR)¹⁰⁰. P-gp efflux pumps operate by removing the anticancer drugs from the cell. They can be activated by environmental stress from foreign chemicals or heat, and display a tendency to over express in cancer cells decreasing the concentration of chemotherapeutics in these cells, which in turn allows the cancer cells to survive¹⁰¹. Because these transporters are the biggest single cause for failure of anticancer chemotherapy, considerable effort has been invested in the development of compounds that behave as blockers of the transport protein and hence can restore the sensitivity of the cell to anticancer drugs.

1.8.1 P- glycoprotein efflux pump inhibitors

P-gp inhibitors are non-cytotoxic agents that, when used in combination with drugs pumped by P-gp, restore the sensitivity of cells to these therapeutic agents maintaining their intracellular concentration¹⁰². This can have implications for the treatment of diseases such as cancer and HIV, since P-gp has the facility to confer resistance by detecting, binding and removing a wide variety of hydrophobic and amphipathic compounds from the cell¹⁰³. The pharmacological approach to circumvention of MDR began with the report by Tsuruo that the calcium channel blocker verapamil and the phenothiazine derivative trifluoperazine potentiate the activity of vincristine¹⁰⁴. Since then the identification of lead compounds in this area has been based mainly on serendipity. P-gp inhibitors, also known as P-gp modulators and chemosensitizers have been classified into several groups distinguished by their structural features. Among them are calcium channel blockers, calmodulin antagonists, protein kinase C inhibitors, natural products such as steroids, cyclic peptides and flavanoids and miscellaneous compounds. They can also be broadly separated into three categories based on their interaction with P-gp: high-

affinity substrates of the P-gp pump, efficient inhibitors of ATP hydrolysis coupled P-gp transport, and partial substrates/inhibitors. Most chemosensitizers display their MDR reversal activities by competitively binding to the drug binding sites on P-gp or non-competitively binding to the modulatory site¹⁰³.

The first generation of P-gp inhibitors embraced compounds that were synthesised for other therapeutic purposes but showed their resistance modulation effect when administered in combination with some anticancer treatments. They showed undesirable side effects at the concentrations necessary to inhibit P-gp clinically. Among them were the calcium channel blocker, verapamil and cyclosporine A. The second group of chemosensitizers includes analogues of the first group, but designed in a way to reduce their toxicity. One of them is dexverapamil **111**, the (*R*)-isomer of verapamil which lacks the cardiac effects of the (*S*)-isomer, but retains the ability to inhibit P-gp.

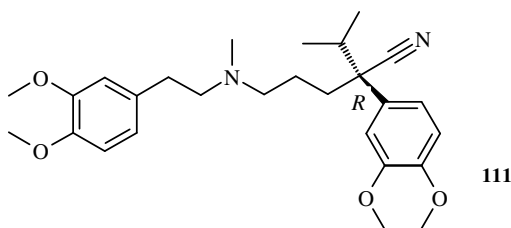


Fig. 1.39 Dexverapamil **111**

Dexverapamil binds reversibly to P-gp and inhibits the binding of many chemotherapeutic agents and other inhibitors of P-gp. Dexverapamil is not the most potent P-gp inhibitor. In fact its analogue Roll-2933 **112**, was found to be ten times more potent than dexverapamil in reversing resistance to doxorubicin¹⁰⁵.

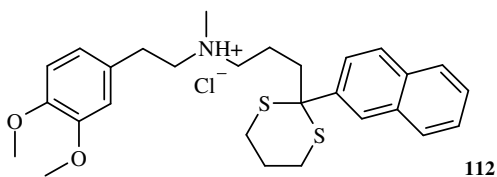


Fig. 1.40 Structure of Roll-2933 the analogue of (*R*)-verapamil

Cyclic peptides and also the immunosuppressants cyclosporine A and tacrolimus **113** are used in organ transplantation and they can also act as P-gp inhibitors¹⁰⁶.

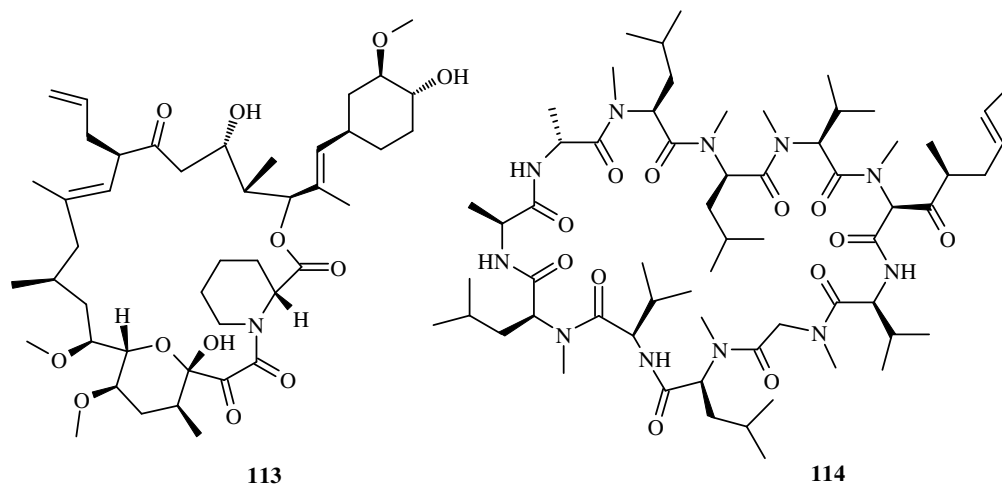


Fig. 1.41 Structures of tacrolimus **113** and valsopodar (PSC-833) **114** an analogue of cyclosporine A

Correspondingly, valsopodar (PSC-833) **114** is a structural analogue of cyclosporine A that lacks its immunosuppressive effects, but remains an effective P-gp inhibitor. It is under phase two clinical studies¹⁰⁷.

Another family of third generation chemosensitizers that have been clinically evaluated are biricodar (VX-710) **115**¹⁰⁸ and dofequidar (MS-209) **116**¹⁰⁹ which inhibit both P-gp and MDR1, whereas zosuquidar (LY-335979) **117** is a selective inhibitor of P-gp¹¹⁰.

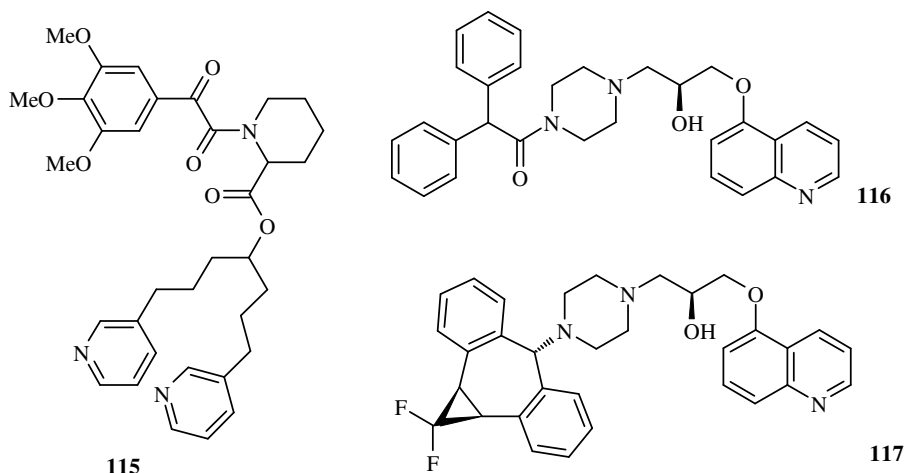


Fig. 1.42 Structures of biricodar (VX-710) **115**, dofequidar (MS-209) **116** and zosuquidar (LY-335979) **117**

Calmodulin antagonists are another class of P-gp inhibitors. These include flupentixol **118**. Both the *cis* and *trans* isomers of flupentixol are P-gp inhibitors, with the *trans* isomer being four times more potent than the *cis* ¹¹¹.

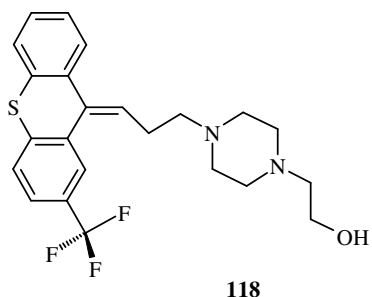


Fig. 1.43 Structure of flupentixol **118**

P-gp has been shown to bind reversibly to most steroids. However, the more hydrophilic steroids are too easily transported and tend to be less useful as P-gp inhibitors. In contrast hydrophobic (lipophilic) steroids are transported less efficiently and as such are more useful P-gp inhibitors. Progesterone **119**, a hormone that occurs naturally in humans, was found to bind to P-gp but appears not to be transported by protein¹¹². This result indicated the possibility of using progesterone as a P-gp inhibitor, but further testing demonstrated that progesterone was found to be less effective than (*R*)-verapamil.

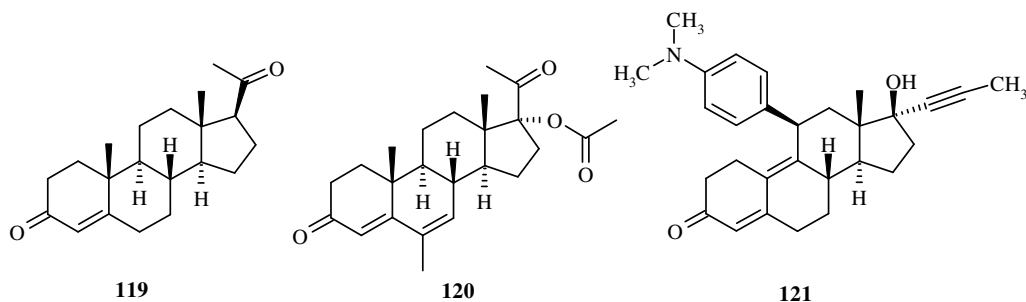


Fig. 1.44 Structures of progesterone **119**, megestrol acetate **120** and mifepristone **121**

Other steroids such as megestrol acetate **120** and mifepristone RU486 **121**, have been tested, and have proved to be more effective inhibitors of P-gp than progesterone, but their activity has not exceeded that of (*R*)-verapamil. Also P-gp inhibitors such as ethacrynic acid **122**, irofulven **123** and SN-22995 **124** are in advanced clinical trials as MDR modulators¹¹³.

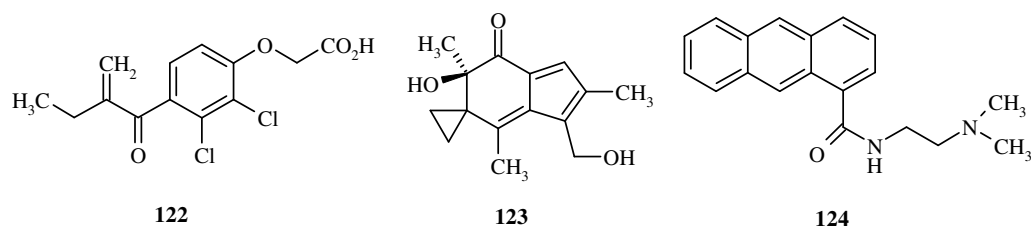


Fig. 1.45 Structures of ethacrynic acid **122**, irofulven **123** and SN-22995 **124**

Elacridar (GF120918) **125** was discovered in the search for potent and selective P-gp inhibitors and was proven to inhibit activity of both the P-glycoprotein drug pump and breast cancer resistance protein (BCRP; A3CG2)¹¹⁴. It proved to be about 100-fold more potent than the widely used P-gp inhibitor cyclosporin A¹¹⁵. In clinical studies with oral dosing of the topotecan, a chemotherapeutic used to treat ovarian and lung cancer, elacridar maximized the bioavailability of the anticancer drug¹¹⁶.

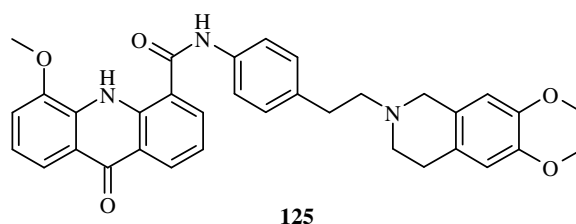


Fig. 1.46 Structure of elacridar **125**

In this short review a few illustrative examples have been included to show the diversity of structures which have been shown to act as P-gp inhibitors. To date a complete structure activity relationship study of each class of P-gp inhibitors has not been carried out. Instead Wang *et al*¹¹⁷ have compiled a list of requirements that potential P-gp inhibitors should have. This list has been compiled from a large group of compounds and categorizes them into seven classes according to their structural features. Studies have indicated that transmembrane sequences of P-gp involved in substrate interaction contain a high number of amino acids with hydrogen bond donor sides such as the OH, NH₂, NH, SH groups of amino acids. Another important feature for maximum binding to P-gp is the presence of *ortho*-substituted aromatic rings and the fragment C-C-X-C-C, where X=O or N and where a tertiary nitrogen is preferential. The lipophilicity as measured by the $(\log P)^2$ parameter was found to be a very important physicochemical property of P-gp inhibitors. Hydrophilic fragments like carboxylic acids, phenols, anilines and quaternary ammonium compounds were

found to possess deactivating inhibiting properties¹¹⁸. This discovery correlates well with an independent study concluding that an effective P-gp modulator candidate should have a minimum log *P* of 2.92, and should have a main chain length of not less than 18 atoms, together with a high energy value for the HOMO and at least one tertiary, basic nitrogen atom¹¹⁹.

1.9 Conclusion

Macrocyclic compounds have been proven to have therapeutic potential in many areas and have been tested as antibacterial and antifungal agents, also as potent hepatitis C virus protease inhibitors, and as cancer therapeutics¹⁰⁶. In the past years several macrocyclic compounds have been found to potentiate the activity of anticancer drugs by inhibiting P-gp in cancer treatment¹²⁰.

Macrocycles have the capability to provide diverse functionality and stereochemical complexity in a conformationally pre-organized ring structure. This ability can result in high affinity and selectivity towards a wide range of targets, including metal cations, amines, amino acids and proteins. Macrocyclic products have evolved to fulfil numerous synthetic and biochemical functions, and their profound properties have led to their development as drugs, sensors and catalysts. Numerous examples of chiral macrocycles containing naturally occurring compounds *e.g.* sugars and amino acids have been presented. Although macrocycles containing opiates *e.g.* morphine and its derivatives have not been synthesised. The strong analgesic properties shown by morphine make it one of the most effective pain killers in the treatment of moderate to severe pain. Also its complexed three-dimensional rigid structure is an interesting subject to investigate. Therefore, it is an appealing challenge to combine the properties of macrocycles with the well known activity of morphine. Such unique compounds could play an advantageous role in asymmetric catalysis especially to control stereoselectivity in Friedel-Crafts reaction products.

2 Friedel-Crafts Chemistry

2.1 Preparation of L-tartramides

A series of tartramides were prepared according to methods reported in the literature. The tartramides **127-129** were synthesised from diethyl-L-tartrate and the corresponding acyclic amine by refluxing in methanol¹²¹, whereas tartramides **130** and **131** were prepared by stirring of diethyl-L-tartrate and the corresponding cyclic amine in methanol at RT for two days¹²². Compounds **127-131** were recrystallized from toluene or benzene to provide crystalline products in good yields varying from 36 to 92 %.

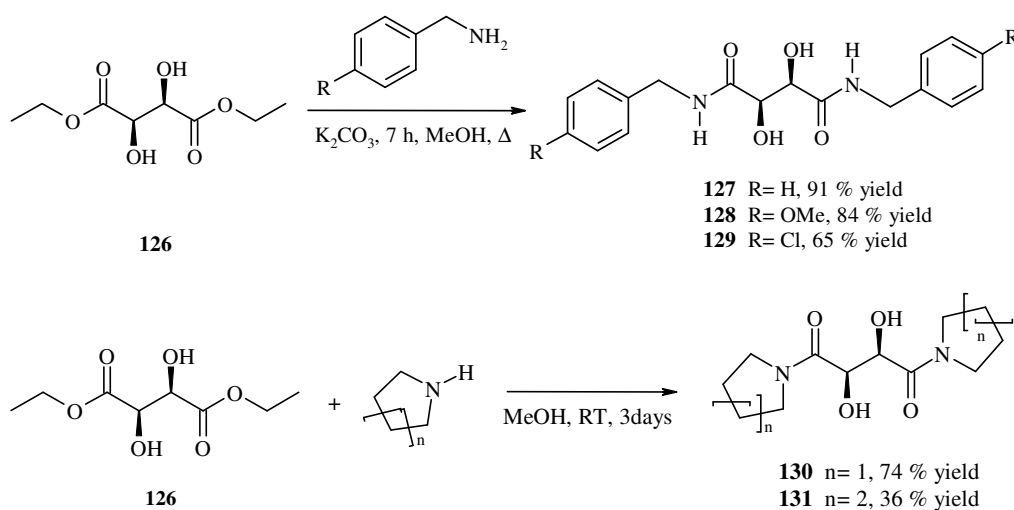


Fig. 2.1 Synthesis of the symmetrical tartramides from diethyl-L-tartrate

Tartramides **127-131** were oxidatively cleaved to form glyoxamides for subsequent Friedel-Crafts chemistry.

2.2 Oxidative cleavage of L-tartramides

Glyoxamides were prepared by oxidative cleavage of tartramides with periodic acid in organic solvents CH_2Cl_2 or Et_2O ¹²³. Oxidation with periodic acid was performed by dissolving the tartramide in the anhydrous solvent and then adding the oxidizing agent (1.1 eq) in small portions over 1 h, and allowing the reaction to continue at 0 °C for an additional hour. The crude was finally poured onto molecular sieves (4Å) to remove any water, filtered and evaporated.

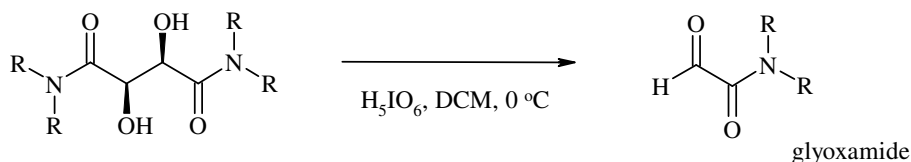


Fig. 2.2 General synthesis of glyoxamides by periodic oxidative cleavage

Attempts to purify the glyoxamides were undertaken by vacuum distillation from toluene, Kugelrohr distillation and sublimation. However, none of these attempts allowed for satisfactory purification of the glyoxamides. Therefore in most cases the crude glyoxamide was used without further purification in subsequent Friedel-Crafts reactions.

2.3 Friedel-Crafts reactions

2.3.1 Catalytic Friedel-Crafts reaction of *N,N*-dimethyl glyoxamides

A series of catalytic Friedel-Crafts reactions between *N,N*-dimethyl glyoxamide **132** and *N,N*-dimethylaniline **104** were carried out in the presence of various Lewis acids under a variety of reaction conditions. First the Lewis acid catalyst was dried under high vacuum for 2 h then the organic solvent, *N,N*-dimethyl glyoxamide **132** and *N,N*-dimethylaniline **104** were added and the reaction stirred at the corresponding temperature for the experiment (Table 2.1). After each experiment crude ¹H NMR analysis was carried out, prior to purification by column chromatography.

However, in each experiment none of the desired compound **133** was observed. Instead *N,N*-dimethylaniline was recovered and *N,N*-dimethyl glyoxamide was found as a mixture of unidentified products.

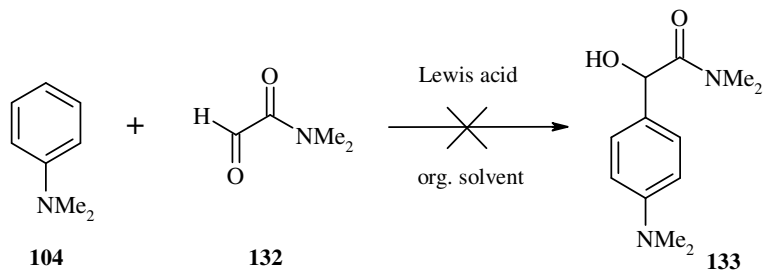


Fig. 2.3 Catalytic Friedel-Crafts reaction of *N,N*-dimethyl glyoxamide **132** with *N,N*-dimethylaniline **104**

Entry	Lewis acid	Catalyst [mol %]	Ratio 1:2	Solvent	Temp. [°C]	Reaction time [h]	Product 133
1	Cu(OTf) ₂	10	1:2	THF	20/65	32/22	0
2	Cu(OTf) ₂	10	1:2	Et ₂ O	20/35	34/32	0
3	Cu(OTf) ₂	50	1:5	CH ₂ Cl ₂	0/20	8/72	0
4	Zn(OTf) ₂	20	1:4	THF	20	62	0
5	Sc(OTf) ₃	30	1:4	THF	20	72	0
6	Al(OTf) ₃	10	1:4	THF	0/20	8/72	0
7	La(OTf) ₃	20	1:4	THF	20	72	0
8	Yb(OTf) ₃	20	1:3	THF	20	72	0
9	SnCl ₂	20	1:3	THF	0/20	8/72	0
10	SnCl ₄	10	1:3	CH ₂ Cl ₂	20	72	0
11	TiCl ₄	10	1:3	CH ₂ Cl ₂	0/20	8/72	0

Table 2.1 Results for the catalytic Friedel-Crafts reaction of *N,N*-dimethyl glyoxamide **132** with *N,N*-dimethyl-aniline **104** under various reaction conditions

2.3.2 Catalytic Friedel-Crafts reaction of 2-oxo-2-(pyrrolidin-1-yl)acetaldehyde

A series of Friedel-Crafts experiments between 2-oxo-2-(pyrrolidin-1-yl)acetaldehyde **134** and *N,N*-dimethylaniline **104** were also performed and carried out in the presence of catalytic amounts of various Lewis acids (Table 2.2). The reaction procedure embraced the drying of the catalyst under high vacuum, then subsequent addition of 2-oxo-2-(pyrrolidin-1-yl)acetaldehyde and *N,N*-dimethylaniline. The reactions were stirred at the corresponding temperature, and then a ^1H NMR of the crude and separation by column chromatography was performed for each experiment. The desired Friedel-Crafts reaction product **135** was not identified, instead *N,N*-dimethylaniline was recovered and product **136** was identified as a side product.

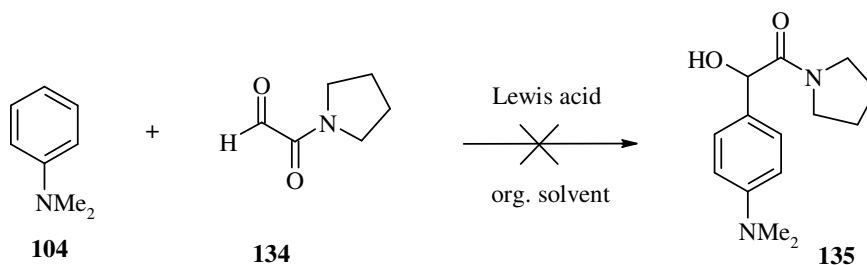


Fig. 2.4 Catalytic Friedel-Crafts reaction of 2-oxo-2-(pyrrolidin-1-yl)acetaldehyde **134** with *N,N*-dimethylaniline **104**

Product **136** was isolated as a white solid after each catalytic Friedel-Crafts experiment employing 2-oxo-2-(pyrrolidin-1-yl)acetaldehyde **134**. This dimeric hemiacetal forms as a result of a reaction between the hydrate and either a second molecule of hydrate or glyoxamide. This dimeric form of 2-oxo-2-(pyrrolidin-1-yl)acetaldehyde was unreactive in catalytic Friedel-Crafts reaction.

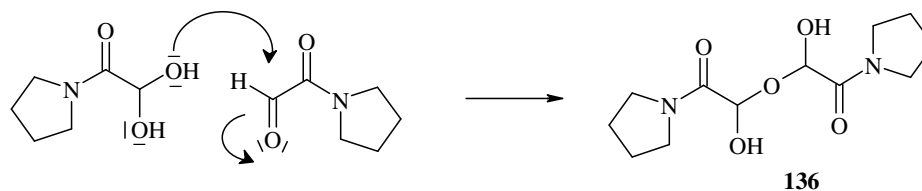


Fig. 2.5 Side product of catalytic Friedel-Crafts reaction of 2-oxo-2-(pyrrolidin-1-yl)acetaldehyde **134** with **104**

Exp. no	Lewis acid	Catalyst [mol %]	Ratio 2:1	Solvent	Temp. [°C]	Reaction time [h]	Product 135
1	Zn(OTf) ₂	20	4:1	CH ₂ Cl ₂	20/35	72	0
2	Zn(OTf) ₂	50	4:1	THF	20/65	48/21	0
3	Zn(OTf) ₂	20	5:1*	toluene	20/35	44/26	0
4	Zn(OTf) ₂	40	5:1*	toluene	20	72	0
5	Cu(OTf) ₂	10	2:1	CH ₂ Cl ₂	20	84	0
6	Cu(OTf) ₂	20	2:1	THF	20	84	0
7	Sc(OTf) ₃	10	2:1	CH ₂ Cl ₂	20	84	0
8	Al(OTf) ₃	10	2:1	CH ₂ Cl ₂	0/20	8/74	0
9	La(OTf) ₃	10	2:1	CH ₂ Cl ₂	20	84	0
10	Sn(OTf) ₂	10	2:1	CH ₂ Cl ₂	20	84	0
11	Yb(OTf) ₃	10	2:1	CH ₂ Cl ₂	20	84	0
12	SnCl ₂	20	2:1	CH ₂ Cl ₂	20	72	0
13	SnCl ₄	20	2:1	CH ₂ Cl ₂	20	72	0
14	TiCl ₄	20	2:1	CH ₂ Cl ₂	0/20	8/72	0

Table 2.2 Results for the catalytic Friedel-Crafts reaction of 2-oxo-2-(pyrrolidin-1-yl)acetaldehyde **134** with *N,N*-dimethylaniline **104** under various reaction conditions

* glyoxamide was added as a mixture with toluene (3 mL)

2.3.3 Catalytic Friedel-Crafts reactions of ethyl glyoxylate

After a series of unsuccessful attempts at performing the Friedel-Crafts with a series of glyoxamides, ethyl glyoxylate **105** was used as a known substrate for the Friedel-Crafts reaction⁹³. Ethyl glyoxylate was prepared from ethyl-L-tartrate **126** by the same oxidative cleavage with H_5IO_6 in CH_2Cl_2 . The Friedel-Crafts reaction were carried out in the presence of 10 mol% of $\text{Cu}(\text{OTf})_2$ in CH_2Cl_2 under N_2 and compound **137** was isolated in 58 % yield, whereas **138** in 42 % yield.

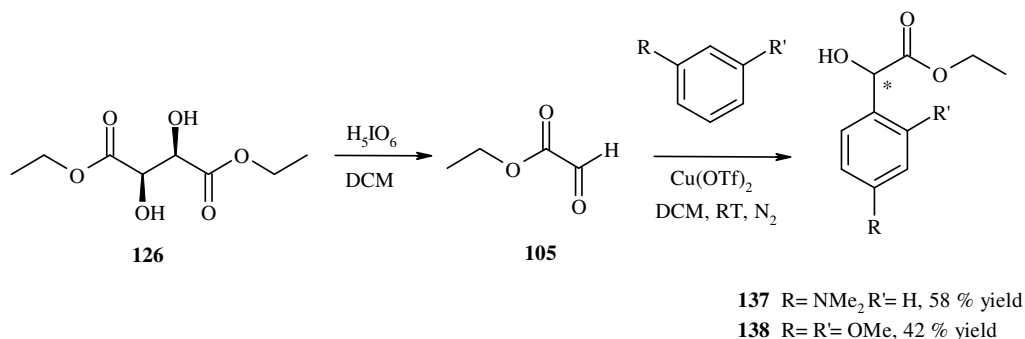


Fig. 2.6 Preparation of **137** and **138** from ethyl glyoxylate **105** by catalytic Friedel-Crafts reaction

2.3.4 Catalytic Friedel-Crafts reactions of ethyl 3,3,3-trifluoropyruvate

Further Friedel-Crafts experiments employing ethyl 3,3,3-trifluoropyruvate **139** and substoichiometric catalytic amounts of Lewis acid were performed according to the reported method⁹⁴. Commercially available ethyl 3,3,3-trifluoropyruvate **139** was reacted with *N,N*-dimethylaniline **104** in the presence of 5 mol% of $\text{Zn}(\text{OTf})_2$ in CH_2Cl_2 at 20 °C under N_2 to give **140** in 76 % isolated yield and with 1,3-dimethoxybenzene to give **141** in 57 % isolated yield.

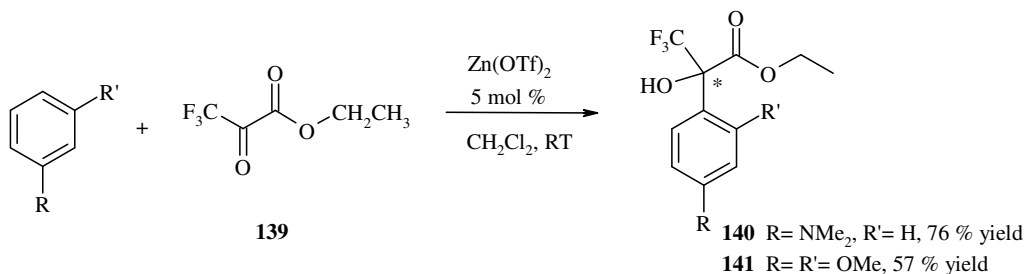


Fig. 2.7 Preparation of **140** and **141** by catalytic Friedel-Crafts reaction

After the success of these experiments more reactive heteroaromatic nucleophiles like indoles and pyrroles were screened. Catalytic Friedel-Crafts reactions were carried out between indole **142** and *N,N*-dimethyl glyoxamide **132** in the presence of a substoichiometric catalytic Lewis acid. The first experiment employed 20 mol% of Cu(OTf)₂ and was run for 32 h at 20 °C in THF. In keeping with the high nucleophilicity of indole the product isolated was found to be that of double addition **143** (Table 2.3). Further experiments carried out over a shorter period of time, and with a ratio of starting materials of 1 to 5 and at 0 °C, still proceeded with formation of product **143**. Formation of the product of monoaddition was not observed.

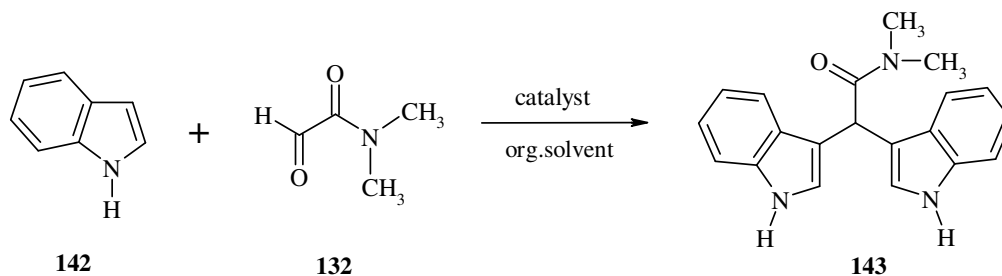


Fig. 2.8 Catalytic Friedel-Crafts reaction of *N,N*-dimethyl glyoxamide **132** with indole **142**

Entry	Catalyst [mol%]	Ratio 142:132	Solvent	Temp. [°C]	Reaction time	Yield [%] 143
1	Cu(OTf) ₂ (20)	1 ^a :2	THF	20	32 h	12
2	Cu(OTf) ₂ (40)	1 ^a :5	CH ₂ Cl ₂	20	10 min.	17
3	Cu(OTf) ₂ (20)	1 ^b :5	THF	0	2 h	14
4	CuCl (20)	1 ^b :5	THF	20	52 h	16
5	Cu(OTf) ₂ (5)	1 ^a :5	CH ₂ Cl ₂	20	10 min.	0

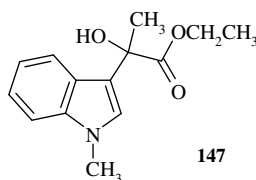
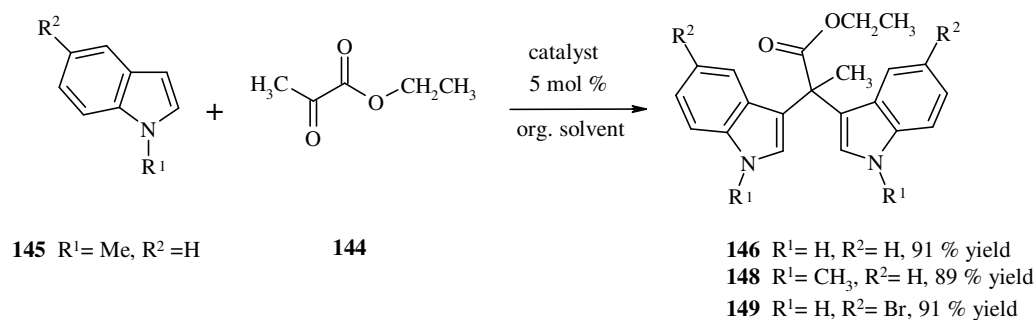
Table 2.3 Results for the catalytic Friedel-Crafts reaction of *N,N*-dimethyl glyoxamide **132** with indole **142** under various reaction conditions

^a 142 added in one portion; ^b 142 added in solution, dropwise

After a series of experiments employing glyoxamide and indole and the unexpected formation of the product of double addition, it was decided to screen the catalytic Friedel-Crafts reaction between indole and ethyl pyruvate under various reaction conditions.

2.3.5 Catalytic Friedel-Crafts reactions of ethyl pyruvate

All reactions presented in Table 2.4 were performed with ethyl pyruvate **144** and *N*-methylindole **145**, however each experiment proceeded with isolation of the product of double addition **146**. For each experiment 5 mol% of catalyst was used and the highest yields were observed when $\text{Zn}(\text{OTf})_2$ and $\text{Cu}(\text{OTf})_2$ were applied. Use of $\text{Sc}(\text{OTf})_3$ gave product **146** in 77 % yield, whereas changing the anion in the scandium Lewis acid resulted in a decrease in yield for ScCl_3 (60 %) and $\text{Sc}(\text{O}^i\text{Pr})_3$ (12 %) with the bulky and electron donating isopropoxy group as a ligand. When CuCl was used it took 96 h for the reaction to reach completion and product **146** was isolated in 78 % yield. However, when ‘harder’ Cu(II) salts were used as the Lewis acid, the reaction was complete after 4 h. Formation of the double addition product was observed even when decreased reaction temperature (-20 °C and 0 °C) and when *N*-methyl indole **145** was added dropwise into the reaction environment. Even under these mild conditions, formation of the mono addition product **147** was not observed. When the relatively weak Lewis acid $\text{Mg}(\text{OTf})_2$ was employed to catalyze the Friedel-Crafts reaction (Entry 10) the formation of any product was not observed and starting materials were recovered.

Fig. 2.9 Friedel-Crafts reaction product of mono addition **147**Fig. 2.10 Catalytic Friedel-Crafts reaction of ethyl pyruvate **144** with indoles

Entry	Ratio 1:2 [mmol]	Catalyst [5 mol%]	Solvent	Temp. [°C]	Reaction time [h]	Yield [%] 146
1	1 : 5	CuCl	CH ₂ Cl ₂	20	76	78
2	1 : 5*	Cu(OTf) ₂	Et ₂ O	20	4	88
3	1 : 5*	CuCl ₂	THF	20	4	83
4	1 : 5*	Zn(OTf) ₂	CH ₂ Cl ₂	0	6	89
5	1 : 5*	Zn(OTf) ₂	CH ₂ Cl ₂	-20	7	66
6	1 : 5*	La(OTf) ₃	CH ₂ Cl ₂	0	6	63
7	1 : 5*	Sc(OTf) ₃	CH ₂ Cl ₂	20	16	77
8	1 : 5	ScCl ₃	CH ₂ Cl ₂	20	14	60
9	1 : 5	Sc(O ^{<i>i</i>} Pr) ₃	CH ₂ Cl ₂	20	48	12
10	1 : 5	Mg(OTf) ₂	THF	20	48	0
11	1 : 5*	Al(OTf) ₃	Et ₂ O	0	7	74

Table 2.4 Results for the catalytic Friedel-Crafts reaction of ethyl pyruvate **144** with *N*-methyl indole **145** under various reaction conditions

* *N*-Methylindole was added dropwise as a solution in the reaction solvent

Products of double addition **148** and **149** were prepared in the presence of 5 mol% of Lewis acid and similarly as in the previous experiments mono addition Friedel-Crafts products were not observed.

2.3.6 Catalytic Friedel-Crafts reaction of ethyl 3,3,3-trifluoropyruvate with indoles

Catalytic Friedel-Crafts reactions between ethyl 3,3,3-trifluoropyruvate **139** and indoles resulted in formation of mono addition Friedel-Crafts products in agreement with the literature⁹⁴. As in previous cases the metal catalyst was pre-dried under high vacuum then freshly distilled solvent and reactants were added and stirred at RT for the duration of the reaction. When CuCl was used to catalyze the reaction, the time required to consume the starting materials was 74 h, whereas with employment of CuCl₂, the reaction was completed after 13 h. In this set of experiments the Friedel-Crafts mono adduct **150** was isolated and formation of the double addition product

was not observed. In two cases (entry 4 and 8) when $\text{Al}(\text{OTf})_3$ and SnCl_4 were employed the formation of neither products occurred.

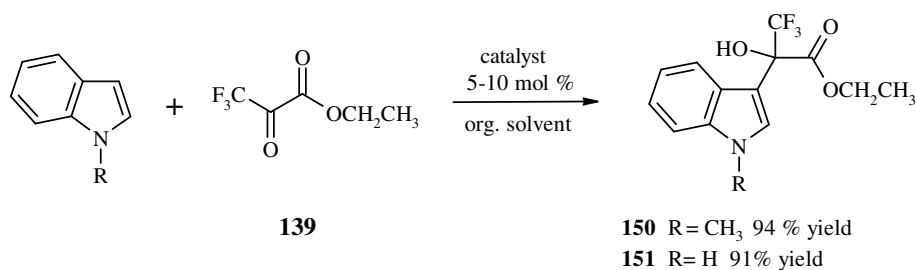


Fig. 2.11 Catalytic Friedel-Crafts reaction of ethyl 3,3,3-trifluoropyruvate **139** with indoles

Entry	Catalyst	Catalyst [mol%]	Ratio 1:2	Solvent	Temp. [°C]	Time [h]	Yield [%] 150
1	CuCl	10	1:2	CH ₂ Cl ₂	20	74	94%
2	CuCl ₂	10	1:2	CH ₂ Cl ₂	20	13	91%
3	Zn(OTf) ₂	5	1:2	CH ₂ Cl ₂	20	13	93%
4	Al(OTf) ₃	5	1:2	CH ₂ Cl ₂	20	12	0
5	La(OTf) ₃	5	1:1	CH ₂ Cl ₂	20	13	91%
6	Sc(OTf) ₃	5	1:1	CH ₂ Cl ₂	20	12	64%
7	SnCl ₂	10	1:1	CH ₂ Cl ₂	20	12	93%
8	SnCl ₄	10	1:1	CH ₂ Cl ₂	20	12	0

Table 2.5 Results for the catalytic Friedel-Crafts reaction of ethyl 3,3,3-trifluoropyruvate **139** with *N*-methylindole **145** under various reaction conditions

Compound **151** was synthesised in the presence of 5 mol% of $\text{Cu}(\text{OTf})_2$ from indole and was isolated in 91 % yield.

2.3.7 Friedel-Crafts reaction of glyoxamides in aqueous solution

Since catalytic Friedel-Crafts reaction between *N,N*-dimethyl glyoxamide **132** and indole **142** proceeded with formation of the Friedel-Crafts double adduct **143** it was decided to perform the reaction in the absence of a Lewis acid and in aqueous solution¹²⁴. Reactions between glyoxamide and indole were carried out in both sat. NaHCO_3 and 1M NaCl solutions (Table 2.6) and an excess of glyoxamide was used.

Reactions were stirred for 16 h at RT and in both cases the isolated product **143** was that of double addition.

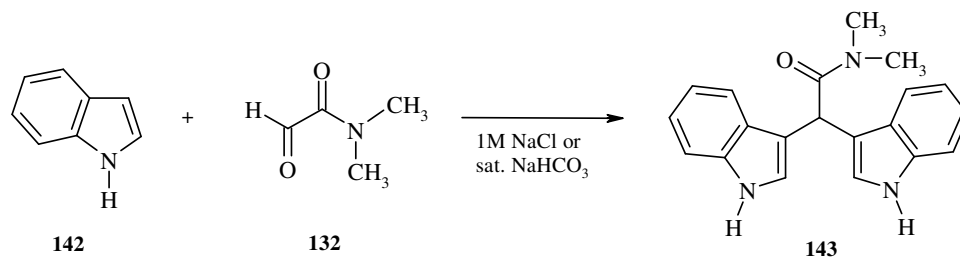


Fig. 2.12 Friedel-Crafts reaction of *N,N*-dimethyl glyoxamide **132** with indole **142**

Entry	Catalyst [mol %]	Ratio 1:2	Solvent	Temp. [°C]	Reaction time	Yield [%] 143
1	no catalyst	1:4	sat. NaHCO ₃	RT	16 h	79
2	no catalyst	1:4	1M NaCl	RT	16 h	86

Table 2.6 Results for the Friedel-Crafts reaction of *N,N*-dimethyl glyoxamide **132** with indole **142** in water solution

The Friedel-Crafts reaction in aqueous solution between *N*-methyl pyrrole **152** and *N,N*-dimethyl glyoxamide **132** proceeded with the formation of the mono-adduct **153** in both saturated NaHCO₃ and 1M NaCl. These results are surprising especially because an excess of glyoxamide was not used. The ratio of aromatic nucleophiles to glyoxamide was 1:1 and mono addition product was isolated by column chromatography in 81 and 86 % yield respectively.

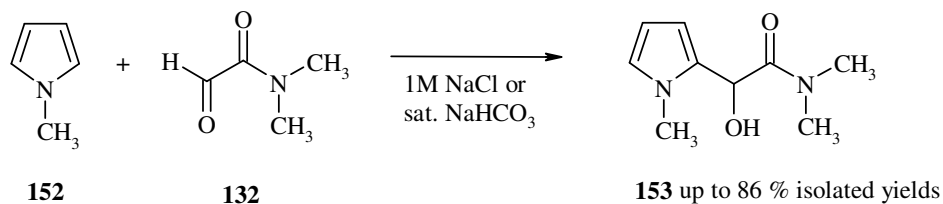


Fig. 2.13 Friedel-Crafts reaction of *N,N*-dimethyl glyoxamide **132** with *N*-methyl pyrrole **152**

Entry	Catalyst [mol %]	Ratio 1:2	Solvent	Temp. [°C]	Reaction time	Yield [%] 153
1	no catalyst	1:1	sat. NaHCO ₃	RT	16 h	81
2	no catalyst	1:1	1M NaCl	RT	16 h	86
3	Cu(OTf) ₂ (15)	1:1	CH ₂ Cl ₂	0	2 h	0
4	Zn(OTf) ₂ (50)	1:1	CH ₂ Cl ₂	RT	36 h	0

Table 2.7 Results for the Friedel-Crafts reaction of *N*-methyl pyrrole **152** with *N,N*-dimethyl glyoxamide **132**

In contrast catalytic Friedel-Crafts experiments carried between **152** and **132** in the presence of Cu(OTf)₂ and Zn(OTf)₂ in organic solvent did not proceed with formation of **153** (Table 2.7). Instead *N*-methyl pyrrole and *N,N*-dimethyl glyoxamide in a polymeric form were recovered.

Similar results were observed for Friedel-Crafts experiments carried out in water and in organic solvents in the presence of a catalyst for 2-oxo-2-(pyrrolidin-1-yl)acetaldehyde **134** and *N*-methyl pyrrole **152**. In the first case the Friedel-Crafts monoadduct product **154** was isolated in 92 and 94 % yield respectively, whereas the catalytic Friedel-Crafts did not take place in CH₂Cl₂ and only starting material was recovered.

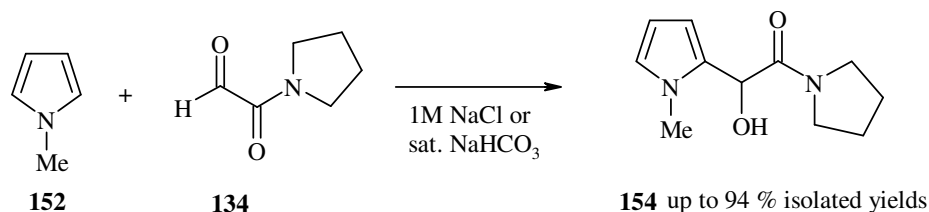


Fig. 2.14 Friedel-Crafts reaction of 2-oxo-2-(pyrrolidin-1-yl)acetaldehyde **134** with *N*-methyl pyrrole **152**

Entry	Catalyst [mol %]	Ratio 1:2	Solvent	Temp. [°C]	Reaction time [h]	Yield [%] 154
1	no catalyst	1:1	sat. NaHCO ₃	RT	16	94
2	no catalyst	1:1	1M NaCl	RT	16	92
3	Zn(OTf) ₂ (15)	1:1	CH ₂ Cl ₂	0	2	0
4	Cu(OTf) ₂ (50)	1:1	CH ₂ Cl ₂	RT	36	0

Table 2.8 Results for the Friedel-Crafts reaction of 2-oxo-2-(pyrrolidin-1-yl)acetaldehyde **134** with *N*-methyl pyrrole **152**

2.3.8 Catalytic Friedel-Crafts reaction in ionic liquids

Since ionic liquids have been reported to be good solvents for Friedel-Crafts chemistry¹²⁵, a series of catalytic Friedel-Crafts experiments using 1-butyl-3-methylimidazolium tetrafluoroborate (BMIMBF₄) and 1-butyl-2,3-dimethylimidazolium tetrafluoroborate (BDMIMBF₄) were performed. First, reactions between commercially available phenylglyoxal monohydrate **155** and *N,N*-dimethylaniline **104** in the presence of 10 mol% of Zn(OTf)₂ were carried out at 40 °C and 60 °C since these two particular ionic liquids required an increased temperature to reduce their viscosity. After stirring for 16 h, the double adduct **156** was isolated by column chromatography in 91 % and 93 % yield, respectively. To evaluate the effect of the solvent, an analogous experiment was performed in CH₂Cl₂, however after 3 days at RT the reaction did not reach completion (monitoring by TLC) and product **156** was isolated in 74 % yield.

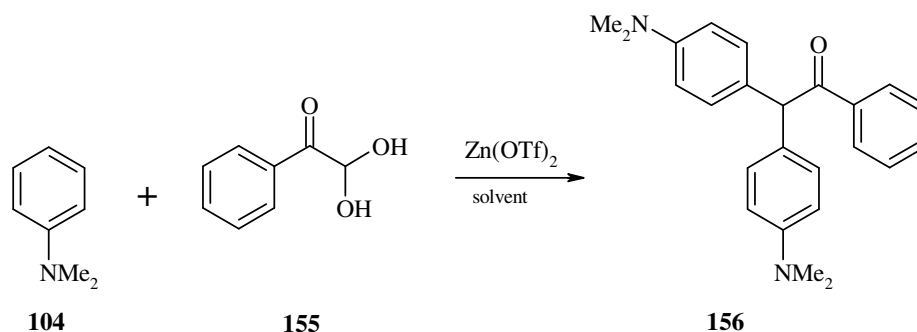


Fig. 2.15 Catalytic Friedel-Crafts reaction of phenylglyoxal monohydrate **155** with *N,N*-dimethylaniline **104**

Exp. no	Catalyst	Catalyst [mol%]	Ratio 1:2	Solvent	Time [h]	Temp. [°C]	Yield [%] 156
1	Zn(OTf) ₂	10	1:4	BMIMBF ₄	16	40	93
2	Zn(OTf) ₂	10	1:4	BDMIMBF ₄	16	60	91
3	Zn(OTf) ₂	10	1:4	CH ₂ Cl ₂	78	RT	74

Table 2.9 Results for the catalytic Friedel-Crafts reaction of phenylglyoxal monohydrate **155** with *N,N*-dimethylaniline **104** under various reaction conditions

Three Friedel-Crafts experiments employing 2-oxo-2-(pyrrolidin-1-yl)acetaldehyde **134** and aromatic nucleophiles were carried out in the presence of $\text{Zn}(\text{OTf})_2$ in BMIMBF_4 at 40 °C. However, with the glyoxamide none of the Friedel-Crafts reactions in ILs gave the desired product.

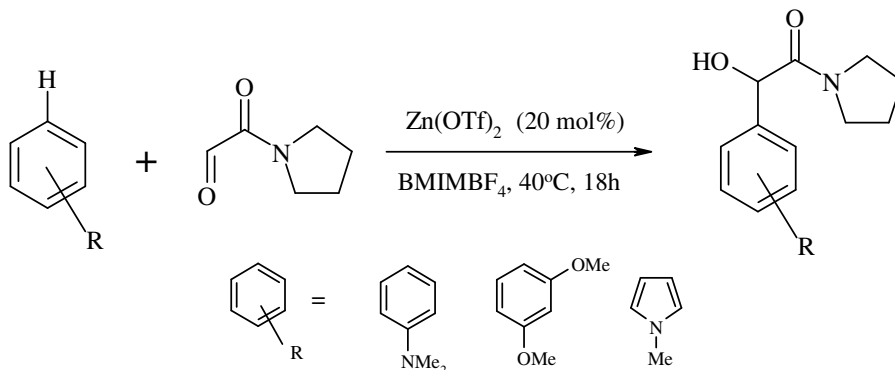


Fig. 2.16 Catalytic Friedel-Crafts reaction of 2-oxo-2-(pyrrolidin-1-yl)acetaldehyde **134** with aromatic compounds

Ionic liquids exhibit the ability to dissolve both metal catalysts and organic reagents which in some cases may increase the activity of the catalyst. Also with this reaction we have demonstrated the feasibility of metal triflates as Lewis acids for Friedel-Crafts acylations in an imidazolium ionic liquid. It was intended that the use of an IL as a solvent for the catalytic Friedel-Crafts reaction might facilitate the reaction between glyoxamide and aromatic nucleophiles. These reactions proved to work more efficiently when $\text{Zn}(\text{OTf})_2$ was used as a catalyst in the IL than when the reaction was performed in a conventional organic solvent (74 %). Nevertheless, the double addition product was the only one isolated despite the fact that an excess of glyoxylate was used.

2.4 Conclusion

Friedel-Crafts chemistry between glyoxamides and aromatic nucleophiles in the presence of a Lewis acid catalyst proved to be more difficult than with α -keto esters and glyoxylate esters. In the case of ethyl 3,3,3-trifluoropyruvate a series of Friedel-Crafts reactions using either *N,N*-dimethylaniline or 1,3-dimethoxybenzene succeeded, giving Friedel-Crafts products in very good yields. Similarly, catalytic Friedel-Crafts reactions with indoles were effective, and gave products of mono or double addition, depending on which carbonyl compound was used as the electrophile. Ethyl 3,3,3-trifluoropyruvate **144** underwent catalytic Friedel-Crafts reaction with indoles to form only the product of mono addition, using a Lewis acid catalyst, whereas experiments with ethyl pyruvate afforded only the double adduct. The difference in reactivity between ethyl pyruvate and ethyl 3,3,3-trifluoropyruvate with indoles is due to the presence of three electronegative fluorine atoms which destabilize the cation **157** required for further reaction giving double addition (Fig. 2.17). The opposite situation takes place for the Friedel-Crafts reaction with ethyl pyruvate where cation **158** is further stabilized by an electron-donating methyl group and undergoes further electrophilic substitution with indole.

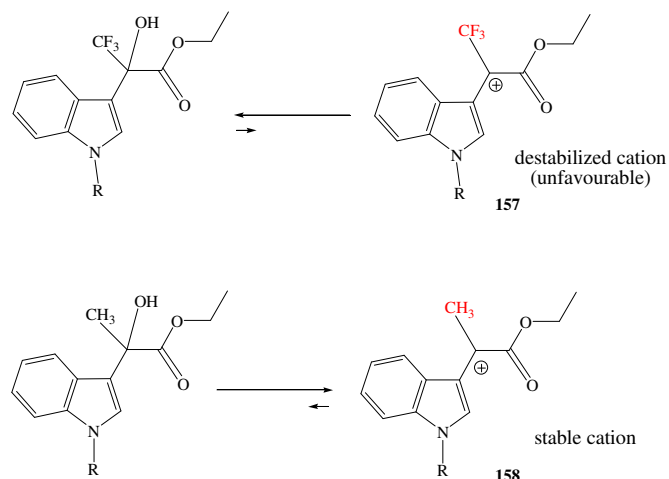


Fig. 2.17 Intermediate cations **157** and **158**

Catalytic F-C reactions between ethyl glyoxylate and aromatic nucleophiles proved to work effectively, despite the fact that ethyl glyoxylate was used as a crude mixture after periodic oxidation of ethyl-L-tartrate. In contrast, glyoxamides exhibit lack of reactivity in the catalytic Friedel-Crafts reaction with substituted benzene rings. However, catalytic Friedel-Crafts reactions between *N,N*-dimethylglyoxamide with an electron rich heteroaromatic indole ring proceeded with formation of the double adduct **143** with yields ranging from 12 to 17 %. Friedel-Crafts reactions between glyoxamides and both indoles and pyrroles in aqueous solution proceeded with preparation of the double adduct **143** with indole in 86 % yield and mono adducts **153** and **154** for *N*-methyl pyrrole (81 to 94 % yield). These reactions occurred in water which suggests that in this case it was not the aldehyde but the hemiacetal form which was the reactive one. Furthermore, catalytic Friedel-Crafts reactions between phenyl glyoxylate monohydrate and *N,N*-dimethylaniline nucleophiles proved to work in ILs and in CH₂Cl₂ to give the double addition product **156** in high yields (74-93 %). It may be speculated (concluded) that the success of these experiments may depend on the form of the carbonylic compound and suggests the more reactive one may be the hydrated form of glyoxyaldehyde.

For catalytic Friedel-Crafts of glyoxamides considerable effort was expended on purifying the glyoxamides. Attempts to purify the glyoxamides were undertaken by vacuum distillation from toluene, Kugelrohr distillation and sublimation. However, none of these attempts allowed for satisfactory purification of the glyoxamides. After each catalytic Friedel-Crafts experiment employing 2-oxo-2-(pyrrolidin-1-yl)acetaldehyde **134** white solid was collected and identified as a compound **136**.

This dimeric hemiacetal (see experimental, page 198 ¹H NMR in CDCl₃ and D₂O) formed as a result of a reaction between the hydrate and either a second molecule of hydrate or glyoxamide. At this stage it should be emphasized that dimer **136** can exist as a cyclic trimer **136a**. Analogically to formaldehyde which trimeric form **136b** was found to be more stable and easily handled source of anhydrous formaldehyde. Therefore, appearance of **136** requires further investigation.

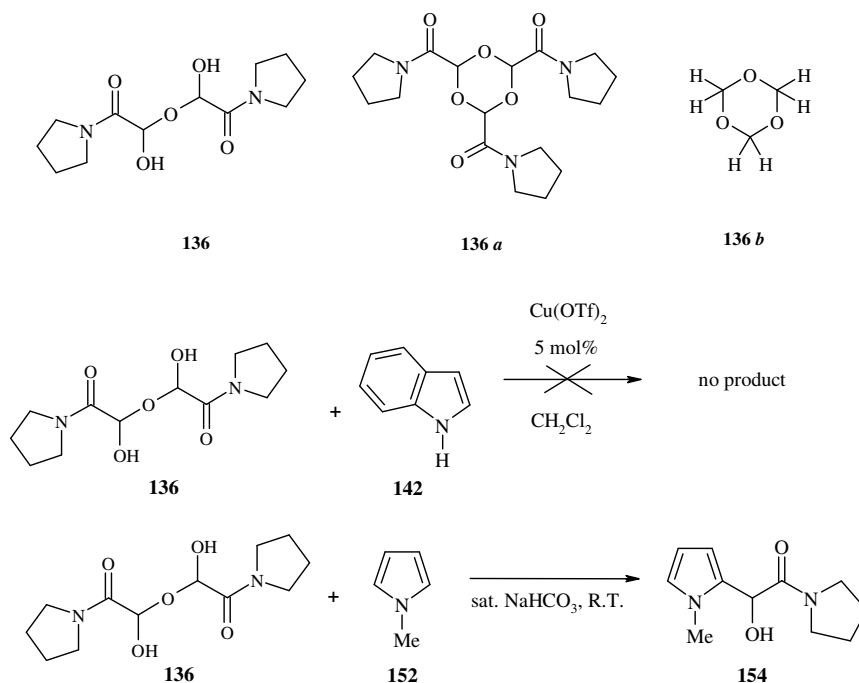


Fig. 2.18 Dimeric **136** and trimeric **136a** form of 2-oxo-2-(pyrrolidin-1-yl)acetaldehyde and 1,3,5-trioxane **136b** trimeric form of formaldehyde and reaction schemes between **136** and heterocycles

The dimeric form of 2-oxo-2-(pyrrolidin-1-yl)acetaldehyde, **136** was then reacted in a catalytic Friedel-Crafts reaction with indole, however without further success. Whereas, when **136** was introduced into the aqueous solution and reacted with *N*-methyl pyrrole, the formation of the mono adduct was observed by analysis of the ^1H NMR of the crude.

An important achievement was the successful preparation of Friedel-Crafts products using more environmentally-friendly, aqueous conditions. It has been demonstrated that the Friedel-Crafts reaction of glyoxamides with heteroaromatic compounds in water can proceed smoothly without the use of traditional Lewis acid catalysis. The reactions proceeded well for indole, however only the double addition adduct was obtained. For pyrroles the mono adduct from electrophilic substitution by glyoxamides at the 2-position was observed as the only product. The results show that the $\text{NaHCO}_3\text{-H}_2\text{O}$ and $\text{NaCl-H}_2\text{O}$ solutions have unique properties for the Friedel-Crafts reaction which results in formation of Friedel-Crafts adducts in high yields. However, at the present stage of this investigation we do not have sufficient mechanistic details to account for the role of the solvent composition in the selectivity of the reaction.

3 Model Macrocycles and their Precursors

In our research we investigated two possible routes for the preparation of macrocyclic model systems. The first synthetic route was a two pot synthesis in which phenoxy-linked open structures undergo ring-closure to the macrocycle *via* an aliphatic linker in the presence of a templating agent and under high dilution conditions. The second synthetic route investigated was a one-pot synthesis, which provided a rapid and straightforward method to perform the sequence, however optimization of reaction conditions may be time consuming.

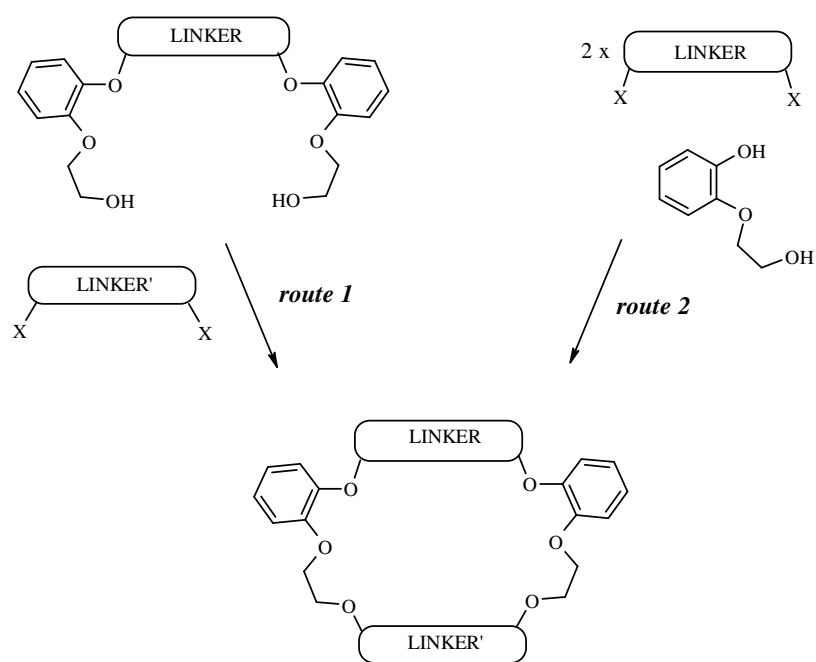


Fig. 3.1 Two different routes for preparation of macrocycles

The macrocyclization process can be promoted either by suppressing the intermolecular reaction (resulting in polymerization) or facilitating the intramolecular one. We chose to combine these approaches by suppressing competing reactions, *via* the use of moderate to high dilution conditions, while promoting cyclization *via* the template effect.

The classical method commonly known as macrocyclization was developed during Ziegler's studies in the 1930s¹²⁶. This method employs an approach based upon the

high dilution technique, and under these conditions the probability of intermolecular reactions between the reacting partners, leading to formation of oligomers is radically decreased. An intramolecular reaction does not require interactions between molecules, so consequently high dilution does not affect the efficiency of cyclization. This method is essentially universal and for the past 70 years numerous compounds with medium to large rings have been synthesised in this way¹²⁷. The technical inconvenience of this method is that even a small amount of product requires large volumes of solvent which is also undesirable from an environmental point of view. A fairly different approach enhancing the probability of the intramolecular pathway emerged with the discovery of crown ethers as a new class of complexing agents. Pedersen's pioneering experiments in this area revealed an unusual phenomenon when 18-membered polyether was formed in high yields by the condensation of two moles of catechol with two moles of 2-chloroethyl ether (Fig. 3.2).

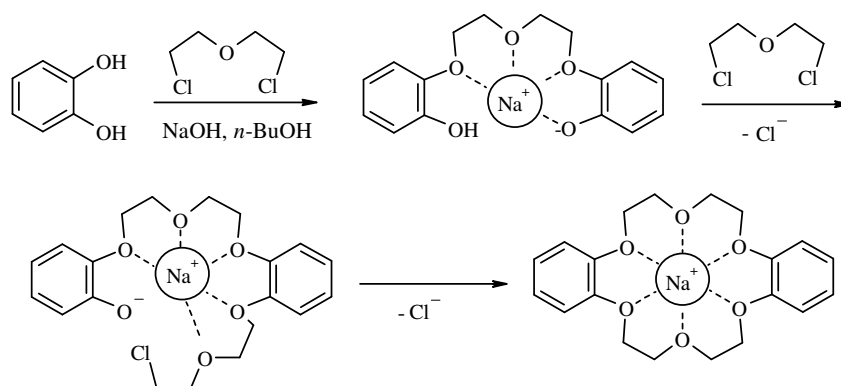


Fig. 3.2 Synthesis of dibenzo-18-crown-6 in the presence of templating agent

The result was truly remarkable as, in this case, the macrocyclization proceeded efficiently without high-dilution conditions. In fact, up to one mole of the product (360 g) was prepared in a volume of just 5 litre of solvent. The striking efficiency of this reaction was correctly ascribed to the forced proximity of the reacting centres induced from the template effect of the sodium ion during the cyclization step. It was suggested that, owing to the coordination effect of the metal ion, the cyclization precursor is formed with a set of donor sites (six ether oxygens) wrapped around a central ion. This pseudo cyclic conformation is ideal for the geometry of the transition state required for the closure of the 18-membered ring and hence formation

of the macrocycle is greatly facilitated. The same reaction performed in the presence of lithium or ammonium bases invariably led to the formation of linear oligomers. Further studies documented the universal validity of using multisite binding and an entry into new areas of organic chemistry was opened.

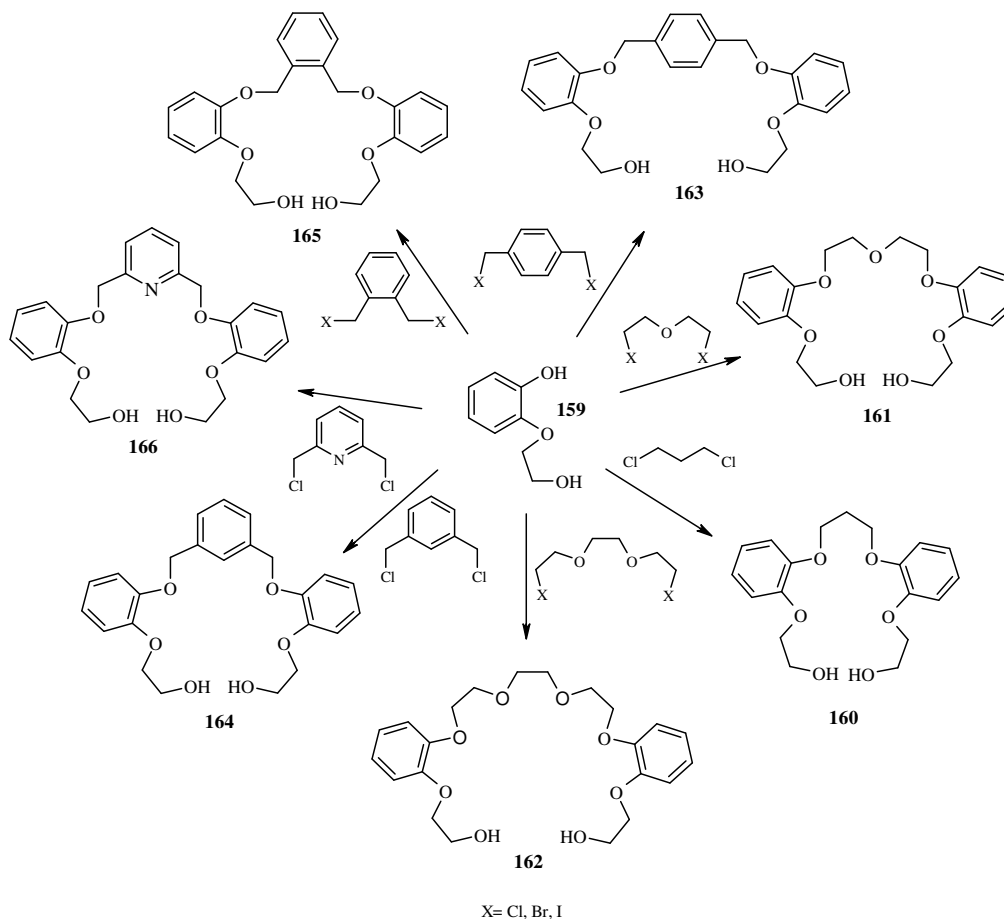
The two methods for macrocycle formation

- 1) by two step synthesis from phenoxy-linked macrocyclic precursors (**160-166**);
 - 2) by one pot approach from 2-(2-hydroxyethoxy)phenol,
- are now presented.

3.1 Preparation of phenoxy-linked open structures

Phenoxy linked open structures **160-166** were synthesised by reacting 2-(2-hydroxyethoxy)-phenol **159** with the corresponding alkyl halides, according to Fig. 3.3.

Seven novel model macrocyclic precursors have been synthesised by the alkylation of commercially available 2-(2-hydroxyethoxy)-phenol **159** with the corresponding alkyl chlorides, bromides or iodides in the presence of K_2CO_3 in DMF. These reactions occurred in moderately to high yields varying from 54 % for **160** to 92 % yield for **166**.


Fig. 3.3 Synthesis of phenoxy-linked open structures

Reaction conditions: Na_2CO_3 or K_2CO_3 , DMF, 120 °C, 7h;

For all the experiments where alkyl chlorides were employed for alkylation of the diol **159** the isolated yields of the products were higher. Whereas the experiments employing alkyl bromides or in the case of **162** an alkyl iodide, open structures have been isolated in slightly lower yields (Table 3.1)

Compound	160	161	162	163	164	165	166
	Isolated yields [%]						
Alkyl chloride	54	86	81	88	91	78	92
Alkyl bromide	-	68	-	77	71	76	-
Alkyl iodide	-	-	54	-	-	-	-

Table 3.1 Isolated yields for phenoxy-linked open structures **160-166**

All the compounds prepared have been characterized by ^1H and ^{13}C NMR and their exact masses have been confirmed by HRMS. The macrocyclic precursors have been used in the next step, for the preparation of macrocyclic structures. Ring closure reactions have been achieved by introduction of alkyl bromides or chlorides into the open structures using high dilution techniques.

3.2 Preparation of macrocycles from their phenoxy-linked precursors

The two-pot synthesis was carried out using phenoxy-linked macrocyclic precursors that were reacted with the corresponding alkyl dichloride, dibromide or diiodide according to the general scheme on Fig. 3.4. Using this approach eighteen novel model macrocyclic structures have been successfully synthesized and isolated.

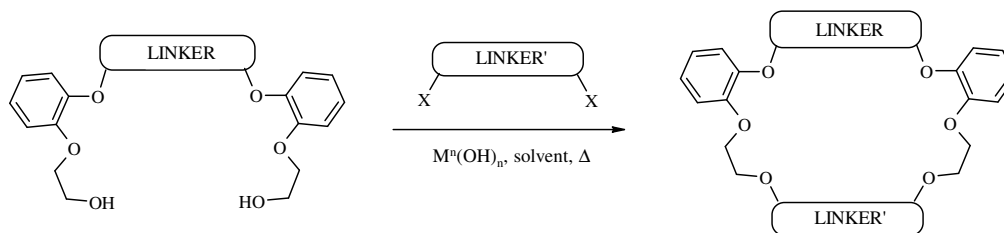


Fig. 3.4 Synthesis of macrocycles from phenoxy-linked precursor

Efforts towards the synthesis of model macrocycles commenced with a series of unsuccessful ring closure experiments using alkyl chlorides and alkyl bromides under mild reaction conditions. Therefore acyl chlorides which are more reactive towards alcohol groups under mild reaction conditions were investigated as alternative linkers. In each case the reaction was carried out in boiling dichloromethane in the presence of K_2CO_3 . The number of equivalents of base used in each reaction was not less than 8 for each phenoxy-linked open structure. Satisfactory results gave us crucial information about the quantity of base required for successful ring closure reactions with the phenoxy-linked macrocyclic precursors. Reaction progress was monitored by TLC and when the reaction was complete it was quenched with water, followed by a standard basic workup. Macrocycles **167** and **168** were isolated in 31 % and 26 % yields respectively.

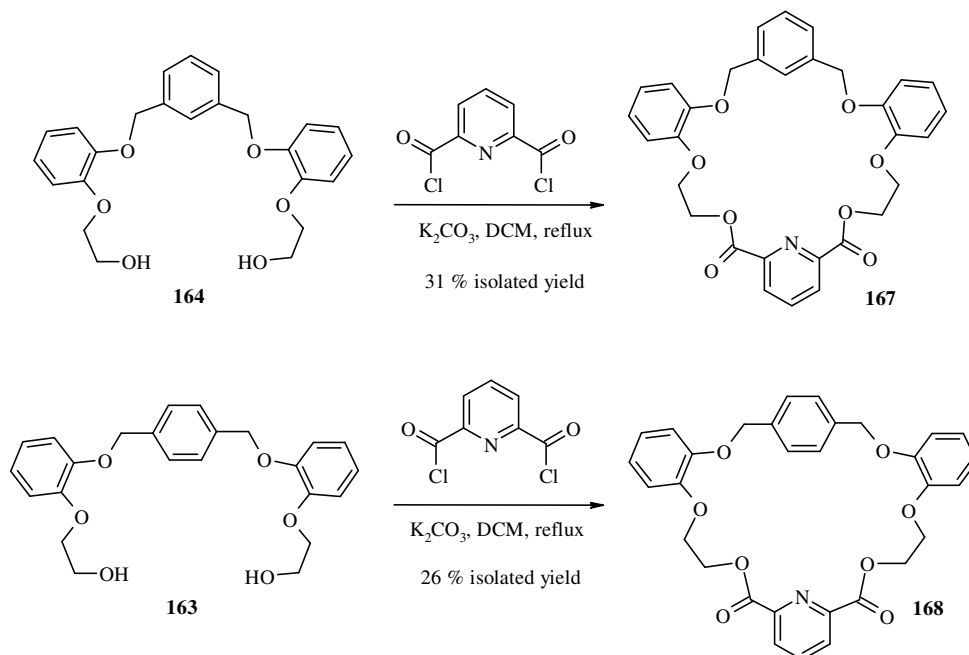


Fig. 3.5 Macrocyclization of macrocyclic precursors **163** and **164** with 2,6-pyridine dicarbonyl dichloride

Based on these promising results new macrocyclic model systems containing both aromatic and aliphatic ether chains were synthesized from 1,5-bis[2-(2-hydroxyethoxy)phenoxy]-3-oxapentane **161** on a 1 mmol scale in 100 mL of 1,4-dioxane. Macrocycle **169** in the Fig. 3.6 was synthesized using 8 mmol of KOH as a base in refluxing solvent with the addition of potassium iodide. The presence of the iodide salt in the reaction environment improved reaction yields by nucleophilic displacement of the Cl with KI to give alkyl iodide, known as a Finkelstein reaction^{128,129}. Presence of 10 mol% of KI in the ring closure reaction environment to synthesise **169** improved conversion by 15% (a 40 % and b 55 %). Preparation of macrocycle **170** with addition of KI into the reaction proceeded with 50% conversion (d), whereas reaction carried out without KI gave 40% conversion (c) (Fig. 3.6). Similar results were obtained for preparation of **171**, without KI the reaction proceed with a conversion of 35% (e) while addition of NaI increased conversion to 45% (f), Fig. 3.6. All three macrocycles were purified by column chromatography on silica gel, using chloroform/ethyl acetate mixtures as the eluent. Surprisingly isolated yields were not as high as was expected. However, the moderate yields may be due to the presence of ethylene oxide chains in each of the compounds that render them

difficult to remove from silica gel. Isolated yields were 32 %, 29 % and 26 %, respectively.

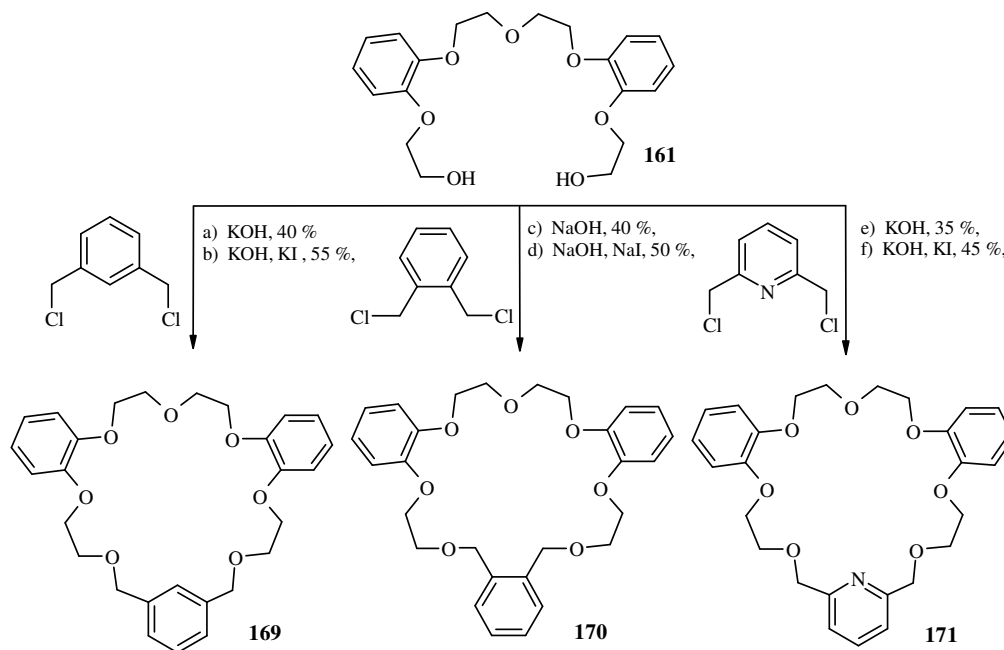


Fig. 3.6 Synthesis of macrocycles **169-171** with 1,5-bis[2-(2-hydroxyethoxy)phenoxy]-3-oxapentane unit **161**

Reaction conditions: a) KOH, 1,4-dioxane, reflux; b) a, KI; c) NaOH, 1,4-dioxane, reflux; d) c, NaI; e) KOH, 1,4-dioxane, reflux; f) e, KI;

The results presented in Fig. 3.6 encouraged us to optimise the reaction conditions in order to maximize yields. A limited study at optimization reactions was carried out on example **169** to determine the most favourable reaction conditions, considering such factors as number of moles of base, additives (NaI, KI), choice of solvent and solvent volume. Various bases (*e.g.* NaH, NaOH, KH, KOH, CsOH and Ba(OH)₂) in different solvents (*e.g.* DMF, THF, 1,4-dioxane) were screened (Table 3.2).

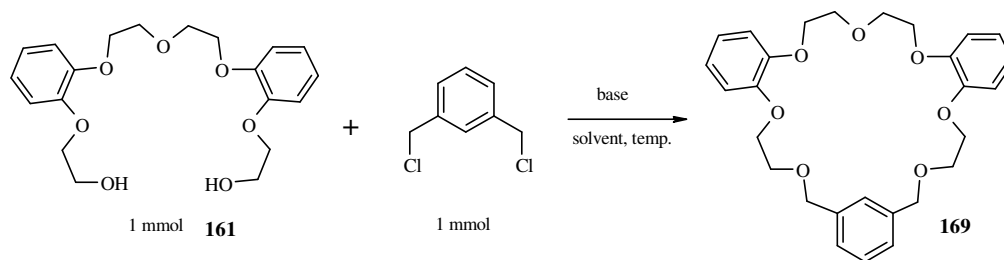


Fig. 3.7 Reaction scheme for preparation of **169**

Entry	Base	Base [mmol]	Additives	Solvent	Temp [°C]	Time [h]	Conv [%]
1	NaOH	10	-	THF	66	46	28
2	NaOH	10	NaI	THF	66	46	30
3	NaOH	10	-	1,4-D ^a	101	46	35
4	NaOH	10	NaI	1,4-D ^a	101	46	38
5	KOH	10	-	THF	66	46	44
6	KOH	10	KI	THF	66	46	50
7	KOH	10	-	1,4-D ^a	101	46	50
8	KOH	10	KI	1,4-D ^a	101	46	60
9	KOH	4	KI	1,4-D ^a	101	46	0
10	KOH	6	KI	1,4-D ^a	101	46	35
11	KOH	8	KI	1,4-D ^a	101	46	55
12	KOH	12	KI	1,4-D ^a	101	46	70
13	KOH	16	KI	1,4-D ^a	101	46	60
14	KOH	20	KI	1,4-D ^a	101	46	60
15	LiOH	12	-	1,4-D ^a	101	46	0
16	CsOH	12	-	1,4-D ^a	101	46	40
17	Ba(OH) ₂	12	-	1,4-D ^a	101	46	0
18	NaH	10	-	THF	0-R.T.	6/18	25
19	KH	10	-	THF	0-R.T.	6/18	30

Table 3.2 Various reaction conditions for preparation of macrocycle **169**. ^a1,4-D; 1,4 Dioxane

This series of experiments proved that the optimal number of moles of base required to effect ring closure varies from 8-12 mmoles (8-12 eq), with the preferred base being sodium or potassium hydroxide in THF or 1,4-dioxane. Experiments carried

out using less than 6 mmol base did not lead to macrocyclization. Also the solvent studies focused on THF and 1,4-dioxane rather than DMF in order to facilitate purification. These experiments also demonstrated that in general, if THF is replaced by a higher-boiling solvent such as 1,4-dioxane conversion of starting materials tends to increase. As presented in Table 3.2 synthesis of **169** was performed under various reaction conditions, with the most efficient ring closure taking place using not less than 10 mmol of KOH and 0.1 mmol of KI in refluxing 1,4-dioxane (entries 8,12). The optimal molar ratio of base to substrate was 12 for the highest conversion, in the presence of an iodide salt. Sodium hydroxide was also effective in promoting alkylation of the primary alcohol, with subsequent macrocyclization. Again maximum product formation was observed in experiments carried out in a solvent with a higher boiling point and in the presence of an iodide salt. Experiments employing hydroxides with small cationic radius *e.g.* LiOH and relatively big cationic radius, such as Ba(OH)₂ gave poor results. In the first case a trace amount of product was observed, whereas formation of the product in the second case was negligible. In addition, the effect of stronger bases *e.g.* sodium and potassium hydrides on the macrocyclization was investigated. Reactions were stirred at 0 °C in THF for 6 h then at room temperature overnight. Considering the hazardous properties of alkali metal hydrides, as well as the unimpressive reaction yield, the use of these bases was not pursued further in our research.

A limited study to establish the optimum quantity of solvent for the macrocyclization reaction was also investigated as an important issue to conclude whether it is the template effect or high dilution that benefits the reaction most. Experiments were carried out with varying amounts of 1,4-dioxane together with 10 mmol of both potassium hydroxide and 0.1 mmol of potassium iodide (Table 3.3).

Entry	Base	Base [mmol]	Additives (0.1mmol)	Solvent	Solvent [mL]	Conv [%]
1	KOH	10	KI	1,4-D	8	trace
2	KOH	10	KI	1,4-D	20	44
3	KOH	10	KI	1,4-D	40	62
4	KOH	10	KI	1,4-D	60	70
5	KOH	10	KI	1,4-D	80	72
6	KOH	10	KI	1,4-D	100	74
7	KOH	10	KI	1,4-D	120	77
8	KOH	10	KI	1,4-D	150	65
9	KOH	10	KI	1,4-D	200	63
10	KOH	10	KI	1,4-D	250	68

Table 3.3 Solvent effect on preparation of macrocycle **169**. ^a1,4-D; 1,4 Dioxane

The experiments in Table 3.3 show that the optimal range for the volume of solvent varies between 60 mL and 120 mL (entry 4-7). This suggests the importance of the template effect, which appears to play a key role in the macrocyclization step. Previous experiments (Table 3.2) show that the use of bases with lithium or sodium counter cations proceeded with lower reaction conversions compared with reactions carried out in the presence of potassium bases. This is most likely due to the fact that the cations with a smaller radius than potassium cannot fit effectively to template the macrocycle for efficient ring closure. Instead oligomeric products are formed. In Fig. 3.8 the two possibilities of behaviour for the macrocyclic precursor, either in the presence or absence of a potassium cation templating agent. The first path depicts the open structure encircling the templating agent. This shape is the consequence of interactions between the metal cation and oxygen-donor atoms. In the absence of a templating agent, the second route is followed in which **161** adopts a linear conformation and in that shape oligomeric products are more likely to be formed.

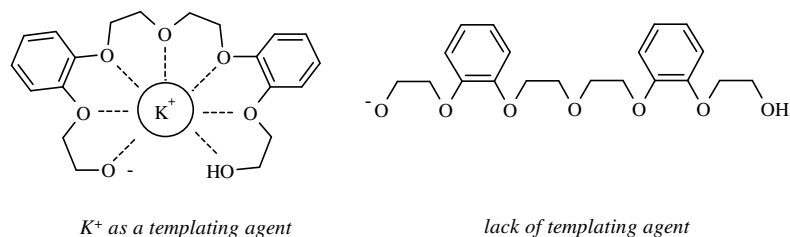


Fig. 3.8 Macrocyclic precursor **161** in the presence and absence of the template

A series of macrocyclic compounds starting from the precursor **162**, 1,8-bis[2-(2-hydroxyethoxy)phenoxy]-3,6-dioxaoctane have been synthesised according to optimized reaction conditions. As shown in Fig. 3.9, for each reaction, potassium hydroxide (12 mmol) and potassium iodide (0.1 mmol) in moderate dilution (80 mL per 1 mmol) were used to synthesise the macrocycles in isolated yields between 38-51 %.

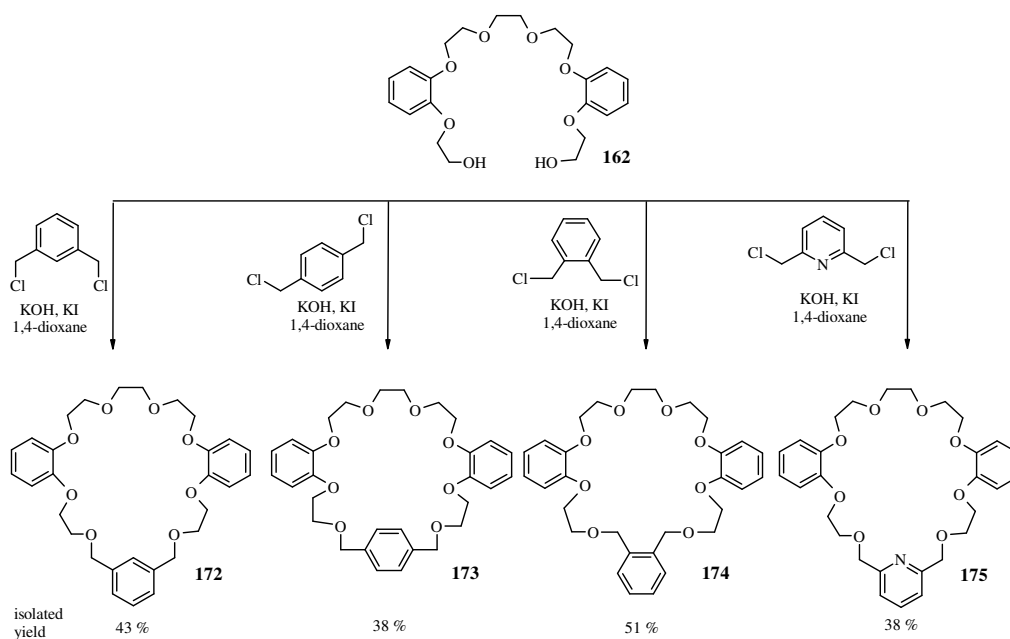


Fig. 3.9 Synthesis of macrocycles from 1,8-bis[2-(2-hydroxyethoxy)phenoxy]-3,6-dioxaoctane **162**

Synthesis of the macrocycles **176**, **177** and **178**, starting from 1,3-bis[2-(2-hydroxyethoxy)phenoxy]-*m*-xylene precursor **164** were carried out as in previous cases on a 1 mmol scale, employing 12 mmol of metal hydroxide under dilute

conditions using 80 mL of 1,4-dioxane (Fig. 3.10) First the macrocyclic precursor was stirred for 1 hour in the presence of the base at 60 °C before addition of the corresponding alkyl dichloride. Macrocyclic precursor **164** was first synthesized in the presence of sodium hydroxide because the introduced *ortho*-xylene unit is “shorter” than the *meta* and *para* isomers and the macrocyclic precursor might better accommodate the smaller sodium cation. However, this was not observed as the subsequent reaction with potassium hydroxide gave a higher conversion (60 %) compared with sodium hydroxide (45 %).

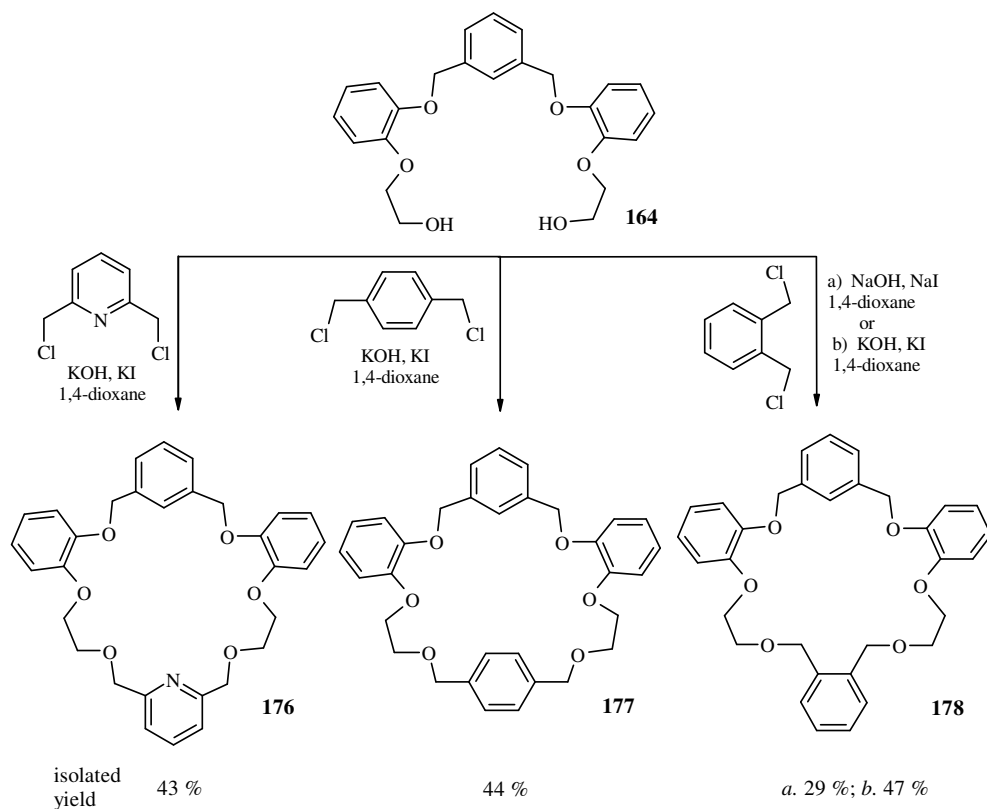


Fig. 3.10 Synthesis of macrocycles **176-178**

All of the macrocycles were purified by column chromatography on silica gel using chloroform as the mobile phase for **177** and **178** and the more polar mobile phase of chloroform and ethyl acetate (3:1) for **176**. Moreover, macrocycle **176** required further recrystallization from $\text{CH}_2\text{Cl}_2/\text{MeOH}$ (5:1) so the final isolated yield of pure compound was 43 % whereas compound **177** was isolated in 44% yield. Macrocycle **178** was isolated in 29 % and 47 % yield, respectively.

Macrocycles prepared from precursor **163** and corresponding α,α' -dichloro-xylenes were synthesized efficiently in the presence of potassium hydroxide and its iodide salt in refluxing 1,4-dioxane (Fig. 3.11). Compounds **179** and **181** were isolated in good yields of 43 % and 48 %, whereas purification of product **182** yielded pure macrocycle in a mere 5 % yield.

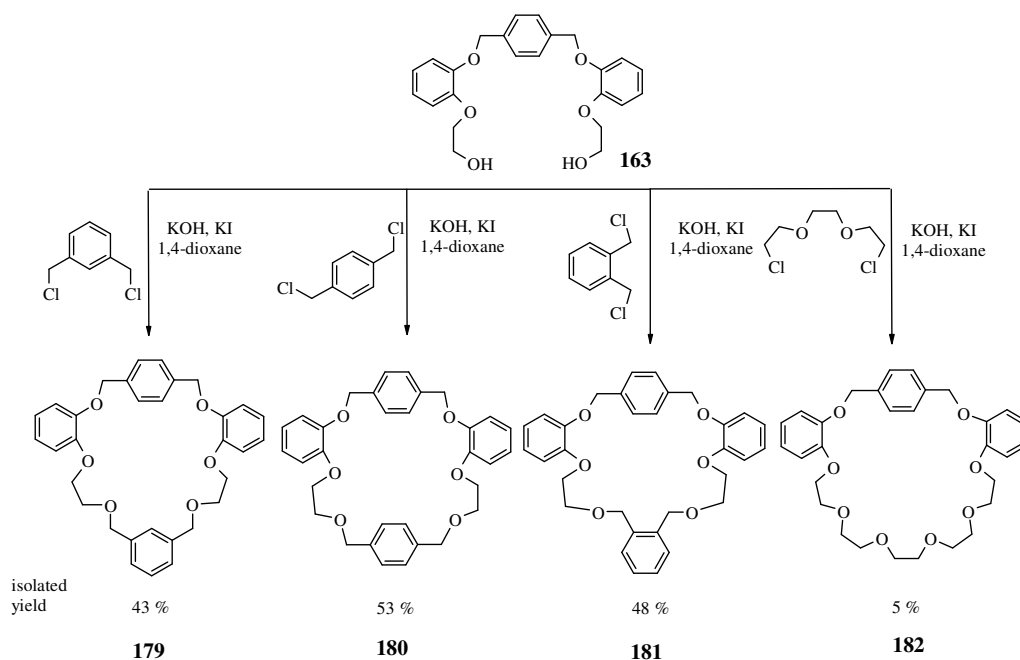


Fig. 3.11 Synthesis of macrocycles **179-182**

Macrocycle **180** was synthesized under a variety of reaction conditions in order to screen the effect of the metal base in cyclising rings of different sizes (Table 3.4). The synthesis of **179** carried out in the presence of potassium hydroxide and its iodide salt proceeded most efficiently, giving 70 % conversion and 53 % isolated yield (entry 6). Sodium hydroxide gave significantly lower yields than the potassium base, whereas lithium hydroxide did not lead to formation of **180**. Moreover, with LiOH the starting material was recovered quantitatively. Reactions carried out in the presence of caesium hydroxide proceeded well and addition of iodide salt improved reaction conversions and increased isolated yields still further. Use of barium hydroxide did not provide with formation of the macrocycle **180**.

	Base (12mmol)	Solvent (80 mL)	Additives	Reaction time [h]	Temp. [°C]	Conv. [%]	Yield [%] 180
1	LiOH	1,4-D ^a	-	48	101	0	0
2	NaOH	THF	NaI	64	66	25	18
3	NaOH	1,4-D ^a	NaI	62	101	32	20
4	NaH	THF	-	6/18	0-R.T.	21	16
5	KOH	THF	KI	46	101	55	46
6	KOH	1,4-D ^a	KI	48	101	70	53
7	KH	THF	-	6/18	0-R.T.	44	35
8	CsOH	1,4-D ^a	-	48	101	45	39
9	CsOH	1,4-D ^a	KI	48	101	54	43
10	Ba(OH) ₂	1,4-D ^a	-	48	101	0	0

Table 3.4 Various reaction conditions for synthesis of macrocycle **180**. ^a1,4-D; 1,4-dioxane

The series of experiments to prepare **180** under different reaction conditions confirmed that the optimal reaction conditions are potassium hydroxide with addition of its iodide salt in an aprotic solvent. According to the results, changing the solvent from THF (b.p. 66 °C) to 1,4-dioxane (b.p. 101 °C) increased the reaction conversion from 55 to 70 % (entries 5,6). Also, the presence of potassium iodide in the reaction flask (Finkelstein modification) increased the yields from 45 % to 54 % (entries 8, 9). Relatively lower conversion was observed for experiments using sodium hydroxide, possibly as a result of reduced template effect. It is also possible that the deprotonated alcohol might form a tighter ion pair with the smaller sodium cation, compared with the larger potassium cation, therefore stabilizing the alkoxide anion and making it less reactive. While not as effective as potassium hydroxide, caesium hydroxide also improved yields compared with reactions carried out using sodium hydroxide.

Macrocycles **183** and **184** were synthesised according to the usual method on a 1 mmol scale and in the presence of potassium hydroxide and potassium iodide in 1,4-dioxane. Macrocycle **183** was purified by column chromatography on silica gel with chloroform/ethyl acetate (3:1) as the mobile phase to give 38 % yield.

Compound **184** was isolated by recrystallization from chloroform/methanol (4:1) and then chloroform to give **184** in 49 % yield.

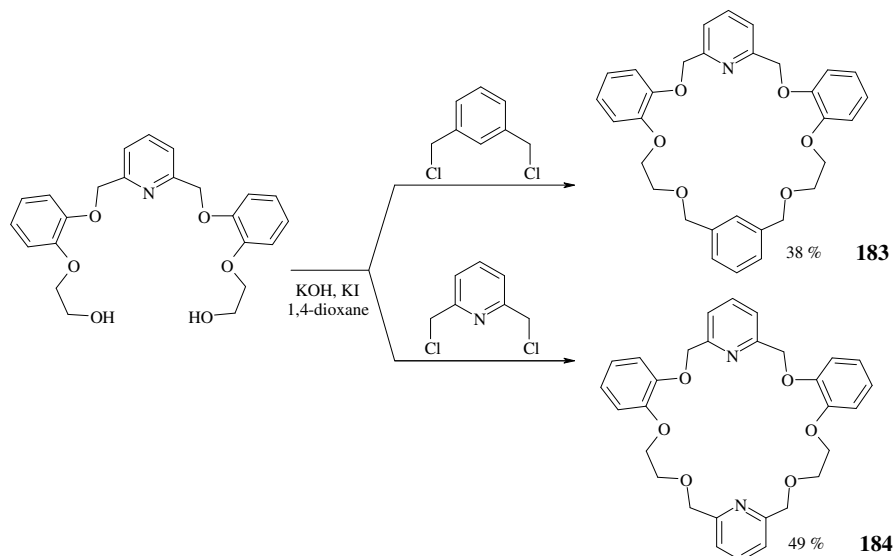


Fig. 3.12 Synthesis of macrocycles **183** and **184**

Macrocycles **170**, **180**, **183** were also synthesized from the corresponding phenoxy-linked macrocyclic precursors and corresponding alkyl bromides.

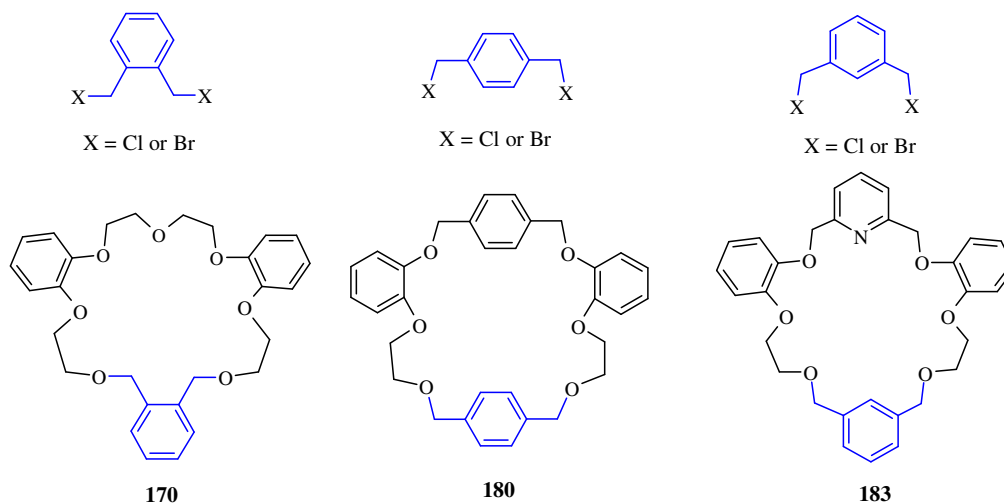


Fig. 3.13 Macrocycles **170**, **180**, **183** synthesized with α, α' -dibromo and α, α' -dichloro-xylenes

These experiments were performed to rapidly determine which of the alkyl halides is a more effective alkylating agent under the optimized reaction conditions. As shown in Table 3.5 reaction conversion and isolated yields were slightly higher for

experiments employing alkyl bromides in the ring closure step. This might be a result of the fact that bromide is a better leaving group than chloride and may react more readily, increasing formation of the desired product. In both cases of purification of **183**, isolated yields were noticeably lower than for the other macrocycles. This may be due to the presence of the pyridine ring which is more likely to interact with silica gel during chromatography separation, therefore it is more difficult to purify.

entry	Macrocycle	Alkyl chlorides		Alkyl bromides	
		conversion	Isolated yield	conversion	Isolated yield
1	170	40 %	32 %	55 %	41 %
2	180	40 %	28 %	55 %	37 %
3	183	50 %	22 %	60 %	38 %

Table 3.5 Results of macrocyclization using alkyl chlorides *versus* bromides

3.3 Preparation of macrocycles by one pot synthesis

Several approaches have been made to synthesize macrocycles by a one-pot synthesis. The advantage of this type of synthesis is that it allows for preparation of a macrocyclic precursor with concomitant macrocyclization. This method not only saves time and reduces the number of synthetic steps but also avoids costly and sometimes difficult purifications. Macrocycle **184** was synthesized using a one pot synthesis in moderate yield by reacting 1 equivalent of 2-(2-hydroxyethoxy)-phenol **159** with 0.5 equivalents of 2,6-*bis*(chloromethyl)pyridine **185** in the presence of a base in 6 mL of 1,4-dioxane. A very important factor in this case is the stoichiometry and choice of base. Sodium or potassium hydroxides are strong enough bases to deprotonate not only the phenol but also the aliphatic alcohol under the reported reaction conditions¹³⁰. Therefore to avoid the formation of polymeric side products, exactly one equivalent of base must be added for each equivalent of 2-(2-hydroxyethoxy)-phenol **159** in the reaction. Formation of macrocyclic precursor **166** was monitored by TLC and additional equivalents of base (up to 5 eq.) and 1,4-dioxane (100 mL) were added to the reaction flask until complete conversion of

starting materials had taken place. The reason for introducing additional solvent is to maintain high dilution conditions for the ring closure step and minimize formation of oligomeric and polymeric side products. Addition of 0.5 eq. of 2,6-bis(chloromethyl)pyridine **185** together with small amounts (0.1 eq) of potassium or sodium iodide was followed by refluxing the reaction mixture for 2 days. Macrocycle **184** was isolated in 6 % yield when sodium hydroxide was used as a base and in 13 % yield when potassium hydroxide was employed.

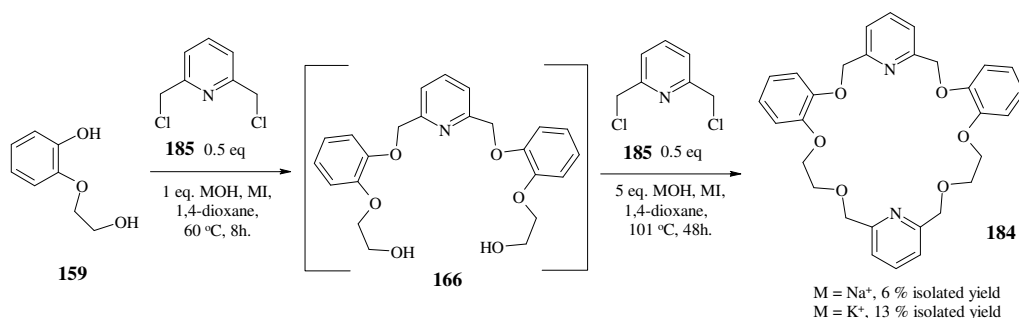


Fig. 3.14 Synthesis of macrocycle **184** in one-pot approach

Identical reaction conditions have been applied to the one-pot synthesis of macrocycle **180**. Isolated yields of product **180** for the reaction with sodium hydroxide (7 %) and potassium hydroxide (11 %) were disappointingly moderate compared with a two-step synthesis, approach.

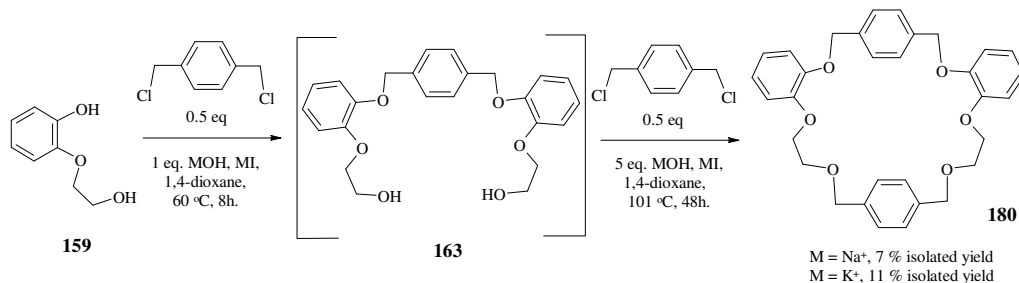


Fig. 3.15 Synthesis of macrocycle **180** in one-pot approach

Analogous attempts to prepare of **180** were performed employing caesium hydroxide or potassium *tert*-butoxide as a base in 1,4-dioxane. However, only trace amounts of the final product **180** were observed and product was not isolated further.

A number of trials were also undertaken to prepare macrocycle **186**. A variety of bases and solvents were screened to promote formation of the intended product,

including lithium, sodium and potassium hydroxide in THF, 1,4-dioxane or DMF. Furthermore, for the second, ring-closing step, even stronger bases such as sodium and potassium hydrides in THF at RT did not lead to the cyclization.

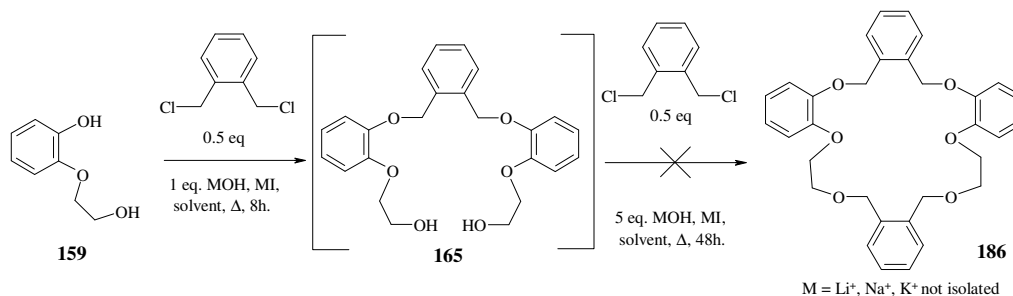


Fig. 3.16 Attempts to synthesis of macrocycle **186**

Every attempt at the preparation of macrocycle **186** was unsuccessful including efforts to synthesize this compound by a two step synthesis. Furthermore, even trials of various base and conditions failed to lead to a successful synthesis of **186**. Preparation of macrocycles **180** and **184** by a one-pot approach proved to be successful, however, isolated yields were unsatisfactory and varied between 6 to 13 %. Therefore the one-pot method was decided not to be explored further, in favour of the more efficient two-pot approach.

3.4 Spectroscopic discussion on model macrocycles

3.4.1 NMR study of **173** and **182**

The ¹H NMR spectra of **173** and **182** are depicted in Fig. 3.18 and Fig. 3.19 respectively. The *para* substituted aromatic CHs for both macrocycles appear as singlets at δ 7.42 for **182** and at δ 7.33 for **173**. Hydrogens adjacent to each other in the catechol ring were expected to appear as a double doublet, but instead merged into a broad multiplet integrating to 8 protons. The benzylic protons of the *para*-xylene groups in **182** and **173** can easily be distinguished since both appear as singlets at distinctly different chemical shifts. In the case of **182** the benzylic methylene group (12,12') is covalently bonded to a phenoxy group and appears at δ 5.05. However, in *para*-xylene **173**, the benzylic methylene (9,9') is covalently

linked to an alkoxy group and so is shifted further upfield and appears as a singlet at δ 4.62. This difference is due to the electron-withdrawing effect of oxygen which is greater for aromatic ethers than for aliphatic ones. The polyethylene protons 7,7' and 8,8' in **182** appear as doublet of doublets at δ 4.11 and δ 3.83 respectively, with a coupling constant of 4.4 Hz. Similarly, the hydrogens at positions 9,9' and 10,10' have resolved as doublet of doublets at δ 3.68 and δ 3.53 with the J value of 4.6 Hz. The singlet at δ 3.51 is due to the chemically equivalent protons of 11,11'. Protons 12,12' and 7,7' in the structure **173** appear as doublet of doublets further downfield at δ 4.11 ($J=4.4\text{Hz}$) and δ 4.06 ($J=4.8\text{Hz}$) due to the electron-withdrawing effect of the catechol ring. This separates them from the doublet of doublets of 13,13' and 8,8' at δ 3.79 ($J=4.4\text{Hz}$) and at δ 3.73 ($J=4.8\text{Hz}$) respectively in which methylenes are linked only to aliphatic ether oxygens. The equivalent hydrogens (14,14') resonate as a singlet at δ 3.55 in the same way that the protons (11,11') did in **182**. The ethylene protons from the ether linkage have been expected merely to couple with each other to give a pair of triplets. The pattern produced in this case is, however, clearly more complicated. The complexity comes from the fact that the pairs of ethylene nuclei are not magnetically equivalent and in consequence produce AA'BB' system.

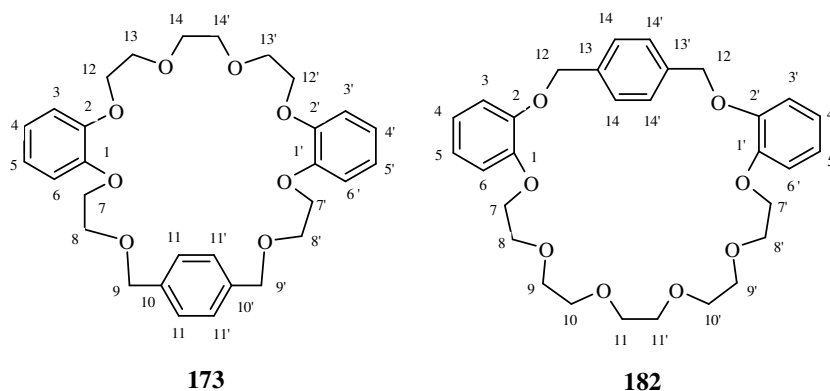


Fig. 3.17 Macrocycles **173** and **182**

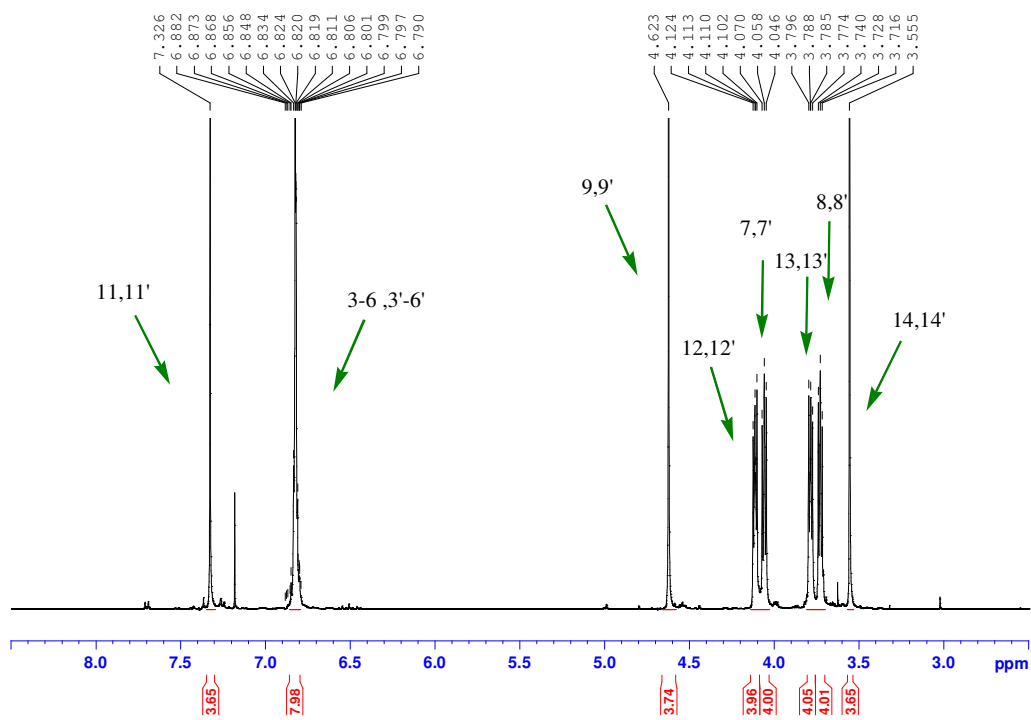


Fig. 3.18 ^1H NMR spectrum of 2,3,14,15,21,24-tribenzo-1,4,7,10,13,16,19,26-octaoxacycloocta-eicosa-2,14,21,22,23-tetraene, **173**

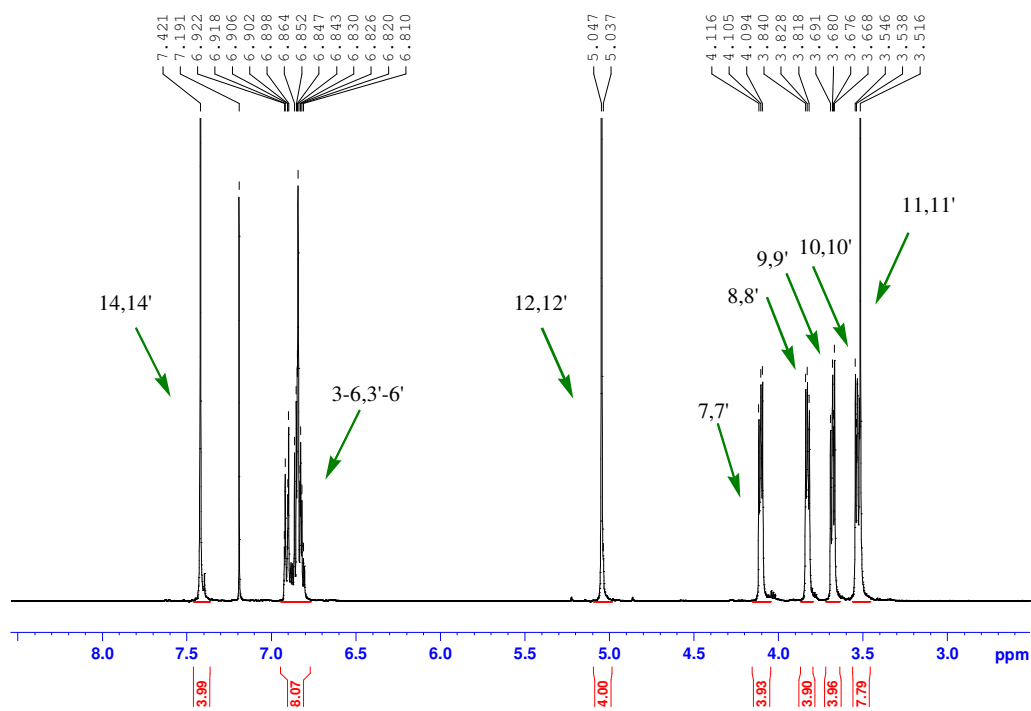


Fig. 3.19 ^1H NMR spectrum of 2,3,6,9,12,13-tribenzo-1,4,11,14,17,20,23,26-octaoxacycloocta-eicosa-2,6,7,8,12-tetraene, **182**

	s	m	s	dd	dd	dd	dd	s
182	14,14'	3-6,3'-6'	12,12'	7,7'	8,8'	9,9'	10,10'	11,11'
	7.42	6.92-6.80	5.05	4.11	3.83	3.68	3.53	3.51
				<i>J</i> =4.4Hz	<i>J</i> =4.4Hz	<i>J</i> =4.6Hz	<i>J</i> =4.6Hz	
173	11,11'	3-6,3'-6'	9,9'	12,12'	7,7'	13,13'	8,8'	14,14'
	7.33	6.85-6.77	4.62	4.11	4.06	3.79	3.73	3.55
				<i>J</i> =4.4Hz	<i>J</i> =4.8Hz	<i>J</i> =4.4Hz	<i>J</i> =4.8Hz	

Table 3.6 ¹H NMR spectroscopic details for macrocycles **173** and **182**

The ¹³C NMR spectrum of **173** (Fig. 3.21), shows some variation from the **182** macrocycle presented in (Fig. 3.20). The most noticeable differences in chemical shift occur for nuclei in the catechol ring. The oxygen substituted aromatic carbons (1,1' and 2,2') in **173** linked to the polyethylene spacer units appear at δ 148.98 as a peak of double intensity, whereas in **182** two separate peaks of weaker intensity for 2,2' at δ 149.38 and 1,1' at δ 148.61 were identified. Subsequently the substitution pattern was found to have a significant effect on the appearance of adjacent tertiary carbons in the catechol unit. In **173** 4,4', 5,5' have virtually identical chemical shift values of δ 121.49 and δ 121.46, while a small variation in the appearance of the corresponding signals in the ¹³C NMR spectrum of **182** was recorded at δ 121.87 (4,4') and δ 121.32 (5,5'). Similarly, minor differences in chemical shift between two macrocycles were observed for 3,3' and 6,6'. Consequently in **173** these tertiary carbons resonate at near identical chemical shifts of δ 114.31 and δ 114.07 respectively, whereas the signals for 6,6' and 3,3' appear at chemical shifts of δ 115.48 and δ 113.82 for **182**. The four tertiary *para*-carbons for both macrocycles **173** and **182** appear as single peaks of double intensity at δ 127.9 for **173** and at δ 127.7 for **182**. In **173** the secondary carbon (9,9') of the benzylic methylene group is shifted downfield to δ 73.15, which is comparable with the value of δ 71.21 for 12,12' in macrocycle **182**.

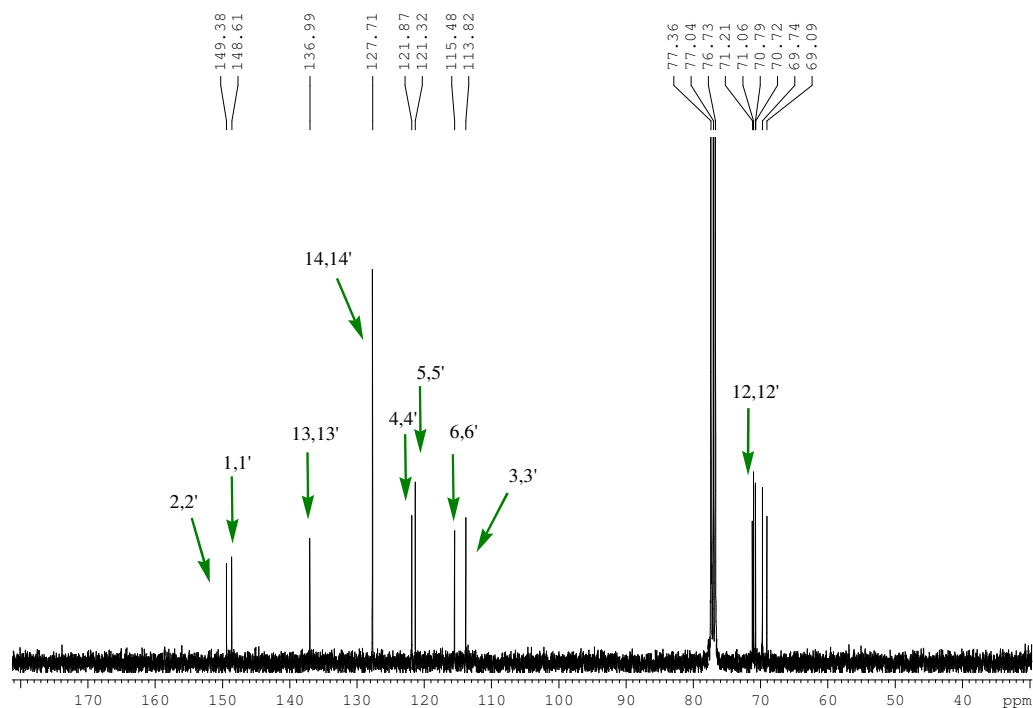


Fig. 3.20 ^{13}C NMR spectrum of 2,3,6,9,12,13-tribenzo-1,4,11,14,17,20,23,26-octaoxacycloocta-eicosa-2,6,7,8,12-tetraene, **182**

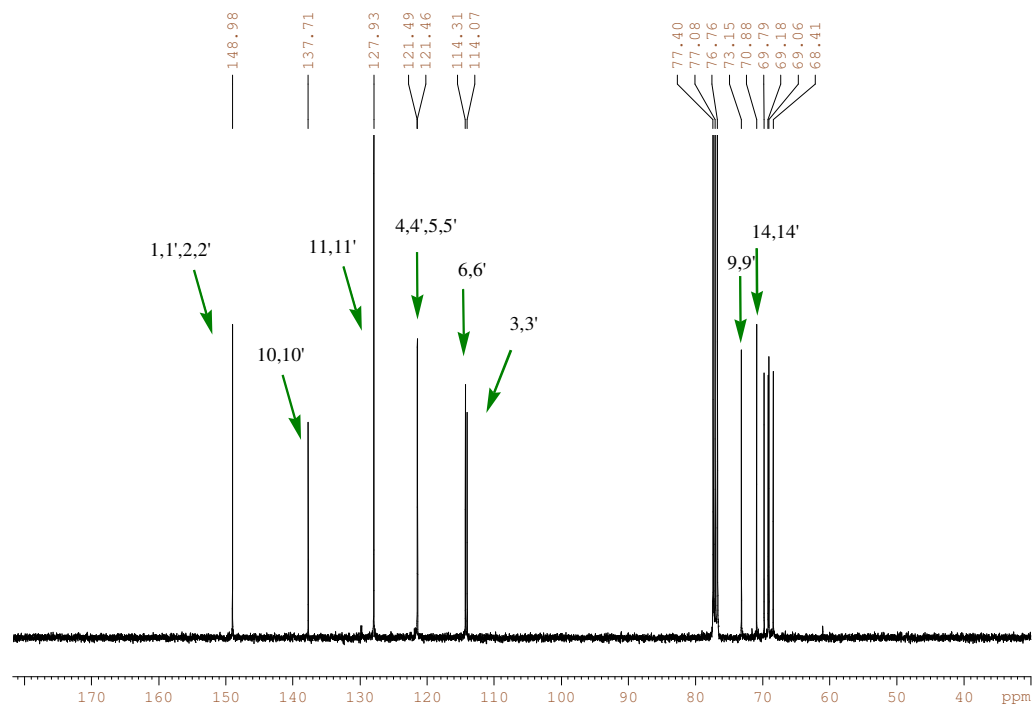


Fig. 3.21 ^{13}C NMR spectrum of 2,3,14,15,21,24-tribenzo-1,4,7,10,13,16,19,26-octaoxacycloocta-eicosa-2,14,21,22,23-tetraene, **173**

3.4.2 NMR study of **174**

In the ^1H NMR of **174** (Fig. 3.23) the major differences in chemical shift compared with **173** appear amongst the polyethylene protons. The 13,13' and 7,7' protons in **174** appear as overlapping doublet of doublets, making it difficult to determine the coupling constants. Overlapping was also observed for protons 8,8' and 14,14' which resonate as a multiplet (δ 3.78-3.75), instead of the anticipated two doublet of doublets integrating to 8 protons. In contrast the ethylene group (15,15') appears as a singlet, integrating to 4 hydrogens at δ 3.62. In the aromatic region the adjacent hydrogens in the *ortho*-xylene ring appear as double doublets, with the *meta*-CH (12,12') at δ 7.35 and the *ortho*-CH (11,11') at δ 7.19 with coupling constants values of 5.6 Hz and 3.2 Hz, respectively. As in previous spectra the aromatic protons of the catechol rings appear as a multiplet in the region δ 6.81-6.76, integrating to 8 hydrogens.

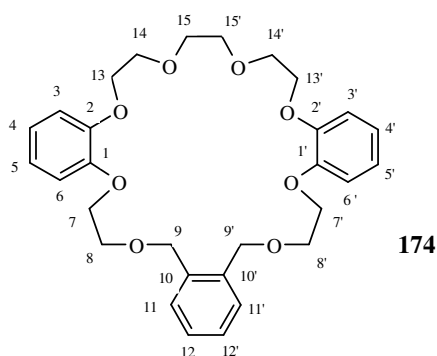


Fig. 3.22 Macrocycles **174**

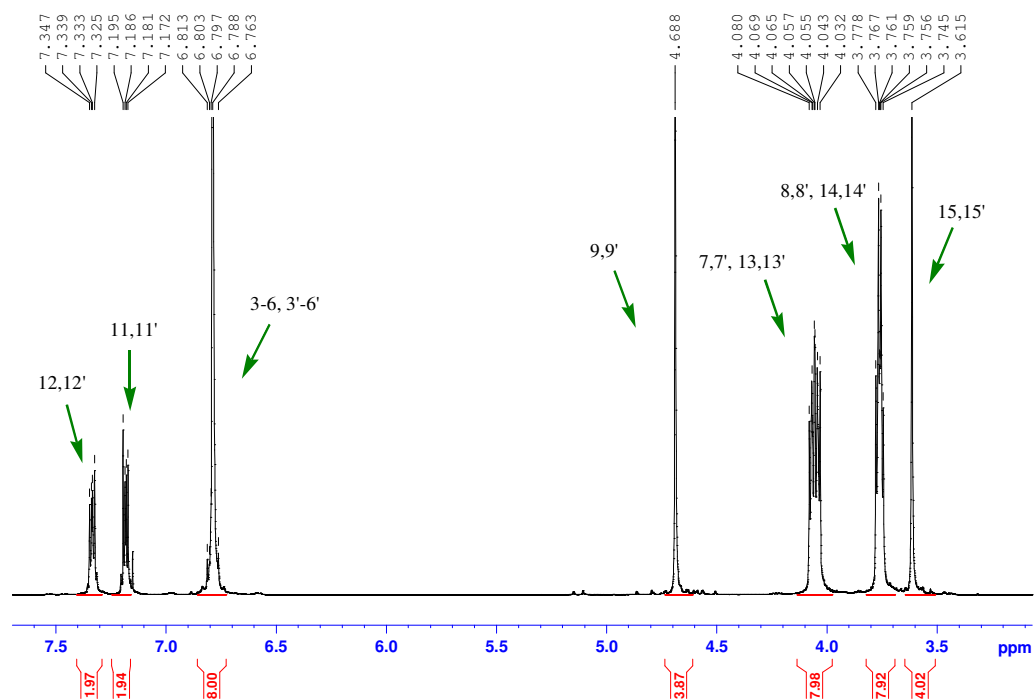


Fig. 3.23 The ^1H NMR spectrum of 2,3,14,15,21,22-tribenzo-1,4,7,10,13,16,19,25-octaoxa-cyclohexaiecosa-2,14,21-triene, **174**

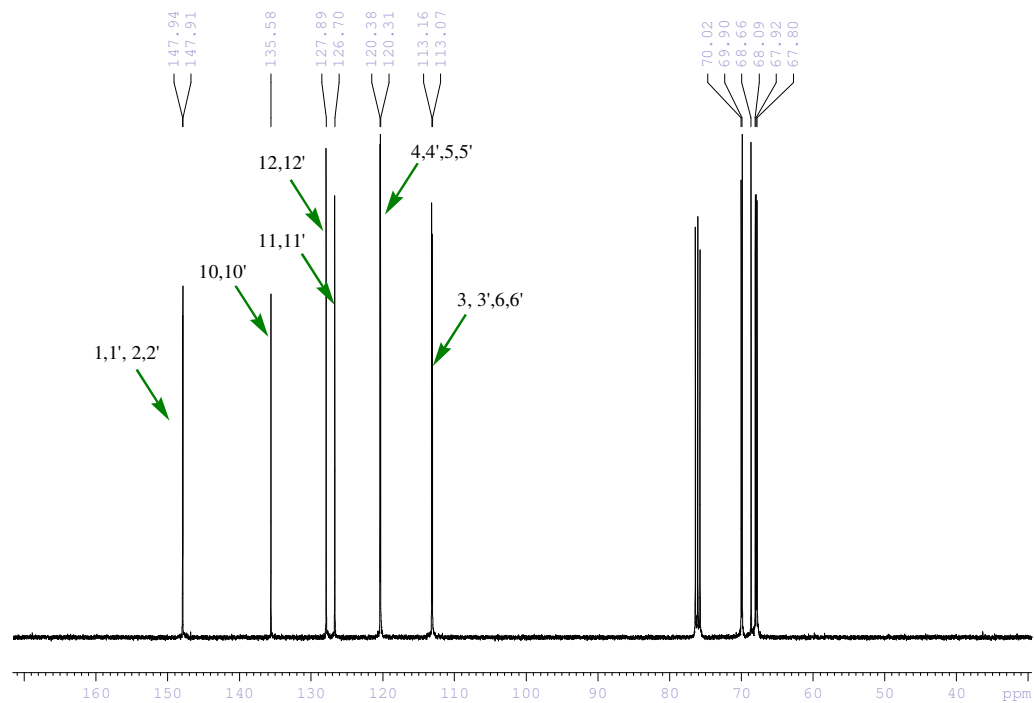


Fig. 3.24 The ^{13}C NMR spectrum of 2,3,14,15,21,22-tribenzo-1,4,7,10,13,16,19,25-octaoxa-cyclohexaiecosa-2,14,21-triene, **174**

In the ^{13}C NMR spectrum of **174** (Fig. 3.24) signals of double intensity due to the quaternary aromatic carbons substituted with oxygen (1,1',2,2') in the catechol ring have been identified at δ 147.9, whereas the aromatic carbons assigned to the *ortho*-xylene unit (10,10') appear at δ 135.58. The *ortho*- and *meta*-CH in the xylene ring (11,11' and 12,12') appear at δ 127.89 and δ 126.7 respectively. The CH signals of the catechol ring *ortho* (3,3',6,6') and *meta* (4,4',5,5') appear upfield, compared with the signals of the xylene unit at δ 120.38 and δ 113.16. The CH's in the catechol system are both markedly shielded compared with an unsubstituted aromatic ring (benzene CH 128). The shielding is greater for the *ortho*-CH 3,3' and 6,6' (δ 113) because of efficient mesomeric electron-donation from the non-bonding electron pairs on oxygen (Fig. 3.25). The *para*-CH 4,4', 5,5' also benefits from mesomeric conjugation, but less efficiently (δ 120).

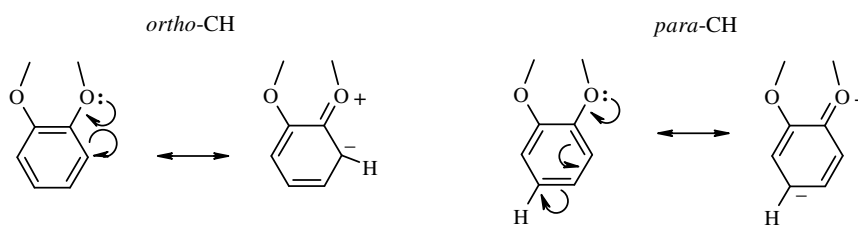


Fig. 3.25 Mesomeric effect, *ortho*-CH and *para*-CH

The benzylic CH_2 9,9' (**174**) situated between an oxygen and the aromatic ring appears as a singlet at δ 70.02. This signal appears upfield with respect to the corresponding benzylic CH_2 of **173** which appears at δ 73.15. Finally, the signals of the polyethylene chain appear in same region as in the previous examples (**174**, **184**) in the region from δ 6.99-6.78.

3.4.3 NMR study of **181**

The proton ^1H NMR of the macrocycle **181** containing four aromatic rings is presented in Fig. 3.27. The protons associated with *para*-phenyl aromatic ring appear as a singlet at δ 7.41 integrating to four hydrogens. The double doublets corresponding to the *ortho*- and *meta*-protons at positions 12,12' and 11,11' have chemical shifts of δ 7.26 and 7.21 respectively. The hydrogens of the *ortho*

substituted catechol appear as a multiplet upfield of the other aromatic hydrogens in the range of δ 6.96-6.82, integrating to eight protons. The benzylic methylene protons for the *ortho*- and *para*-xylene rings, both appear as singlets at different chemical shifts. The first singlet at δ 5.00 is due to the *para* 13,13' hydrogens, whereas the *ortho*-methylene protons 9,9' are shifted upfield by approximately 0.33 ppm to a chemical shift of δ 4.67, with both singlets integrating to four protons. The two doublet of doublets at δ 4.12 and 3.77 refer to the protons of the ethylene units 7,7' and 8,8' as a consequence of a AA'BB' system.

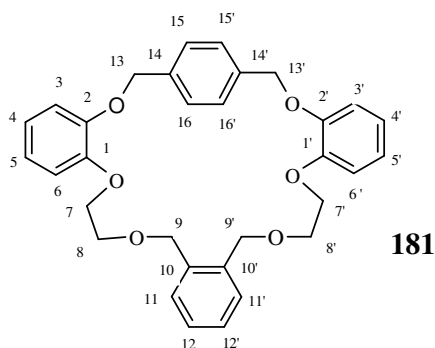


Fig. 3.26 Structure of **181**

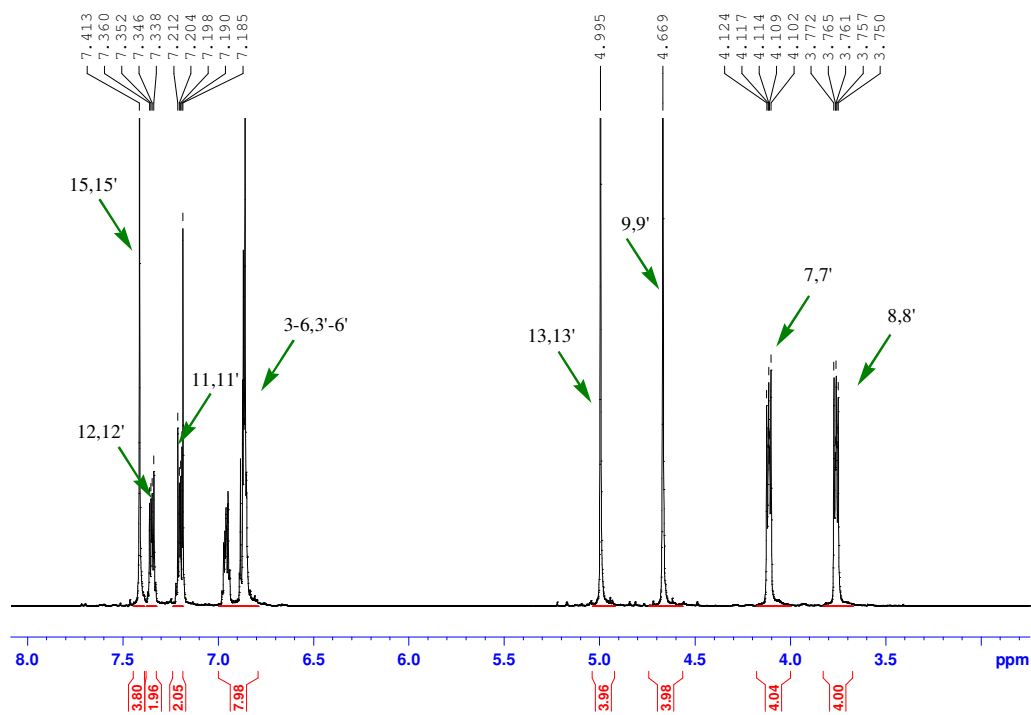


Fig. 3.27 The ^1H NMR spectrum of 2,3,6,9,12,13,19,20-tetrabenzo-1,4,11,14,17,22-hexaoxa-cyclotetraeicosa-2,6,7,8,12,19-hexaene, **181**

In the ^{13}C NMR spectrum of **181** (Fig. 3.28) the aromatic carbons bonded to the oxygen atoms have chemical shifts of δ 149.49 (2,2') and δ 149.05 (1,1'), respectively. The aromatic CH groups *para* to the oxygens (14,14') appear at δ 136.85, while the CHs *ortho* to oxygen (10,10') resonate at δ 136.44. The other aromatic carbons from the *ortho*-xylene unit (11,11' and 12,12') resonate at δ 127.79 and δ 128.95, respectively. Tertiary aromatic carbons of *para*-xylene ring (15,15',16,16') have merged into a signal of double intensity at δ 127.43. Analogously to **182** the tertiary carbons associated with the catechol rings resonate as separate signals, with 4,4' at δ 121.83 and 5,5' at δ 121.59. Carbons labelled as 6,6' and 3,3' have also resolved into separate signals, however with close chemical shifts of δ 115.19 and at δ 114.52, respectively. The signals for the secondary aliphatic carbons in the methylene group "spacers" appear at δ 71.21 for 13,13' and at δ 70.99 for 9,9'.

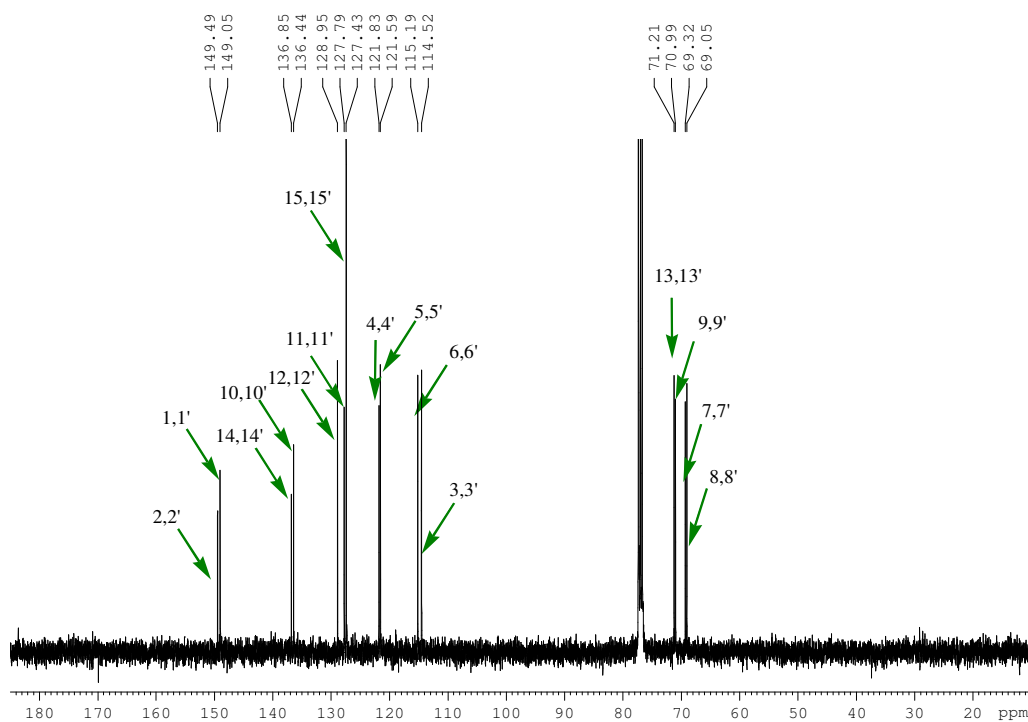
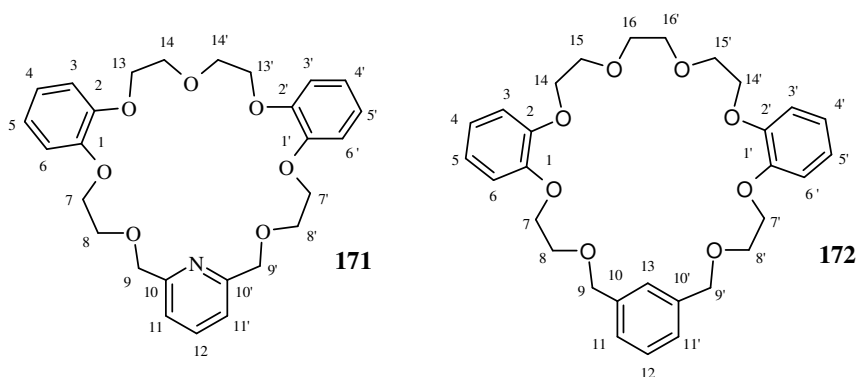


Fig. 3.28 The ^{13}C NMR spectrum of 2,3,6,9,12,13,19,20-tetrabenzo-1,4,11,14,17,22-hexaoxa-cyclotetraeicosa-2,6,7,8,12,19-hexene, **181**

3.4.4 The ^1H NMR studies of **171** and **172**Fig. 3.29 Macrocycles **171** and **172**

The ^1H NMR of **171** and **172** are shown in Fig. 3.30 and Fig. 3.31 respectively. The aromatic proton 12 of the pyridine ring in **171** appears as a triplet, representing the highest chemical shift of δ 7.67 with a coupling constant of 7.6 Hz. The protons adjacent to 12 appear as a doublet with identical J values and integrating to two hydrogens. As in previous cases protons at positions 3-6 and 3'-6' appear as a multiplet in the chemical shift range δ 6.85-6.80. The methylene groups (9,9') linking the pyridine ring to the ether oxygen appear as a singlet at δ 4.82. In the region from δ 3.75 to 4.25 typical of glycol ethers, the four doublet of doublets ethylene units appear at δ 4.14 (13,13') and 3.93 (14,14') (both J values of 4.4 Hz) and at δ 4.03 (7,7') and δ 3.83 (8,8'), both with a J value of 4.8 Hz. This complexity comes from the fact that the pairs of nuclei 7,7', 8,8', 13,13', 14,14' are not magnetically equivalent. All of them are examples of AA'BB' system.

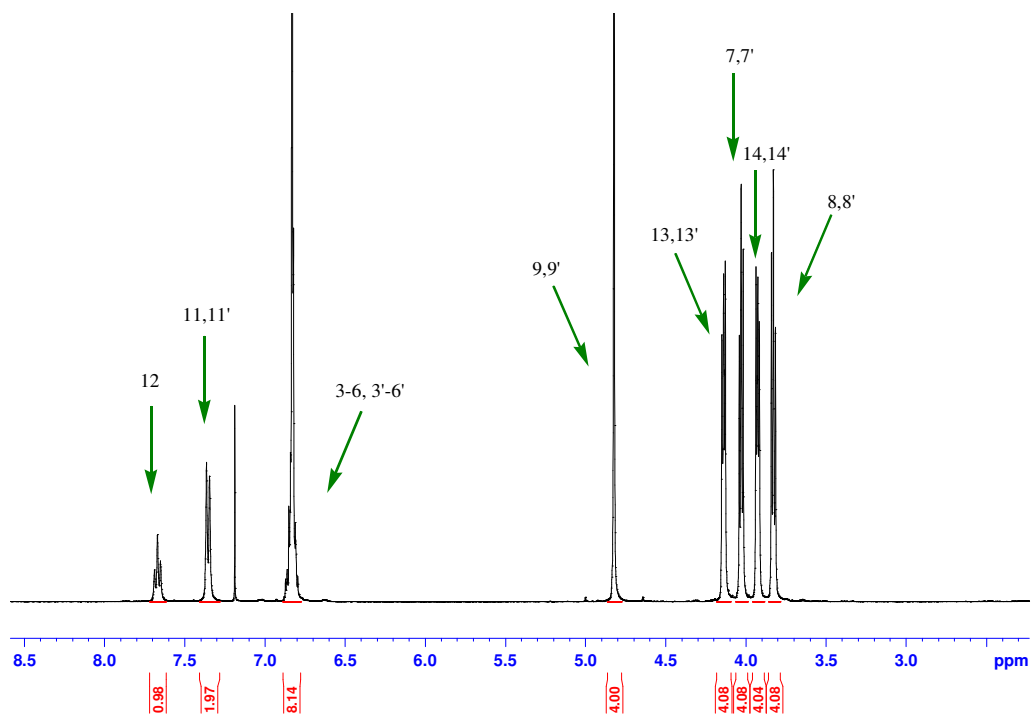


Fig. 3.30 The ^1H NMR spectrum of 2,3,11,12,18,20-tribenzo-19-aza-1,4,7,10,13,16,22-heptaoxa-cyclotetra-eicosa-2,11,18,19-tetraene, **171**

Fig. 3.31 shows the ^1H NMR spectrum of **172** containing a *meta*-xylene unit as part of the macrocyclic ring. Proton 13 in the *meta*-substituted aromatic system appears as a singlet at δ 7.28, whereas protons 11,11' and 12 appear as a multiplet at δ 7.25 to 7.22. A second multiplet at δ 6.82-6.78 is due to the *ortho* catechol system and integrates to eight protons. The methylene hydrogens 9,9' resolve as a singlet at δ 4.60. Ethylene units from the ether linkages have merged into double doublets with coupling constants of 4.4 Hz and chemical shifts of δ 4.11 and δ 3.79 for 14,14' and 15,15', respectively, and δ 4.05 and δ 3.71 for 7,7' and 8,8', with coupling constants of 4.8 Hz.

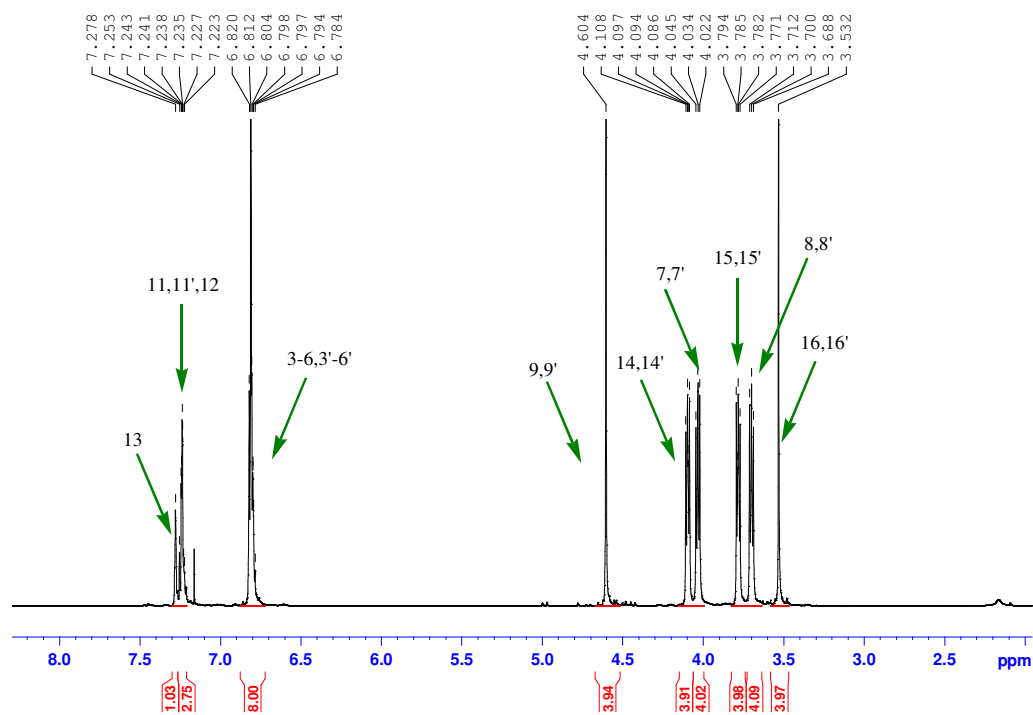


Fig. 3.31 The ^1H NMR spectrum of 2,3,14,15,21,23-tribenzo-1,4,7,10,13,16,19,25-octaoxacycloheptaecosa-2,14,21,22-tetrene, **172**

3.5 Conclusion

New phenoxy-linked precursors of macrocyclic compounds have been successfully prepared by alkylation of 2-(2-hydroxyethoxy)phenol **159** with a variety of alkyl dihalides in DMF in the presence of K_2CO_3 . Synthesised compounds were isolated in high yields varying between 54 to 91 %. All seven structures have been identified by NMR and HRMS. For six of the macrocyclic precursors, it was possible to confirm their structures by X-ray crystallography (Chapter 5).

All these phenoxy-linked macrocyclic precursors were subjected to ring closure reactions employing the template effect and high dilution techniques.

Two routes of synthesis of model macrocycles were investigated:

- A. from phenoxy-linked open structures,
- B. one pot synthesis from 2-(2-hydroxyethoxy)phenol.

The one-pot approach proved to be a straightforward method, however isolated yields for compounds prepared according to this method were unsatisfactory (6-13 %) The approach of synthesis of model macrocycles from their phenoxy-linked

open structures was more extensively investigated. Various bases and solvents were screened which established that the greatest yields for the macrocyclization step were accomplished in the presence of KOH and KI in refluxing 1,4-dioxane. It was established that the presence of a templating agent plays a crucial role in that step. A series of alkali metal bases were screened with the presence of K^+ compared to Cs^+ , Na^+ or Li^+ enabling the reaction to proceed with the highest yield. The advantage of this method compared to the one pot synthesis is good overall yields of synthesised macrocycles, which varied between 24-47% isolated yields. Eighteen model macrocyclic structures based on 2-(2-hydroxyethoxy)phenol unit and both aromatic and aliphatic ethereal linkers were successfully synthesised and isolated. A library of macrocycles and their phenoxy linked precursors were screened as therapeutics as part of our cancer program (Chapter 7). Assay of binding extraction studies of synthesized compounds towards a selection of metal picrates was also performed (Chapter 6).

A further reason for synthesising a variety of macrocyclic model systems based on 2-(2-hydroxyethoxy) phenol and optimizing reaction conditions was to explore the reactivity and behaviour of the two hydroxyl groups in diol to established reaction procedures on the preparation of morphine macrocycles.

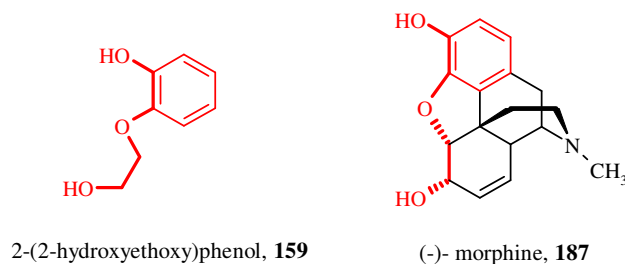


Fig. 3.32 Similar features in structures of 2-(2-hydroxyethoxy) phenol **159** and morphine **187**

It was expected that both alcohol groups in morphine will react in the same order (would exhibit similar reactivity) as per the 2-(2-hydroxyethoxy) phenol system. Therefore extensive effort was undertaken for optimization for the alkylation of diol and ring closure step conditions, especially that the diol substrate is sterically less rigid and more easily available.

“Of all the remedies which a kind Providence has bestowed upon mankind for the purpose of lighting its miseries, there is not one which equals opium in its power to moderate the violence of so many maladies and even to cure some of them”

Thomas Sydenham 1624-1689

4 Morphine compounds

The powerfully euphoric and analgesic opium alkaloids have fascinated mankind since the days of antiquity. The active principles of opium have been known for years to be highly powerful pain relievers. Morphine and its 3-*O*-methylated form, codeine are principal constituents of opium and can be obtained by isolation from the unripe seed pods of the opium poppy, *Papaver somniferum*¹³¹.

In 1805 the active principle of opium was isolated in pure form as a white crystalline powder and named “morphium” after Morpheus, the ancient Greek god of dreams¹³². Since then morphine became one of the most commonly prescribed drugs in medical practice and was widely employed to treat ailments as diverse as diabetes, asthma, diarrhoea and ulcers as well as being used in the relief of moderate to severe pain. However, the dark side of morphine is that it is highly addictive and tolerance, physical and psychological dependence develop very rapidly.

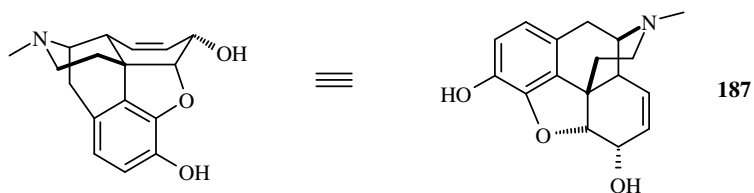


Fig. 4.1 (-)- Morphine 187

The activity shown by morphine including both analgesic potency and narcotic side effects, has been proven to depend on its structural arrangement. The specific set of structural features common to the opioid family are: a tertiary nitrogen with a small alkyl substituent, a quaternary carbon, a phenyl group or its isosteric equivalent directly attached to the quaternary carbon and finally a two carbon spacer between the quaternary carbon and the tertiary nitrogen. All of the derivatives of morphine which possess this basic ring structure can act as either an agonist or antagonist of the opioid receptor. Therefore, some of them are used as effective analgesics for the treatment of pain while others are useful as opioid antagonists for the treatment of narcotic overdose or opioid addiction.

Codeine is one of the constituents of opium and is approximately one-sixth as effective an analgesic as morphine. It is commonly prescribed as a cough suppressant and mild pain reliever. One of the better known examples of a morphine derivative is

heroin. Heroin (diamorphine) presents the same structural features as morphine, except that both of the hydroxyl groups have been modified by acetylation. Diamorphine has physiological effects that are essentially the same as those of morphine except that it acts faster and so has a greater potency. The presence of the two acetyl units on the hydroxyl groups makes heroin very lipid-soluble and so it readily enters the brain where it is rapidly hydrolyzed to morphine, whereas morphine itself is less lipid-soluble and thus crosses the blood-brain barrier more slowly.

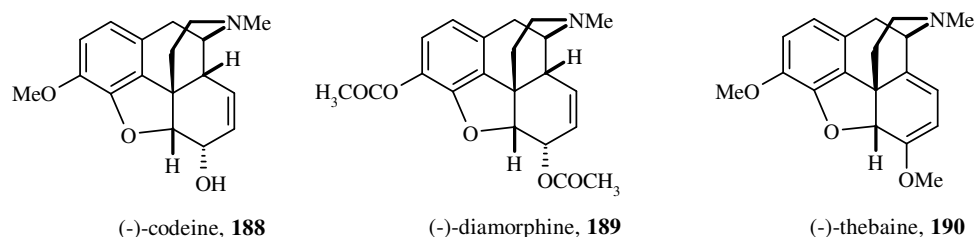


Fig. 4.2 Morphine derivatives codeine **188**, diamorphine **189** and thebaine **190**

Another ingredient of opium, thebaine has been found to be a biochemical precursor of morphine and codeine. Thebaine has no therapeutic application, but is used industrially for the production of synthetic opiates such as oxymorphone **191**, naloxone **192** and etorphine **193**.

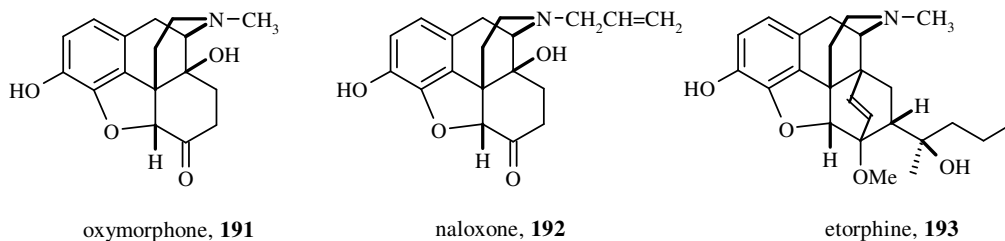


Fig. 4.3 Morphine derivatives oxymorphone **191**, naloxone **192** and etorphine **193**

Opiates induce such an intense biological response because of their binding properties to specific receptor sides within the central nervous system and gastrointestinal tract¹³³. The opioid receptors (G protein-coupled receptors) have been identified as a large protein family of transmembrane receptors which can be activated by binding to ligand structures like peptides, proteins, hormones,

pheromones or neurotransmitters (including the skeleton of morphine). Three distinct classes of mammalian opioid receptor μ , κ and δ have been identified and have been the subject of intense studies^{134,135,136}.

Morphine itself is a selective μ -type receptor agonist, and so the analgesia it elicits is also accompanied by euphoria, decreased gastrointestinal motility (leading to constipation), physical dependence, and respiratory depression^{137,138}. The latter is usually the cause of death upon morphine overdose. The synthetic opiate oxymorphone has been found to be a μ -agonist with ten times the potency of morphine, whereas the closely related naloxone actually antagonises all types of opioid receptors and is a useful antidote to morphine overdosage. Etorphine has a thousand times the potency of morphine as a μ -agonist and greatly depresses respiration. That is why its use is mainly reserved for the immobilisation of very large animals, such as elephants.

The harrowing addiction to morphine continues to provide impetus to the quest for alternative drugs, based on the morphine skeleton, that are powerful analgesics but do not have the undesirable side effects. The opium alkaloids and their analogues are called opioids and all of these compounds bear a strong structural resemblance one to another, which first suggested that there are receptors in animals complementary in structure to morphine and its family¹³⁹.

Synthesis of the morphine skeleton has been a great challenge for organic chemistry for the past decade¹⁴⁰. There is continuing interest in developing total synthetic routes because of the broad range of pharmacological properties of morphine alkaloids and related compounds. Many routes and possibilities for analogues have been already reported, however, at an industrial scale none of them can be considered an efficient alternative to isolation of morphine from poppies^{141,142}.

4.1 Preparation of morphine macrocycle precursors

Vögtle and Frensch have reported a method for preparation of open chain oligomeric ethylene glycol ethers **194** and **195** with two terminal morphine groups¹⁴³. The reaction was carried out by refluxing the oligomeric dichloride with morphine in wet butanol in the presence of sodium hydroxide as a base. Structure **194** was isolated in 8% yield and **195** in 10 % yield. Attempts to join two morphines with 2,6-*bis*(bromomethyl)pyridine were also undertaken. However, in this case 6-(3-morphinylmethylene)-2-pyridinyl-methanol **196** was isolated as the major product in 10 % yield.

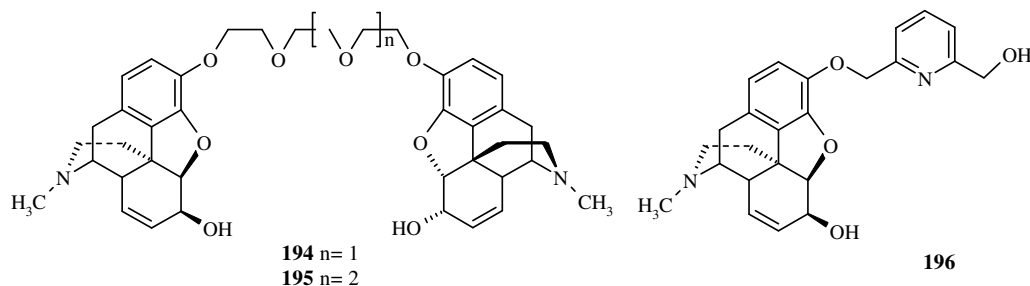


Fig. 4.4 n=1; 1,8-*bis*(3-morphinyl)-3,6-dioxaoctan, **194**; n=2; 1,11-*bis*(3-morphinyl) -3,6,9-trioxaundecane **195**, 6-(3-morphinylmethylene)-2-pyridinylmethanol **196**

In our research a series of novel macrocyclic precursors containing two morphine units in the structure were successfully synthesized and isolated. Methodology used for this purpose was however, different from the one established by Frensch. Also reaction conditions developed for preparation of phenoxy-linked model systems based on the 2-(2-hydroxyethoxy)-phenol unit **159** did not prove useful.

Developing a satisfactory method which allows preparation of the desired compounds in high yields and purity was achieved by screening of series of reactions employing a variety of bases *e.g.* Na_2CO_3 , K_2CO_3 , Cs_2CO_3 , NaOH, NaOMe, KOH and DMAP in different solvents: MeOH, acetone, DMF, THF and 1,4-dioxane. The best base/solvent combination for preparation of compounds **194**, **198**, **199** and **200** proved to be NaOMe in refluxing MeOH. By employing these conditions the final products were synthesized in isolated yields ranging from 64 % to 94 %. However,

synthesis of **201** and **202** by this method did not give satisfactory yields, and instead for synthesis of **201** and **202** potassium *tert*-butoxide in refluxing THF was preferred. Under these conditions **197**, **201** and **202** were isolated in 28 %, 51 % and 37 % yields, respectively. Notably, in all cases, the use of bromides or iodides instead of chlorides leads to a significant increase in the quantity and purity of the products.

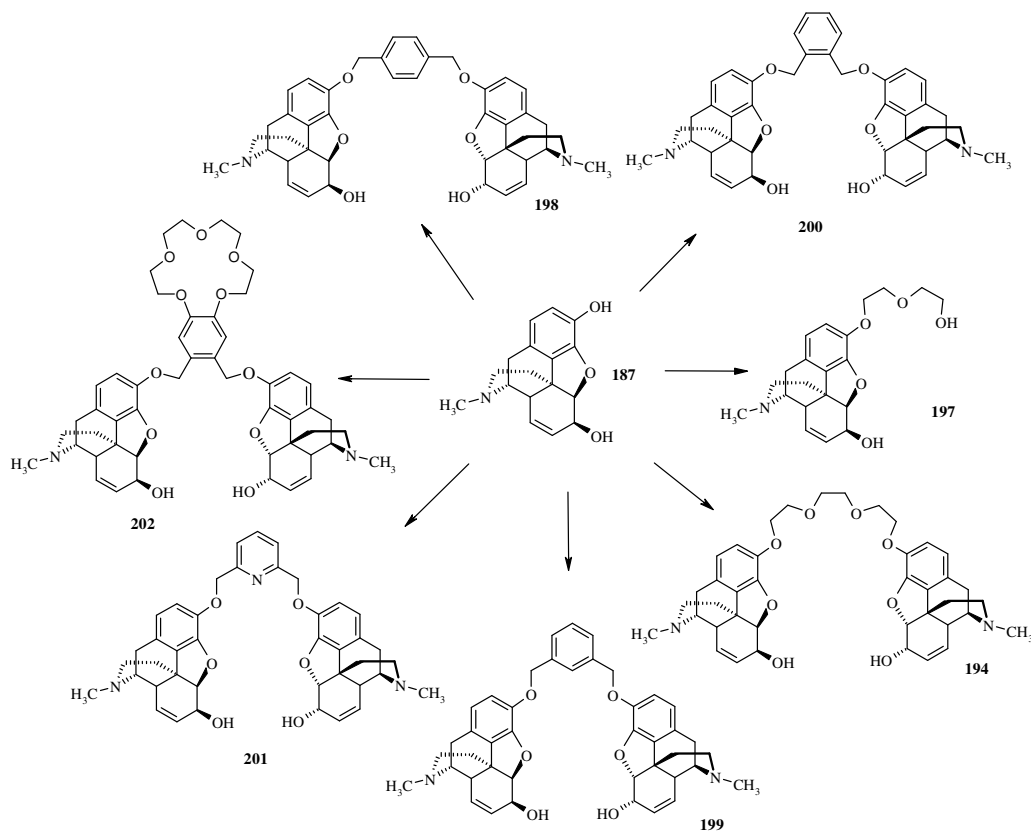


Fig. 4.5 Precursors of morphine macrocycles

Compounds **194**, **198-200** were prepared by alkylation of morphine with the corresponding alkyl halides in absolute methanol in the presence of 3 eq of sodium methoxide as a base. First the morphine hydrochloride salt was suspended in solvent and then while stirring the suspension of salt, a solution of sodium methoxide in methanol was added dropwise over 1 hour. Next, the alkylating agent was added in one aliquot and the reaction was stirred at 64 °C for 48 h. In each case the reaction mixture was purified by column chromatography, to give the linked morphine in yields varying between 36-94%. Several attempts to prepare **194** using 1,2-*bis*(2-chloroethoxy)ethane **203** in the presence of sodium methoxide in methanol or sodium ethoxide in ethanol were undertaken and in both cases product was isolated in 42 %

yield. However, the highest yield (94 %) of **194** was obtained for reaction of 1,2-bis-(2-iodoethoxy)ethane **204** in methanol in the presence of sodium methoxide. Compound **198** was prepared in a one step synthesis by reaction of morphine with α,α' -dibromo-*p*-xylene **206** in the presence of sodium methoxide in absolute methanol. The crude product was purified by column chromatography, to give **198** in a 68 % yield, a considerable improvement over the yield of 36 % obtained by refluxing of morphine with α,α' -dichloro-*p*-xylene **205** and sodium carbonate in THF.

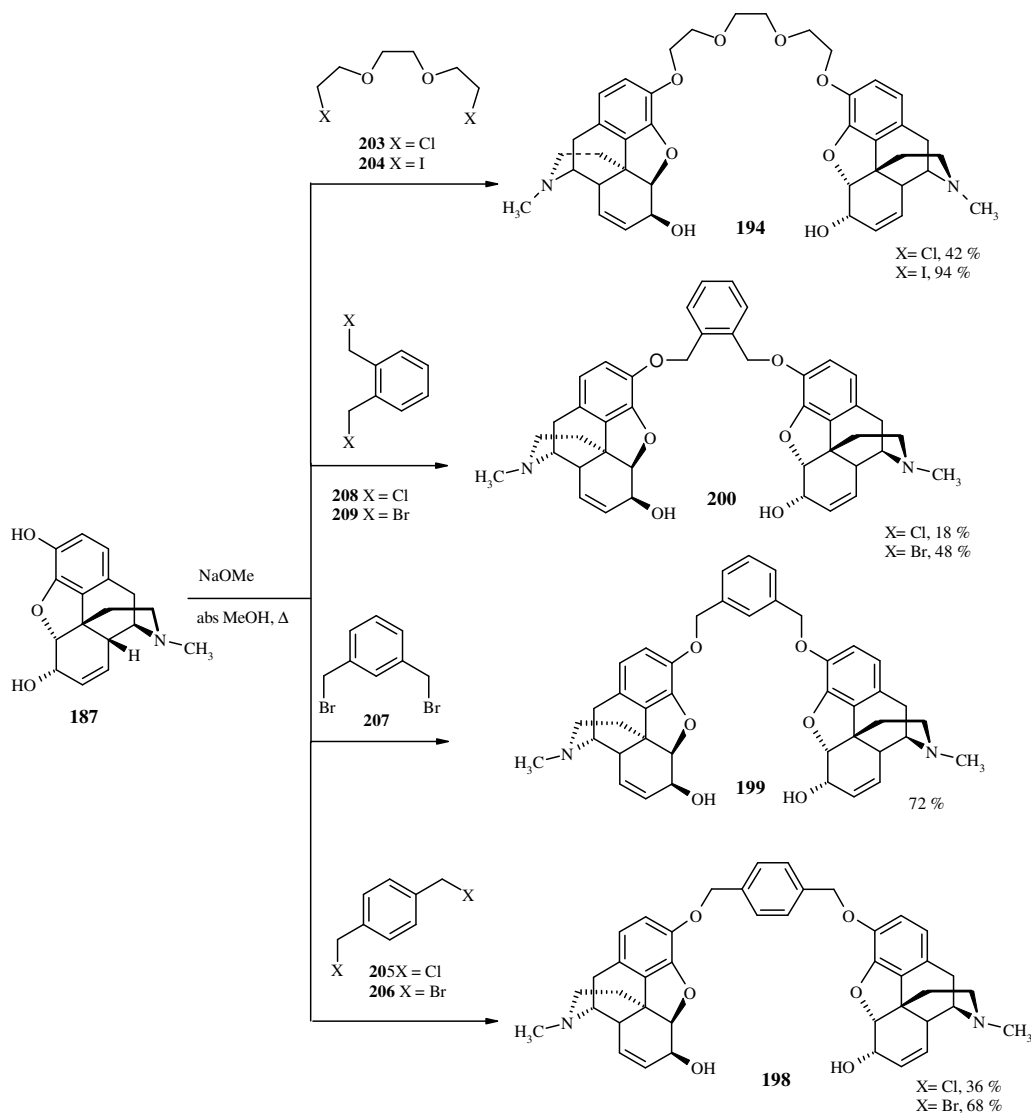


Fig. 4.6 Synthesis of **194**, **198**, **199**, **200**

Likewise, compound **199** was synthesised from morphine hydrochloride and α,α' -dibromo-*m*-xylene **207** then isolated by column chromatography in 72 % yield.

Again the use of alternative bases led to less satisfactory yields, with potassium hydroxide in THF giving 17 %, potassium carbonate in 1,4-dioxane 27 % and sodium carbonate in DMF no product at all.

Compound **200** was also synthesized using the optimum conditions of NaOMe/abs. MeOH and then purified by column chromatography, to give the crystalline macrocyclic precursor in 48 % yield. **200** was again prepared, however, in lower yields (18 %) using α,α' -dichloro-*o*-xylene **208** and sodium carbonate in 1,4-dioxane. Attempts to prepare **202** by reaction in NaOMe and abs MeOH did not succeed, therefore synthesis of intended **202** was repeated, however in boiling THF in the presence of potassium *tert*-butoxide. **202** was isolated by column chromatography in 37 % yield.

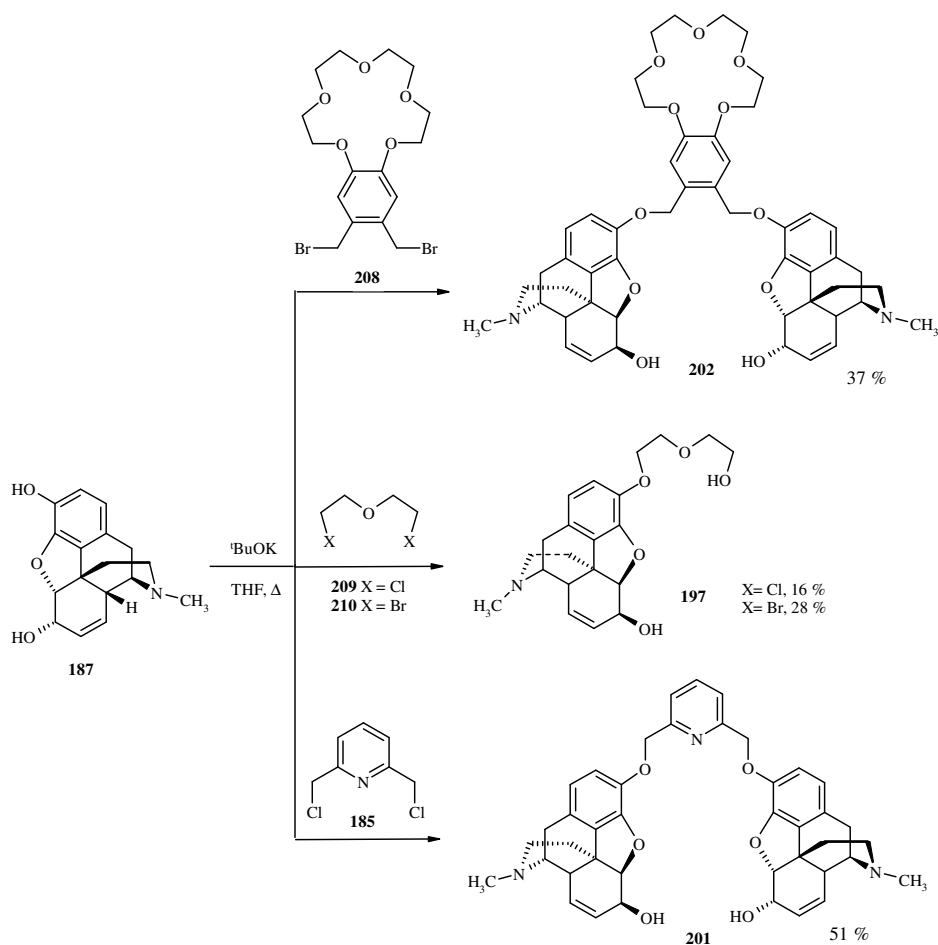


Fig. 4.7 Synthesis of **197**, **201** and **202**

Isolated yields for the preparation of **201** by reaction of morphine and 2,6-*bis*(chloromethyl)pyridine **185** in MeOH and NaOMe were disappointingly low

(12 %). However, the synthesis using t BuOK in THF again proved superior and under these conditions **201** was prepared in 42 % isolated yield after column chromatography. In common with the general pattern, attempts to prepare **211** were undertaken using both NaOMe in abs MeOH and t BuOK in THF, reaction conditions. Both 2-chloroethyl ether **209** and 2-bromoethyl ether **210** were employed, however formation of **211** was not observed.

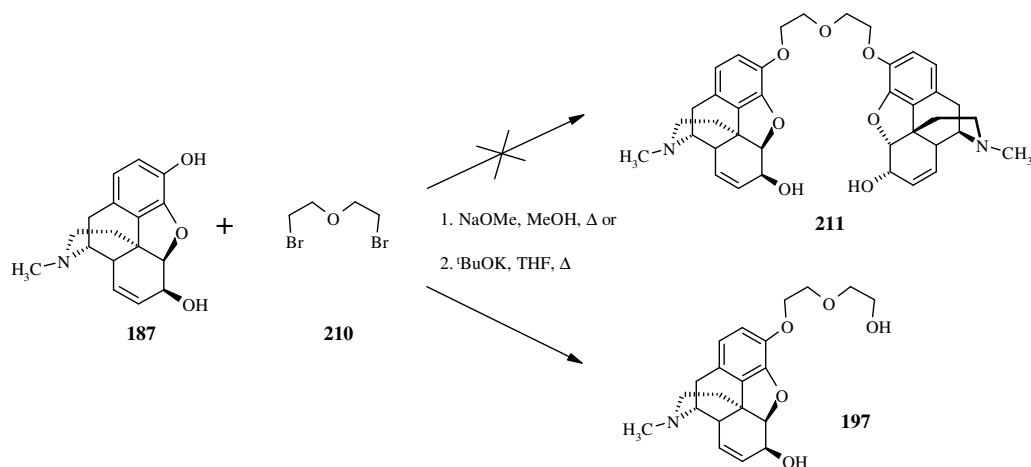


Fig. 4.8 Synthesis of **197**

Instead considerable amounts of **197** were isolated with the higher yields observed when 2-bromoethyl ether **210** replaced 2-chloroethyl ether **209** as the alkylating agent. Furthermore, replacing sodium methoxide with the preferred base t BuOK in refluxing THF increased the yield from 16 to 28 %. Perhaps low quality of the alkylating agent and simultaneous hydrolysis of one of the halide groups was the main reason for the formation of mono-morphineglycol **197**.

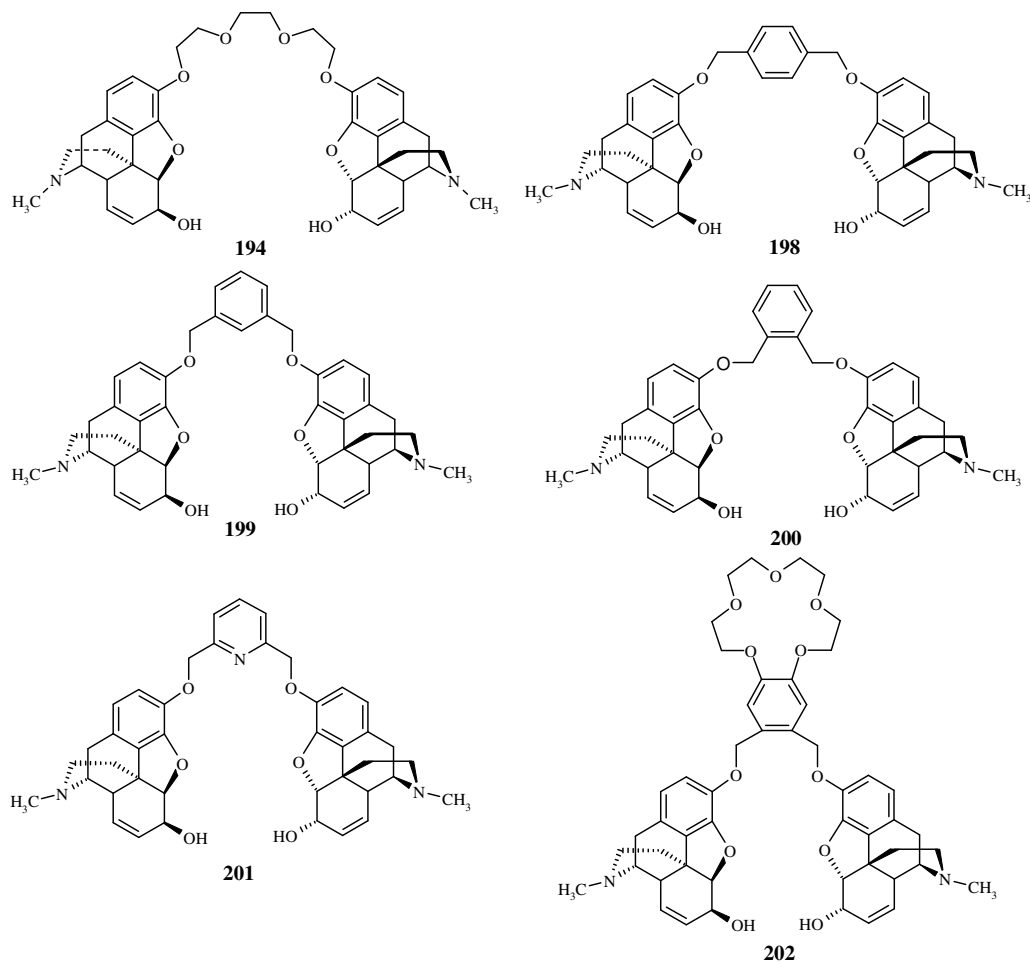


Fig. 4.9 Structures of morphine macrocyclic precursors **194**, **198-202**

All six morphine macrocyclic precursors **194**, **198**, **199**, **200**, **201** and **202**, containing two morphine units in the structures, were prepared by our developed concise synthetic route. The most difficult part was the purification and isolation of the products. Attempts at recrystallization, Soxhlet extraction and conversion of selected structures into their hydrochloride salts to facilitate purification proved unsuccessful and finally every compound was only obtained in a pure form after column chromatography on silica gel, using a DCM/MeOH/NH₄OH mixture. All compounds were identified by ¹H, ¹³C NMR, IR and HRMS.

4.2 Modifications on 6-hydroxyl group of morphine

As has been established codeine and morphine derivatives are favourable from a pharmacological point of view as targets for SAR studies. Another example is morphine 3,6-dinicotinate **213** which shows decreased physical dependence and respiratory depression compared with morphine¹⁴⁴. The synthetic route to 3,6-dinicomorphine **213** and 6-nicocodeine **214** commences with conversion of nicotinic acid into nicotinic chloride **212** with thionyl chloride. After evaporation of excess chlorinating agent, chloroform and pyridine were added to the residue, followed by either morphine or codeine. Depending on the reaction conditions either one, or both of the hydroxyl groups in morphine can be esterified to form either 3,6-dinicomorphine or 3-nicomorphine¹⁴⁵.

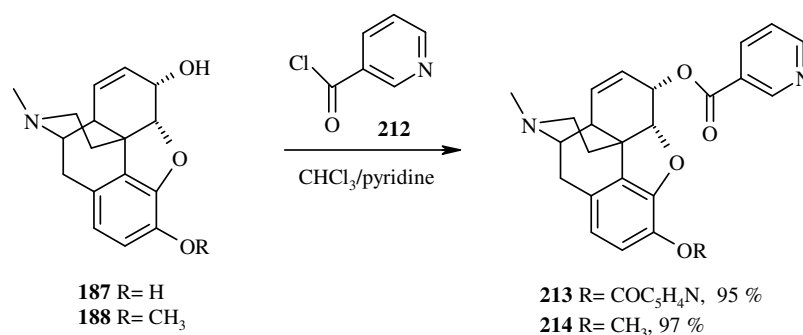
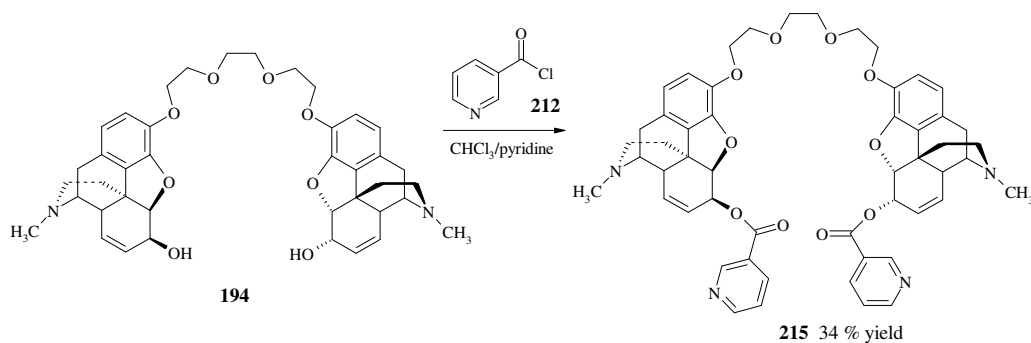


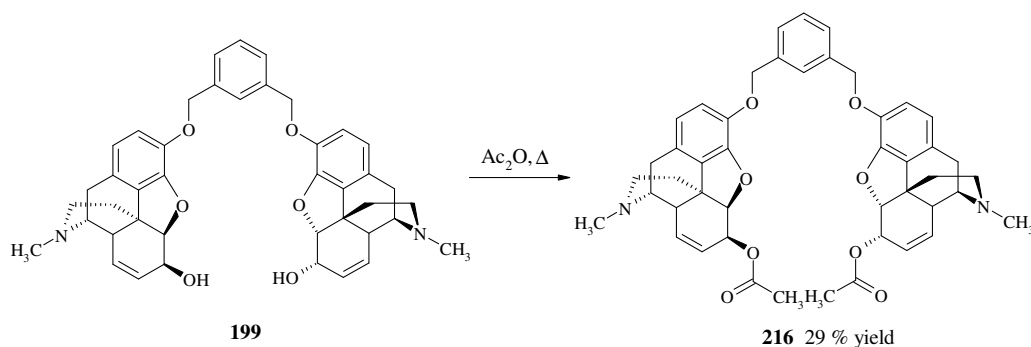
Fig. 4.10 Synthesis of **213**, **214**

Nicotinate of codeine **214** did not show any analgesic activity, however morphine 3,6- dinicotinate **213** proved to have the same analgesic potency as morphine.

In our laboratory compound **213** was prepared according to Hosztafi's procedure in 74 % isolated yield. This encouraged us to employ the same reaction conditions to introduce nicotinyl units onto the secondary alcohol functions of compound **194**.

Fig. 4.11 Synthesis of **215**

In a first step nicotinic chloride **212** was again obtained from nicotinic acid and thionyl chloride and then dry chloroform and dry pyridine were added to the residue and refluxed. While cooling the mixture down 10 °C **194** was added in small portions over 30 min, allowed to warm to RT and then stirred for 16 h. The crude was loaded directly onto a silica column and chromatographed to give **215** as a crystalline solid in 34 % yield. Furthermore, acetylation of **199** with acetic anhydride was also studied and this experiment afforded the product **216** in 29 % isolated yield. These successful experiments encouraged us to investigate alkylating linkers as a means of accessing the target macrocyclic compounds.

Fig. 4.12 Synthesis of **216**

4.3 Preparation of morphine macrocycles

We succeeded with successful synthesis and isolation of four morphine macrocycles (Fig. 4.13). Previously optimized reaction conditions for the ring closure step of the model systems were employed.

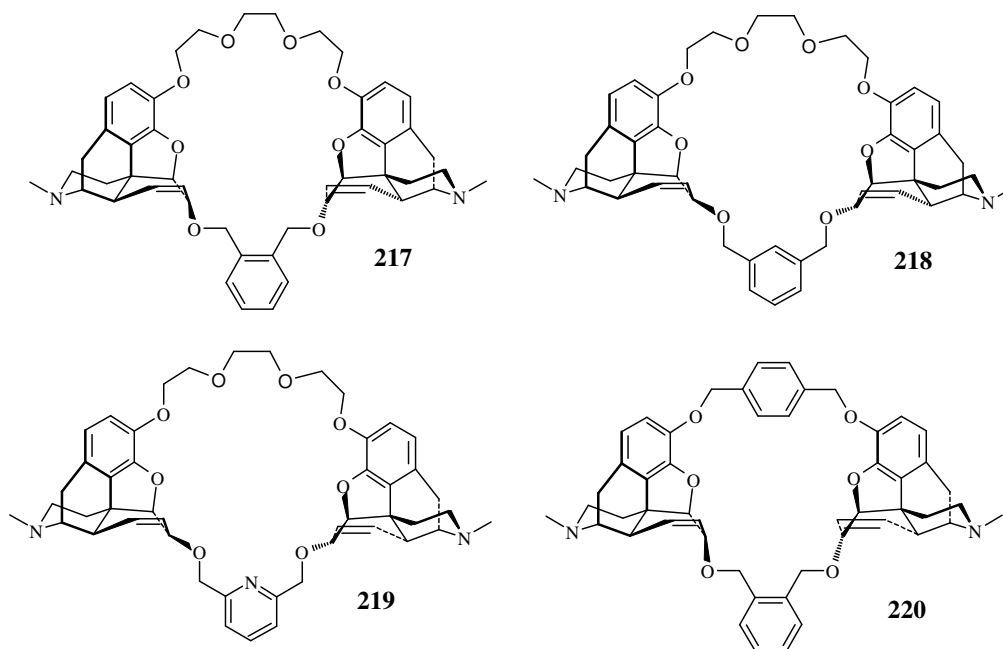


Fig. 4.13 Morphine macrocycles **217-220**

After a series of unsuccessful attempts at ring closure reactions on macrocyclic precursors, it turned out that the success of this reaction largely depends on the choice of the spacer linking the phenol groups. We discovered that macrocyclic precursor **194** with the longer and more likely flexible alkyl linker (dioxaoctane) would accept the shortest spacers between the secondary alcohol functions (*e.g.* *meta*-xylene).

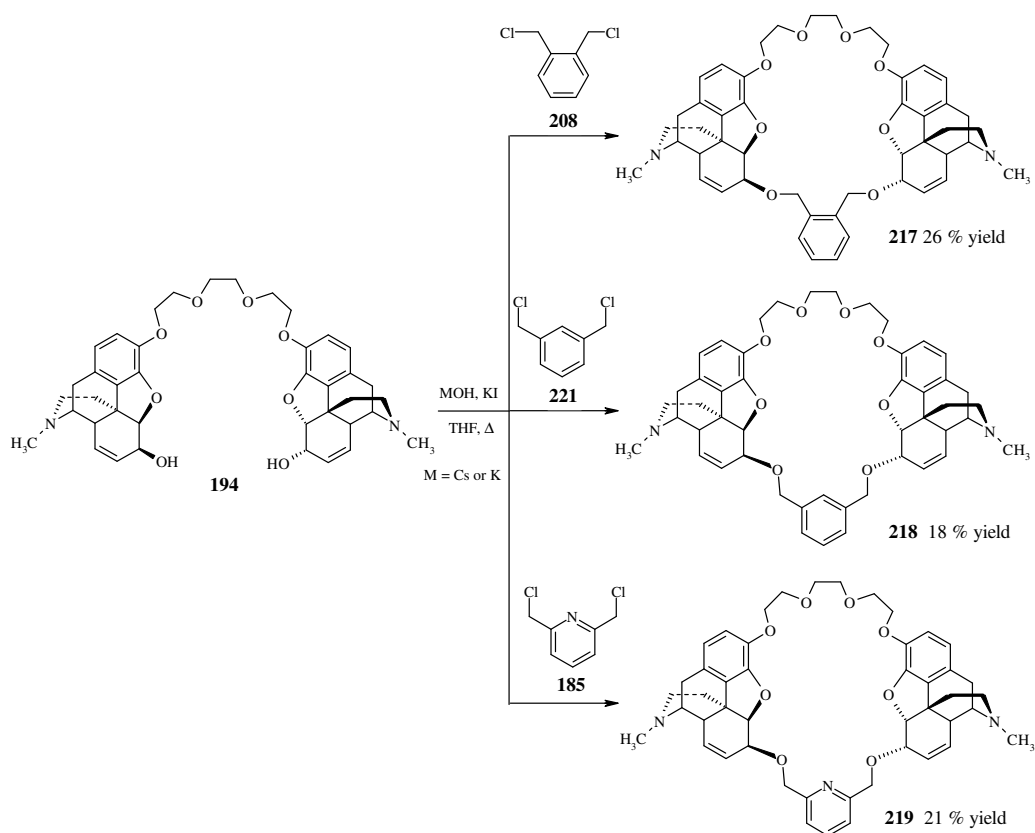


Fig. 4.14 Synthesis of macrocycles **217**, **218**, **219** containing morphine units

Even with such favourable systems, the metal template is still a key factor and successful macrocyclization reactions generally required potassium or caesium hydroxide in refluxing THF. As was already established, morphine open structure **194** containing the longest ethereal chain reacted with α,α' -dichloro-*o*-xylene **208** in the presence of KOH and KI or CsOH and KI to form the target compound **217** in 26% and 17% isolated yields, respectively. The effectiveness of potassium as a template may correspond to the similarity between this molecule and 18-crown-6.

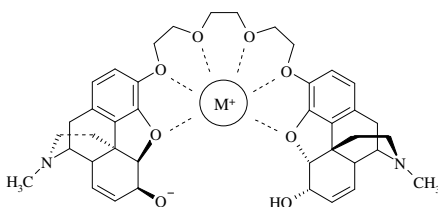


Fig. 4.15 Etheral oxygens of **194** templating metal cation

Identical reaction conditions were applied to the preparation of macrocycle **218**, however this time higher yields were obtained with CsOH as the base, instead of KOH. Purification was carried out by column chromatography to give **218** in 11 % and 18 % yields, respectively. Ring closure of **194** with 2,6-bis-(chloromethyl)pyridine **185** was carried out using various reaction conditions. As shown in Table 4.1 (entries 7-10) formation of the product was not observed using sodium or barium hydroxide. However, macrocycle **219** was successfully isolated from reactions carried out in the presence of KOH or CsOH in 13 % and 21 % yields, respectively. The most difficult macrocycle to synthesise was **220**, which is derived from macrocyclic precursor **198** which incorporates a *para*-xylene spacer. As a result it is less flexible than the polyetheral chain in **194**, which possibly resulted in the relatively low isolated yields for **220** (Table 4.1, entries 11,12).

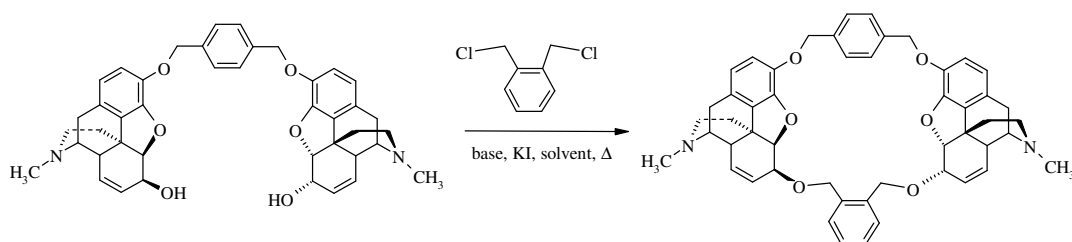


Fig. 4.16 Synthesis of morphine macrocycle **220**

Entry	Compound	Base	Additive	Solvent	Temp [°C]	Yield [%]
1	217	NaOH	NaI	THF	64	0
2	217	KOH	KI	THF	64	26
3	217	CsOH	KI	THF	64	17
4	218	KOH	KI	THF	64	11
5	218	CsOH	KI	THF	64	18
6	218	Ba(OH) ₂	KI	THF	64	0
7	219	NaOH	NaI	THF	64	0
8	219	KOH	KI	THF	64	13
9	219	CsOH	KI	THF	64	21
10	219	Ba(OH) ₂	KI	THF	64	0
11	220	KOH	KI	THF	64	17
12	220	CsOH	KI	THF	64	9

Table 4.1 Reaction conditions for preparation of morphine macrocycles **217-220**

At the beginning of this chapter it was hypothesised that morphine macrocycles can be successfully synthesised under the condition that the linkers connecting the two morphine structures should differ in terms of length and flexibility. To support this conclusion a series of negative results from ring closure experiments are recorded (Table 4.2-4.6).

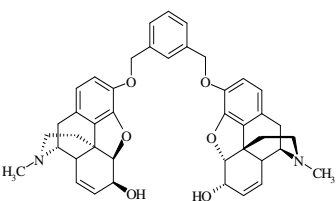
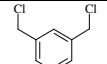
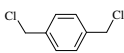
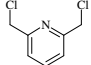
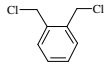
Open structure	Alkyl linker	Base/additive	Solvent	Yield [%]
		KOH/KI	THF	0
		CsOH/KI	THF	0
		CsOH/KI	THF	0
		KOH/KI	THF	0

Table 4.2 Attempted preparation of morphine macrocycles from **199**

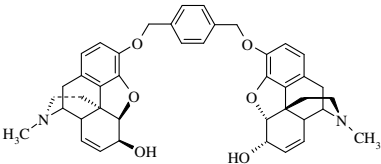
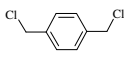
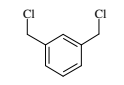
Open structure	Alkyl linker	Base/additive	Solvent	Yield [%]
		KOH/KI or CsOH/KI	THF	0
		KOH/KI or CsOH/KI	THF	0

Table 4.3 Attempted preparation of morphine macrocycles from **198**

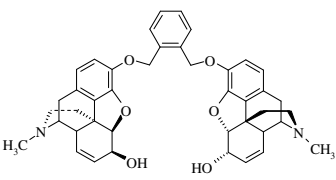
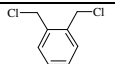
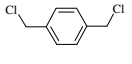
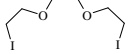
Open structure	Alkyl linker	Base/additive	Solvent	Yield [%]
		KOH/KI or CsOH/KI	THF	0
		KOH/KI	THF	0
		CsOH/KI	THF	0

Table 4.4 Attempted preparation of morphine macrocycles from **200**

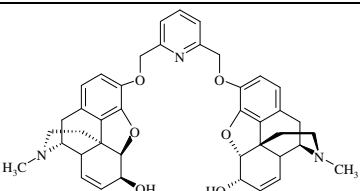
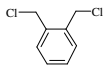
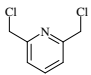
Open structure	Alkyl linker	Base/additive	Solvent	Yield [%]
		KOH/KI	THF	0
		KOH/KI	THF	0

Table 4.5 Attempted preparation of morphine macrocycles from **201**

Attempts to prepare morphine macrocycles (Table 4.2-4.5) were carried out in boiling THF in the presence of potassium or caesium hydroxide and potassium iodide, according to the usual protocol, without success. All the reaction conditions and working procedures were identical to those undertaken for the synthesis of **217-220**, therefore we believe the reason for the lack of cyclization may be the rigidity of the morphine moiety.

The approach of introducing a propylene chain into **194** failed because of the competing elimination reaction which occurs, yielding product **222** in 19 % isolated yields. The reaction was carried out as in the previous cases, using potassium hydroxide and potassium iodide in boiling THF.

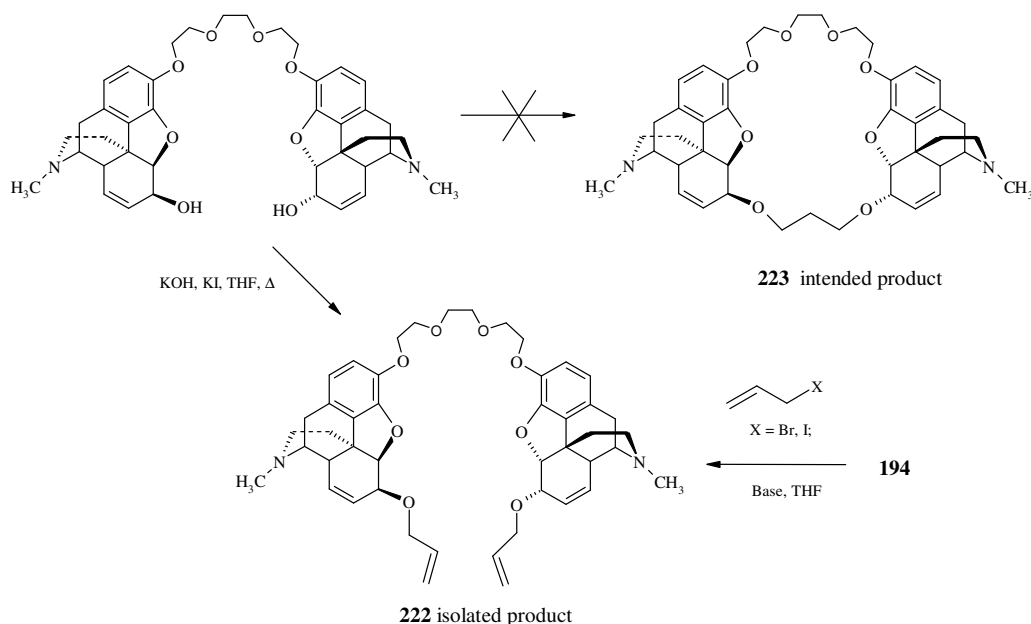


Fig. 4.17 Synthesis of **222**

Instead of the desired macrocyclic structure **223**, the compound allylated on the secondary alcohol groups **222** was identified. This occurrence motivated us to attempt a ring closure reaction by olefin metathesis using Grubbs catalyst¹⁴⁶, therefore **222** was prepared in larger quantities by a more practical method. **222** was preferably synthesised by treating **194** with allyl bromide or allyl iodide in the presence of potassium hydride in THF at -20 °C. Higher yields were observed with allyl iodide. However, in refluxing THF and potassium hydroxide alkylation with allyl bromide proved to proceed more smoothly. In the best case, **222** was isolated in 37 % yield (Table 4.6).

Entry	Alkylating agent	Base	solvent	Temp [°C]	Isolated yield [%] 222
1	Allyl bromide	KH	THF	-20 to RT	16
2	Allyl bromide	KOH	THF	66	24
3	Allyl iodide	KH	THF	-20 to RT	37
4	Allyl iodide	KOH	THF	66	12

Table 4.6 Reaction conditions for preparation of **222**

Attempt of ring closure by an olefin metathesis reaction on **222** employing 1st ¹⁴⁷ and 2nd generation Grubbs catalysts ¹⁴⁸.

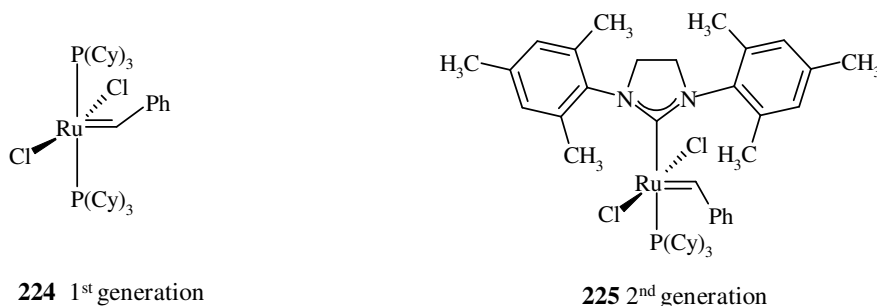


Fig. 4.18 1st and 2nd Generation of Grubbs catalysts **224** and **225**

Despite our efforts to perform this reaction under a variety of conditions, including refluxing in toluene and xylene with a stream of nitrogen to remove ethylene gas and shift the equilibrium, formation of the product was not observed in any case.

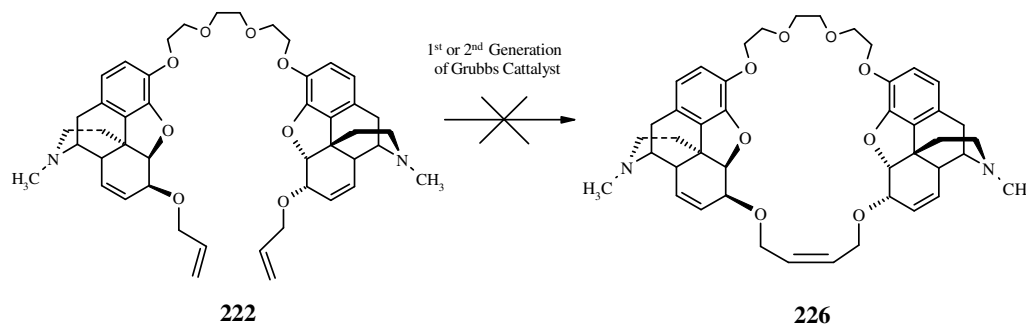


Fig. 4.19 Attempt of ring closure by metathesis on **222**

Synthesis of **226** using ring closure metathesis (RCM) was attempted using the 1st Generation Grubbs catalyst **224** in various solvents at molar concentrations of 5-

10 mol%. First 1 mmol of **222** and 5 mol% of **224** was stirred under nitrogen in DCM at 40 °C for 2 days with no conversion of starting material. Next, **222** with 10 mol % catalyst loading in 1,2-dichloroethane (b.p. 84 °C) and then toluene (b.p. 110 °C) were investigated as solvents because they have higher boiling points that might promote the reaction. However, no success was achieved using Grubbs type I. It was then decided to perform trials using the 2nd generation Grubbs catalyst **225** since it has been reported to be more useful in macrocyclization reactions¹⁴⁹. Reactions in four different solvents were screened, dichloromethane, 1,2-dichloroethane, toluene and *para*-xylene (b.p. 138 °C). In each case the reaction was refluxed under a stream of nitrogen to drive off ethylene and shift the equilibrium towards the product, but nevertheless in no case was macrocyclization achieved. In cases where the reaction temperature was below 100 °C starting material was recovered from the reaction mixture, whereas in synthesis performed at 105-110 °C only degradation of starting material was observed.

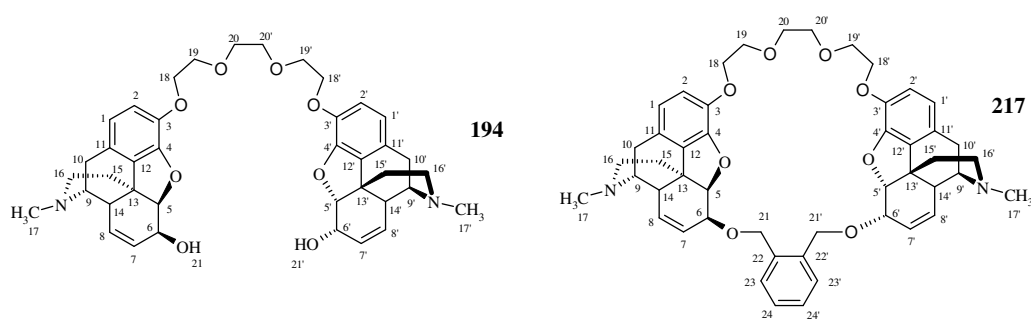
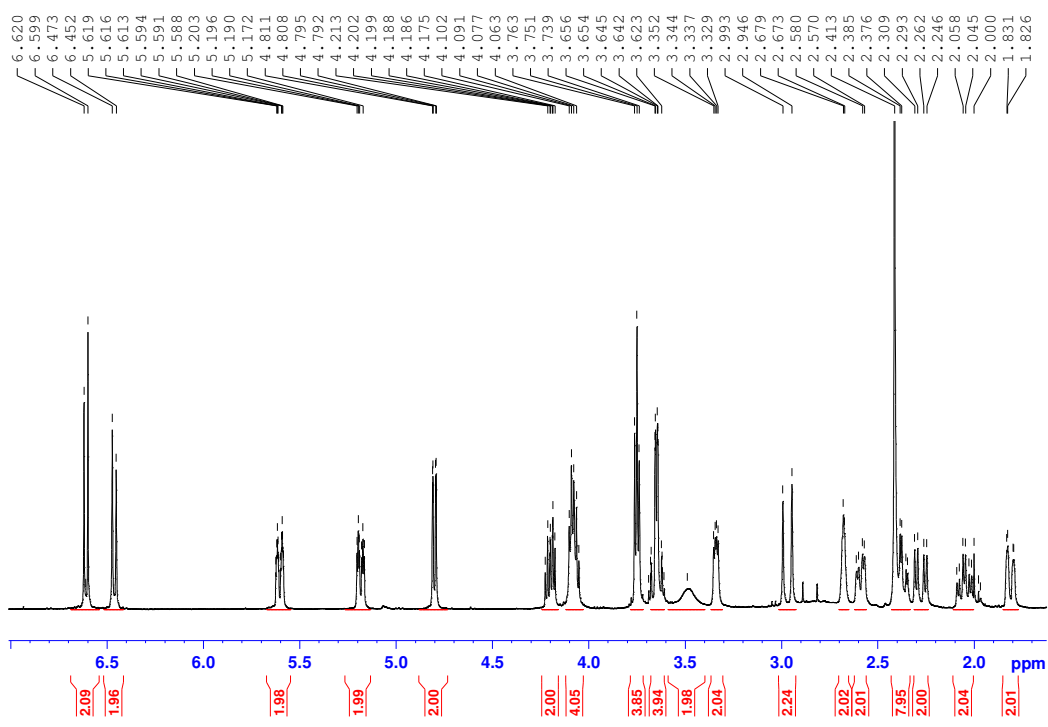
4.4 Spectroscopic discussion on morphine macrocycles

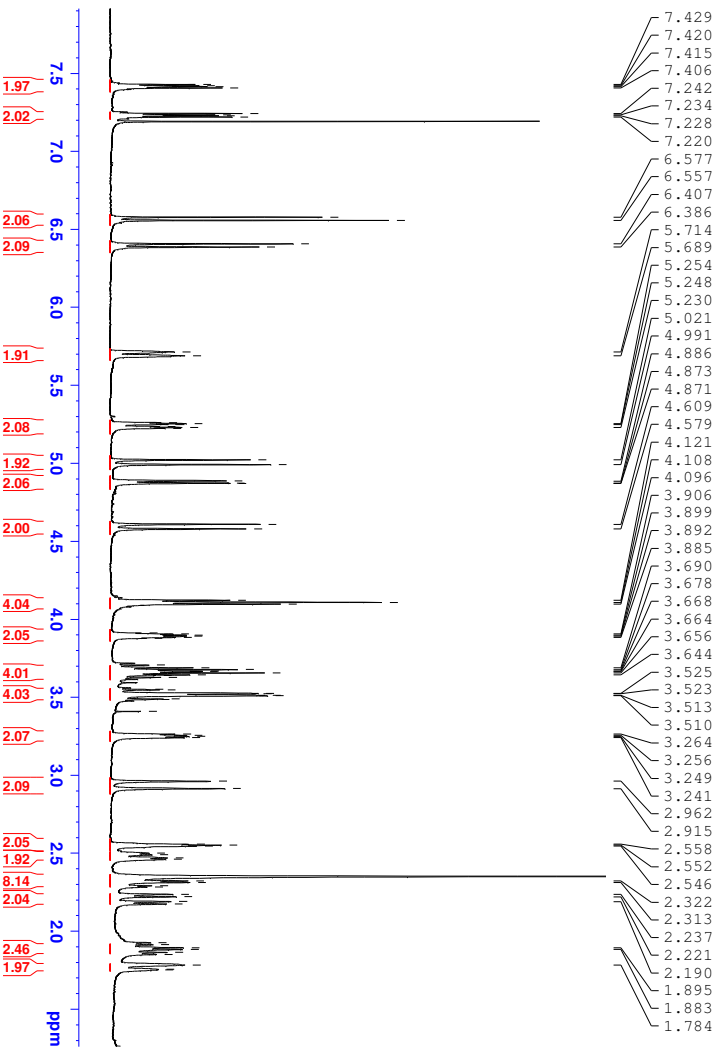
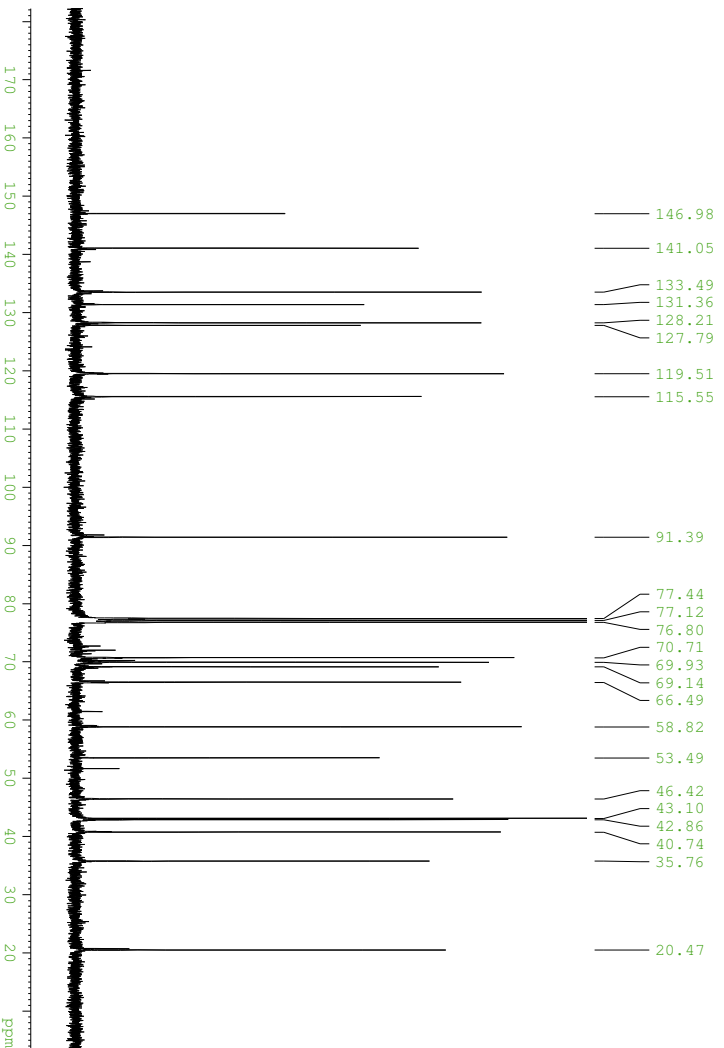
4.4.1 NMR study of **194** and its macrocycles **217** and **218**

As expected from a chiral scaffold, the ^1H NMR spectra of the macrocycles and their precursors containing the morphine moiety is more complex than for analogous model macrocycles. In the ^1H NMR spectrum of **194** the protons of the morphine moiety gave resonances identical to those reported for morphine¹⁵⁰. **194** is the phenoxy-linked morphine open structure, which has been used for the synthesis of novel morphine macrocycles **217**, **218** and **219**. The ^1H NMR spectrum of the morphine macrocyclic precursor **194** and macrocycle **217** are shown in Fig. 4.21 and Fig. 4.22, respectively. Protons 18,18' in **194** appear as a two doublets of double doublets at δ 4.22 and δ 4.10, with J values of 10.8, 5.2 and 1.2 Hz and these values could be calculated only for the first signal since the second one overlapped with the 6,6' protons of the morphine moiety. This multiplicity is due to the diastereotopic nature of these protons and is a result of geminal coupling between the two 18,18' hydrogens and further coupling between 18,18' and the adjacent hydrogens, 19,19'. The signal from the hydrogens 20, 20' which also exhibit diastereotopicity, appear at δ 3.69 as two doublets of double doublets which overlap with one another, therefore exact calculation of the coupling constants was not possible.

In the spectrum of **217** the appearance of protons in the ethereal chain has slightly changed, compared with **194**. Specifically, the protons of 18,18' in **217** appear as a triplet with a J value of 5.0 Hz, whereas protons 19,19' which resonate as a triplet at δ 3.76 ppm with a J value of 4.8 Hz in **194**, in **217** appear as a multiplet in the range δ 3.72-3.64. Protons 20,20' at δ 3.56 are also diastereotopic and appear as two doublets of double doublets overlapping one another.

The aromatic protons of the *ortho*-xylene unit (23,23',24,24') in **217** appear as double doublets at δ 7.43 and δ 7.24 with coupling constants of 5.6 and 3.6 Hz, respectively. Additional peaks arise from the xylene unit, in which the benzylic methylene groups appear as two individual doublets at δ 5.02 and δ 4.61 with coupling constants of 12.0 Hz. These protons (21,21') are diastereotopic and therefore appear as two individual doublets, a consequence of their mutual coupling.

Fig. 4.20 Morphine macrocycle **217** and its precursor **194**Fig. 4.21 The ^1H NMR spectrum of **194**

Fig. 4.22 The ¹H NMR spectrum of 217Fig. 4.23 The ¹³C NMR spectrum of 194

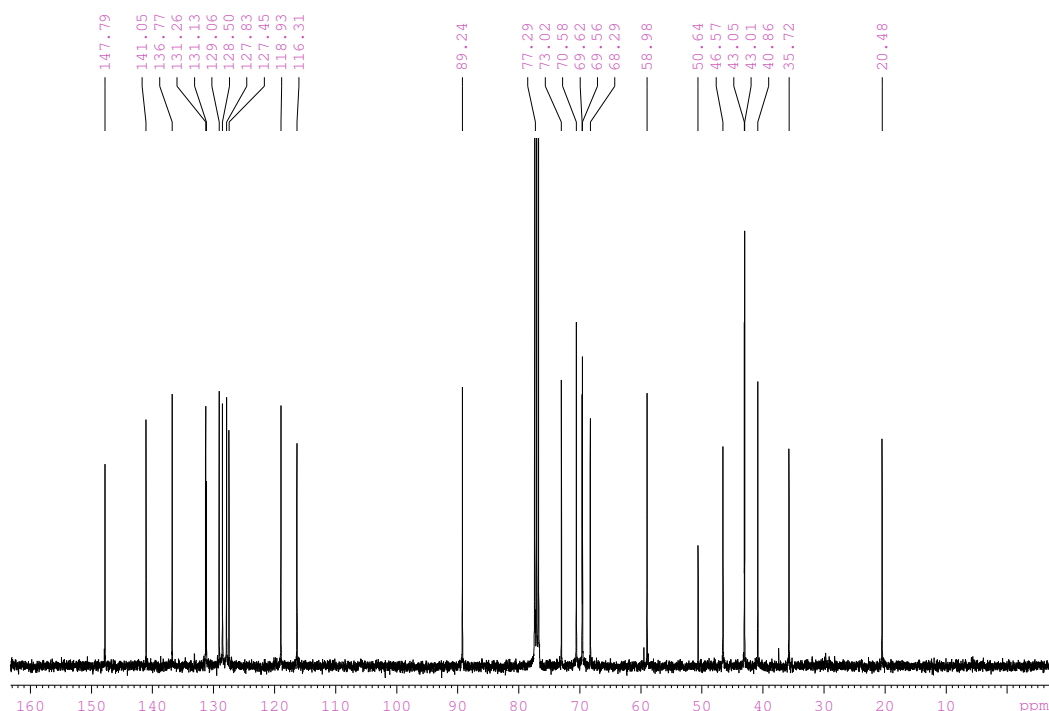


Fig. 4.24 The ^{13}C NMR spectrum of **217**

The ^{13}C NMR spectra of **194** and **217** are depicted in Fig. 4.23 and Fig. 4.24. The resonance for the ethereal chain in **194** and **217** carbons also appear at very similar chemical shifts, however the order of appearance of ethereal carbons in **194** is 20, 20' (at δ 70.71), 19,19' (at δ 69.93) and 18,18' (at δ 69.14), whereas in **217** this arrangement has changed, with 18,18' appearing at a higher chemical shift (δ 69.77) than 19,19' at δ 69.54. The main difference in shifts between those two structures was observed for carbons 6, 6' in the morphine moiety. In the spectrum of **194** 6,6' appears at δ 66.49 whereas in **217** it is shifted downfield to δ 73.07. Furthermore, the peaks related to the *ortho*-xylene ring differentiated these two spectra. The *ortho*- and *meta*-CH in the xylene ring (24,24' and 23,23') in **217** appear at δ 128.53 and δ 127.54 respectively, whereas the quaternary aromatic carbons 22,22' resonate at δ 136.79. The secondary benzylic methylene carbons 21,21' appear at δ 68.29.

In the ^1H NMR spectrum of the morphine macrocycle, **218** (Fig. 4.26) the isolated aromatic hydrogen of *meta*-xylene (25) appears as a singlet at δ 7.34 integrating to one proton, whereas aromatic protons 23,23' and 24 resonate as a multiplet integrating to 3 protons at δ 7.23-7.18. The protons of the benzylic methylene group appear as two individual doublets at δ 5.55 and δ 4.84, each with a coupling constant value of 11.4 Hz. This coupling is due to the diastereotopic nature of these protons

and corresponds to a coupling between the two methylene protons. In **194** the protons 18,18' appear as two doublets of double doublets, whereas in **218** their appearance is still more complex, and they resolve as a multiplet, absorbing in the range δ 4.15-4.07. Furthermore, protons 19,19' which appear as a triplet at δ 3.76 in **194**, appear as a multiplet in **218** at a chemical shift from δ 3.65-3.55. Protons 20,20' appear as a singlet at δ 3.42 integrating to 4 protons, in contrast to the corresponding protons in **194** which exhibit chemical non-equivalence.

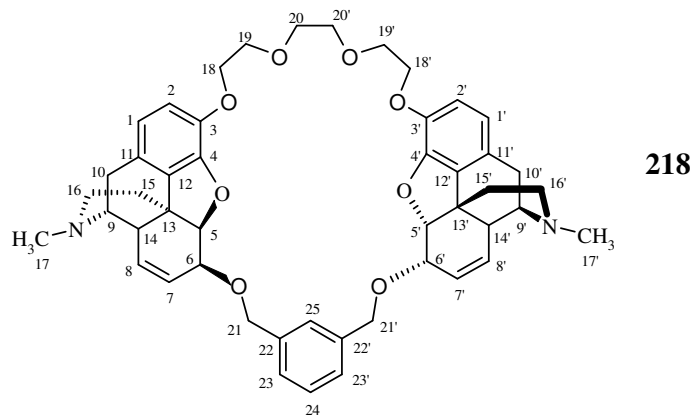


Fig. 4.25 Morphine macrocycle **218**

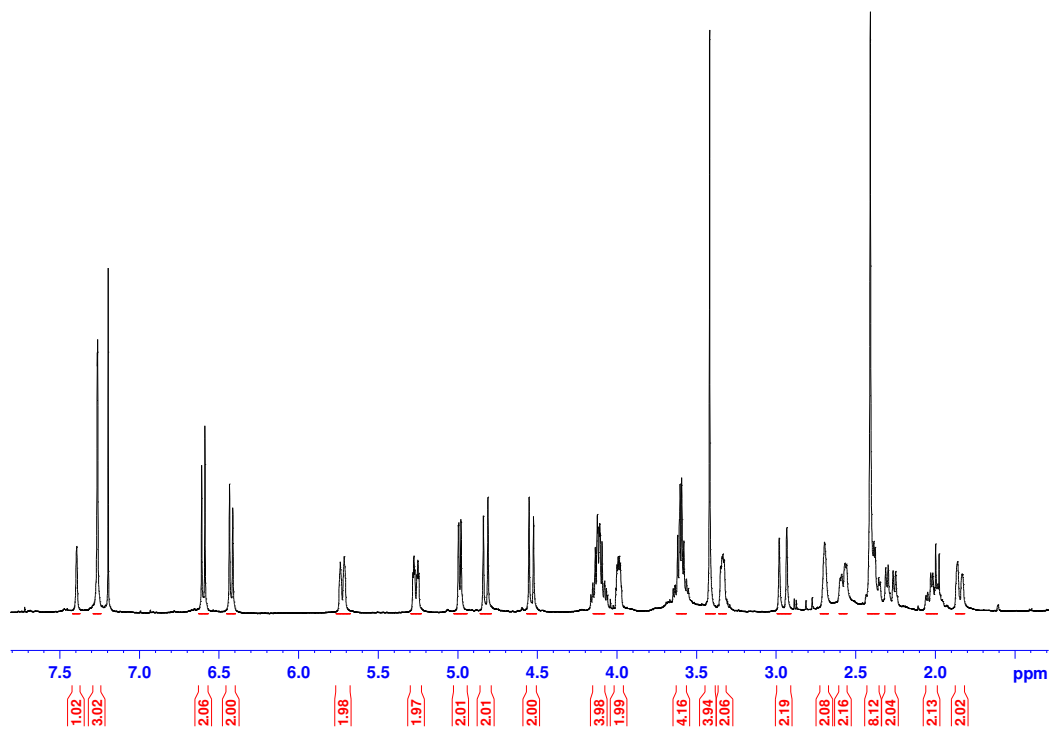


Fig. 4.26 The ^1H NMR spectrum of **218**

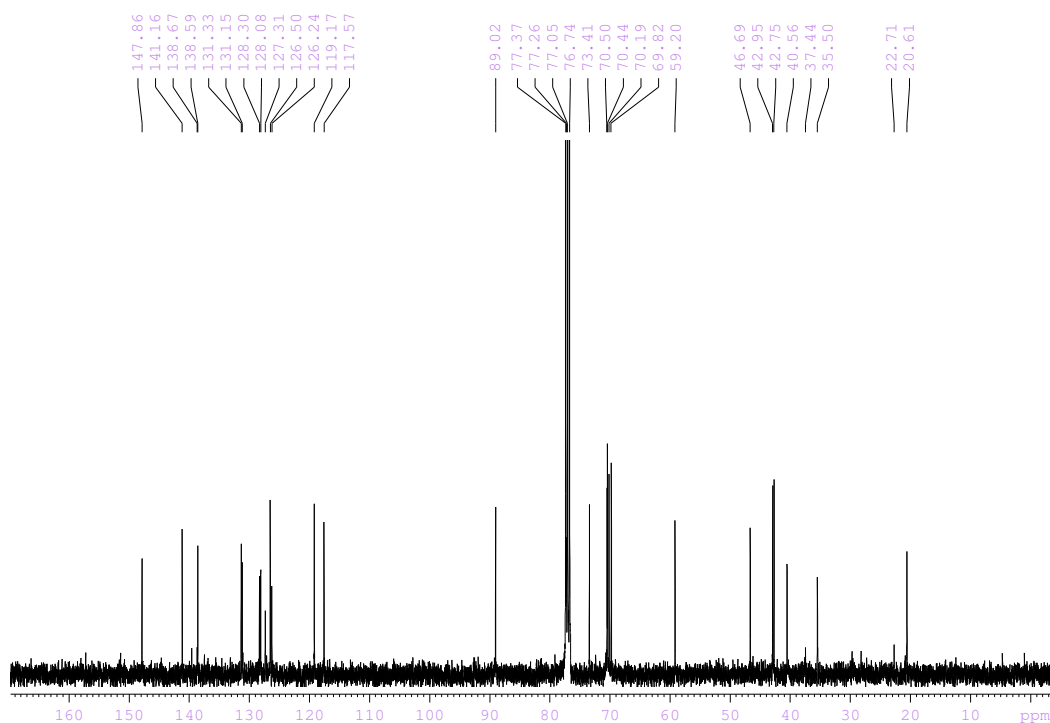


Fig. 4.27 The ^{13}C NMR spectrum of **218**

In the ^{13}C NMR spectrum (Fig. 4.27) of **218** signals appear in the aromatic region due to the quaternary carbons of the *meta*-xylene ring (22,22'), resonating as a peak of double intensity at δ 138.59. At higher field, peaks of single intensity assigned to aromatic CHs 24 and 25 appear at chemical shifts of δ 127.31 and δ 126.24, respectively. Finally the signals for the tertiary aromatic carbons 23,23' resonate at δ 126.50. Benzylic methylene carbons (21,22') resonate at δ 70.44 and are shifted downfield compared with the signal of the corresponding carbons in **217** (δ 68.29). The carbons of 6,6' in **194** appear at δ 66.49, whereas the corresponding carbons in **218** are shifted downfield and can be seen at δ 73.41. In **218** remaining ethereal carbons appear at δ 70.50 for 20,20', at δ 70.19 for 18,18' and at δ 69.82 for 19,19' as peaks of double intensity.

4.5 Conclusion

The synthesis and structural characterization of a series of macrocyclic structures and their precursors with morphine moiety has been carried out.

Synthesis of macrocyclic precursors with two morphine units have been developed and reaction conditions were optimised, therefore designed opens structures were prepared in moderate to high yields. Each of the phenol linked morphine open structures were synthesised for further employment in the synthesis of morphine macrocycles. Metal binding studies were carried out on each of the successfully synthesised and isolated phenol linked morphine open structures with a variety of metal ions. Ring closure reactions by introducing *ortho* and *meta*-xylenes and *bis*-(2,6-methyl)pyridine linkers was achieved by employing potassium and caesium hydroxides under high dilution conditions in boiling THF. The purpose of the base was to deprotonated the secondary alcohol group to generate an alkoxide while the metal template may serve to orient the reactive groups close to one another and lower the free energy of activation for the entropically disfavoured end-to-end cyclization.

On the basis of the limited available evidence, it would appear that to facilitate cyclization of morphine macrocycles a small linker (*e.g.* *ortho*-xylene) is required to link the secondary alcohols in morphine macrocyclic precursor. This situation contrasts with reactions carried out on the more flexible 2-(2-hydroxyethoxy)phenol moiety which facilitates introduction of a variety of alkyl linkers that could not be incorporated into the *bis*-morphine macrocycle precursor. This experiment data can now be used to assist with future molecular modelling studies in the group, since computer modelling was not the remit of this PhD.

Firstly the aims of the project with this group of compounds were achieved, especially as the synthesis of these novel structures had not been reported previously. Secondly when we consider the properties of these species and their potential applications as analgesic compounds, P-gp inhibitors and chiral ligands in asymmetric catalysis it opens numerous possibilities for future work.

An advantage of preparing morphine macrocycles is that they may have applications as chiral ligands for asymmetric synthesis. Moreover, morphine's three-dimensional rigid structure could then increase the likelihood of preferential binding of chiral guests. Furthermore, the rigid chiral structure may impart chirality onto the products

in any potential catalysed reactions, controlling stereoselectivity of the reaction, *i.e.* increase the enantiomeric excess of either the *R* or *S* enantiomer.

5 Crystallographic studies

An understanding of the interactions in the crystals of a potential ion receptor can provide valuable information on the bonding mode and binding sites of “host” molecule in solution studies¹⁵¹. The crystallographic analysis of therapeutic compounds has also proven invaluable to chemists and biologists in understanding the key binding sites and modes of action of these therapeutic agents¹⁵². From the X-ray crystallographic analysis of the macrocyclic structures **179** and **184** and their precursors **160**, **161**, **163-166** the cavity sizes of the cyclic species were estimated using Mercury 1.4.2 software. These data were based on solid state and it must be emphasised that the macrocycles and their precursors may undergo significant conformational changes when in solution or when binding to guest species. However the X-ray data regarding the cavity size of the macrocycles can be used to estimate which of the guest species might have a significant chance of binding to the macrocycle. In this project the guest species of interest are metal cations. The full data for each of the compounds is specified in the appendix A. By comparing trends in X-ray data with actual trends of metal cation binding this may lead to a more accurate predictive model for future work.

5.1 Structural studies of macrocycle **179**

Crystals suitable for single crystal X-ray crystallographic determination of **179** were grown by slow evaporation from chloroform : hexane (4:1), yielding colourless block shaped crystals of m.p.=159-161 °C. Selected bond distances and angles of non-hydrogen atoms are given in Table 5.1 and Table 5.2. Figure 5.2 shows perspective views of the crystal structure with the atomic numbering.

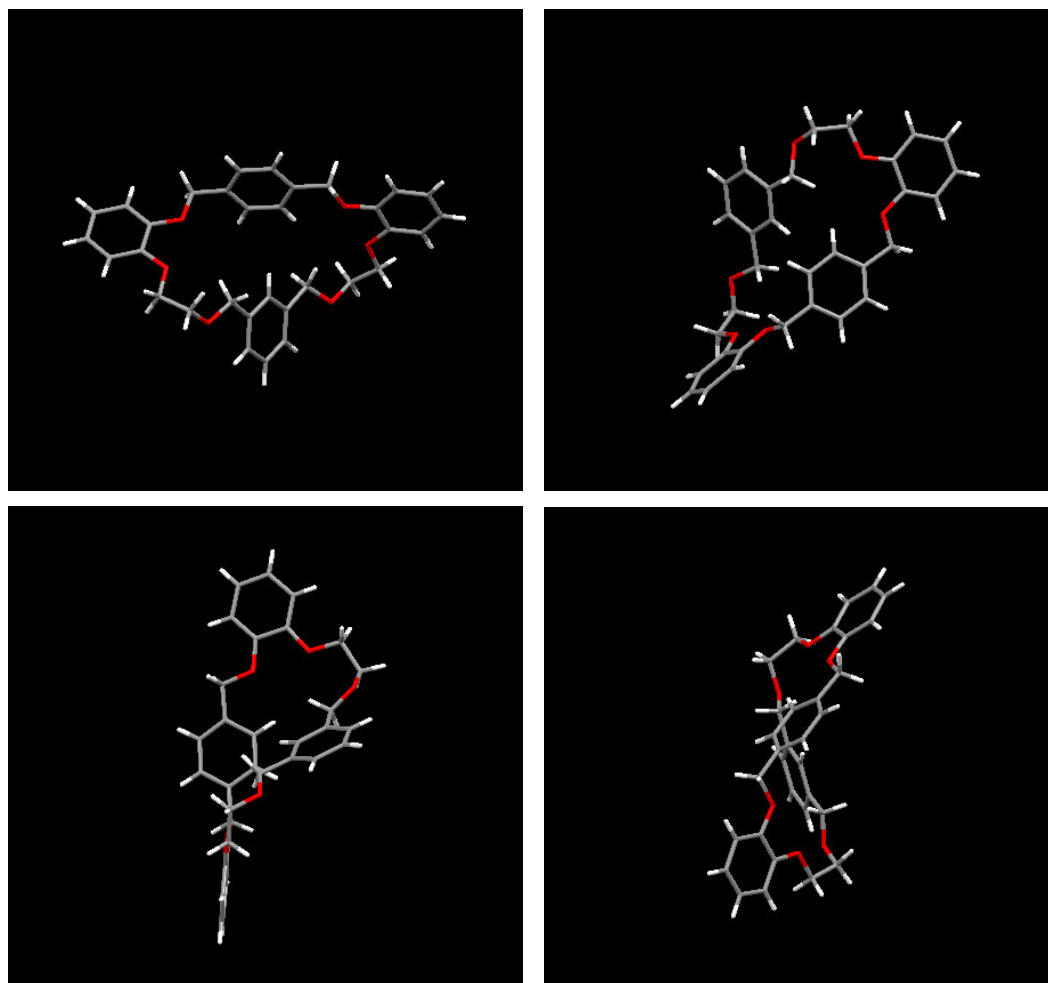


Fig. 5.1 X-ray structure of **179**

The presence of the four six member rings deformed the structure, severely restricting the flexibility commonly recognized for ethereal aliphatic crown ethers. The structure takes on the form of a flattened and slightly deformed ellipsoid.

Bond distances	
C(7)–C(8)	1.468(10)
C(11)–C(14)	1.480(10)
C(14)–O(3)	1.404(8)
O(2)–C(7)	1.421(9)
O(3)–C(15)	1.359(9)
C(6)–O(2)	1.360(8)
O(5)–C(23)	1.365(8)

Bond angles	
C(6)–O(2)–C(7)	117.4(6)
O(2)–C(7)–C(8)	106.7(6)
O(3)–C(14)–C(11)	108.1(6)
C(23)–O(5)–C(22)	113.8(6)
O(6)–C(30)–C(28)	110.9(6)
C(30)–O(6)–C(31)	113.9(5)

Table 5.1 Selected bond distances [Å] angles [°] for **179** with estimated standard deviations

O(2)–C(7)–C(8)–C(13)	84.7(9)
C(12)–C(11)–C(14)–O(3)	2.3(10)
O(5)–C(23)–C(24)–C(29)	157.0(7)
C(29)–C(28)–C(30)–O(6)	166.7(6)

Table 5.2 Selected torsion angles [°] for **179**

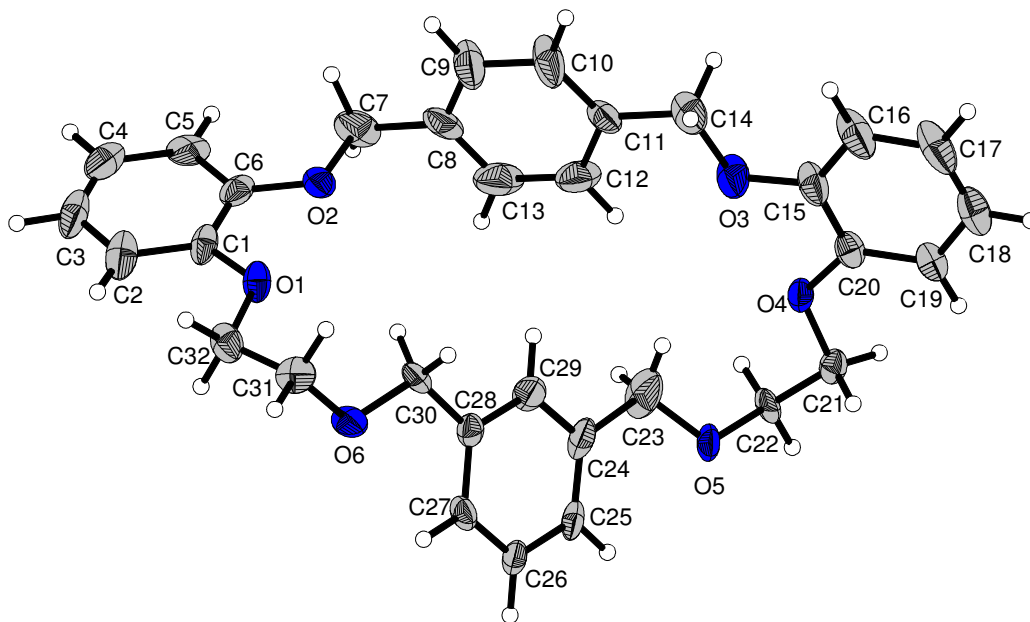


Fig. 5.2 X-ray crystal structure of 2,3,6,9,12,13,19,21-tetrabenzo-1,4,11,14,17,23-hexaoxacyclopentaicosa-2,6,7,8,12,19,20-hexaene, **179**

2-O6	O3-O5	O2-O4	O2-O5	O3-O1	O3-O6	C7-30	C14-23
4.67	4.71	8.19	7.85	8.16	7.83	5.11	5.46

Table 5.3 Dimensions of the cavity of compound **179**

Macrocycle **179** crystallizes in the monoclinic space group $P2_1/n$ with four independent molecules per asymmetric unit. The bond length for C(7)–C(8) is 1.468 Å and for C(11)–C(14) is 1.480 Å, whereas for O(2)–C(7) it is 1.421 Å and for C(14)–O(3) the bond length is slightly shorter at 1.404 Å. Bonds C(6)–O(2) and O(3)–C(15) are almost the same distances at 1.360 Å and 1.359 Å respectively. The angle for O(2)–C(7)–C(8) is 106.7° and is close to O(3)–C(14)–C(11) angle of 108.1°. However, torsion angles for O(2)–C(7)–C(8)–C(13) and C(12)–C(11)–C(14)–O(3) are 84.7° and 2.3° respectively. This gives an indication that the compound is not completely symmetrical in the solid state. However, torsion angle values associated with the *meta*-xylene unit are similar and equal 166.7° for C(29)–C(28)–C(30)–O(6) and 157.0° for O(5)–C(23)–C(24)–C(29).

5.2 Structural studies of macrocycle **184**

Macrocycle **184** containing two pyridine rings, with four aromatic rings in total is conformationally quite rigid. It is clearly depicted in Fig. 5.3 that the pyridine rings are almost perpendicular to each other, essentially shielding one side of the macrocycle, creating a potential binding pocket. Crystals suitable for single crystal X-ray crystallographic determination of **184** were grown from chloroform by slow solvent evaporation, yielding colourless block shaped crystals of m.p.=145-147 °C.

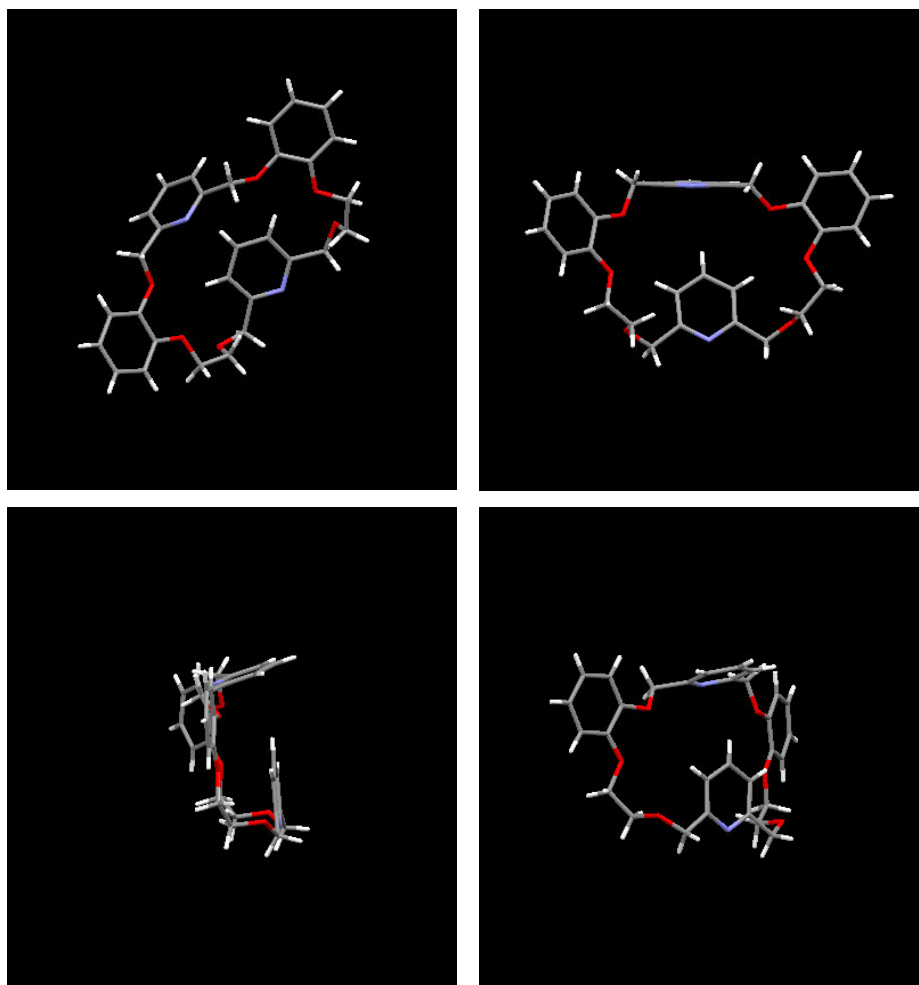


Fig. 5.3 X-ray structure of **184** visioned in Mercury 1.4.2

Macrocycle **184** crystallizes in the monoclinic space group $P2_1/n$ with two independent molecules per asymmetric unit. The bond length for O(1)–C(7) is 1.376 Å which is slightly longer than the C(29)–O(6) which equals 1.360 Å, however both are shorter than C(14)–O(3) and O(4)–C(22) which are 1.410 Å and 1.406 Å respectively. A similar correlation which highlights the influence of the aromatic rings was observed for bonds C(5)–C(6), 1.473 Å and C(1)–C(30) 1.499 Å. These are slightly shorter than the corresponding bonds on the other pyridine ring C(15)–C(16), 1.507 Å and C(20)–C(21), 1.508 Å. The angles for O(1)–C(6)–C(5) and O(6)–C(30)–C(1) display close values which are 110.5° and 108.2° respectively, and the angles for C(7)–O(1)–C(6) 118.0° and C(29)–O(6)–C(30) 119.6° are also similar. The angle of O(3)–C(15)–C(16) is 112.8 and is identical to O(4)–C(21)–C(20), while C(14)–O(3)–C(15) and C(22)–O(4)–C(21) differ slightly at 111.5° and 113.4°.

The torsion angles for C(5)–C(6)–O(1)–C(7) and C(29)–O(6)–C(30)–C(1) are 174.9° and 145.4° respectively, whereas C(6)–O(1)–C(7)–C(8) is 15.4° and C(28)–C(29)–O(6)–C(30) is -42.6° . The torsional angles of C(14)–O(3)–C(15)–C(16) and C(20)–C(21)–O(4)–C(22) are -75.2° and 84.8° , whereas the values for O(3)–C(15)–C(16)–C(17) and C(19)–C(20)–C(21)–O(4) are -32.8° and 22.4° , suggesting that **184** is not completely symmetrical in the solid state.

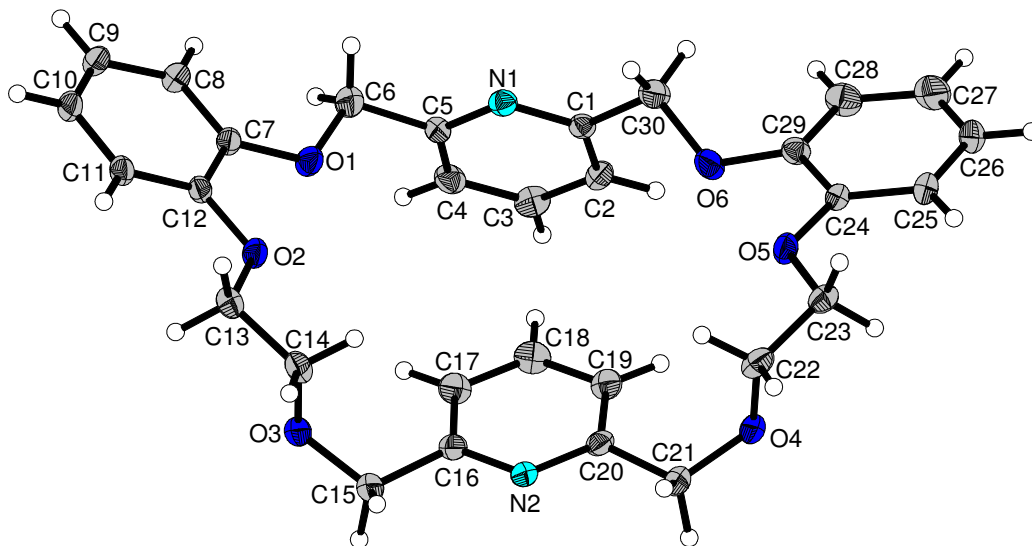


Fig. 5.4 View of the X-ray structure of 2,3,6,8,11,12,18,20-tetrabenzo-7,19-diaza-1,4,10,13,16,22-hexaoxacyclo-tetraeicosa-2,6,7,11,18,19-hexaene, **184**

C3–C18	N1–C18	O1–O3	O6–O4	O1–O5	O1–O4	O6–O2	O6–O3
4.029 Å	4.096 Å	4.834 Å	4.793 Å	7.346 Å	7.859 Å	7.844 Å	8.498 Å

Table 5.4 Dimensions of the cavity of compound **184**

O(1)–C(6)–C(5)	110.5(3)
C(14)–O(3)–C(15)	111.5(3)
O(3)–C(15)–C(16)	112.8(3)
C(7)–O(1)–C(6)	118.0(2)
O(4)–C(21)–C(20)	112.8(3)
C(22)–O(4)–C(21)	113.4(3)
C(29)–O(6)–C(30)	119.6(2)
O(6)–C(30)–C(1)	108.2(2)

Table 5.5 Selected bond angles [°] for **184** with estimated standard deviations

C(1)–C(30)	1.499(4)
C(5)–C(6)	1.473(4)
C(20)–C(21)	1.508(4)
O(1)–C(7)	1.376(3)
C(14)–O(3)	1.410(4)
O(4)–C(22)	1.406(4)
C(29)–O(6)	1.360(3)

Table 5.6 Selected bond lengths [Å] for **184** with estimated standard deviations

C(5)–C(6)–O(1)–C(7)	174.9(3)
C(6)–O(1)–C(7)–C(8)	15.4(5)
C(14)–O(3)–C(15)–C(16)	–75.2(4)
O(3)–C(15)–C(16)–C(17)	–32.8(5)
C(28)–C(29)–O(6)–C(30)	–42.6(5)
C(29)–O(6)–C(30)–C(1)	145.4(3)
C(19)–C(20)–C(21)–O(4)	22.4(5)
C(20)–C(21)–O(4)–C(22)	84.8(4)

Table 5.7 Torsion angles [°] for **184**

5.3 Structural studies of macrocyclic precursor **160**

Compound **160** crystallizes in the monoclinic space group C2 with four independent molecules per asymmetric unit. Bond lengths within the phenyl ring are normal with C-C distances of 1.365(6) Å to 1.407(5) Å, mean 1.386 Å. The ethereal C-O distances for O(2)–C(3) and C(8)–O(3) are 1.359(5) Å and 1.364(4) Å respectively. Refinement has shown that there are two types of disorder associated with **160**. The atoms in the ethanol chain C2–C1–O1 are disordered over two sites C2A–C1A–O1A/C2B–C1B–O1B which differ in their orientation with respect to the aromatic ring moiety and with site occupancy factors subsequently fixed at 50% each. Therefore particular bond lengths for C(2A)–O(2) and C(2B)–O(2) are noticeably different at 1.513 Å and 1.417 Å, whereas O(1A)–C(1A) is 1.466 Å and O(1B)–C(1B) 1.369 Å. The O–C–C bond angles range from 107.9° to 125.5° while distortions between C(3)–O(2)–C(2B) at 132.3° and C(3)–O(2)–C(2A) at 108.7° can be also observed. Distances measured between O1–O1' = 9.861 Å, O3–O3' = 3.464 Å, O2–O2' = 7.078 Å.

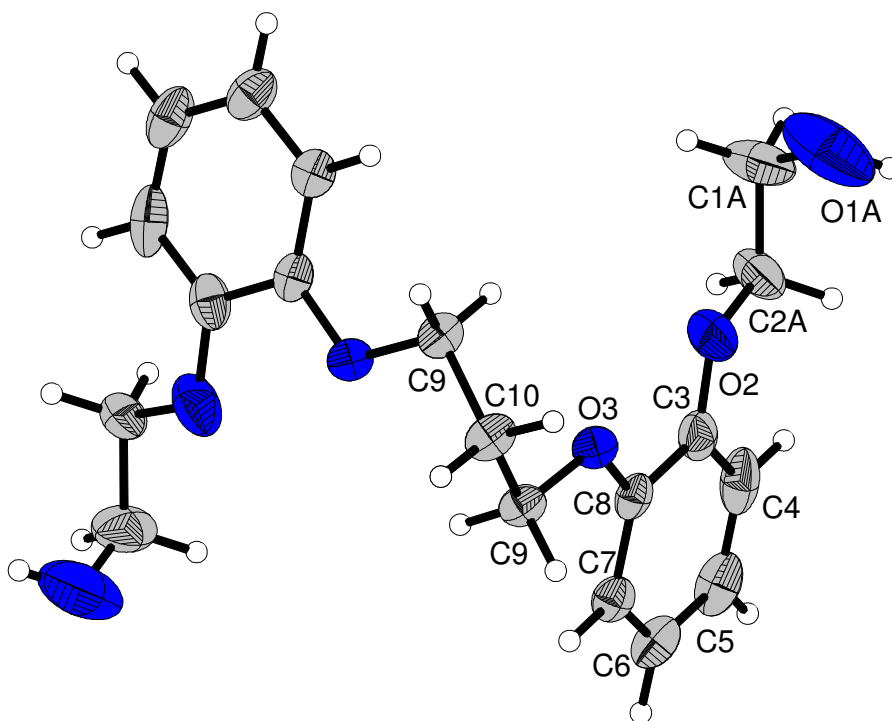


Fig. 5.5 View of the X-ray crystal structure of 1,3-bis[2-(2'-hydroxyethoxy)phenoxy]propane, **160**, disorder neglected for clarity

Bond distances		Bond angles	
O(1A)–C(1A)	1.466(15)	C(3)–O(2)–C(2B)	132.3(8)
C(2A)–O(2)	1.513(9)	C(3)–O(2)–C(2A)	108.7(5)
O(1B)–C(1B)	1.369(15)	C(2B)–O(2)–C(2A)	33.5(6)
C(2B)–O(2)	1.417(10)	O(2)–C(3)–C(4)	125.5(4)
C(3)–C(4)	1.393(6)	O(2)–C(3)–C(8)	115.4(4)
C(3)–C(8)	1.407(5)	O(3)–C(8)–C(3)	116.2(3)
C(4)–C(5)	1.383(6)	C(7)–C(8)–C(3)	118.9(3)
C(5)–C(6)	1.365(6)	C(8)–O(3)–C(9)	116.7(2)
C(6)–C(7)	1.391(5)	O(3)–C(9)–C(10)	107.9(2)
C(7)–C(8)	1.382(5)	C(9)–C(10)–C(9)	113.3(5)

Table 5.8 Selected bond lengths [Å] and angles [°] for **160**

5.4 Structural studies of macrocyclic precursor **161**

For macrocyclic precursor **161** the presence of a water molecule in the crystal has been detected. The water molecule is bound by hydrogen-bond interactions to the primary alcohol groups (Fig. 5.6). The flexible ether chain connecting the two diol units allows the structure to adopt twisted conformations, with distances between O1–O4 of 5.331 Å, O4–O5 of 7.897 Å and O1–O3 of 4.707 Å.

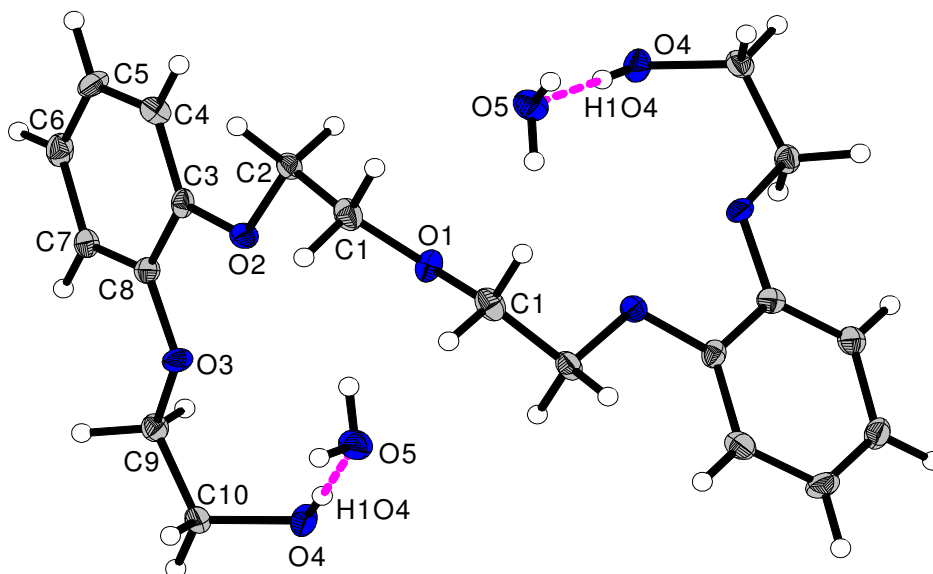


Fig. 5.6 X-ray crystal structure of 1,5-bis[2-(2'-hydroxyethoxy) phenoxy]-3-oxapentane, **161**

161 crystallizes in the monoclinic space group C2 with two independent molecules per asymmetric unit. Bond lengths within the phenyl ring are normal with C-C distances of 1.374 Å to 1.406 Å, mean 1.390 Å. Etheral bonds O(1)–C(1), C(2)–O(2) and O(3)–C(9) show very similar bond lengths at around 1.434 Å, whereas shorter distances, about 1.372 Å have been detected for O(2)–C(3) and C(8)–O(3). Bond angles O(2)–C(2)–C(1) and C(3)–O(2)–C(2) are 108.6° and 116.1° respectively, whereas the angle O(3)–C(9)–C(10) was measured at 107.7° and O(4)–C(10)–C(9) at 113.6°. Significant hydrogen bonding is taking place between H(104) and O(5) (separation of 1.87 Å) and also between H(2O5) and O(4) (separation of 1.94 Å).

O(1)–C(1)	1.430(3)
C(2)–O(2)	1.437(3)
O(2)–C(3)	1.375(3)
C(3)–C(4)	1.383(4)
C(3)–C(8)	1.406(4)
C(4)–C(5)	1.395(5)
C(5)–C(6)	1.374(5)
C(6)–C(7)	1.395(4)
C(7)–C(8)	1.384(4)
C(8)–O(3)	1.372(3)
O(3)–C(9)	1.436(3)
C(10)–O(4)	1.423(3)

Table 5.9 Selected bond lengths [Å] for **161** with estimated standard deviations

O(2)–C(2)–C(1)	108.6(2)
C(3)–O(2)–C(2)	116.1(2)
O(3)–C(8)–C(3)	115.7(2)
C(8)–O(3)–C(9)	116.7(2)
O(3)–C(9)–C(10)	107.7(2)
O(4)–C(10)–C(9)	113.6(2)

Table 5.10 Selected bond angles [°] for **161** with estimated standard deviations

D–H...A	d(D–H)	d(H...A)	d(D...A)	<(DHA)
O(4)–H(1O4)...O(5)	0.84	1.87	2.710(3)	176.1
O(5)–H(2O5)...O(4)	0.843(19)	1.94(2)	2.782(3)	174(4)

Table 5.11 Hydrogen bonds for **161** [Å and °]

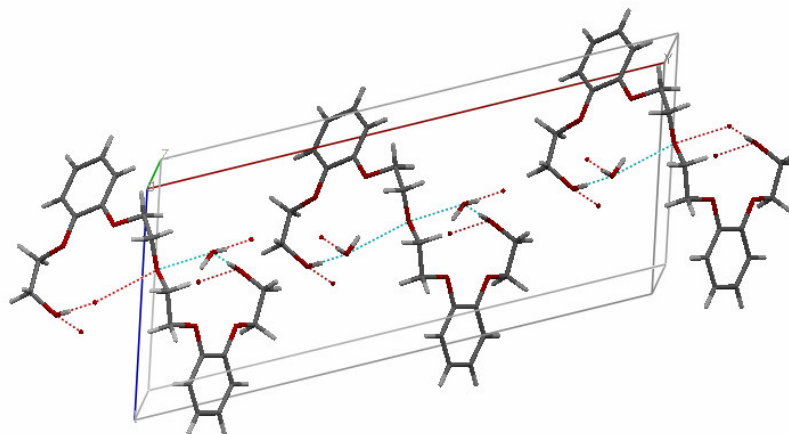


Fig. 5.7 X-ray crystal structure and unit cell of 1,5-bis[2-(2'-hydroxyethoxy) phenoxy]-3-oxapentane, **161** depicting the hydrogen bond interactions

5.5 Structural studies of macrocyclic precursor **163**

Compound **163** crystallizes in the monoclinic space group $C2/c$ with four independent molecules per asymmetric unit. The bond lengths for the aromatic region are as expected with C–C distances of 1.355 Å to 1.396 Å, mean 1.375 Å also single bonds appear regular with C(1)–C(2) and C(9)–C(10) distances of 1.501 Å and 1.503 Å respectively. The bond distances of C(8)–O(3) 1.371 Å and O(2)–C(3) 1.374 Å between aromatic carbon and oxygen are shorter than the bond lengths of O(3)–C(9) (1.427 Å) and C(2)–O(2) (1.426 Å) formed between oxygen and the aliphatic carbon. The O–C–C and C–O–C bond angles range from 107.3° to 117.9°. The torsion angle between the *ortho*-substituted phenyl ring and alkyl alcohol functionality, C(1)–C(2)–O(2)–C(3) is 178.7°, whereas C(8)–O(3)–C(9)–C(10) is 71.7°. Refinement has shown that there are two types of disorder associated with **163**. The alcohol oxygen atom is disordered over two sites O1A/O1B which differ in their orientation with respect to the alcohol chain moiety and with site occupancy factors subsequently fixed at 50 % (probability level) each.

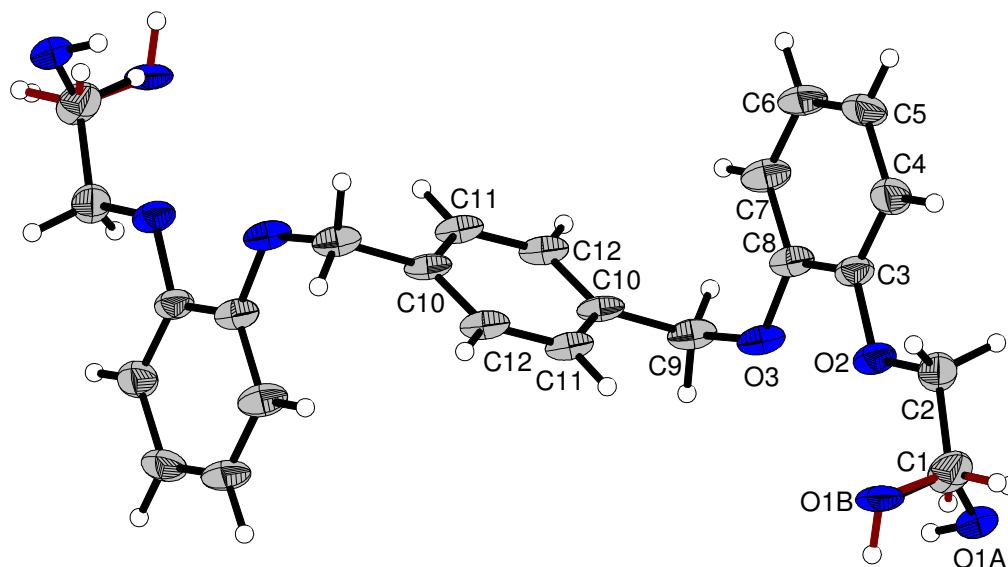


Fig. 5.8 X-ray crystal structure of 1,4-bis[2-(2'-hydroxyethoxy)phenoxy]xylene, **163**

Bond distances		Bond angles	
C(1)–C(2)	1.501(5)	O(2)–C(2)–C(1)	107.3(3)
C(2)–O(2)	1.426(4)	C(3)–O(2)–C(2)	117.3(2)
O(2)–C(3)	1.374(3)	C(8)–O(3)–C(9)	117.9(2)
C(3)–C(8)	1.390(4)	O(3)–C(9)–C(10)	113.4(2)
C(4)–C(5)	1.396(4)		
C(5)–C(6)	1.355(5)	Torsion angles	
C(6)–C(7)	1.387(5)	C(1)–C(2)–O(2)–C(3)	178.7(3)
C(7)–C(8)	1.385(4)	C(2)–O(2)–C(3)–C(4)	–0.4(4)
C(8)–O(3)	1.371(4)	C(7)–C(8)–O(3)–C(9)	5.2(4)
O(3)–C(9)	1.427(4)	C(8)–O(3)–C(9)–C(10)	71.7(3)
C(9)–C(10)	1.503(5)	O(3)–C(9)–C(10)–(11)	41.9(4)
C(10)–C(12)	1.383(4)	O(2)–C(3)–C(8)–O(3)	1.9(4)
C(10)–C(11)	1.390(4)	O(3)–C(9)–C(10)–(12)	–140.6(3)
C(11)–C(12)	1.374(5)		

Table 5.12 Selected bond distances [\AA] and angles [$^\circ$] for **163** with estimated standard deviations

The crystal structure of **163** shows the spatial arrangement which the aromatic rings and alcohol chains adopt with respect to one another. The alcohol chains are orientated in opposite directions to one another so it can be concluded that formation of a macrocycle from this precursor would pose a considerable challenge without a templating agent. A templating agent would enable rearrangement of **163** to a conformation where ring closure by introduction of an alkyl linker would be preferred over oligomers formation. Table 5.13 shows distances between particular atoms measured for **163** in the solid state.

2-O6	O3-O5	O2-O4	O2-O5	O3-O1	O3-O6	C7-30	C14-23
4.67	4.71	8.19	7.85	8.16	7.83	5.11	5.46

Table 5.13 Dimensions of the cavity of compound **163**

5.6 Structural studies of macrocyclic precursor **164**

Compound **164** crystallizes in the monoclinic space group $P2_1/c$ with four independent molecules per asymmetric unit. Bond lengths within the phenyl ring are normal, with C-C distances of 1.374 Å to 1.411 Å, mean 1.392 Å. The bond distances of C(2)–O(2) (1.444 Å) and O(5)–C(23) (1.433 Å) are similar to those of O(3)–C(9) (1.439 Å) and C(16)–O(4) (1.437 Å) and are in agreement with typical bond lengths for aliphatic ethers (1.430 Å)¹⁵³. Furthermore the C-O bond in the phenol ring has been reported to be considerably shorter (1.37 Å)¹⁵⁴ and this includes bond lengths of C8-O3 (1.367 Å), C17-O4 (1.364 Å), C3-O2 (1.367 Å) and C22-O5 (1.368 Å). The bond angles of O(3)–C(9)–C(10) and O(4)–C(16)–C(14) are practically identical and equal, 107.78° and 107.00° respectively, also C(15)–C(10)–C(9) and C(15)–C(14)–C(16) exhibit very similar values of 120.36°. The torsion angles of C(8)–O(3)–C(9)–C(10) and C(14)–C(16)–O(4)–C(17) between the two aromatic rings are 175.12° and 176.38° respectively, while O(2)–C(3)–C(8)–O(3) and O(4)–C(17)–C(22)–O(5) are –1.47° and 1.49° which emphasises the regularity of the structure **164** in the solid state.

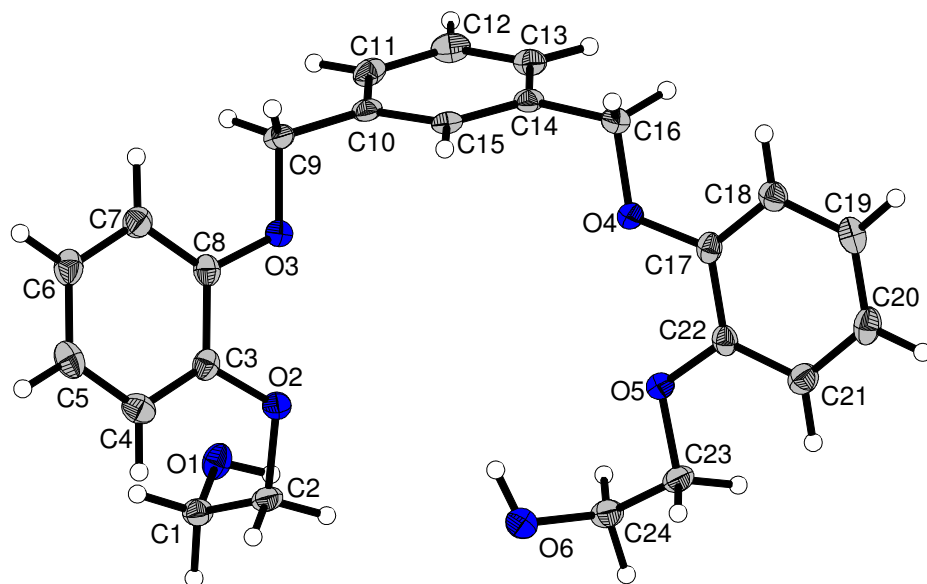


Fig. 5.9 X-ray crystal structure of 1,3-bis[2-(2'-hydroxyethoxy) phenoxy]xylene, **164**

Bond lengths			
C(2)–O(2)	1.4445(16)	C(12)–C(13)	1.384(2)
O(2)–C(3)	1.367(16)	C(13)–C(14)	1.392(2)
C(3)–C(4)	1.381(2)	C(14)–C(15)	1.388(2)
C(3)–C(8)	1.406(2)	C(16)–O(4)	1.437(16)
C(4)–C(5)	1.396(2)	O(4)–C(17)	1.364(16)
C(6)–C(7)	1.392(2)	C(17)–C(22)	1.411(19)
C(8)–O(3)	1.367(17)	C(19)–C(20)	1.374(2)
O(3)–C(9)	1.439(17)	C(20)–C(21)	1.396(2)
C(10)–C(11)	1.394(2)	C(22)–O(5)	1.368(17)
C(11)–C(12)	1.388(2)	O(5)–C(23)	1.433(17)
Bond angles		Torsion angles	
O(3)–C(9)–C(10)	107.78(11)	C(8)–O(3)–C(9)–C(10)	175.12(11)
C(15)–C(10)–C(9)	120.08(13)	C(14)–C(16)–O(4)–C(17)	176.38(11)
C(15)–C(14)–C(16)	120.65(13)	O(2)–C(3)–C(8)–O(3)	–1.47(17)
O(4)–C(16)–C(14)	107.00(11)	O(4)–C(17)–C(22)–O(5)	1.49(17)

Table 5.14 Selected bond distances [\AA] bond angles [$^\circ$] and torsion angles [$^\circ$] for **164** with estimated standard deviations

The crystal structure of the single **164** unit shows the two OH groups to be in close proximity which is preferential for successful ring closure reactions. We believe that it is because of the *meta*-substituted xylene ring that macrocyclic precursor **164** adopts this cyclic, hydrogen bonded conformation with a perfect arrangement for introduction of an alkyl linker to perform the ring closure step. The distances between particular atoms have been depicted in Table 5.15.

O4-O2	O3-O5	O3-O4	O1-O6	O4-O1	O3-O6
5.97 Å	6.12 Å	5.23 Å	4.87 Å	7.57 Å	5.71 Å
O4-H6	O3-H6	O3-H1	H1-H6	O4-H1	H6-H15
4.376	4.875	4.560	3.804	7.135	5.159

Table 5.15 Dimensions of the cavity of compound **164**

The presence of intermolecular hydrogen bonds in **164** has been observed which links two neighbouring molecules on H106-O1 and H101-O2 and according to the literature can be classified as a medium hydrogen bond¹⁵⁵.

D-H...A	d(D-H)	d(H...A)	d(D...A)	<(DHA)
O(6)-H(1O6)...O(1)	0.88(2)	1.89(2)	2.7628(16)	175.6(19)
O(1)-H(1O1)...O(2)	0.867(19)	2.087(19)	2.8072(14)	140.0(16)

Table 5.16 Hydrogen bonds for **164** [Å and °]

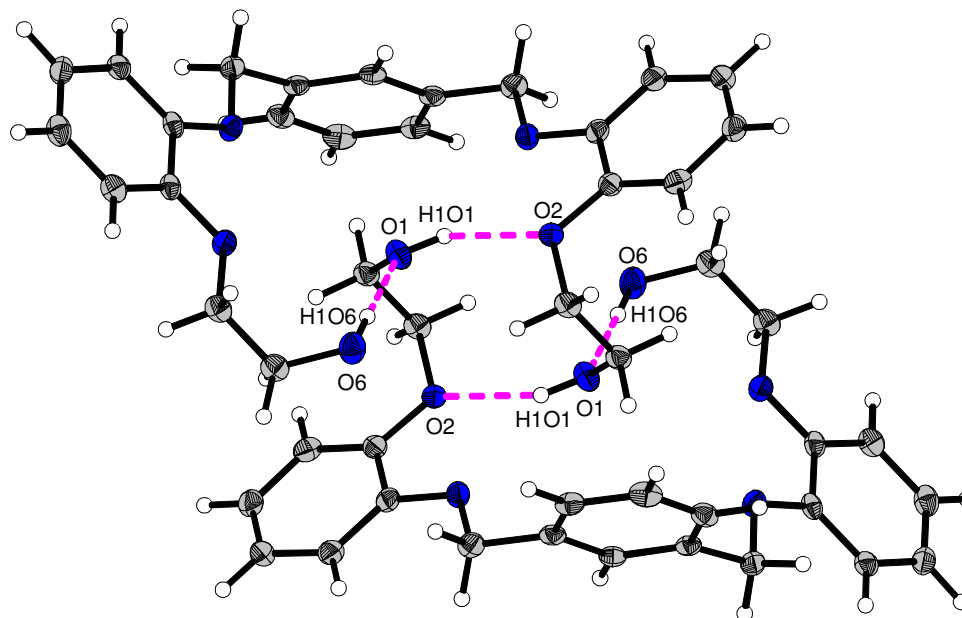


Fig. 5.10 The crystal structure of two molecules of **164** linked with intermolecular hydrogen bonds

5.7 Structural studies of macrocyclic precursor **165**

Compound **165** crystallizes in the monoclinic space group $C2/c$ with four independent molecules per asymmetric unit. Bond lengths within the phenyl rings are regular with C-C distances of 1.368 Å to 1.405 Å, mean 1.386 Å. The bond distances of O(2)–C(3) and C(8)–O(3) exhibit close values of 1.372 Å and 1.380 Å respectively, which are significantly shorter bond lengths than C(2)–O(2), at 1.426 Å. The bond angles of O(3)–C(8)–C(3) and C(8)–O(3)–C(9) are quite similar, with values of 115.39° and 115.07° respectively. The torsion angle of the O(2)–C(3)–C(8)–O(3) is 0.45°, in contrast to the values for **163** and **164** which are 1.9° and –1.47° respectively. Furthermore the torsion angle of C(8)–O(3)–C(9)–C(10) in **165** is –179.70(12)°, whereas identically situated atoms in **163** and **164** created torsion angles of 71.7(3)° and 176.38(11)° respectively. Refinement has shown that there are two types of disorder associated with **165**. The alcohol oxygen atom is disordered over the two sites O1A/O1B which differ in their orientation with respect to the alcohol chain moiety and with site occupancy factors subsequently fixed at 50 % (probability level) each.

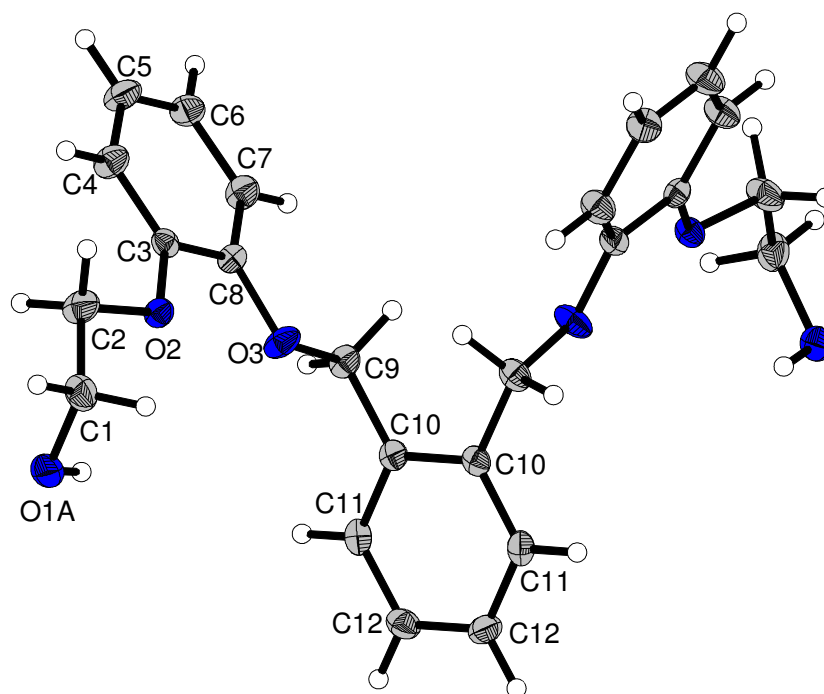


Fig. 5.11 X-ray crystal structure of 1,2-bis[2-(2'-hydroxyethoxy) phenoxy]xylene **165**, disorder neglected for clarity

Bond distances		Bond angles	
O(2)–C(3)	1.372(17)		
C(3)–C(4)	1.376(2)	O(3)–C(8)–C(3)	115.39(12)
C(3)–C(8)	1.404(2)	C(8)–O(3)–C(9)	115.07(11)
C(5)–C(6)	1.368(2)	O(3)–C(9)–C(10)	109.02(11)
C(6)–C(7)	1.392(2)	C(10)–C(10)–C(9)	121.07(8)
C(10)–C(11)	1.389(2)		
C(8)–O(3)	1.380(17)	Torsion angles	
C(2)–O(2)	1.426(4)	O(2)–C(3)–C(8)–O(3)	0.45(18)
C(10)–C(10)	1.405(3)	C(8)–O(3)–C(9)–C(10)	–179.70(12)
C(11)–C(12)	1.385(2)	O(3)–C(9)–C(10)–C(11)	97.51(15)

Table 5.17 Selected bond distances [Å] bond angles [°] and torsion angles [°] for **165** with estimated standard deviations

Crystallographic data for **165** provides constructive information about the arrangement of the aromatic rings and alcohol chains of **165** in the solid state. Steric interactions between the *ortho*-xylene units hinder the entire molecule adopting a pseudo-cyclic structure resembling the macrocyclic precursor **164**. Furthermore, the measured distance between the two hydrogens of the alcohol groups (H1-H1) is 11.157 Å and is too far apart for another *meta*-, *para*- or especially *ortho*-xylene unit to be introduced. This fact could perhaps shed some light on the unsuccessful results of ring closure reactions employing **165**. Even trials to promote macrocyclization by introducing a *para*-xylene linker (7.45 Å) into the **165** failed, and also employment of a variety of templating agents (Li⁺, Na⁺, K⁺, Cs⁺) in that particular case did not promote the ring closure. In fact, only formation of oligomeric products was observed.

O1-O1	O2-O2	O3-O3	C9-C9	H1-H1	O3-H1
12.641	8.472	4.146	2.963	11.157	7.639

Table 5.18 Dimensions of the cavity of compound **165**

By viewing the structure of **165** in Mercury 1.4.2, it is evident that the two 2-(2'-hydroxyethoxy)phenoxy units are orientated antiperiplanar to the aromatic linker. The steric torsions introduced by the *ortho*-xylene ring joining the two diol units are the most likely reason for the unsuccessful macrocyclization reaction attempted in that particular case.

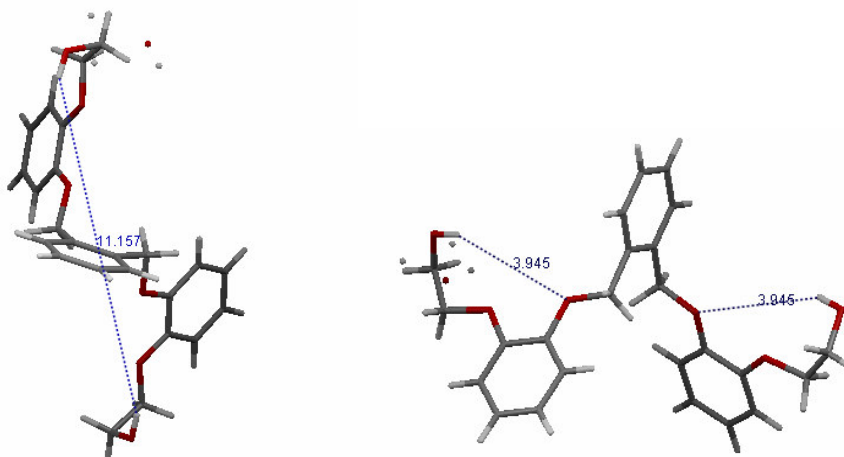


Fig. 5.12 Drawing of the X-ray crystal structure of **165** depicting different 3D perspectives

5.8 Structural studies of macrocyclic precursor **166**

Compound **166** crystallizes in the monoclinic space group $P2_1/c$ with four independent molecules per asymmetric unit. The phenyl C-C bond distances range from 1.364 Å to 1.406 Å (mean 1.385 Å) whereas in the pyridine moiety the range of C-C bond length is shorter (between 1.379 Å and 1.387 Å, mean 1.383 Å). Both C-N bond distances in the pyridine ring are around 1.342 Å in length, and are in agreement with reported data¹⁵⁶. The O-C-C bond angles range from 108.69° to 110.42°. The torsional angles of C(8)–O(3)–C(9)–C(10) and C(14)–C(15)–O(4)–C(16) are -178.74° and -179.65° respectively, which are also close to the values for C(3)–C(8)–O(3)–C(9) and C(15)–O(4)–C(16)–C(21) (177.86° and 179.45°). All these features indicate that in the solid state the compound **166** adopts a planar form, apart from the disorder of the alcohol chains. Refinement has shown that there are two types of disorder associated with **166**. One of the alcohol chains is disordered over two sites O1A/O1B which differ in their orientation with respect to the phenyl moiety and with site occupancy factors subsequently fixed at 50 % (probability level) each.

Bond distances		Bond angles	
C(3)–C(4)	1.381(2)	C(8)–O(3)–C(9)	116.17(12)
C(3)–C(8)	1.406(2)	O(3)–C(9)–C(10)	108.69(13)
C(17)–C(18)	1.388(3)	O(4)–C(15)–C(14)	110.42(13)
C(18)–C(19)	1.364(4)	C(16)–O(4)–C(15)	115.19(13)
C(10)–N	1.343(2)	Torsion angles	
C(10)–C(11)	1.387(2)	C(8)–O(3)–C(9)–C(10)	-178.74(13)
N–C(14)	1.341(2)	O(3)–C(9)–C(10)–N	178.12(13)
C(14)–C(15)	1.498(2)	O(3)–C(9)–C(10)–C(11)	-1.3(2)
C(15)–O(4)	1.418(2)	N–C(14)–C(15)–O(4)	-178.61(13)
O(3)–C(9)	1.416(2)	C(13)–C(14)–C(15)–O(4)	1.3(2)
O(4)–C(16)	1.373(2)	C(14)–C(15)–O(4)–C(16)	-179.65(13)
C(8)–O(3)	1.372(2)	C(15)–O(4)–C(16)–C(21)	179.45(17)

Table 5.19 Selected bond distances [Å] bond angles [°] and torsion angles [°] for **166** with estimated standard deviations

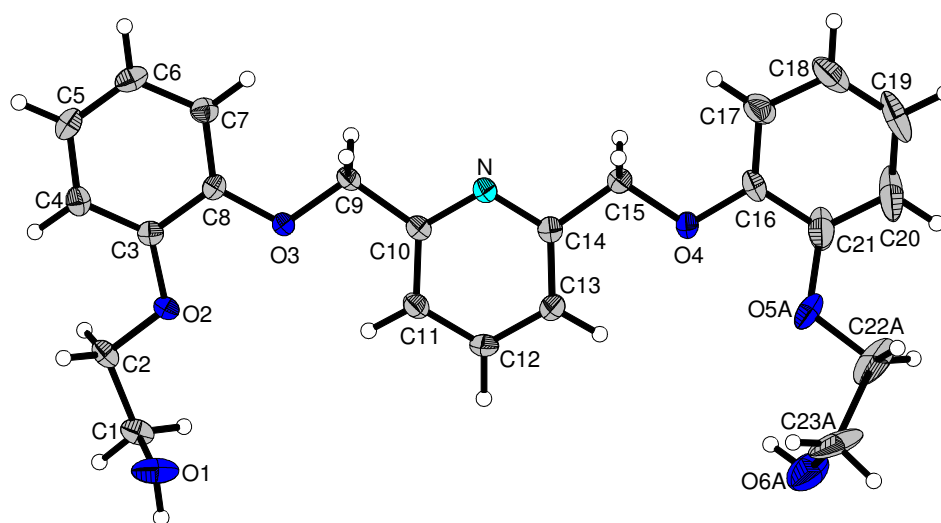


Fig. 5.13 X-ray crystal structure of 1,6-bis[2-(2'-hydroxyethoxy) phenoxy]methylene pyridine, **166**, disorder neglected for clarity

O1-O6	O2-O6	O1-O5	O1-O3	O4-O6	H1-H6	O1-H12	O3-H1
11.426	11.573	11.772	4.848	4.850	10.746	5.893	5.550

Table 5.20 Dimensions of the cavity of compound **166**

In the Appendix A structure of macrocycle **176** and morphine macrocycle precursor **200** have been attached.

5.9 Conclusion

Crystal data and crystallographic descriptions of macrocyclic precursors **160**, **161**, **163-166** provide information about spatial arrangement of particular atoms and chemical groups. This data highlights conformational differences between these structures. Apart from structure **165**, the orientation of atoms in macrocyclic precursors **160**, **161**, **163**, **164**, **166** in the solid state ‘suggest’ potential for successful further ring closure steps. For example the crystal structure of **164** shows that it adopts a cyclic hydrogen bonded conformation with a perfect arrangement for introduction of an alkyl linker to perform the macrocyclization step. For that compound each of the ring closure step experiments were successful. This is in contrast to crystallographic data for **165**. Steric interactions in the *ortho*-xylene unit hinder the entire molecule preventing it from adopting a pseudo-cyclic structure resembling the macrocyclic precursor **164**. Therefore the two hydrogens of the alcohol groups in **165** are too far apart for another linker unit to be introduced. This fact could perhaps provide a reasonable explanation of the unsuccessful results of ring closure reactions employing **165**, for which only formation of oligomeric products was observed.

From the measurements of the cavity sizes and cation metal diameters it is possible to roughly estimate which metal “guest” would fit best into the macrocyclic cavity. Both **179** and **184** exhibit quite large cavity sizes (4.029 Å on 4.096 Å on 7.346 Å on 8.498 Å) and therefore would be expected to bind preferentially to metal guests with diameters ranging from 2.66 to 3.34 Å (Table 6.2, Chapter 6) *e.g.* K⁺ (2.66 Å) Cs⁺ (3.34 Å), Rb⁺ (2.94 Å), Sr²⁺ (2.26 Å) or Ba²⁺ (2.68 Å). Macrocyclic **184** in contrast to **179** contains two pyridine rings which provide an alternative binding pocket. For macrocycle **184** binding affinity towards metal cations such as La³⁺ (2.30 Å) or Pb²⁺ (2.40 Å) would also be expected, in view of the presence of donor nitrogens in the two pyridine rings. Macrocycles **179** and **184** apart from having a relatively large polycyclic scaffold contain 4 aromatic rings each. This feature may reduce the potential flexibility of **179** and **184** which would surely influence the binding affinity towards metal cations.

It is hard to make any estimation of binding preferences of macrocyclic precursors **160-163** and **165**, since the X-ray measurements reveal that they do not adopt a

pseudocyclic arrangement in the solid state. Therefore adequate measurement of the distances between donor atoms would not be possible.

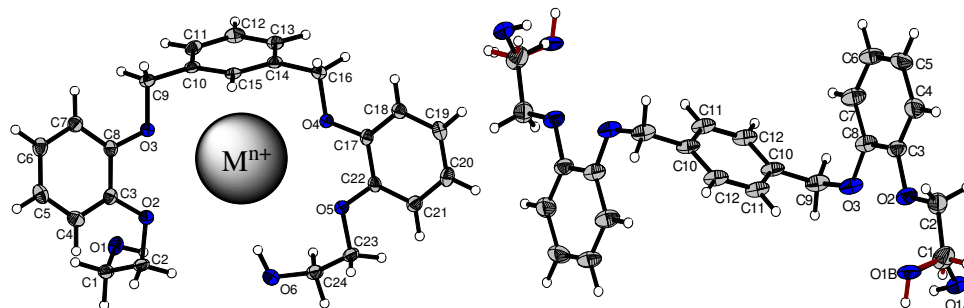


Fig. 5.14 Pseudocyclic structure adopted by **164** and linear arrangement of **163** in the solid state

From the estimation of the cavity size of the **164** (5.97 Å on 6.12 Å and 5.23 Å on 5.71 Å) in the solid state, **164** would fit metal “guests” such as K^+ , Cs^+ , Ba^{2+} and Sr^{2+} . Therefore this might be the answer of significant templating role of K^+ and Cs^+ in the macrocyclization step.

Based on the X-ray crystallographic data representative measurements of the cavity sizes and distances between selected atoms in the macrocycles **179**, **184** and their precursors **164** have been presented. These measurements are based purely on physical size of the cavity in the solid state and the potential guest cation and do not take into account the rigidity/flexibility of the “hosts”, the charge on the metal cations and the stability of the host-guest complex. This estimated data is likely to change in solution or on binding to the “guest” species.

6 Metal binding studies

6.1 Introduction

This chapter describes metal picrate extraction studies carried out on selected products synthesized in this project. A general view of the binding affinity of the macrocycles and their precursors, to a variety of metal cations, indicating which metal cation would bind to the corresponding macrocyclic compound, is the aim. The picrate method is commonly used to determine extracting efficiencies of macrocyclic ethers and their precursors by measuring the relative distribution of a coloured alkali metal salt (in this case picrate) between water and an immiscible organic solvent in the presence of the crown ether Fig. 6.1¹⁵⁷. If the polyether host is a powerful complexing agent, most of the colour will remain in the organic phase, whereas a colourless organic phase after extraction, indicates a low binding affinity.

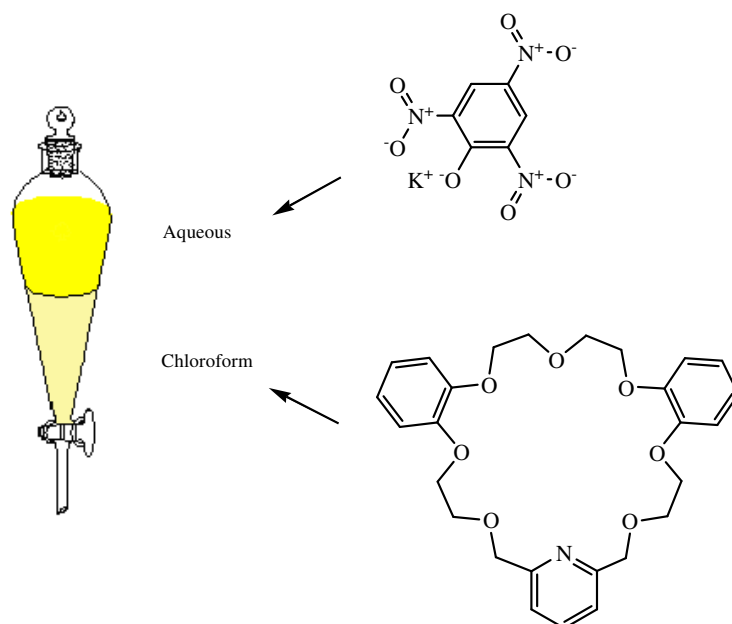


Fig. 6.1 Partitioning of crown ether and potassium picrate between water and chloroform solution

The relationship between the diameter of an alkali cation and the crown ether has been noted in earlier literature of crown ethers and this is best referred by Pedersen as the “hole-size-rule”¹⁵⁸. The diameters of the macrocyclic polyethers (A-E) are presented in Table 6.1, while cation diameters are shown in Table 6.2¹⁵⁹.

	Macrocyclic Polyethers	Diameters [\AA]
<i>A</i>	All 14-crown-4	1.2-1.5
<i>B</i>	All 15-crown-5	1.7-2.2
<i>C</i>	All 18-crown-6	2.6-3.2
<i>D</i>	All 21-crown-7	3.4-4.3
<i>E</i>	All 24-crown-8	4.5-5.2

Table 6.1 Diameter of cavity in Ångström Units

Group I		Group II		Group III		Group IV	
Li	1.36						
Na	1.94	Mg	1.44				
K	2.66	Ca	1.98				
Cu(I)	1.92	Zn	1.48				
Rb	2.94	Sr	2.26				
Ag	2.52	Cd	1.94				
Cs	3.34	Ba	2.68	La	2.30	Pb(II)	2.40
NH ₄	2.86						

Table 6.2 Cations and their Diameters in Ångström Units

6.2 Results and discussion

Macrocyclic compounds and their precursors synthesised for this project were tested for cation selectivity using UV picrate extraction techniques. Each of the thirty compounds was tested against thirteen metal picrates and the results are presented in Tables 6.3-6.32. The metal picrate extraction experiments were performed by using host solutions of macrocycle or its precursor in chloroform and picrate solutions in deionised water according to the procedure described by Pedersen. The absorption of the extracted picrate was measured from the aqueous layer at 356 nm and compared against a blank solution (no host in chloroform) of the appropriate picrate. The average of three samples is reported with standard deviation < 0.01. It has to be mentioned that preparation of cadmium picrate was troublesome, despite several attempts to synthesize that particular salt only minimal amounts of it were obtained.

However the calibration curves constructed from the standard solutions were not complementary with the required standards therefore all the results obtained for extraction of the cadmium picrate had to be rejected.

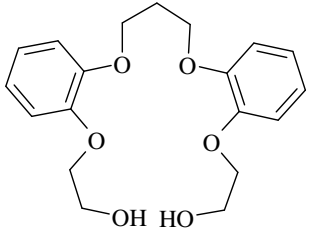
Binding Agent	Cation	% Extraction	Cation	% Extraction
 <p style="text-align: center;">160</p>	Li ⁺	12.7		
	Na ⁺	4.1	Zn ²⁺	0.3
	K ⁺	1.4	Co ²⁺	2.3
	Cs ⁺	1.1	Cu ²⁺	0.3
	Ca ²⁺	0.7	Sr ²⁺	0.3
	Ba ²⁺	1.7	Pb ²⁺	1.4
	Mg ²⁺	1.4	La ³⁺	4.9

Table 6.3 Extraction results with **160**

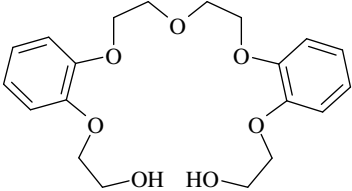
Binding Agent	Cation	% Extraction	Cation	% Extraction
 <p style="text-align: center;">161</p>	Li ⁺	24.1		
	Na ⁺	7.9	Zn ²⁺	1.6
	K ⁺	5.9	Co ²⁺	1.0
	Cs ⁺	1.1	Cu ²⁺	2.5
	Ca ²⁺	2.5	Sr ²⁺	0.2
	Ba ²⁺	2.0	Pb ²⁺	1.1
	Mg ²⁺	1.9	La ³⁺	9.6

Table 6.4 Extraction results with **161**

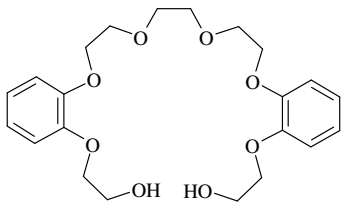
Binding Agent	Cation	% Extraction	Cation	% Extraction
 <p style="text-align: center;">162</p>	Li ⁺	20.2		
	Na ⁺	78.2	Zn ²⁺	1.6
	K ⁺	40.8	Co ²⁺	1.7
	Cs ⁺	7.5	Cu ²⁺	1.5
	Ca ²⁺	2.3	Sr ²⁺	0.5
	Ba ²⁺	3.4	Pb ²⁺	0.8
	Mg ²⁺	0.9	La ³⁺	9.6

Table 6.5 Extraction results with **162**

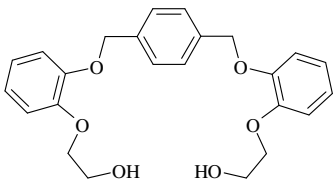
Binding Agent	Cation	% Extraction	Cation	% Extraction
 <p style="text-align: center;">163</p>	Li ⁺	0.0		
	Na ⁺	3.5	Zn ²⁺	1.9
	K ⁺	8.0	Co ²⁺	0.1
	Cs ⁺	2.8	Cu ²⁺	1.9
	Ca ²⁺	0.1	Sr ²⁺	1.1
	Ba ²⁺	3.1	Pb ²⁺	1.1
	Mg ²⁺	2.1	La ³⁺	4.8

Table 6.6 Extraction results with **163**

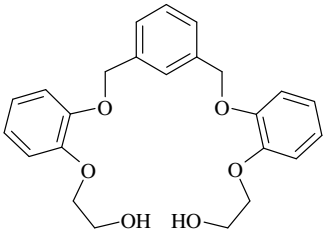
Binding Agent	Cation	% Extraction	Cation	% Extraction
 <p style="text-align: center;">164</p>	Li ⁺	6.2		
	Na ⁺	59.1	Zn ²⁺	1.9
	K ⁺	13.3	Co ²⁺	0.1
	Cs ⁺	1.9	Cu ²⁺	2.5
	Ca ²⁺	2.4	Sr ²⁺	1.1
	Ba ²⁺	2.7	Pb ²⁺	1.5
	Mg ²⁺	0.8	La ³⁺	4.9

Table 6.7 Extraction results with **164**

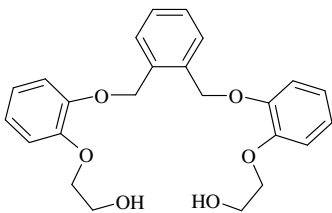
Binding Agent	Cation	% Extraction	Cation	% Extraction
 <p style="text-align: center;">165</p>	Li ⁺	8.5		
	Na ⁺	54.1	Zn ²⁺	0.4
	K ⁺	13.0	Co ²⁺	0.6
	Cs ⁺	2.5	Cu ²⁺	1.9
	Ca ²⁺	1.6	Sr ²⁺	1.2
	Ba ²⁺	2.3	Pb ²⁺	1.5
	Mg ²⁺	2.1	La ³⁺	4.5

Table 6.8 Extraction results with 165

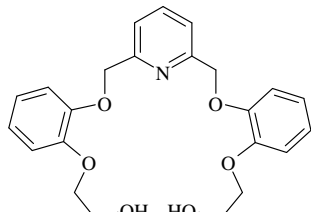
Binding Agent	Cation	% Extraction	Cation	% Extraction
 <p style="text-align: center;">166</p>	Li ⁺	1.1		
	Na ⁺	48.0	Zn ²⁺	0.7
	K ⁺	4.7	Co ²⁺	0.4
	Cs ⁺	2.4	Cu ²⁺	2.1
	Ca ²⁺	1.6	Sr ²⁺	1.1
	Ba ²⁺	0.8	Pb ²⁺	0.8
	Mg ²⁺	0.1	La ³⁺	10.3

Table 6.9 Extraction results with 166

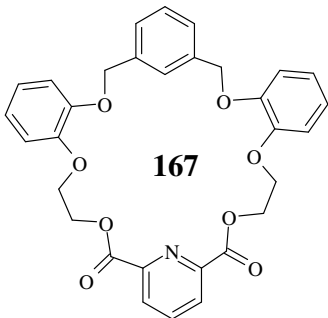
Binding Agent	Cation	% Extraction	Cation	% Extraction
 <p style="text-align: center;">167</p>	Li ⁺	0.1		
	Na ⁺	64.3	Zn ²⁺	0.0
	K ⁺	2.3	Co ²⁺	1.0
	Cs ⁺	0.7	Cu ²⁺	2.1
	Ca ²⁺	2.1	Sr ²⁺	1.3
	Ba ²⁺	1.2	Pb ²⁺	0.62
	Mg ²⁺	0.8	La ³⁺	9.0

Table 6.10 Extraction results with 167

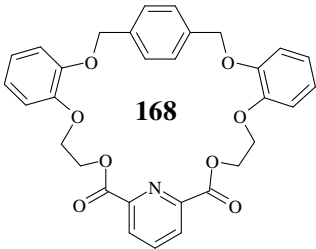
Binding Agent	Cation	% Extraction	Cation	% Extraction
 <p style="text-align: center;">168</p>	Li ⁺	1.0		
	Na ⁺	54.6	Zn ²⁺	0.6
	K ⁺	3.1	Co ²⁺	0.5
	Cs ⁺	0.3	Cu ²⁺	2.2
	Ca ²⁺	1.2	Sr ²⁺	1.2
	Ba ²⁺	2.0	Pb ²⁺	0.7
	Mg ²⁺	0.8	La ³⁺	10.1

Table 6.11 Extraction results with 168

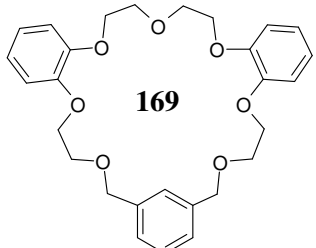
Binding Agent	Cation	% Extraction	Cation	% Extraction
 <p style="text-align: center;">169</p>	Li ⁺	1.3		
	Na ⁺	21.1	Zn ²⁺	0.9
	K ⁺	6.8	Co ²⁺	1.4
	Cs ⁺	0.4	Cu ²⁺	1.9
	Ca ²⁺	1.3	Sr ²⁺	1.0
	Ba ²⁺	2.1	Pb ²⁺	0.0
	Mg ²⁺	0.8	La ³⁺	4.3

Table 6.12 Extraction results with 169

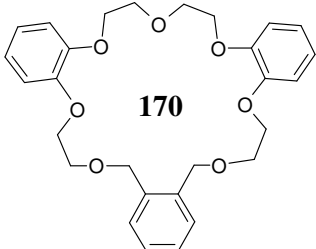
Binding Agent	Cation	% Extraction	Cation	% Extraction
 <p style="text-align: center;">170</p>	Li ⁺	1.7		
	Na ⁺	5.8	Zn ²⁺	0.0
	K ⁺	1.3	Co ²⁺	0.2
	Cs ⁺	0.6	Cu ²⁺	2.1
	Ca ²⁺	1.0	Sr ²⁺	0.0
	Ba ²⁺	0.7	Pb ²⁺	0.5
	Mg ²⁺	0.9	La ³⁺	2.3

Table 6.13 Extraction results with 170

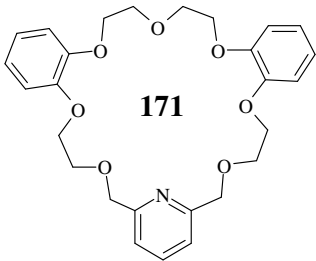
Binding Agent	Cation	% Extraction	Cation	% Extraction
	Li ⁺	0.2		
	Na ⁺	4.6	Zn ²⁺	0.3
	K ⁺	0.1	Co ²⁺	0.1
	Cs ⁺	0.0	Cu ²⁺	1.9
	Ca ²⁺	0.3	Sr ²⁺	0.2
	Ba ²⁺	0.1	Pb ²⁺	0.2
	Mg ²⁺	0.2	La ³⁺	5.5

Table 6.14 Extraction results with 171

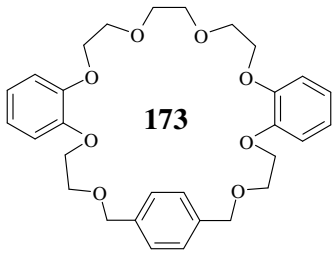
Binding Agent	Cation	% Extraction	Cation	% Extraction
	Li ⁺	0.00		
	Na ⁺	41.7	Zn ²⁺	0.00
	K ⁺	4.0	Co ²⁺	0.1
	Cs ⁺	0.34	Cu ²⁺	1.9
	Ca ²⁺	0.0	Sr ²⁺	1.2
	Ba ²⁺	1.0	Pb ²⁺	0.3
	Mg ²⁺	0.0	La ³⁺	4.7

Table 6.15 Extraction results with 173

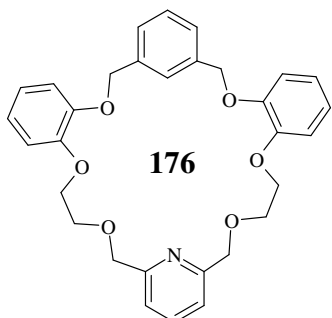
Binding Agent	Cation	% Extraction	Cation	% Extraction
	Li ⁺	0.2		
	Na ⁺	52.6	Zn ²⁺	1.4
	K ⁺	1.7	Co ²⁺	1.2
	Cs ⁺	1.2	Cu ²⁺	2.0
	Ca ²⁺	1.3	Sr ²⁺	1.1
	Ba ²⁺	0.7	Pb ²⁺	0.7
	Mg ²⁺	1.4	La ³⁺	7.2

Table 6.16 Extraction results with 176

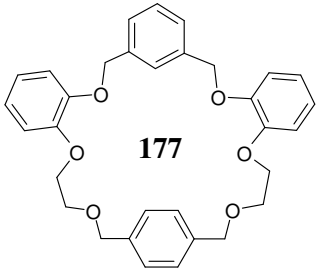
Binding Agent	Cation	% Extraction	Cation	% Extraction
	Li ⁺	1.2		
	Na ⁺	72.0	Zn ²⁺	0.0
	K ⁺	4.8	Co ²⁺	0.29
	Cs ⁺	0.1	Cu ²⁺	1.9
	Ca ²⁺	0.0	Sr ²⁺	0.0
	Ba ²⁺	0.0	Pb ²⁺	0.5
	Mg ²⁺	0.0	La ³⁺	4.3

Table 6.17 Extraction results with 177

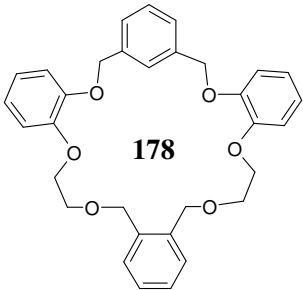
Binding Agent	Cation	% Extraction	Cation	% Extraction
	Li ⁺	0.8		
	Na ⁺	71.0	Zn ²⁺	0.88
	K ⁺	3.1	Co ²⁺	0.54
	Cs ⁺	16.1	Cu ²⁺	1.97
	Ca ²⁺	0.9	Sr ²⁺	0.53
	Ba ²⁺	0.7	Pb ²⁺	0.06
	Mg ²⁺	1.1	La ³⁺	2.62

Table 6.18 Extraction results with 178

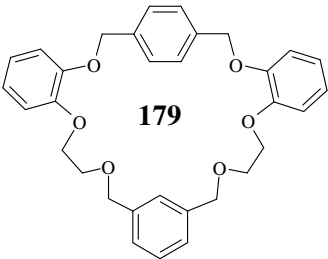
Binding Agent	Cation	% Extraction	Cation	% Extraction
	Li ⁺	0.7		
	Na ⁺	29.7	Zn ²⁺	0.9
	K ⁺	3.8	Co ²⁺	1.1
	Cs ⁺	1.2	Cu ²⁺	2.0
	Ca ²⁺	1.2	Sr ²⁺	1.0
	Ba ²⁺	2.1	Pb ²⁺	1.5
	Mg ²⁺	0.9	La ³⁺	9.7

Table 6.19 Extraction results with 179

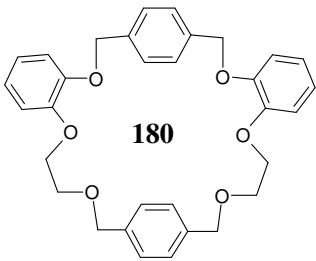
Binding Agent	Cation	% Extraction	Cation	% Extraction
	Li ⁺	1.9		
	Na ⁺	57.4	Zn ²⁺	1.9
	K ⁺	13.8	Co ²⁺	1.7
	Cs ⁺	3.0	Cu ²⁺	1.6
	Ca ²⁺	1.5	Sr ²⁺	1.6
	Ba ²⁺	0.9	Pb ²⁺	1.00
	Mg ²⁺	1.2	La ³⁺	10.6

Table 6.20 Extraction results with 180

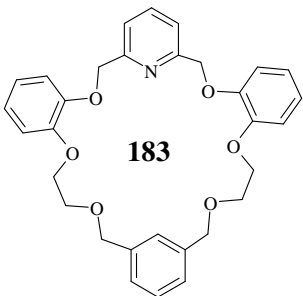
Binding Agent	Cation	% Extraction	Cation	% Extraction
	Li ⁺	0.2		
	Na ⁺	32.5	Zn ²⁺	1.7
	K ⁺	5.8	Co ²⁺	1.1
	Cs ⁺	1.0	Cu ²⁺	1.2
	Ca ²⁺	0.3	Sr ²⁺	1.0
	Ba ²⁺	0.7	Pb ²⁺	0.7
	Mg ²⁺	1.2	La ³⁺	6.7

Table 6.21 Extraction results with 183

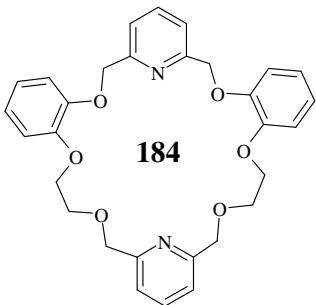
Binding Agent	Cation	% Extraction	Cation	% Extraction
	Li ⁺	0.5		
	Na ⁺	30.1	Zn ²⁺	0.9
	K ⁺	4.7	Co ²⁺	0.5
	Cs ⁺	0.0	Cu ²⁺	2.3
	Ca ²⁺	1.4	Sr ²⁺	1.0
	Ba ²⁺	0.9	Pb ²⁺	0.8
	Mg ²⁺	0.1	La ³⁺	7.4

Table 6.22 Extraction results with 184

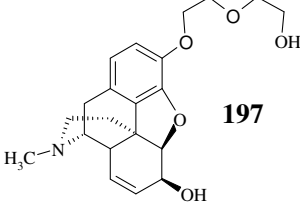
Binding Agent	Cation	% Extraction	Cation	% Extraction
 197	Li ⁺	3.7		
	Na ⁺	16.2	Zn ²⁺	0.4
	K ⁺	3.3	Co ²⁺	16.2
	Cs ⁺	1.1	Cu ²⁺	14.2
	Ca ²⁺	8.3	Sr ²⁺	11.1
	Ba ²⁺	10.4	Pb ²⁺	19.5
	Mg ²⁺	2.7	La ³⁺	11.2

Table 6.23 Extraction results with 197

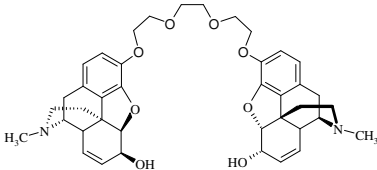
Binding Agent	Cation	% Extraction	Cation	% Extraction
 194	Li ⁺	1.9		
	Na ⁺	4.2	Zn ²⁺	12.2
	K ⁺	21.6	Co ²⁺	28.6
	Cs ⁺	24.0	Cu ²⁺	45.7
	Ca ²⁺	20.4	Sr ²⁺	20.3
	Ba ²⁺	16.4	Pb ²⁺	40.4
	Mg ²⁺	4.5	La ³⁺	16.5

Table 6.24 Extraction results with 194

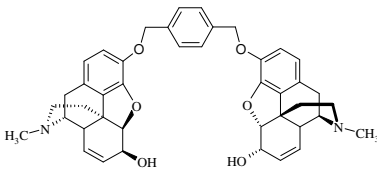
Binding Agent	Cation	% Extraction	Cation	% Extraction
 198	Li ⁺	0.00		
	Na ⁺	0.2	Zn ²⁺	4.2
	K ⁺	2.5	Co ²⁺	8.1
	Cs ⁺	3.3	Cu ²⁺	8.9
	Ca ²⁺	8.7	Sr ²⁺	4.9
	Ba ²⁺	16.3	Pb ²⁺	24.7
	Mg ²⁺	8.0	La ³⁺	17.6

Table 6.25 Extraction results with 198

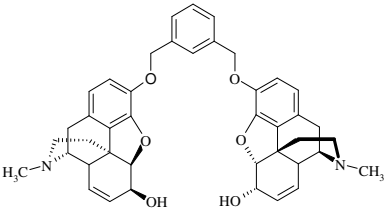
Binding Agent	Cation	% Extraction	Cation	% Extraction
 <p style="text-align: center;">199</p>	Li ⁺	0.00		
	Na ⁺	0.6	Zn ²⁺	4.4
	K ⁺	0.2	Co ²⁺	12.7
	Cs ⁺	3.1	Cu ²⁺	20.5
	Ca ²⁺	3.5	Sr ²⁺	5.8
	Ba ²⁺	3.9	Pb ²⁺	28.9
	Mg ²⁺	2.0	La ³⁺	19.6

Table 6.26 Extraction results with **199**

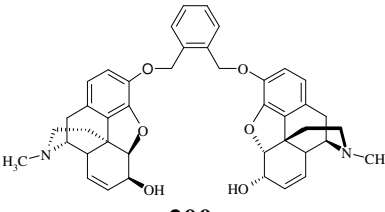
Binding Agent	Cation	% Extraction	Cation	% Extraction
 <p style="text-align: center;">200</p>	Li ⁺	1.2		
	Na ⁺	41.9	Zn ²⁺	8.1
	K ⁺	3.8	Co ²⁺	17.0
	Cs ⁺	1.3	Cu ²⁺	28.8
	Ca ²⁺	16.0	Sr ²⁺	12.2
	Ba ²⁺	19.8	Pb ²⁺	45.9
	Mg ²⁺	11.1	La ³⁺	20.1

Table 6.27 Extraction results with **200**

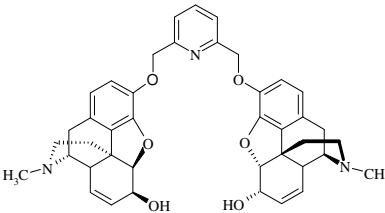
Binding Agent	Cation	% Extraction	Cation	% Extraction
 <p style="text-align: center;">201</p>	Li ⁺	1.3		
	Na ⁺	23.1	Zn ²⁺	16.7
	K ⁺	20.0	Co ²⁺	20.4
	Cs ⁺	4.5	Cu ²⁺	60.6
	Ca ²⁺	12.1	Sr ²⁺	12.0
	Ba ²⁺	11.6	Pb ²⁺	72.5
	Mg ²⁺	4.2	La ³⁺	23.9

Table 6.28 Extraction results with **201**

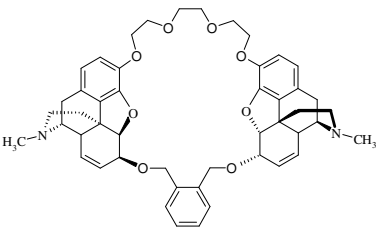
Binding Agent	Cation	% Extraction	Cation	% Extraction
 <p style="text-align: center;">217</p>	Li ⁺	3.1		
	Na ⁺	11.9	Zn ²⁺	41.8
	K ⁺	17.5	Co ²⁺	54.6
	Cs ⁺	41.9	Cu ²⁺	72.6
	Ca ²⁺	19.8	Sr ²⁺	38.7
	Ba ²⁺	13.5	Pb ²⁺	78.0
	Mg ²⁺	21.3	La ³⁺	43.2

Table 6.29 Extraction results with 217

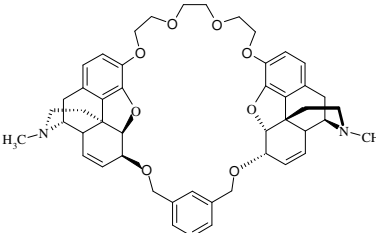
Binding Agent	Cation	% Extraction	Cation	% Extraction
 <p style="text-align: center;">218</p>	Li ⁺	0.8		
	Na ⁺	0.2	Zn ²⁺	24.3
	K ⁺	0.0	Co ²⁺	16.1
	Cs ⁺	0.9	Cu ²⁺	34.0
	Ca ²⁺	12.9	Sr ²⁺	8.8
	Ba ²⁺	4.8	Pb ²⁺	53.2
	Mg ²⁺	13.0	La ³⁺	17.1

Table 6.30 Extraction results with 218

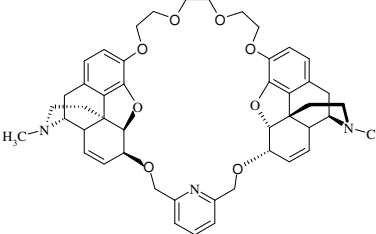
Binding Agent	Cation	% Extraction	Cation	% Extraction
 <p style="text-align: center;">219</p>	Li ⁺	0.9		
	Na ⁺	4.7	Zn ²⁺	4.2
	K ⁺	2.6	Co ²⁺	23.7
	Cs ⁺	1.6	Cu ²⁺	32.6
	Ca ²⁺	0.9	Sr ²⁺	20.3
	Ba ²⁺	4.3	Pb ²⁺	62.3
	Mg ²⁺	0.8	La ³⁺	16.7

Table 6.31 Extraction results with 219

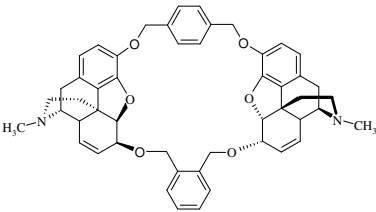
Binding Agent	Cation	% Extraction	Cation	% Extraction
 <p style="text-align: center;">220</p>	Li ⁺	0.4		
	Na ⁺	0.4	Zn ²⁺	23.5
	K ⁺	4.4	Co ²⁺	36.6
	Cs ⁺	8.7	Cu ²⁺	60.6
	Ca ²⁺	5.2	Sr ²⁺	27.4
	Ba ²⁺	7.2	Pb ²⁺	48.2
	Mg ²⁺	0.5	La ³⁺	39.8

Table 6.32 Extraction results with **220**

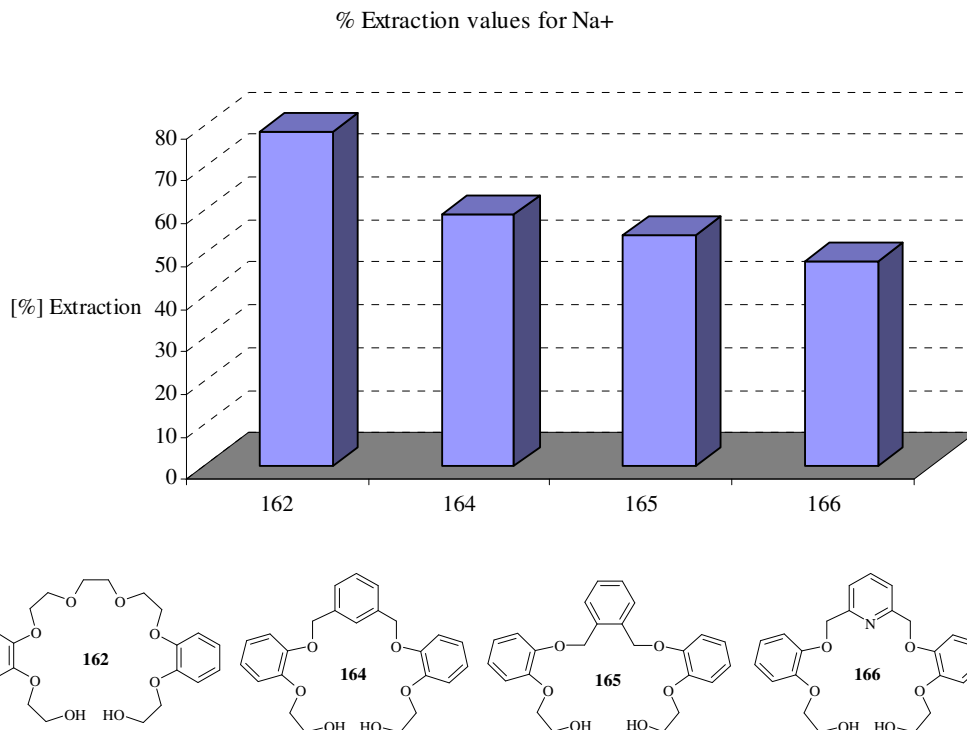
Pedersen reported extraction values for crown ethers with various ring sizes and incorporating both cyclohexyl and benzene rings. The general conclusion according to the Table 6.33 is that crown ethers with benzene rings are more rigid and less flexible than their cyclohexyl analogues, therefore macrocycles with the same cavity size but with carbocyclic rings would extract the same metal picrate with different efficacies.

The measured dimensions of the cavities of macrocycles **179** and **184** (Chapter 5) are quite large and these parameters correspond to the scaffold of 24-crown-8. Since macrocycles of the 24-crown-8 type exhibit moderate complexation of cations like K⁺ and Cs⁺ with diameters of 2.66 and 3.34 Å respectively, complexation of the potassium cation, despite its smaller diameter is slightly preferred over the caesium cation. A similar trend was observed for dicyclohexyl-21-crown-7 which extracted K⁺ and Cs⁺ from aqueous solution with good efficiency (Table 6.33), though preferential complexation of the potassium cation was spotted. According to the cavity size, similar binding properties would be expected from **179** and **184**, however these macrocycles contain different number of donor oxygens which might influence their binding preferences.

Crown Ether	Picrate Extracted [%]			
	Li ⁺	Na ⁺	K ⁺	Cs ⁺
Dicyclohexyl-14-crown-4	1.1	0	0	0
Cyclohexyl-15-crown-5	1.6	19.7	8.7	4.0
Dibenzo-18-crown-6	0	1.6	25.2	5.8
Dicyclohexyl-18-crown-6	3.3	25.6	77.8	44.2
Dicyclohexyl-21-crown-7	3.1	22.6	51.3	49.7
Dicyclohexyl-24-crown-8	2.9	8.9	20.1	18.1

Table 6.33 Extraction results, two-phase liquid extraction: methylene chloride and water

Macrocyclic compounds and their precursors described in this thesis contain at least two aromatic rings or rigid morphine units, therefore especially in the case of the cyclised structures we do not expect much flexibility and minimal conformational change is expected on binding to the metal cation making binding more entropically favourable. The acyclic polyethers **160**, **161**, **163** did not complex appreciably to any of the metal picrates. Among the thirty compounds tested twelve of them showed significant extraction values for sodium picrate. Pedersen's crown ethers dibenzo-18-crown-6 and dicyclohexyl-18-crown-6 exhibit higher affinity towards K⁺ over Na⁺. The same trend was observed for macrocycles with bigger cavities, dicyclohexyl-21-crown-7 and dicyclohexyl-24-crown-8, whereas binding studies performed for this project showed the opposite trend. The highest extraction value for Na⁺ was observed for model macrocyclic precursor **162** (78.2 %). This result was quite surprising, considering the size of its cavity. Regrettably, of all the macrocyclic precursors **162** was the only one that did not give good quality crystals for X-ray analysis.



Graph 6.1 % Extraction values for macrocyclic precursors **162**, **164**, **165**, **166**

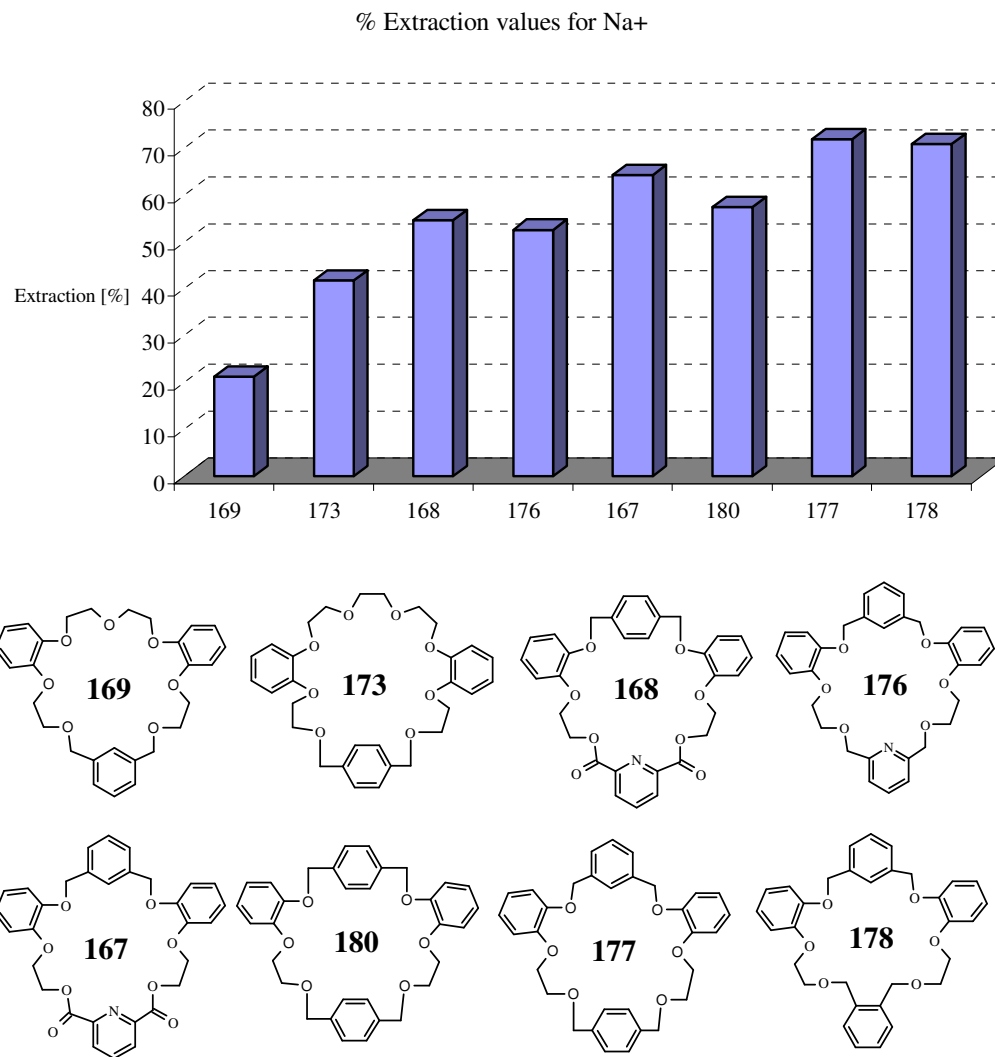
The extraction data showed significant binding of several macrocyclic structures and their precursors towards sodium picrate. Among the nineteen model macrocyclic systems the highest extraction values were observed for **177** (72.0 %), **178** (71.0 %), **167** (64.3%), **180** (57.4 %) and **168** (54.6 %). The common feature linking all these compounds is the presence of four aromatic rings in their structures arranged in such a way as to form a rigid cavity surrounded by six donor oxygen atoms. According to the data in the table and from analysis of cavity sizes in the crystallographic (relevant) literature we would expect metal picrates with cation diameters larger than sodium to be bound more effectively. Also the most efficient extractions were observed in the case of model macrocycles containing 4 aromatic rings instead of 3 in which the xylene linker is replaced by an ethereal chain. This may suggest that the presence of 4 aromatic rings in the macrocycle may facilitate binding process by arrangement of aromatic rings in a way which prevents from binding to the bigger cation.

Macrocycles **169**, **173**, **167**, **168**, **176**, **177** and their extraction values for Na⁺ and K⁺ are presented in Table 6.34. Macrocycle **169** exhibits relatively low extraction values

for Na⁺ 21.1 % and even lower for K⁺ 6.8 %, whereas macrocycle **173** the cavity selectivity towards Na⁺ over K⁺ increased and extraction values were 41.7 and 4.0 %, respectively. Macrocycles containing a pyridine ring **167**, **168** and **176**, gave high extraction values for Na⁺ (64.3 %, 54.6 % and 52.6 %, respectively) and proved to have significant binding affinity for La³⁺ (9.0 % and 10.1 %, 7.2 %) and to bind relatively weakly to K⁺. Macrocycle **177** showed an excellent 72 % extraction value for Na⁺ and about 5 % for K⁺.

	169	173	167	168	176	177
Na ⁺	21.1	41.7	64.3	54.6	52.6	72.0
K ⁺	6.8	4.0	2.3	3.1	1.7	4.8
La ³⁺	4.3	4.7	9.0	10.1	7.2	4.3

Table 6.34 Extraction values of **167**, **168**, **169**, **173**, **176**, **177** for Na⁺, K⁺ and La³⁺

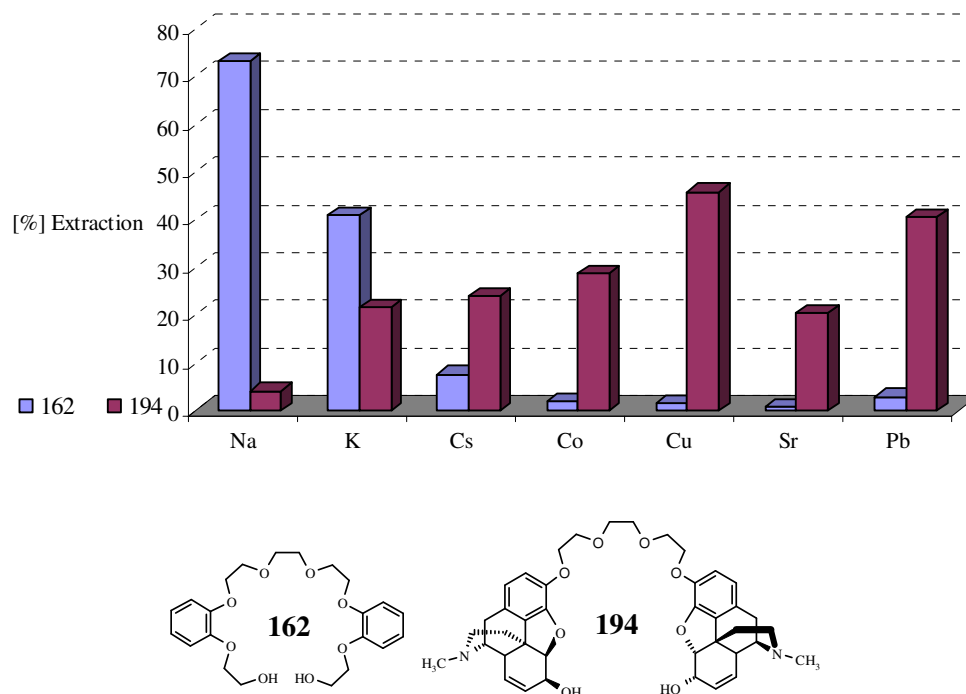


Graph 6.2 % Extraction values of **167, 168, 169, 173, 176, 177, 178, 180** for Na⁺

Apart from interactions between the cation and donor oxygen atoms, the complexation process may also be favoured by cation- π interactions with π -electrons from the aromatic rings. None of the tested ligands exhibited a high affinity for potassium and caesium whose hydroxides played a significant role in the ring closure step. The optimal metal for the preorganization of the acyclic precursor to facilitate ring closure does not necessarily have optimal fit with the macrocyclic product. Careful selection of templates to assist synthesis *versus* binding metal studies is always an important compromise.

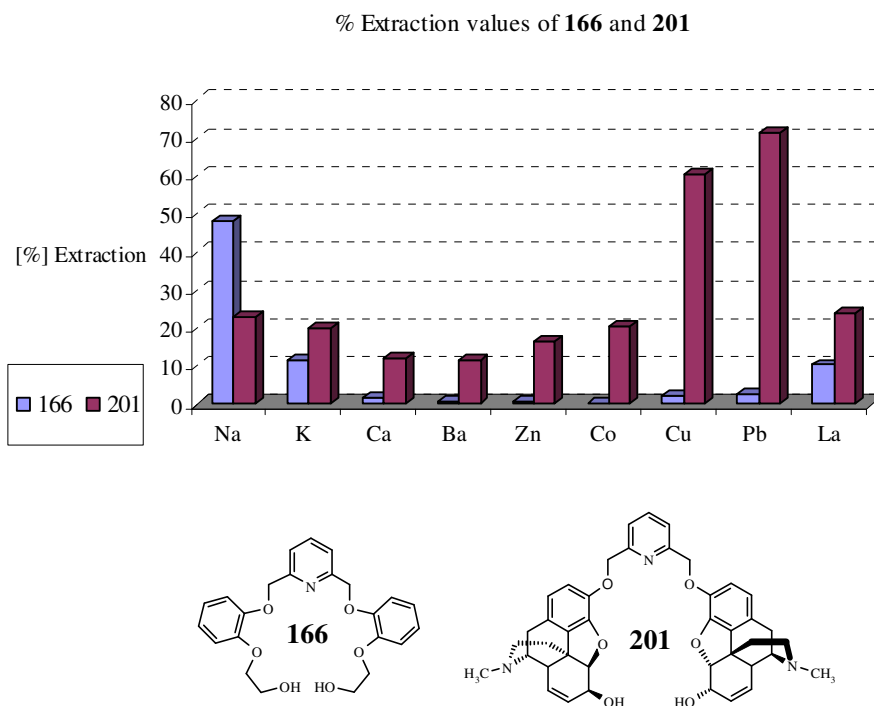
If a comparison is made between the extraction values of two macrocyclic precursors, one based on the 2-(2-hydroxyethoxy)phenol unit **162** and the second one incorporating two morphine units **194** interesting affinity can be observed. From the Graph 6.3 it is clear that **162** exhibits high extraction values for sodium 78.2 % and potassium 40.8 % and moderate values for caesium 7.5 % picrates, whereas noticeable signs of efficient binding towards transition metal cations (apart from lanthanum, 9.6 %) were not observed. However, increased extraction values with **194** were observed towards copper (45.7 %), lead (40 %), cobalt (28.6 %) and strontium (20.3 %) picrates.

% Extraction values of **162** and **194**



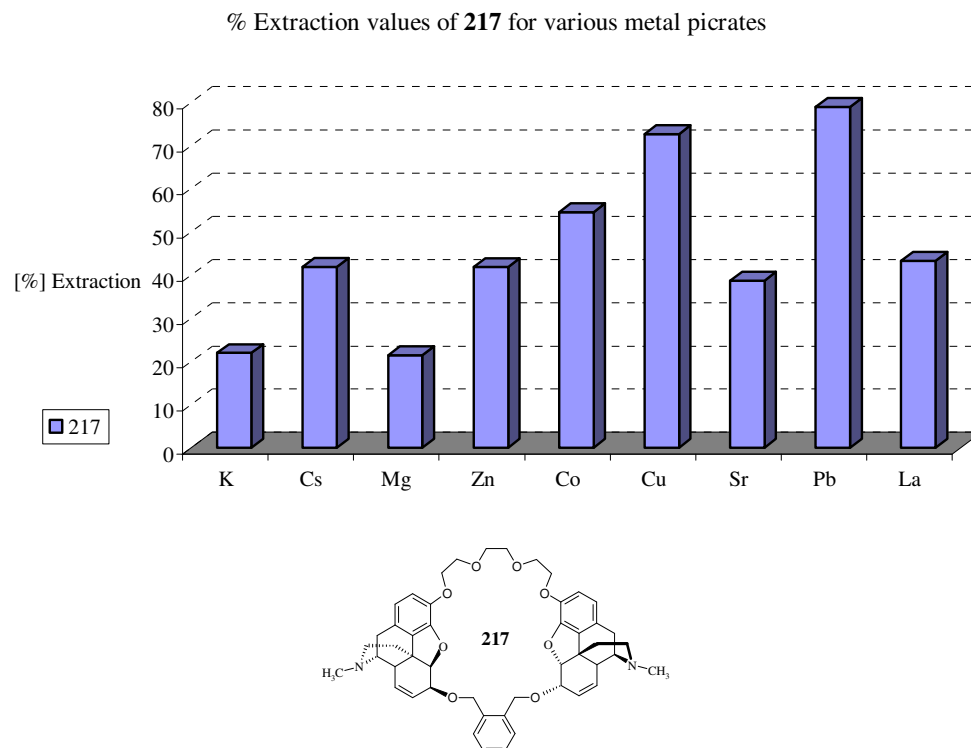
Graph 6.3 % Extraction values of **162** and **194** for series of various metal cations

Similar properties were observed for open structure **201** which preferentially extracted lead and copper, whereas **166** shows binding preference towards sodium picrate. Significant extraction values for the transition metal cations was not observed.



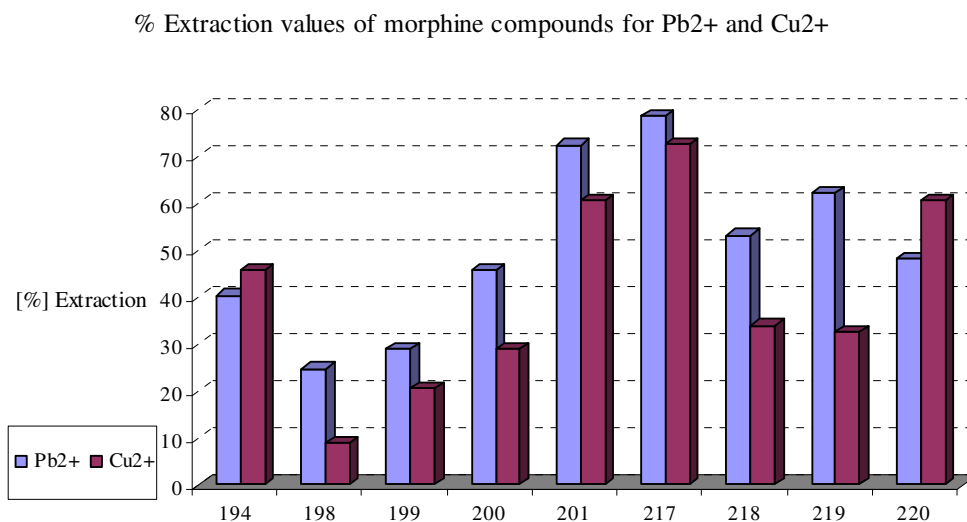
Graph 6.4 % Extraction values of **166** and **201** for series of various metal cations

217 was the only morphine macrocycle to show appreciable binding to the series of metal picrates. 41.9 % of the caesium picrate was extracted from the aqueous layer by **217** and this is the highest binding ability towards this metal picrate among all the compounds tested. Potassium, magnesium and calcium picrates were also extracted from the aqueous layer to the extent of 17.5 %, 21.3 % and 19.8 % respectively. **217** proved to be an especially effective extracting agent towards lead (78.0 %) and copper (72.6 %) picrates, although quite significant values were also observed for cobalt (54.6 %), zinc (41.8 %), strontium (38.7 %) and lanthanum (43.2 %) picrates.



Graph 6.5 % Extraction values of **217** for series of various metal cations

Graph 6.6 emphasizes the high affinity of morphine macrocycles and their precursors towards lead and copper cations. Amongst all the ligands based on morphine, the highest extraction values were observed for lead and copper picrates, especially in the cases of **201** and **217**. Further testing would be required in order to determine whether these macrocycles with their affinity for copper and lead might have applications as possible co-catalysts.



Graph 6.6 % Extraction values of morphine compounds for Pb²⁺ and Cu²⁺

As can be seen from the graphs, the morphine macrocycles and their precursors showed higher affinity towards transition metals compared with aromatic polyether model systems. This is not just a result of modifying the host cavity, but rather may be due to the tertiary amino group of morphine, a soft ligating site which is known to increase the affinity of crown ethers for transition metals^{160,161}. Therefore it was decided to perform a control experiment with morphine for copper and lead picrates.

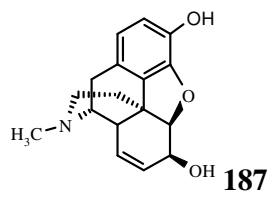
	Cation	% Extraction	Cation	% Extraction
		Pb ²⁺	10.7	Cu ²⁺

Table 6.35 Extraction results for Pb²⁺ and Cu²⁺ with morphine **187**

Control experiments were performed in order to establish whether the significant binding values of morphine compounds toward Pb²⁺ and Cu²⁺ were due to the presence of morphine moiety in the tested compounds. Since tests showed that morphine itself exhibits a binding value of 10.7 % for Pb²⁺ and 8.4 % for Cu²⁺ it may be concluded that additional functional groups *e.g.* polyetheral chains, aromatic rings and also the effect of the cyclic structure play an important role in binding of transition metal cations.

6.3 Conclusion

The macrocycles and their precursors synthesised in this project were tested for metal extraction ability against a variety of metal picrates. Some of these products did not exhibit significant extraction values for any of the metal picrates, although an ability to extract multiple metal picrates was more common. Furthermore, the preference exhibited by several crown ethers to bind with sodium suggests that the binding affinities of the novel crown ethers for cations are not based only on ionic size.

It was interesting to note that morphine macrocycles and their precursors bind strongly to transition metals and that they are able to extract lead and copper picrates most effectively. For the calculations we have assumed the formation of 1:1 complexes, but it is possible that the actual binding of metal picrates to crown ethers is a result of aggregation of metal ions and crown ethers, however, this aspect requires further investigation¹⁶². Steric effect from the opiate backbone may make 1:2 or 2:3 complexes difficult to prepare. However, until X-ray structure of the opiate linker ligand and preferably the metal inclusion complex are solved, this is open to debate.

The morphine macrocycles and their precursors could have applications as potential sensors or as co-catalysts with metals for asymmetric catalysis, for example in the catalytic Friedel-Crafts reaction¹⁶³. This was an initial goal of the project, which was unaccomplished, therefore we are obliged to pass the idea to be investigated by following researchers.

It has to be mentioned that these extraction studies do not take into account stoichiometry of the complexes, because the ratio of complexing agent:metal picrate is assumed to be 1:1 for the purpose of the calculations. However it is well known that the ratio can be more complex and formation of 1:2 or 2:3 complexes could also take place.

6.4 Experimental

Thirty macrocyclic structures and their precursors were tested for their ability to extract a number of metal picrates.

Picric acid (0.77g, 65% suspension in water) was suspended in 20 mL of water and warmed to 70 °C to make a saturated solution. The metal carbonate was added slowly to the hot solution with stirring until evolution of CO₂ ceased. The solution was allowed to cool to 0 °C slowly and the yellow solid that precipitated was isolated by gravity filtration, washed with 5 mL of cold water and allowed to air-dry. All the following metal picrates were synthesised according to the same method:

LiC₆H₂N₃O₇, NaC₆H₂N₃O₇, KC₆H₂N₃O₇, CsC₆H₂N₃O₇, Mg(C₆H₂N₃O₇)₂, Ca(C₆H₂N₃O₇)₂, Ba(C₆H₂N₃O₇)₂, Zn(C₆H₂N₃O₇)₂, Co(C₆H₂N₃O₇)₂, Cu(C₆H₂N₃O₇)₂, Sr(C₆H₂N₃O₇)₂, Pb(C₆H₂N₃O₇)₂, and La(C₆H₂N₃O₇)₃. According to an agreement with the head of safety it was not permitted to completely dry the metal picrates and therefore accurate isolated yields products could not be recorded.

1000 mL of 7x10⁻⁵ M solutions of each of the picrate salts were made up in deionised water. The solutions of extracting agents (500 mL each) were made up to a concentration of 1.75x10⁻⁵ M in chloroform. Each metal picrate was extracted with each of the 30 macrocyclic structures and their precursors.

6 mL each of both the picrate solution and the macrocycle solution were transferred into a glass vial and shaken on an automatic shaker for 15 minutes and the same procedure was repeated 3 times. The UV absorption spectrum for each picrate salt was measured at 356 nm and then this was compared with the aqueous layer of each mixture after shaking.

Blank extractions with chloroform were carried out for each of the picrate solutions. The recorded absorbance for each case was oscillating around the same value recorded for deionised water. Blank experiments showed that no picrate extraction occurred in the absence of crown ethers or their precursors.

Picrate extraction studies were carried out and the % extraction values of various ions were calculated using the following equation:

$$\%E = 100 \cdot \left(\frac{(Mol_{picrate})_0 - (Mol_{picrate})_E}{Mol_{binding\ agent}} \right)$$

Where $(Mol_{picrate})_0$ is the number of moles of metal picrate in the aqueous layer originally, $(Mol_{picrate})_E$ is the number of moles of the picrate salt in the aqueous layer after extraction and $(Mol_{binding\ agent})$ is the number of moles of binding agent in the organic layer.

The calibration curves for each of the metal picrates were drawn according to data collected from standard solutions of metal picrates. The coefficient of determination (R^2 value) for each calibration curve was $> 99\%$ and these records were used to calculate the percentage extraction of metal picrates into the organic layer.

7 Biological activity of model macrocycles and their precursors

7.1 Lung cell carcinoma assay

For the purpose of this project, the bioactivity of macrocyclic compounds and their precursors was assessed by screening against non-small cell lung carcinoma cell lines. The *in vitro* model chosen for investigating the potential of synthesised compounds was DLKP and DLKP-A cell lines. The DLKP-A cell line is a daughter cell line of DLKP, a poorly differentiated squamous cell lung carcinoma. The main mechanism of multidrug resistance (MDR) for DLKP is *via* MRP1 and it is a poor expresser of P-glycoprotein (P-gp). DLKP-A's line is a daughter cell line of DLKP and the main mechanism of MDR is *via* the P-gp membrane pump. DLKP-A mainly expresses P-gp, while expressing very low levels of multidrug resistance protein 1 (MRP1). The compounds obtained in this project were designed with the idea of aiding the delivery of drug to the cell, thereby increasing the effectiveness of a dose. A range of macrocyclic compounds and their precursors were synthesized and their anti-proliferative effectiveness was studied, alone and in combination with a chemotherapeutic drugs, epirubicin **227** and taxotere **228**.

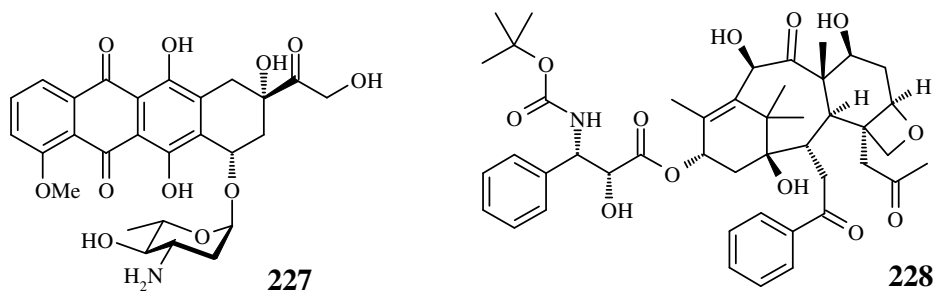


Fig. 7.1 Structures of epirubicin **227** and taxotere **228** chemotherapeutics

7.2 MultiDrug Resistance Proteins

MultiDrug Resistance (MDR) is a major factor in the failure of cancer chemotherapy. MDR is a phenomenon whereby tumour cells *in vitro* that have been exposed to one cytotoxic agent develop cross-resistance to a range of structurally and functionally unrelated compounds. This resistance is often due to an elevation in the expression of particular proteins, such as cell membrane transporters, which can result in an increased efflux of cytotoxic drugs from the cancer cells¹⁶⁴.

The two MDR proteins of interest in this report are P-gp and MRP1. Both of which are also members of the ATP-binding cassette (ABC) family. These proteins bind ATP and use the energy to drive the transport of various molecules across all cell membranes.

P-gp is a transmembrane protein with a very broad specificity for the structures it pumps out of cells. One effective way to overcome P-gp-mediated drug resistance is either to block the drug pumping function of P-gp or to inhibit its expression. Many agents that modulate the function of P-gp have been identified, including calcium channel blockers, calmodulin antagonists, steroidal agents, protein kinase C inhibitors, immunosuppressive drugs, antibiotics, and surfactants¹⁶⁵. MRP1 is located in the cytoplasm and is responsible for carrying cellular drugs to the cell membrane and expelling them from the cell. It is thought to play both a role in protecting cells from chemical toxicity and oxidative stress and to mediate inflammatory responses. Out of all the compounds synthesised, several were selected for biological investigation. Commercially purchased samples of 15-crown-5, benzo-15-crown-5, 18-crown-6, benzo-18-crown-6, dibenzo-18-crown-6 and their linear precursors, tri-, tetra-, penta-, and hexaethylene glycols (Sigma Aldrich) were also screened. These compounds were primarily selected on the basis of solubility properties in aqueous solutions. Dimethylsulfoxide was used to solubilise the compounds in question, before solubility of the solution was tested in aqueous media. A minimum concentration of 0.5 mg/mL in the medium was required for a compound to undergo biological evaluation.

7.3 Biological results

Compounds **160-166**, **169**, **170**, **173** and **178** were examined for inhibition of the P-gp efflux pump. These compounds were also studied for their anti-proliferative effectiveness against DLKP and DLKP-A cell lines, alone and in combination with the widely used chemotherapeutic drugs epirubicin and taxotere.

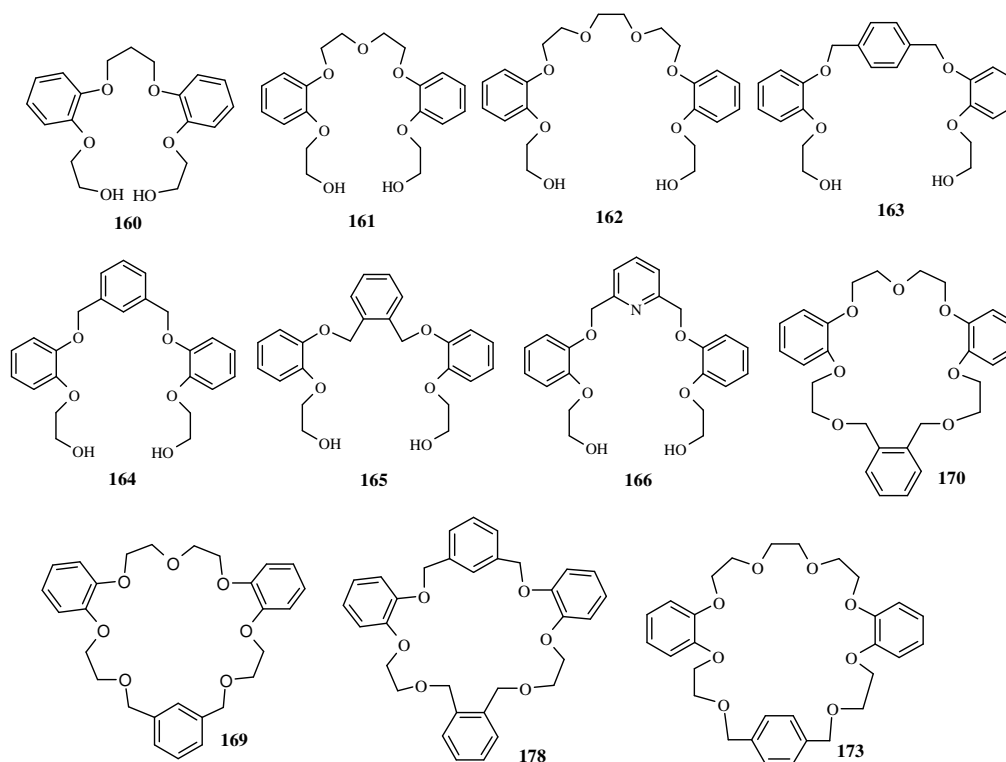


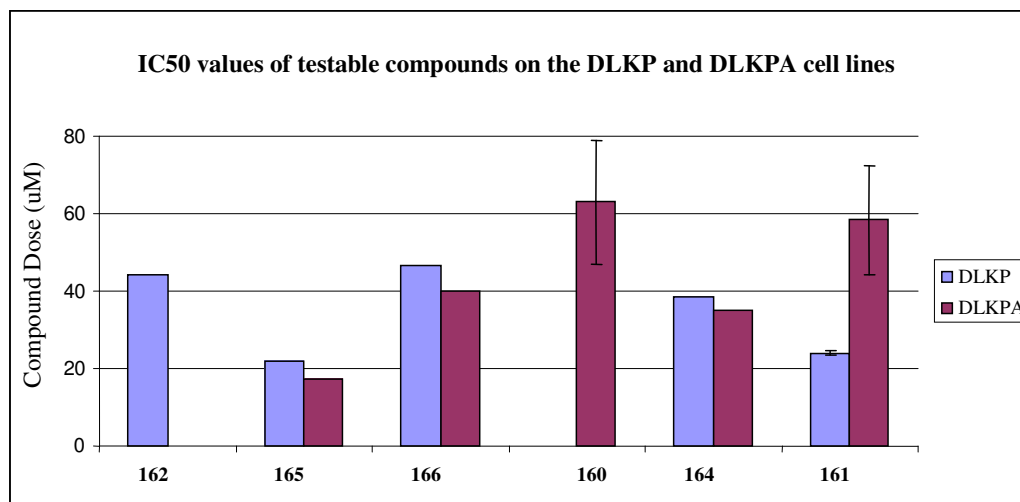
Fig. 7.2 Macrocycles and their precursors screened for the inhibition of the P-gp

Of the 16 macrocyclic compounds and their precursors submitted for testing only 11 had acceptable solubility properties. However, the majority of candidates with good water solubility did not inhibit P-gp, therefore full data with bar charts for those are separately included in the Appendix B.

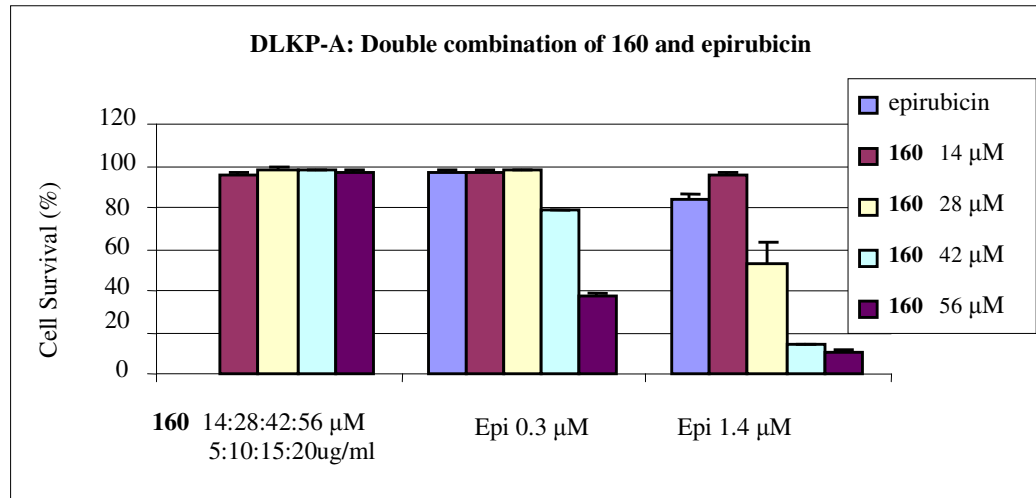
7.3.1 Biological activity of macrocyclic precursors

The determination of IC_{50} values for the eight macrocyclic precursors was carried out on both the DLKP and DLKP-A cell lines. **165** (22 μ M and 17.4 μ M, respectively)

was found to have the greatest effect on cell proliferation whereas **160** (>50 μM and $63.16 \pm 16 \mu\text{M}$, respectively) was the least toxic.



Graph 7.1 The IC₅₀ values of the six testable compounds on both the DLKP and DLKPA cell lines. Experiments with no errors bars were only carried out once whereas those with error bars were carried out twice.

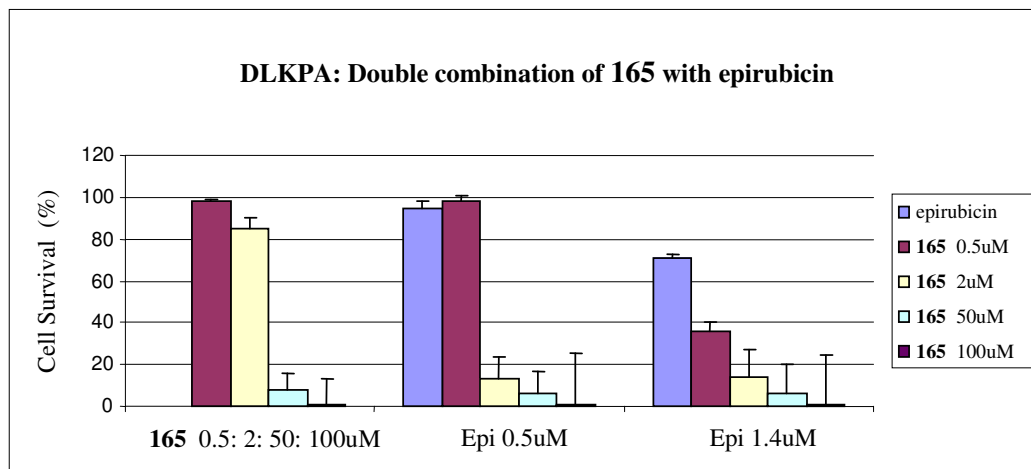


Graph 7.2 Combination of **160** with epirubicin on the DLKP-A cell line

The bar charts shown in Graphs 7.2 and 7.3 demonstrate the increase in activity when **160** and **165** are combined with the epirubicin. In the assay of cell line DLKP-A, **160** inhibits cell growth by over 60 % at an epirubicin concentration of 0.3 μM

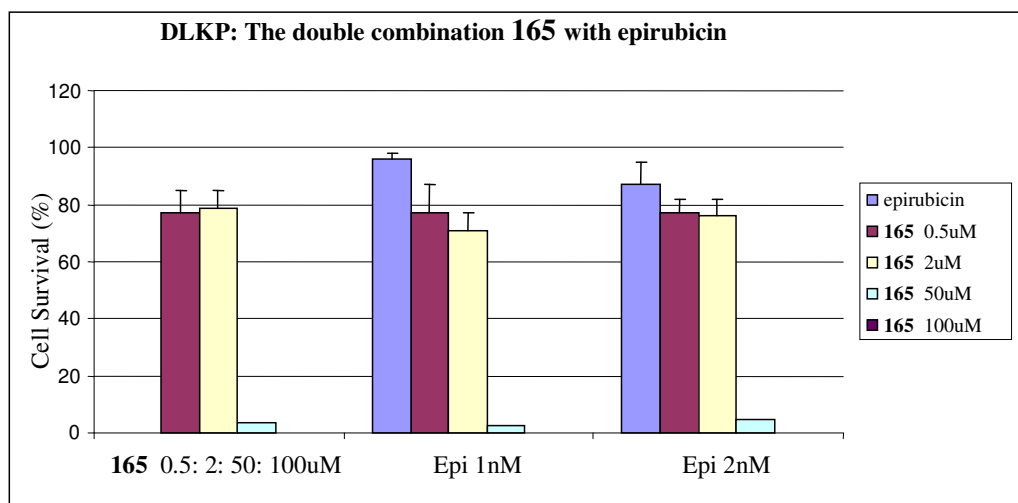
and **160** at 56 $\mu\text{g/mL}$. **160** was also found to be nontoxic to DLKP-A cells up to a concentration of 20 $\mu\text{g/mL}$.

Synergy was observed with **165** at a concentration of 2 μM and epirubicin at 0.5 μM . With a lower concentration of **165**, 0.5 μM , and a slightly higher concentration of epirubicin, 1.4 μM , synergy was also observed. The IC_{50} for this compound was found to be 17.4 μM .

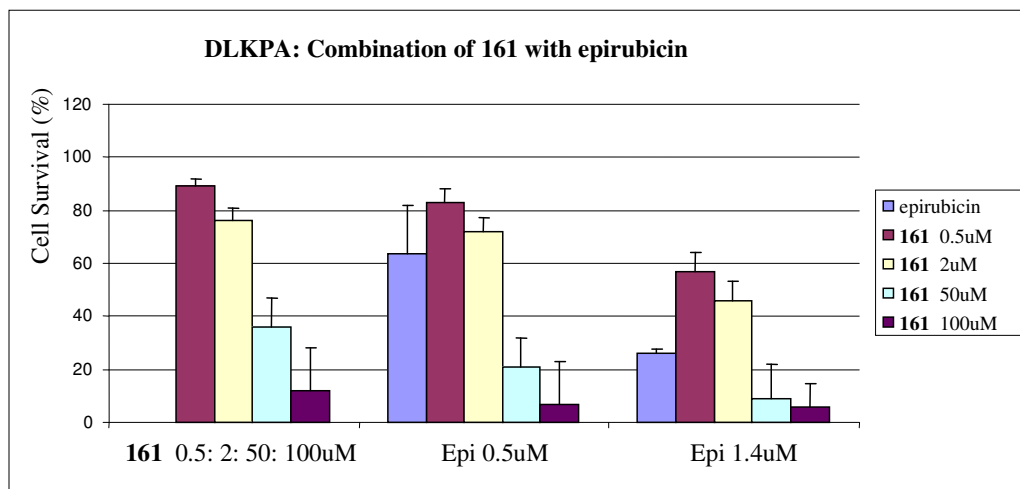


Graph 7.3 Combination of **165** with epirubicin on the DLKP-A cell line.

No effect was seen for the drug interaction study with epirubicin for **165** on the DLKP cell lines. The IC_{50} for **165** was found to be 22 μM .

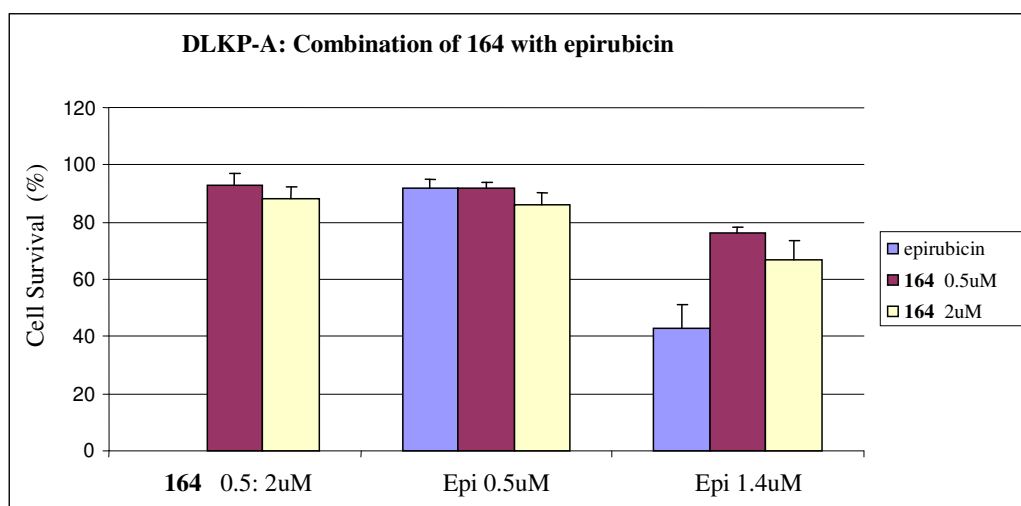


Graph 7.4 The double combination of **165** with epirubicin on the DLKP cell line



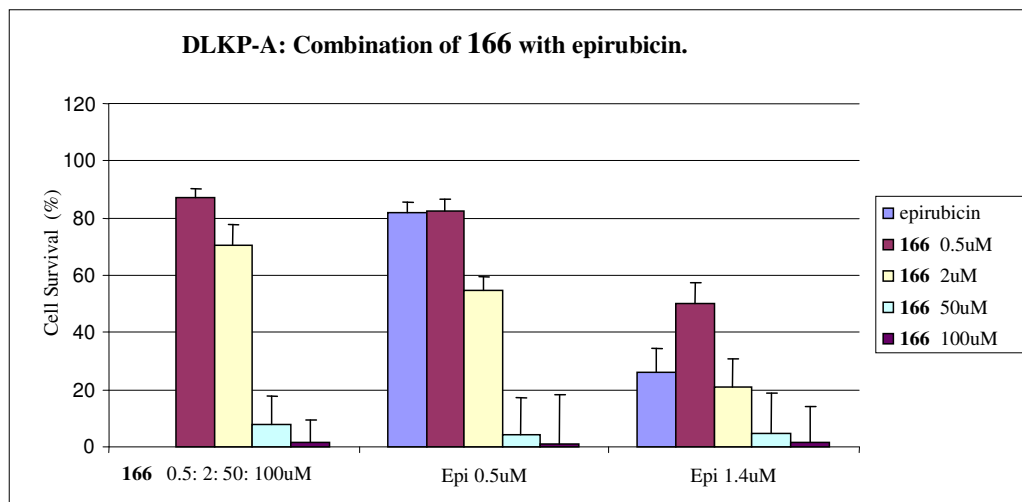
Graph 7.5 Combination of **161** with epirubicin on the DLKP-A cell line

A slightly antagonistic interaction was observed between **161** and epirubicin on the DLKP-A cell line (Graph 7.5). This can be seen at the two lower concentrations of **161** with both concentrations of epirubicin. The IC_{50} for this compound was found to be $58.4 \pm 14 \mu M$. Analogical, antagonistic interaction between **164** and epirubicin was observed at the higher concentration of epirubicin with both concentrations of **164** on the DLKP-A cell line (Graph 7.6). The IC_{50} for this compound was found to be $35 \mu M$.



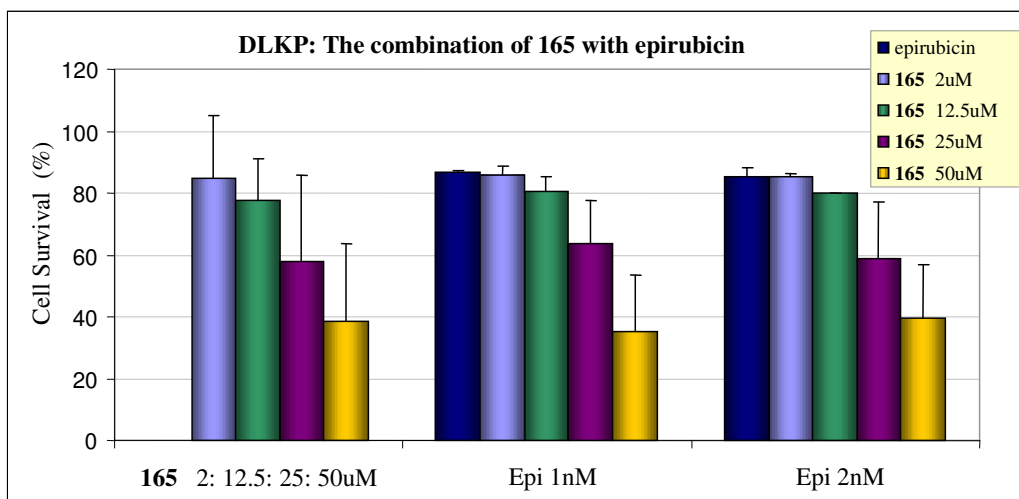
Graph 7.6 Combination of **164** with epirubicin on the DLKP-A cell line

Graph 7.7 shows that at the lowest **166** concentration, 0.5 μM , **166** acted antagonistically with 1.4 μM epirubicin, whereas no antagonism or synergy was noted at any other concentration. A separate IC_{50} curve was carried out and a concentration of $40.4 \pm 5 \mu\text{M}$ was required to kill 50% of the cells.



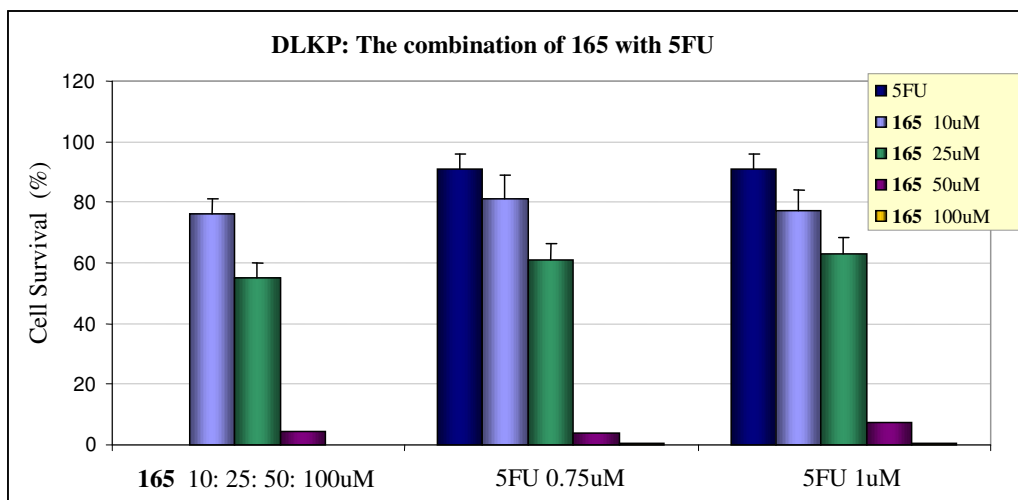
Graph 7.7 Combination of **166** with epirubicin on the DLKP-A cell line

Each of the macrocyclic precursors **160-166** was dissolved in ethanol but only six of them were found to be soluble in the cell culture medium, ATCC +5% FCS. The six compounds were tested for any anti-proliferation effects and also for a possible synergistic interaction with epirubicin in both the P-gp and MRP1 rich cell lines. It became clear that combinations of **160**, **161**, **162**, **164**, **165**, **166** with epirubicin gave no synergistic interactions on the DLKP cell lines. This suggests that none of these five compounds have an effect on MRP1. **161** and **162** showed no effect in either assay, either by themselves or in combination with epirubicin on the DLKP-A cell line, whereas **160**, **164** and **166** acted antagonistically with epirubicin on the DLKP-A cell line. Compound **165** gave a synergistic interaction with epirubicin at all concentrations with 1.4 μM epirubicin on the DLKP-A cell line, providing a valuable lead for further testing. The calculated IC_{50} value for **165** with respect to both cell lines was found to be in the micromolar ranges for DLKP 19 ± 3 and DLKP-A 34 ± 4 , respectively. Additionally when compared with other commonly used chemotherapeutic compounds, **165** is non-toxic to both the cell lines tested.



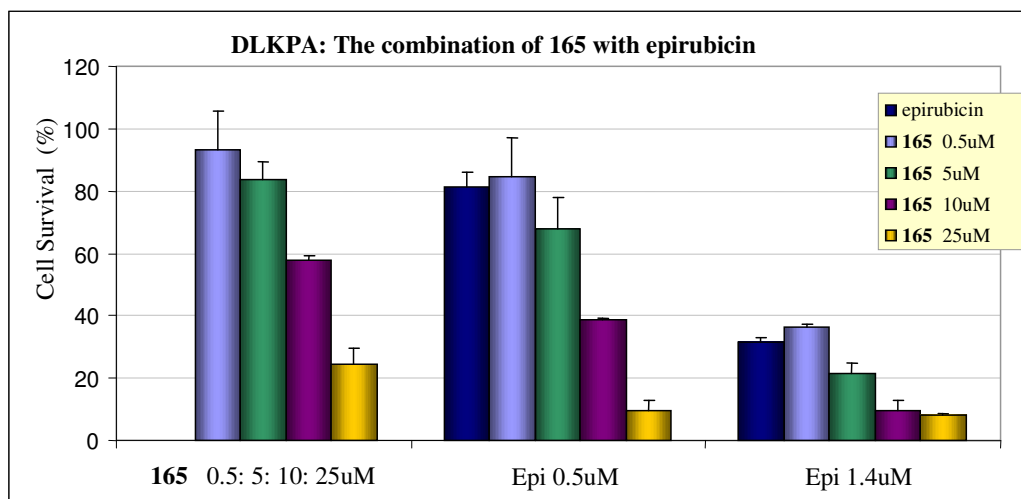
Graph 7.8 The effect of a combination of **165** with epirubicin on the DLKP cell line

No synergy, additivity or antagonism is evident in Graph 7.8. This suggests that **165** is neither a substrate nor an inhibitor of MRP1. Graph 7.8 is the result of two separate experiments and no synergy or antagonism is observed as a result of this combination.



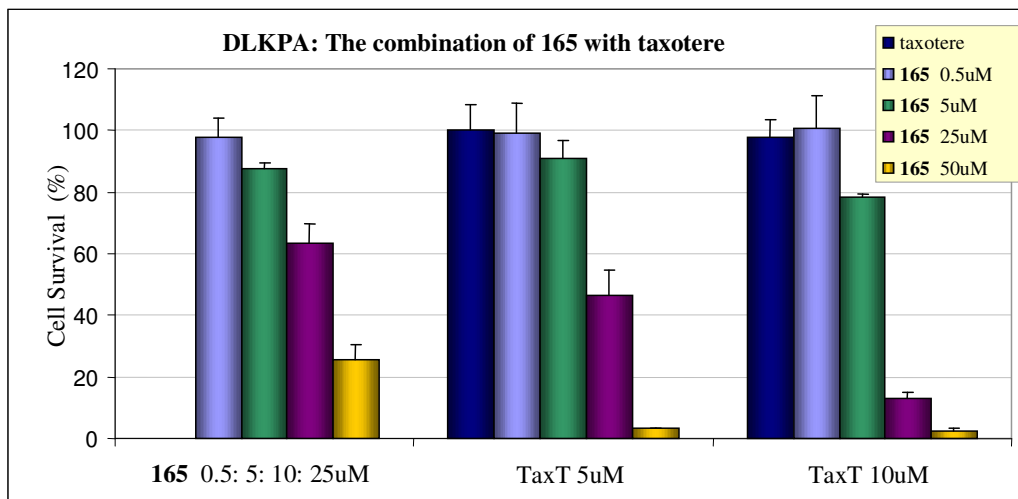
Graph 7.9 The effect of a combination of **165** and 5FU on the DLKP cell line

When **165** was combined with 5FU on DLKP cell line (Graph 7.9), the combination showed neither synergism, antagonism nor additivity. This gives weight to the theory that the mechanism of action of compound **165** involves the inhibition of the P-gp pump.



Graph 7.10 Effect of a combination of **165** with epirubicin on the DLKP-A cell line

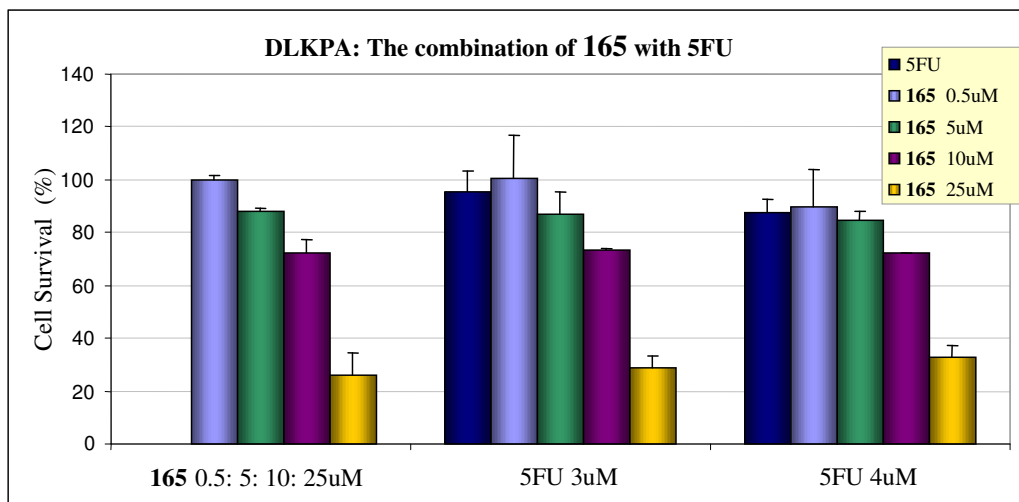
The chart above, which is the result of two separate experiments, demonstrates that **165** acts in neither a synergistic nor an antagonistic manner but rather has an additive effect when co-incubated with epirubicin on the DLKP-A cell line.



Graph 7.11 Effect of a combination of **165** with taxotere on the DLKP-A cell line

When **165** was combined with taxotere it appears to act synergistically at a concentration of 10 uM **165** and 10 μM taxotere. The observed increase in cell kill was roughly 50 % (Graph 7.11). Taxotere is pumped from the cell by P-gp and at a concentration of 25 μM **165** and 10 μM taxotere an even higher cell kill was observed. **165** was also tested with 5-flurouracil (5FU) which is not affected by P-gp

and as such no improvement in cell kill occurred when **165** was added as shown in Graph 7.12. The combination exhibits neither synergism, antagonism nor additivity.



Graph 7.12 Effect of a **165** with 5FU on the DLKP-A cell line

To date **165** has proven to be non-toxic on the two non-small cell lung carcinoma cell lines used, and toxic at 19 μM in the DLKP and 34 μM concentration in the DLKP-A cell lines. However after a second series of tests no synergy, additivity or antagonism was evident in combination with epirubicin and 5FU on the DLKP cell line. Therefore, **165** was ruled out as a compound that can overcome MRP1 resistance. In combination with epirubicin on the DLKP-A cell line, **165** appears to act in an additive manner but acts synergistically with taxotere. This indicates that **165** may have some form of inhibitory effect on P-gp.

7.3.2 Biological activity of compounds with ester groups

Compounds **229**, **230**, **231** (Fig. 7.3) were synthesised by another member of the group and tested as P-gp inhibitors. Both **229** and **230** exhibited a pronounced synergistic effect among the rest of tested compounds.

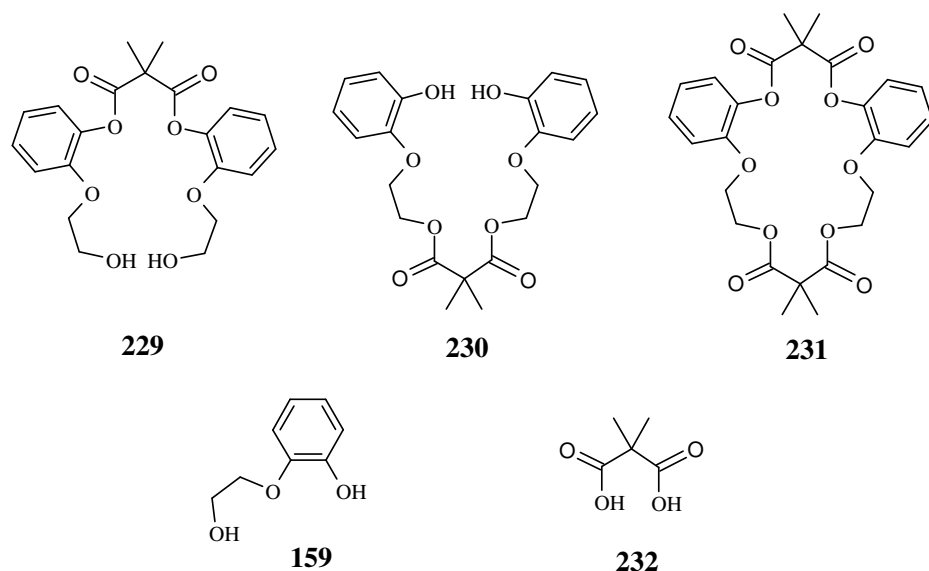
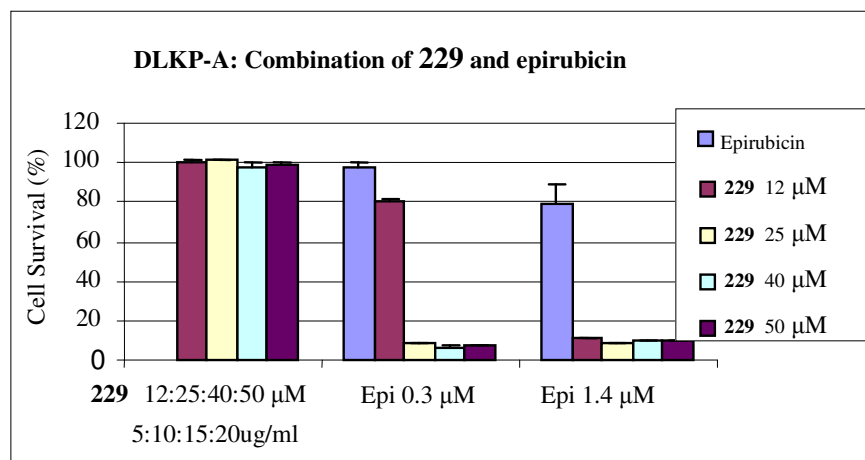
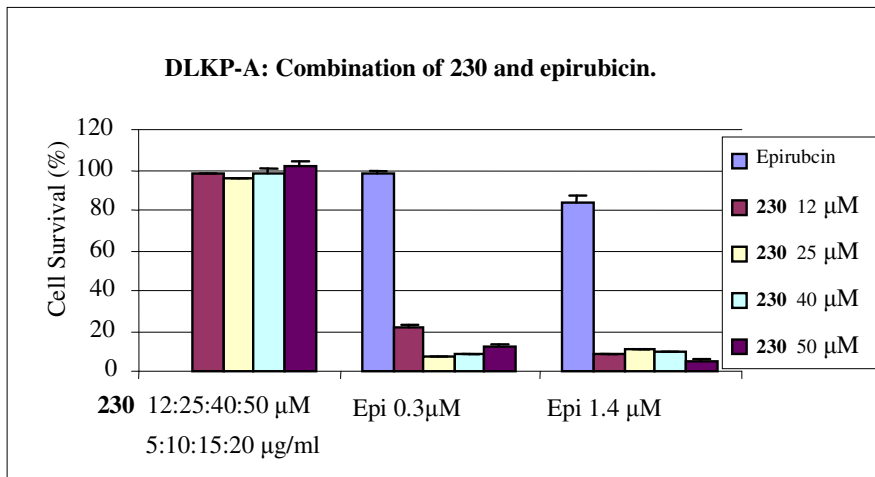


Fig. 7.3 Screened compounds containing ester groups

In contrast with **165** in the DLKP-A assay, **229** at a concentration of 25 μM combined with 0.3 μM epirubicin inhibited cell survival by over 90%, whereas a combination of higher concentration of epirubicin (up to 1.4 μM) and **229** at 12 μM gave a similar cell survival rate.

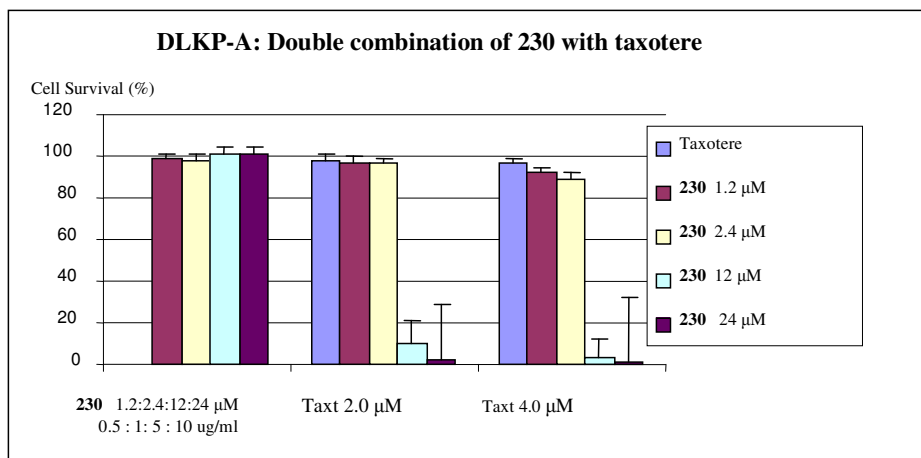


Graph 7.13 Effect of a combination of **229** with epirubicin on the DLKP-A cell line



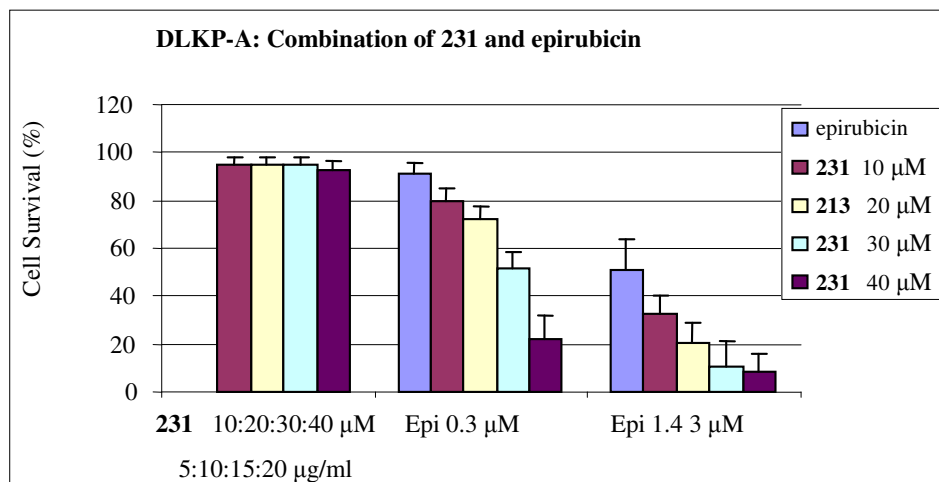
Graph 7.14 Effect of a combination of **230** with epirubicin on the DLKP-A cell line

The combination of **230** and epirubicin showed a significant increase in cell kill with increasing non-toxic concentrations of **230**. **230** at concentrations of 12 μM with 0.3 μM epirubicin cause a significant increase in cell kill, furthermore increased of the concentrations of **230** to 25 μM at the same level of epirubicin inhibits cell growth by over 90 %.



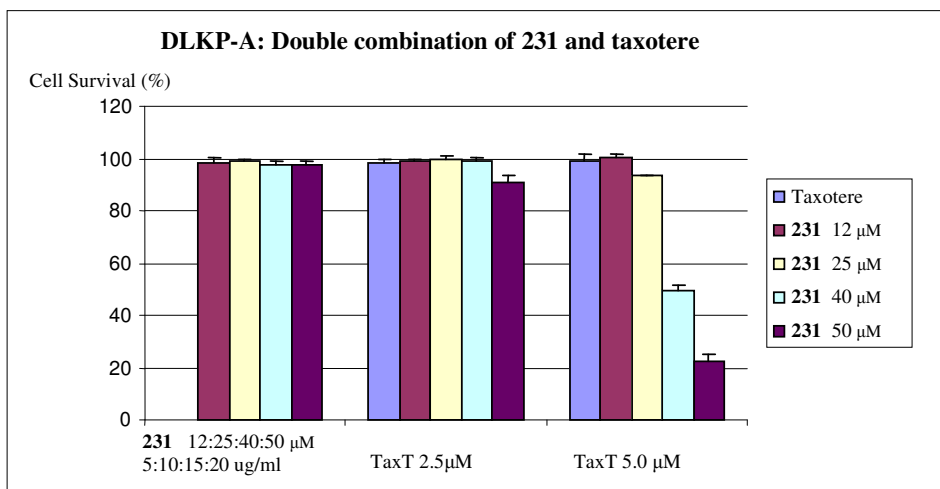
Graph 7.15 Combination of **230** with taxotere on DLKP-A cell line

The combination of **230** with taxotere on DLKP-A cell line showed a significant increase in cell kill with increasing non-toxic concentrations of **230**. **230** at the concentration of 12 μM with 2.0 μM of taxotere caused over 90 % cell kill. The assay performed for the combination of **231** with 5FU and taxotere gives weight to the theory that the mechanism of action of compound **231** involves the inhibition of the P-gp pump.



Graph 7.16 Combination of **231** with epirubicin on the DLKP-A cell line

Initial testing showed that **231** at concentrations of 40 μM with 0.3 μM epirubicin significantly increased cell kill in DLKP-A, whereas under the same conditions but with DLKP no significant increase occurred.



Graph 7.17 Bar chart illustrating the double combination of **231** with taxotere on the DLKP-A cell line

The combination of **231** and taxotere on the DLKP-A cell line appears to act synergistically at a concentration of 40 μM **231** and 5.0 μM taxotere. The observed increase in cell kill was roughly 50 %.

Next 2-(2-hydroxyethoxy)phenol **159** and 2,2-dimethylmalonic acid **232** the hydrolytic decomposition products of **229**, **230** and **231** were screened in order to exclude the possibility that they were increasing cell kill in the assay. The results from this round of testing indicated that 2-(2-hydroxyethoxy)phenol **159** and dimethylmalonic acid **232** exhibit inhibition of P-gp.

7.3.3 Summary of carcinoma assay for ester compounds

The results presented above show that both **229** and **230** have a significant effect on cell survival in conjunction with epirubicin. This suggests that **229** and **230** are effective P-gp inhibitors, compared with **160-166**. From the set of compounds containing ether groups it has been found that **165** containing the *ortho*-xylene moiety is the best P-gp inhibitor. Both **229** and **230** have suffered in consistent data between batches. The high activity observed with the first batch has not been reproduced. Work is ongoing in the group to determine the reason. Compound **165** was found to give reproducible data in several batches. Presented data also indicate that the presence of ester groups may play a significant role in the inhibition of P-gp. The mechanism of P-gp inhibition has yet to be determined, however, these studies may aid future research into the design of P-gp inhibitor candidates.

7.3.4 Biological activity of commercially available compounds

Following analysis of the data from the compounds screened it was decided to subject a range of commercially available macrocycles and their linear precursors to biological investigation. Among them were triethylene **233**, tetraethylene **234**, pentaethylene **235** and hexaethyleneglycols **236** as well as benzo-15-crown-5 **237**, 18-crown-6 **4** and benzo-18-crown-6 **238**. Amongst these commercially available chemicals only benzo-18-crown-6 **238** exhibited a synergistic effect with epirubicin on the DLKP-A cell line.

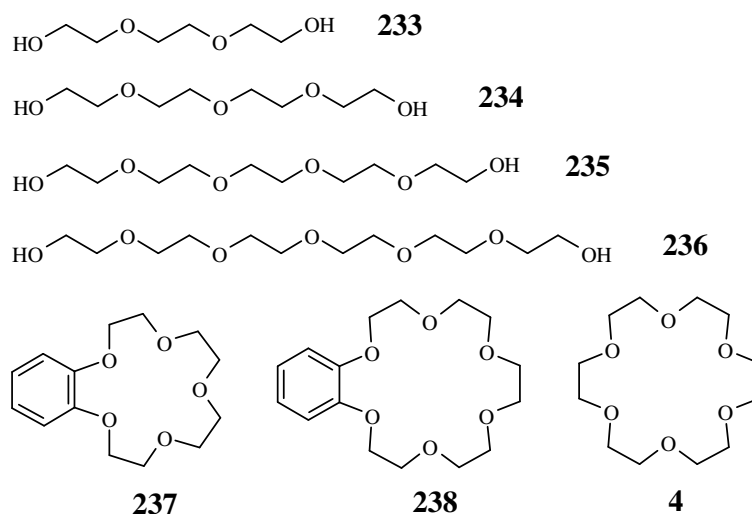
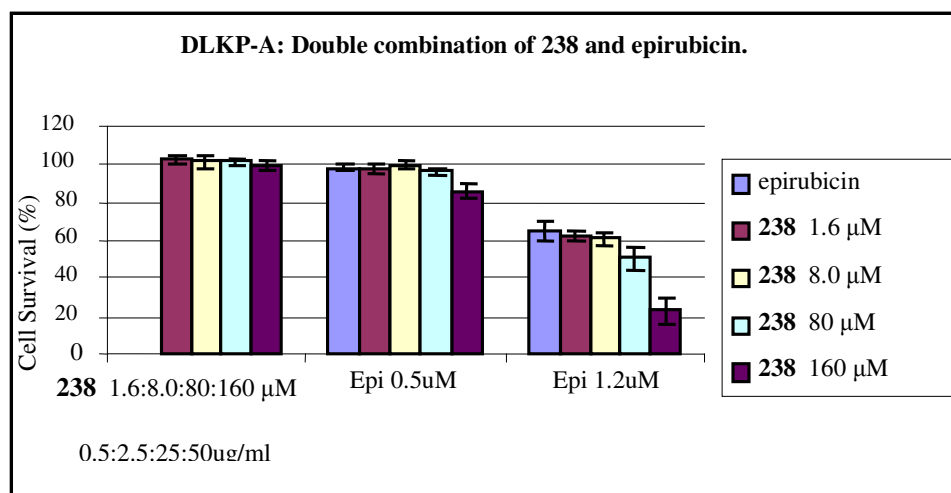


Fig. 7.4 Commercially available compounds screened in carcinoma assay

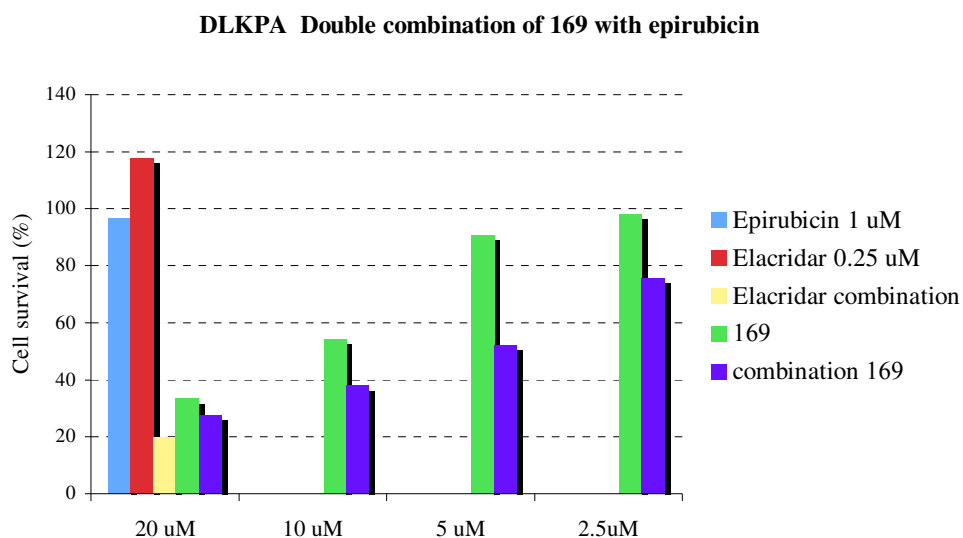


Graph 7.18 Bar chart for the combination of 238 with epirubicin in the DLKP-A cell line

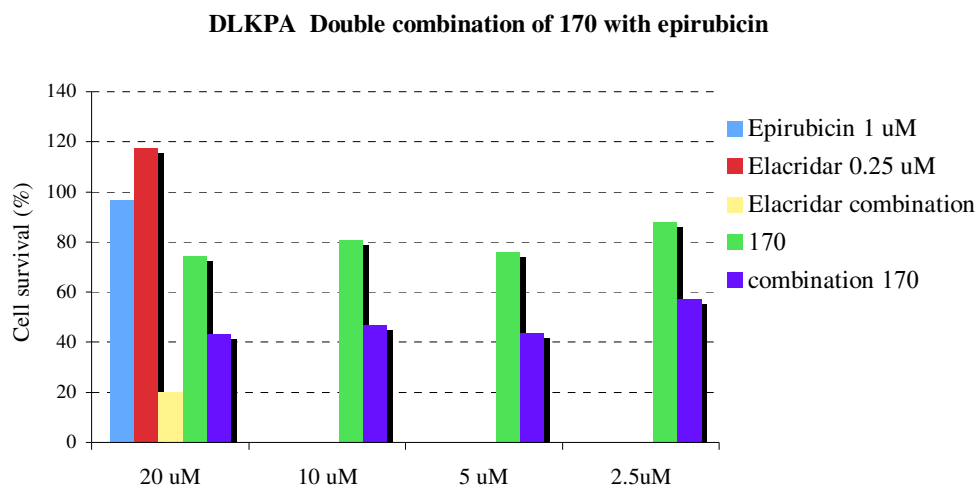
The combination of epirubicin with benzo-18-crown-6 238 gave a slight synergistic interaction at the same concentration as the highest concentration (100 μM) of 238 tested against DLKP-A cell line. 238 gave a slight synergy with epirubicin but only in the DLKP-A cell line. When the extent of the interaction is compared with that of 230 with epirubicin in the same cell line, it is clear that 230 has a much greater effect. 238 only acts synergistically at 160 μM and above, whereas the required concentration of 230 lies between 12 μM and 25 μM.

7.3.5 Biological activity of macrocycles

The macrocyclic compounds were then subjected to simple toxicity screening in control experiments to establish P-gp inhibition properties for these compounds. A combination assay with epirubicin and taxotere was carried out with macrocycle concentrations of 20.0, 10.0, 5.0 and 2.5 μ M. Control experiments were compared with results for elacridar **125**, a drug used in cancer treatment as a reverser of P-gp activity. The bioassays were carried out on the P-gp rich cell line DLKP-A with epirubicin **227** and taxotere **228** as anticancer drugs.

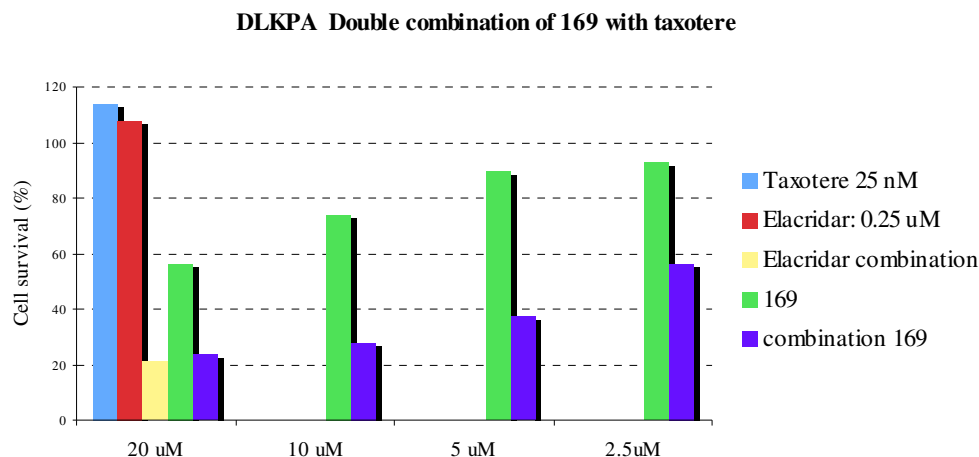


Graph 7.19 Combination assay of **169** with epirubicin on the DLKP-A cell line



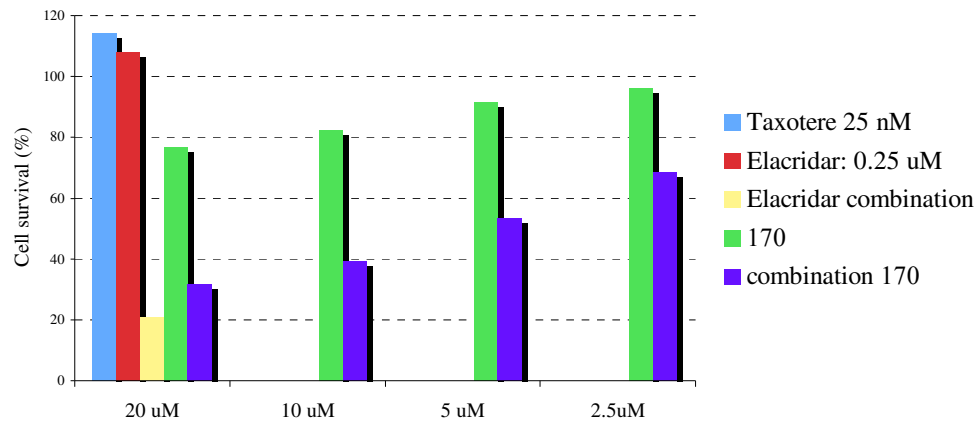
Graph 7.20 Combination assay of **170** with epirubicin on the DLKP-A cell line

Graph 7.19 and Graph 7.20 show bar charts demonstrating the increase of activity against the DLKP-A cell line when **169** and **170** are administered in combination with epirubicin. In the presence of potent P-gp inhibitor, elacridar an increase in cell growth was recorded after assay incubation. However when elacridar was combined with epirubicin a dramatic reverse in cell growth was observed. Inhibition of P-gp was also evident for the combination of either **169** or **170** with epirubicin at concentrations of 10 μ M for **170** and 20 μ M for **169**. The combination of **170** with epirubicin exhibited an encouraging 40 % cell kill. Both compounds **169** and **170** in combination with taxotere showed positive result in the DLKP-A assay. The combination of elacridar at 0.25 μ M with taxotere at 25 nM inhibits growth by over 80 %. Likewise combinations **170** or **169** with taxotere also give significant cell kill, but only in the higher concentration ranges. In both cases cell survival was the lowest at the highest concentration of 20 μ M.



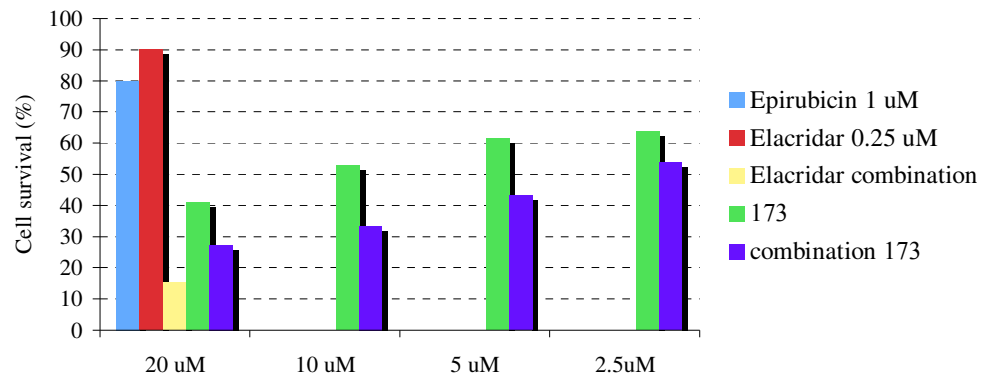
Graph 7.21 Combination assay of **169** with taxotere on the DLKP-A cell line

DLKPA Double combination of 170 with taxotere



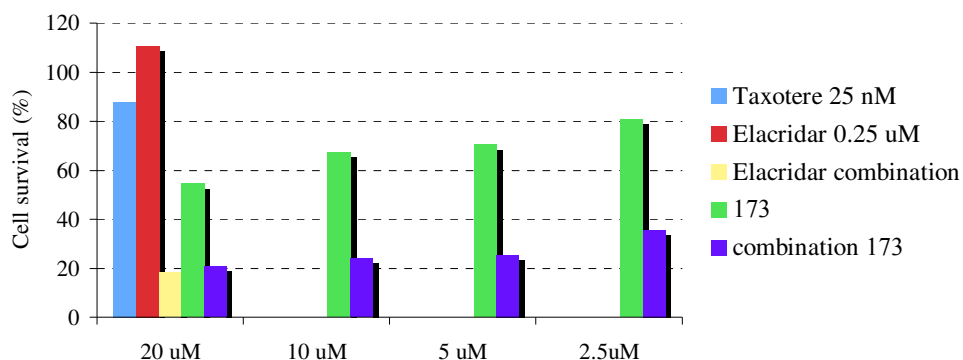
Graph 7.22 Combination assay of 170 with taxotere on the DLKP-A cell line

DLKPA Combination of 173 with epirubicin



Graph 7.23 Combination assay of 173 with epirubicin on the DLKP-A cell line

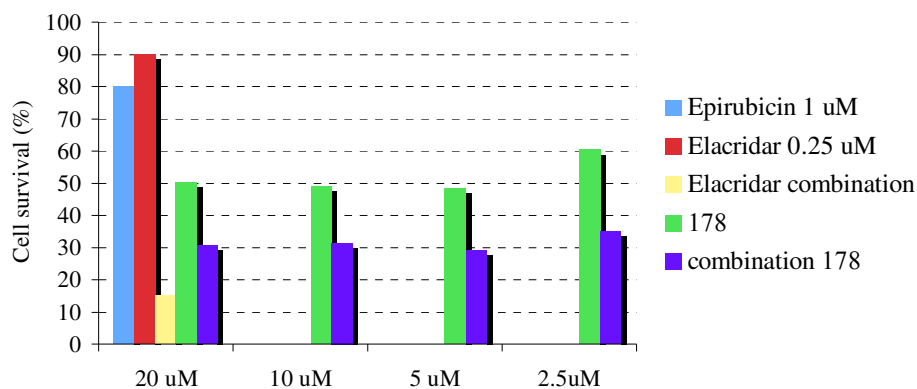
DLKPA Combination of 173 with taxotere



Graph 7.24 Combination assay of **173** with taxotere on the DLKP-A cell line

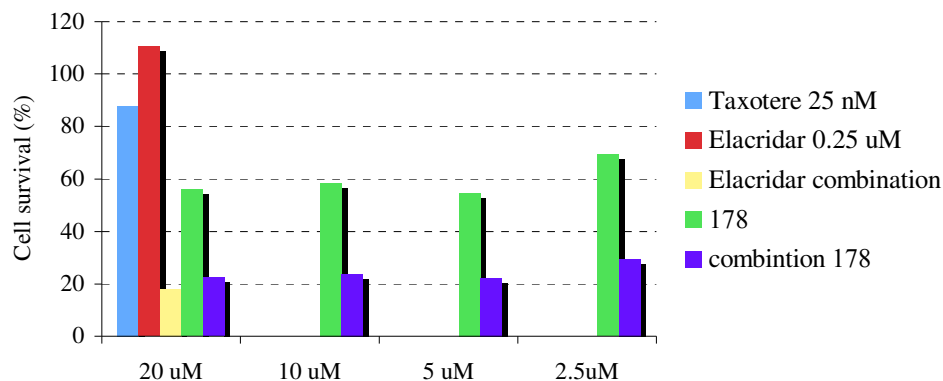
Macrocycle **173** was also subjected to biological evaluation against a DKLP-A cell line as a combination with either epirubicin or taxotere. The results are depicted in Graph 7.23 and graph 7.24 which also present cell survival data for elacridar combined with epirubicin and taxotere, respectively on the lung cancer cell line. In both cases addition of elacridar (0.25 μM) together with the chemotherapeutic agent inhibits cell growth dramatically. As seen from the graphs **173** seems to have a toxic effect on the cells itself. However, when combined with taxotere a still more pronounced increase in cell kill occurred.

DLKPA Combination of 178 with epirubicin



Graph 7.25 Combination assay of **178** with epirubicin on the DLKP-A cell line

DLKPA Combination of 178 with taxotere



Graph 7.26 Combination assay of **178** with taxotere on the DLKP-A cell line

Similar observations were made when the bioactivity of macrocycle **178** and its effect in combination with epirubicin (Graph 7.25) and taxotere (Graph 7.26) was investigated. In the DLKP-A assay **178** inhibits growth by over 30 % at the lowest concentration used. In both assays synergy was noted, however combination with taxotere at the usual range of concentrations led to cell survival of about 20 %.

The usual control experiments were performed to determine whether the compounds screened exhibited any level of P-gp inhibition worthy of further investigation. These tests are not elaborate enough to determine bioactivity, but nevertheless resulted in important structure activity data regarding P-gp inhibition.

7.4 Conclusion

The efforts made in this project towards identification of an anti P-gp pharmacophore do not yet constitute a complete structure activity relationship study. However, key information guiding future studies has been gained. It can be seen that the aromatic rings in the acyclic P-gp inhibitors are an important feature, although aromaticity alone does not indicate that similar compounds will act as P-gp inhibitors. Macrocyclic precursor **162** showed no effect on P-gp, either when screened in combination with epirubicin on DLKP or a DLKP-A cell line. Nevertheless, simple toxicity assay of **173** indicate a definite synergistic effect when **173** was combined with epirubicin and taxotere. It seems that introduction of an additional aromatic ring into **162** could improve P-gp inhibition behaviour as in compound **173**. A similar trend was observed for macrocyclic precursor **161** and its macrocycles **169** and **170**. When a biological investigation into compound **161** with combination of epirubicin on DLKP and DLKP-A cell lines was carried out, neither a significant increase nor a decrease in the effect of the drug was seen. However, when **169** and **170** were assayed with DLKP-A in the absence of a cytotoxic anticancer agent, toxicity levels towards the cell line was found to be low (5-30%). In contrast when the macrocycles were administered to the cells with taxotere, synergistic effect and considerable cell kill level was observed. Amongst the four macrocycles screened, **173** (20 to 60% of cell kill) and **178** (40 to 50% cell kill) were most cytotoxic at the concentration range of 2.5 to 20 μ M towards the DLKP-A cell line. This compares favourably with **170** (5-25%) and **169** (5-45%). These results emphasize the significance of retaining aromatic rings when designing the cyclic P-gp inhibitors. This observation, drawn from compounds synthesized during this project, was supported by the bioassay results from commercially available 15-crown-5, 18-crown-6 and benzo-18-crown-6. The first two cyclic polyethers did not exhibit P-gp inhibiting properties whatsoever, while benzo-18-crown-6 shows signs of a slight synergistic interaction with epirubicin, at the highest concentration (100 μ M) in the DLKP-A cell line. However, this difference, particularly between 15-crown-5 and benzo-18-crown-6 could merely be a result of the difference in the size of the rings.

The investigation carried out on the cancer cell lines indicated that the macrocyclic precursors containing ester groups **229** and **230** are more effective as P-gp inhibitors than macrocyclic precursors with aliphatic linker joining two 2-(2-hydroxyethoxy)phenol units. Moreover, availability of phenolic hydroxyl groups in the structure may play an important role since **230** with free aromatic alcohol groups instead of primary alkyl alcohol acted more sufficiently towards P-gp than **229**. **230** at the concentration range of 12-24 μM proved to act synergistically with epirubicin (0.3 and 1.4 μM) causing cell kill over 80 %. Furthermore, **230** at the lower concentration range of 1.2-2.4 μM with taxotere (2.0-4.0 μM) increases cell kill over 90 %. Macrocyclic precursor **165** showed neither synergy nor antagonism as a combination with epirubicin on DLKP and DLKP-A cell lines. However, combination with taxotere appears to act synergistically at a concentration of 10 μM of **165** and 10 μM of taxotere causing 30 % of cell kill.

This investigation is just an opening for the work which needs to be done to prove claimed statements conclusively. It would be necessary for future research to synthesize and submit for a SAR study a number of other macrocycles of varying size and constituents. Few constructive conclusions can be made based on the structural properties of tested compounds.

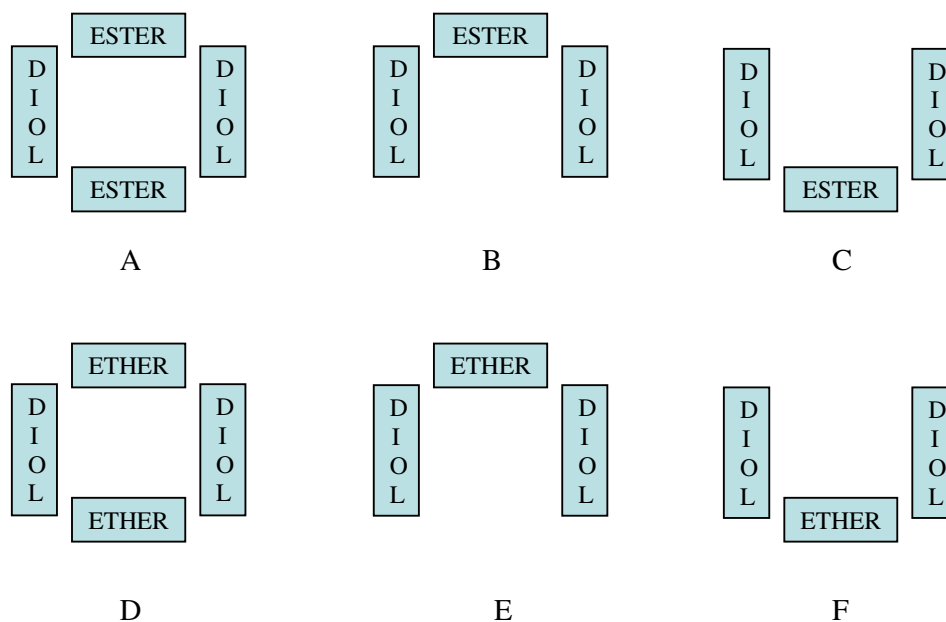


Fig. 7.5 Schematic view of screened compounds

In the Fig. 7.5 a simple view of screened compounds is presented. From the results of the cancer studies it can be concluded that:

- Presence of aromatic rings, particularly *ortho*-substituted aromatic rings, increase P-gp inhibition
- Macrocyclic precursors with ester linkers showed higher potency as a P-gp inhibitors compared to macrocyclic precursors with ethereal linkers
- Macrocyclic precursors, both alkoxy-(C) and phenoxy-linked (B) with ester linkers showed higher potency as P-gp inhibitors than their macrocycles (A)
- Macrocyclic precursors with ester linkers (B,C) exhibit high synergy with both epirubicin and taxotere
- Presence of the aromatic ring in the macrocycle, increases P-gp inhibition activity (18-crown-6, benzo-18-crown-6)
- Macrocycle with ester groups (A) exhibit higher synergy with epirubicin than taxotere
- Macrocyclic precursors with ethereal linkers (E) showed higher P-gp inhibition when in combination with taxotere than epirubicin.
- Macrocycles (D) with ethereal linkers exhibit higher P-gp inhibition when combined with taxotere than epirubicin.

8 Experimental

All chemicals were purchased from Sigma-Aldrich, and used without further purification. Morphine hydrochloride trihydrate was purchased from Johnson Matthey Macfarlan Smith, Edinburgh, and was dried for one week under vacuum before use. Commercial grade reagents were used without further purification procedures. THF was distilled from sodium with benzophenone as indicator under nitrogen. Dichloromethane was distilled from CaH₂ and triethylamine distilled and stored over potassium hydroxide pellets¹⁶⁶. DMF, 1,4-dioxane and pyridine were purchased anhydrous from Sigma-Aldrich.

Thin layer chromatography was performed on Fluka silica gel (60 F254) coated on aluminium plates. TLC plates were visualised by UV (254 nm) and/or developed using potassium permanganate. Davisil 60Å silica gel was used for column chromatography.

Melting point determinations were carried out using a Stuart, SMP3 melting point apparatus. Infrared spectra were recorded on an Perkin Elmer FT-IR system, spectrum GX spectrometer. Optical rotations were measured on a Perkin Elmer 343 Polarimeter in HPLC grade chloroform. High Resolution Mass Spectrometry was carried out on Liquid Chromatography Time of flight mass spectrometer from Micromass MS Technologies Centre by the Microanalytical Laboratory at University College Dublin. NMR spectra were obtained on a Bruker AC 400 NMR spectrometer operating at 400 MHz for ¹H NMR and 100 MHz for ¹³C NMR. The ¹H and ¹³C NMR shifts are expressed in ppm relative to tetramethylsilane and were internally referenced to the residual solvent signal. Coupling constants values (*J*) are in Hertz (Hz). Chemical-shift assignments for ¹H and ¹³C spectra were assisted with COSY, DEPT and HMQC experiments. The splitting patterns for NMR spectra are designated as follows: s (singlet), d (doublet), t, (triplet), q, (quartet), p, (pentet), dd (doublet of doublets), ddd (doublet of doublet of doublets), dt (doublet of triplet) and m (multiplet).

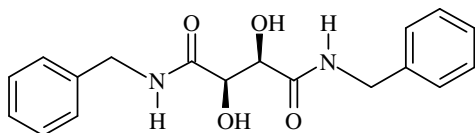
8.1 Friedel-Crafts chemistry

General procedure (127, 128, 129)

Diethyl-L-tartrate (10 mmol) and the corresponding benzylamine (24 mmol) were added to the K_2CO_3 (1.0 mmol) in abs. methanol (15 mL). The mixture was heated at 64 °C for 7 h and then allowed to cool to RT. The white solid was filtered and washed with copious of methanol. The crude product was then recrystallized from toluene.

N,N'-dibenzyl-L-tartaric acid amide (127)

The general procedure was used with the starting materials diethyl-L-tartrate (10 mmol, 2.06 g) and benzylamine (24 mmol, 2.57 g). Recrystallization from toluene gave the title product as white crystalline needles (2.98 g, 9.1 mmol, 91% yield).



1H and ^{13}C NMR data were in agreement with the literature¹²¹.

1H NMR (400 MHz, DMSO) 8.29 (2H, t, $J=6.0$ Hz, NH) 7.31-7.20 (10H, m, Ar-H)

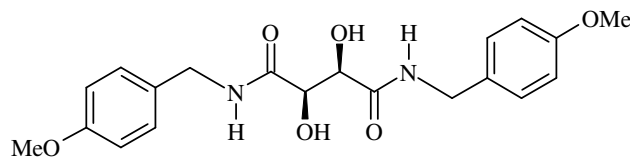
5.72 (2H, d, $J=6.0$ Hz, OH) 4.41-4.28 (6H, m, OCH, Ar-CH₂)

^{13}C NMR (100 MHz, DMSO) 171.48, 139.45, 128.02, 127.10, 126.55, 72.52, 41.04.

m.p.=200-201 °C

N,N'-di-(4-methoxybenzyl)-L-tartaric acid amide (128)

The general procedure was used with the starting materials diethyl-L-tartrate (0.52 g, 2.5 mmol) and 4-methoxy-benzylamine (0.82 g, 6.0 mmol). Recrystallization from toluene gave the title product as white crystalline needles (0.81 g, 2.1 mmol, 84 % yield).



1H and ^{13}C NMR data were in agreement with the literature¹²¹.

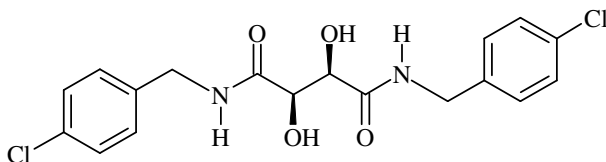
^1H NMR (400 MHz, DMSO) 8.16 (2H, t, $J=6.0\text{ Hz}$, NH) 7.23 (4H, d, $J=8.4\text{ Hz}$, ArH) 6.85 (4H, d, $J=8.4\text{ Hz}$, Ar-H) 5.71 (2H, d, $J=7.2\text{ Hz}$, OH) 4.32 (2H, d, $J=7.2\text{ Hz}$, OCH) 4.27 (4H, t, $J=6.0\text{ Hz}$, ArCH₂) 3.72 (6H, s, CH₃)

^{13}C NMR (100 MHz, DMSO) 171.96, 157.98, 131.02, 127.86, 112.76, 72.02, 55.01, 40.96.

m.p.=220-222 °C

***N,N'*-di-(4-chlorobenzyl)-L-tartaric acid amide (129)**

The general procedure was used with the starting materials diethyl-L-tartrate (0.52 g, 2.5 mmol) and 4-chloro-benzylamine (0.85 g, 6.0 mmol). Recrystallization from toluene gave the title product as white crystalline needles (0.64 g, 1.6 mmol, 65 % yield).



^1H and ^{13}C NMR data were in agreement with the literature¹²¹.

^1H NMR (400 MHz, DMSO) 8.42 (2H, t, $J=6.2\text{ Hz}$, NH) 7.35-7.20 (8H, m, ArH) 5.76 (2H, s, OH) 4.40-4.15 (6H, m, OCH, ArCH₂)

^{13}C NMR (100 MHz, DMSO) 171.94, 138.45, 130.52, 129.01, 127.49, 71.00, 41.02.

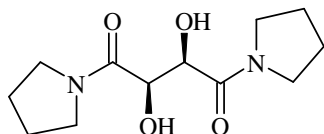
m.p.=180-182 °C

General procedure (130, 131)

To a solution of diethyl-L-tartrate (131 mmol, 27.0 g) in abs. methanol (40 mL) was added freshly distilled cyclic amine (420 mmol, 29.83 g). After 3 days at RT solvent and excess of amine were removed *in vacuo*. After period of time white crystals appeared. The crude product was recrystallised from benzene. The residue was dried *in vacuo* to give the corresponding tartramides.

Diazacyclopentane-L-tartaric acid amide (130)

The general procedure was used with the starting materials diethyl-L-tartrate (27.04 g, 131 mmol) and freshly distilled pyrrolidine (420 mmol, 29.83 g). Recrystallization from benzene gave the title product as white crystalline needles (24.45 g, 96 mmol, 74 % yield).



^1H and ^{13}C NMR data were in agreement with the literature¹²².

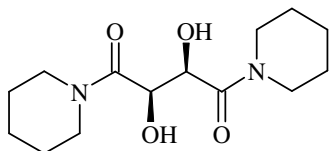
^1H NMR (400 MHz, DMSO) 5.19 (2H, d, $J=7.2\text{Hz}$, OH) 4.29 (2H, d, $J=7.2\text{Hz}$, CH) 3.65-3.22 (8H, m, NCH₂) 1.89-1.71 (8H, m, CH₂)

^{13}C NMR (100 MHz, DMSO) 169.57, 70.53, 45.95, 44.29, 23.04, 21.82.

m.p.=128-130 °C

Diazacyclohexane-L-tartaric acid amide (131)

The general procedure was used with the starting materials diethyl-L-tartrate (18.81 g, 93 mmol) and freshly distilled piperidine (31.48 g, 370 mmol). Recrystallization from toluene gave the title product as white crystalline needles (8.73 g, 31 mmol, 36 % yield).



^1H and ^{13}C NMR data was in agreement with the literature¹²²

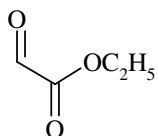
^1H NMR (400 MHz, DMSO) 5.21 (2H, d, $J=6.2\text{ Hz}$, OH) 4.41 (2H, d, $J=6.2\text{Hz}$, CH) 3.49-3.43 (8H, m, NCH₂) 1.59-1.44 (12H, m, CH₂)

^{13}C NMR (100 MHz, DMSO) 169.14, 70.12, 46.64, 45.86, 26.17, 25.56, 24.89.

m.p.=179-181 °C

Preparation of ethyl glyoxylate (105)

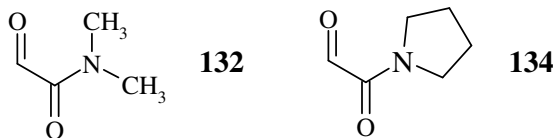
Diethyl-L-tartrate **126** (1.03 g, 5.0 mmol) was dissolved in freshly distilled CH₂Cl₂ (5 mL). Periodic acid (1.05 g, 5.0 mmol) was added in portions over 1 h and the reaction mixture was stirred at RT for an additional hour and then poured onto molecular sieves (4 Å) for 15 minutes to remove any water. The solid was filtered off and the solvent was evaporated under reduced pressure (20 °C) to give the crude aldehyde as a colourless oil.



The presence of the aldehyde group was confirmed by ^1H NMR, in which a singlet at 9.36 ppm was observed. This material was not purified further, but instead used directly in the Friedel-Crafts reaction.

Preparation of glyoxamides (132, 134)

Tartramide (5.0 mmol) was dissolved in freshly distilled DCM (8 mL). Periodic acid (5.0 mmol) was added in portions over 1 h and the reaction mixture was stirred at RT for an additional hour and then poured onto molecular sieves (4 Å) and allowed to stand for 15 minutes to remove any water. The solid was filtered off and the solvent was evaporated under reduced pressure (20 °C) to give crude glyoxamide as a white solid.



The presence of the aldehyde group was confirmed by ^1H NMR, in which a singlet at 9.38 ppm was observed. This material was not purified but used directly in the Friedel-Crafts reaction.

Catalytic Friedel-Crafts reaction in organic solvent

To a flame-dried flask fitted with stirring bar was added the Lewis acid catalyst MX_n (0.05 mmol, 10 mol %) and then the flask and catalyst were dried under vacuum for 4 h. Freshly distilled solvent (4 mL) and carbonyl compound (2-5 mmol) were added and stirred for 20 min. Subsequently the aromatic or heteroaromatic nucleophile (1 mmol) was added. After stirring for 1 to 2 days at RT the reaction mixture was filtered through a pad of silica with CH_2Cl_2 , solvent was removed in *vacuo* and the product was purified by column chromatography.

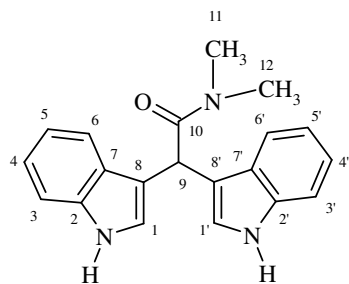
2,2-di(1*H*-indol-3-yl)-*N,N*-dimethylacetamide (**143**)

Catalytic Friedel-Crafts reaction

The general procedure was used with the starting materials indole **142** (0.059 g, 0.5 mmol) and *N,N*-dimethyl glyoxamide **132** (2.5 mmol as a crude mixture) in the presence of Cu(OTf)₂ (0.045 g, 0.125 mmol, 25 mol %) in CH₂Cl₂. Product **143** was isolated as a dark orange solid after column chromatography on silica gel using ethyl acetate (0.014 g, 0.04 mmol, 17 % yield).

Friedel-Crafts reaction in aqueous solution (**143**)

A flask was charged with 1M NaCl (4 mL) and then crude *N,N*-dimethyl glyoxyamide (0.28 g, 2.2 mmol) and indole (0.059 g, 0.50 mmol) were added. The reaction mixture was stirred for 3 h at RT then extracted with CH₂Cl₂ and dried over MgSO₄. Solvent was evaporated and the reaction mixture was separated by flash chromatography on silica gel (EtOAc) to give product **143** (0.075 g, 0.21 mmol, 86 % yield) as a dark orange solid.



¹H NMR (400 MHz, CDCl₃) 8.26 (2H, s, NH) 7.50 (2H, dd, *J*=7.6, 1.2 Hz, (H3,3')) 7.13 (2H, d, *J*=7.6, 1.0 Hz, (H6,6')) 7.08 (2H, td, *J*=7.6, 1.0 Hz, (H4,4')) 6.99 (2H, td, *J*=7.6, 1.2 Hz, (H5,5')) 6.13 (2H, d, *J*=2.0 Hz, (H1,1')) 5.61 (1H, s, (H9)) 3.01 (3H, s, (H11 or 12)) 2.96 (3H, s, (H11 or 12))

¹³C NMR (100 MHz, CDCl₃) 173.23 (C10), 136.41 (C2,2'), 126.67 (C7,7'), 123.87 (C1,1'), 121.81 (C5,5'), 119.28 (C4,4'), 118.66 (C8,8'), 114.1 (C6,6'), 111.46 (C3,3'), 46.34 (C9), 37.80 (C11 or 12), 37.29 (C11 or 12).

IR (KBr) ν (cm⁻¹) 3446, 2938, 1628, 1294, 1186.

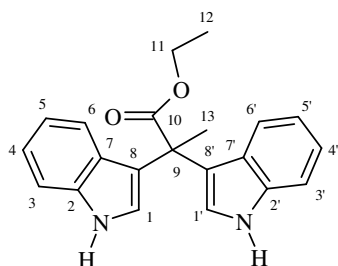
HRMS (EI, 70 eV) Calculated for 350.2227; Found 350.2234

m.p.=167-169 °C

R_fEtOAc=0.49

2,2-(di-indole-3-yl)-propionic acid ethyl ester (146)

The general procedure was used with the starting materials indole **142** (0.117 g, 1.0 mmol) and ethyl pyruvate **144** (0.58 g, 0.54 mL, 5.0 mmol) in the presence of $\text{Al}(\text{OTf})_3$ (0.024 g, 0.05 mmol, 5 mol %) in CH_2Cl_2 . Product **146** was isolated by column chromatography on silica gel using dichloromethane/petroleum ether (4:1) as a white solid (0.149 g, 0.45 mmol, 91 % yield).



^1H NMR (400 MHz, CDCl_3) 7.92 (2H, s, NH) 7.47 (2H, dd, $J=8.0, 1.0\text{Hz}$, (H3,3')) 7.29 (2H, dd, $J=8.0, 0.8\text{Hz}$, (H6,6')) 7.09 (2H, td, $J=8.0, 0.8\text{Hz}$, (H4,4')) 6.94 (2H, td, $J=8.0, 1.0\text{Hz}$, (H5,5')) 6.89 (2H, d, $J=2.8\text{Hz}$, (H1,1')) 4.11 (2H, q, $J=7.0\text{Hz}$, (H11)) 2.04 (3H, s, (H13)) 1.05 (3H, t, $J=7.0\text{ Hz}$, (H12))

^{13}C NMR (100 MHz, CDCl_3) 175.31 (C10), 136.80 (C2,2'), 126.14 (C7,7'), 122.86 (C1,1'), 121.75 (C5,5'), 121.47 (C4,4'), 119.33 (C8,8'), 119.14 (C6,6'), 111.23 (C3,3'), 61.08 (C11), 46.32 (C9), 25.89 (13), 14.23 (C12).

IR (KBr) ν (cm^{-1}) 3401, 2982, 1726, 1454, 1372, 1295, 1176.

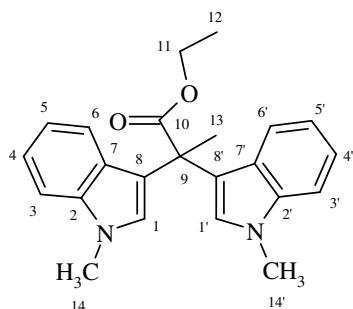
HRMS (EI, 70 eV) Calculated for 333.1598; Found 333.1611

m.p.=160-162 °C

R_f Hex:EtOAc (4:1)=0.54

2,2-(di-1-methyl-indole-3-yl)-propionic acid ethyl ester (148)

The general procedure was used with the starting materials *N*-methylindole **145** (0.131 g, 0.12 mL, 1.0 mmol) and ethyl pyruvate **144** (0.29 g, 0.27 mL, 2.5 mmol) in the presence of $\text{Zn}(\text{OTf})_2$ (0.05 mmol, 5 mol %) in CH_2Cl_2 . Product **148** was isolated by column chromatography on silica gel using dichloromethane/petroleum ether (1:1) as a white solid (0.158 g, 0.44 mmol, 89 % yield).



^1H NMR (400 MHz, CDCl_3) 7.48 (2H, dd, $J=8.0, 1.2\text{Hz}$, (H3,3')) 7.23 (2H, dd, $J=8.0, 1.0\text{Hz}$, (H6,6')) 7.14 (2H, td, $J=8.0, 1.0\text{Hz}$, (H4,4')) 6.96 (2H, td, $J=8.0, 1.2\text{Hz}$, (H5,5')) 6.76 (2H, s, (H1,1')) 4.08 (2H, q, $J=7.2\text{Hz}$, (H11)) 3.67 (6H, s, (H14,14')) 2.40 (3H, s, (H13)) 1.05 (3H, t, $J=7.2\text{Hz}$, (H12))

^{13}C NMR (100 MHz, CDCl_3) 175.45 (C10), 137.52 (C2,2'), 127.56 (C7,7'), 126.48 (C1,1'), 121.61 (5,5'), 121.34 (C4,4'), 118.57 (C8,8'), 117.65 (C6,6'), 109.21 (3,3'), 61.07 (C11), 46.34 (C9), 32.78 (C14,14'), 26.29 (C13), 14.23 (C12).

IR (KBr) ν (cm^{-1}) 2986, 1728, 1618, 1305, 1226, 1161.

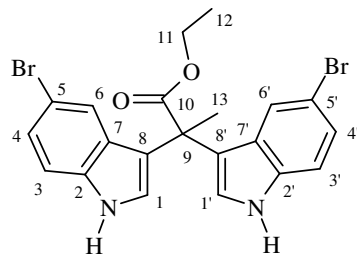
HRMS (EI, 70 eV) Calculated for 361.1911; Found 361.1921

m.p.=201-203 °C

R_f EtOAc=0.48

2,2-(di-5-bromo-1H-indole-3-yl)-propionic acid ethyl ester (**149**)

The general procedure was used with the starting materials 5-bromoindole (0.194 g, 1.0 mmol) and ethyl pyruvate **144** (0.58 g, 0.54 mL, 5.0 mmol) in the presence of $\text{Al}(\text{OTf})_3$ (0.023 g, 0.05 mmol, 5 mol %) in CH_2Cl_2 . Product **149** was isolated by column chromatography on silica gel using dichloromethane/petroleum ether (5:1) as a white solid (0.213 g, 0.45 mmol, 91 % yield).



^1H NMR (400 MHz, CDCl_3) 8.04 (2H, s, NH) 7.55 (2H, s, (H6,6')) 7.17 (2H, d, $J=7.6\text{Hz}$, (H3,3')) 7.05 (2H, d, $J=7.6\text{Hz}$, (H4,4')) 6.91 (2H, s, (H1,1')) 4.12 (2H, q, $J=7.2\text{Hz}$, (H11)) 1.99 (3H, s, (H13)) 1.10 (3H, t, $J=7.2\text{Hz}$, (H12))

^{13}C NMR (100 MHz, CDCl_3) 174.67 (C10), 135.46 (C2,2'), 127.57 (C7,7'), 124.86 (C1,1'), 124.03 (C6,6'), 123.82 (C4,4'), 119.47 (C8,8'), 118.56 (C5,5'), 112.73 (C3,3'), 61.48 (C11), 46.08 (C9), 25.76 (C13), 14.1 (C12).

IR (KBr) ν (cm^{-1}) 3401, 2984, 2081, 1732, 1620, 1543, 1462, 1304, 1227.

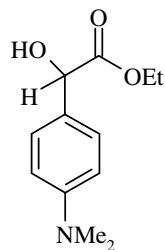
HRMS (EI, 70 eV) Calculated for 474.9651; Found 474.9667

m.p.=82-84 °C

R_f DCM/PET (5:1) =0.40

2-(4-Dimethylaminophenyl)-2-hydroxyacetic acid ethyl ester (137)

The general procedure was used with the starting materials *N,N*-dimethylaniline **104** (0.097 g, 0.101 mL, 0.8 mmol) and ethyl glyoxylate **105** (1.76 mmol in a crude mixture) in the presence of $\text{Cu}(\text{OTf})_2$ (0.029g, 0.08 mmol 10 mol %) in THF. Product **137** was isolated by column chromatography on silica gel using petroleum ether/diethyl ether (3:1) as a white powder (0.098 g, 0.44 mmol, 56 % yield)



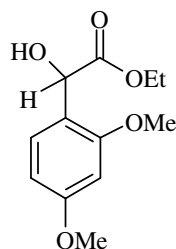
^1H and ^{13}C NMR data were in agreement with the literature⁹³.

^1H NMR (400 MHz, CDCl_3) 7.66 (2H, d, $J=9.2\text{Hz}$, Ar-H) 6.76 (2H, d, $J=9.2\text{Hz}$, Ar-H) 5.05 (1H, d, $J=5.8\text{Hz}$, CH) 4.31 (1H, dq, $J=10.8, 7.2\text{Hz}$, CH_2CH_3) 4.22 (1H, dq, $J=10.8, 7.2\text{Hz}$, CH_2CH_3) 3.42 (1H, d, $J=5.8\text{Hz}$, OH) 3.00 (6H, s, NCH_3) 1.29 (3H, t, $J=7.2\text{Hz}$, CH_2CH_3)

^{13}C NMR (100 MHz, CDCl_3) 172.37, 150.86, 127.56, 126.25, 112.79, 73.02, 62.19, 40.43, 14.91

2-(2,4-Dimethoxyphenyl)-2-hydroxyacetic acid ethyl ester (138)

The general procedure was used with the starting materials 1,3-dimethoxybenzene (0.138 g, 0.132 mL, 1.0 mmol) and ethyl glyoxylate **105** (1.52 mmol in a crude mixture) in the presence of $\text{Cu}(\text{OTf})_2$ (0.036g, 0.1 mmol 10 mol %) in THF. Product **138** was isolated by column chromatography on silica gel using petroleum ether/diethyl ether (5:1) as a colorless oil (0.134 g, 0.56 mmol, 56 % yield)



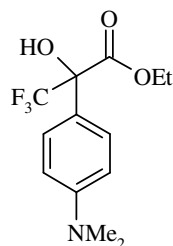
^1H and ^{13}C NMR data were in agreement with the literature⁹³.

^1H NMR (400 MHz, CDCl_3) 7.32 (1H, d, $J=8.6\text{Hz}$, Ar-H) 6.43 (1H, dd, $J=8.6$, 2.4Hz , Ar-H) 6.38 (1H, d, 2.4Hz , Ar-H) 5.07 (1H, d, $J=6.0\text{Hz}$, CH) 4.33 (1H, d, $J=6.0\text{Hz}$, OH) 4.31 (1H, dq, $J=10.4$, 7.2Hz , CH_2CH_3) 4.24 (1H, dq, $J=10.4$, 7.2Hz , CH_2CH_3) 3.71 (3H, s, OCH_3) 3.67 (3H, s, OCH_3) 1.29 (3H, t, $J=7.2\text{Hz}$, CH_2CH_3)

^{13}C NMR (100 MHz, CDCl_3) 171.10, 161.18, 158.94, 128.13, 114.98, 112.09, 105.06, 72.04, 62.14, 55.53, 55.40, 14.84.

2-(4-Dimethylaminophenyl)-3,3,3-trifluoro-2-hydroxypropionic acid ethyl ester (140)

The general procedure was used with the starting materials *N,N*-dimethylaniline (0.06 g, 0.06 mL, 0.5 mmol) and ethyl 3,3,3-trifluoropyruvate **139** (0.16 g, 0.13 mL, 0.96 mmol) in the presence of $\text{Cu}(\text{OTf})_2$ (0.009 g, 0.025 mmol, 5 mol %) in THF. Product **140** was purified by column chromatography on silica gel using petroleum ether/diethyl ether (4:1) mixture as a pale yellow oil (0.129 g, 0.48 mmol, 98 %)



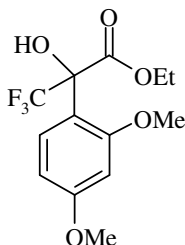
^1H and ^{13}C NMR data were in agreement with the literature⁹⁴.

^1H NMR (400 MHz, CDCl_3) 7.65 (2H, d, $J=9.2\text{Hz}$, Ar-H) 6.75 (2H, d, $J=9.2\text{Hz}$, Ar-H) 4.46 (1H, dq, $J=10.8$, 7.2Hz , CH_2CH_3) 4.40 (1H, dq, $J=10.8$, 7.2Hz , CH_2CH_3) 4.28 (1H, s, OH) 3.00 (6H, s, NCH_3) 1.41 (3H, t, $J=7.2\text{Hz}$, CH_2CH_3)

^{13}C NMR (100 MHz, CDCl_3) 169.38, 150.79, 127.61, 127.50 (q, $J_{\text{C-F}}=283.8\text{Hz}$), 112.56, 111.93, 77.06 (q, $J_{\text{C-F}}=30.0\text{Hz}$), 64.09, 40.41, 13.95

2-(2,4-dimethoxyphenyl)-3,3,3-trifluoro-2-hydroxypropionic acid ethyl ester (141)

The general procedure was used with the starting materials 1,3-dimethoxybenzene (0.069 g, 0.070 mL, 0.5 mmol) and ethyl 3,3,3-trifluoropyruvate **139** (0.16 g, 0.13 mL, 0.96 mmol) in the presence of Cu(OTf)₂ (0.009 g, 0.025 mmol, 5 mol %) in THF. Product **141** was purified by column chromatography on silica gel using petroleum ether/diethyl ether (5:1) mixture as a colorless oil (0.113 g, 0.37 mmol, 73 %).



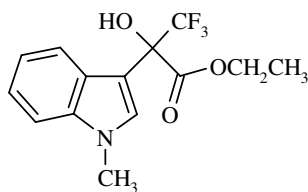
¹H and ¹³C NMR data were in agreement with the literature⁹⁴.

¹H NMR (400 MHz, CDCl₃) 7.34 (1H, d, *J*=9.0Hz, Ar-H) 6.47 (1H, dd, *J*=9.0, 2.2Hz, Ar-H) 6.43 (1H, d, 2.2Hz, Ar-H) 4.47 (1H, s, OH) 4.24 (1H, dq, *J*=10.8, 7.2Hz, CH₂CH₃) 4.18 (1H, dq, *J*= 10.8, 7.2 Hz, CH₂CH₃) 3.73 (3H, s, OCH₃) 3.68 (3H, s, OCH₃) 1.21 (3H, t, *J*=7.2Hz, CH₂CH₃)

¹³C NMR (100 MHz, CDCl₃) 169.71, 161.63, 158.44, 129.01, 122.60 (q, *J*_{C-F}= 285.8Hz), 115.63, 112.36, 109.41, 77.86 (q, *J*_{C-F}= 29.8Hz), 63.39, 55.59, 55.44, 13.81.

3,3,3-trifluoro-2-hydroxy-2-(1'-methyl-indole-3'-yl)-propionic acid ethyl ester (150)

The general procedure was used with the starting materials *N*-methylindole (0.066 g, 0.5 mmol) and ethyl 3,3,3-trifluoropyruvate (0.43 g, 0.33 mL, 2.5 mmol) in the presence of Cu(OTf)₂ (0.018 g, 0.05 mmol, 10 mol %) in CH₂Cl₂. Product **150** was purified by column chromatography on silica gel using petroleum ether/diethyl ether (4:1) mixture as a white powder (0.143 g, 0.47 mmol, 94 %).



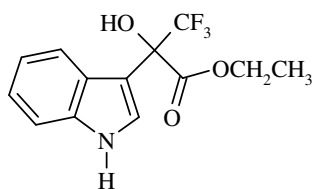
^1H and ^{13}C NMR data were in agreement with the literature⁹⁴.

^1H NMR (400 MHz, CDCl_3) 7.94 (1H, d, $J=8.2\text{Hz}$, Ar-H) 7.37 (1H, s, Ar-H) 7.31-7.25 (2H, m, Ar-H) 7.18 (1H, ddd, $J=8.2, 6.6, 1.2\text{Hz}$, Ar-H) 4.44 (1H, dq, $J=10.6, 7.4\text{Hz}$, CH_2CH_3) 4.41 (1H, s, OH) 4.38 (1H, dq, $J=10.6, 7.4\text{Hz}$, CH_2CH_3) 3.74 (3H, s, NCH_3) 1.31 (3H, t, $J=7.4\text{ Hz}$, CH_2CH_3)

^{13}C NMR (100 MHz, CDCl_3) 169.61, 136.87, 129.01, 125.86, 123.12 (q, $J_{\text{C-F}}=284.2\text{Hz}$), 121.97, 121.13, 120.04, 109.76, 106.95, 77.02 (q, $J_{\text{C-F}}=28.9\text{Hz}$), 65.01, 33.25, 14.40.

3,3,3-trifluoro-2-hydroxy-2-(indole-3'-yl)-propionic acid ethyl ester (151)

The general procedure was used with the starting materials indole (0.059 g, 0.048 ml, 0.5 mmol) and ethyl 3,3,3-trifluoropyruvate (0.43 g, 0.33 mL, 2.5 mmol) in the presence of $\text{Cu}(\text{OTf})_2$ (0.018 g, 0.05 mmol, 10 mol %) in CH_2Cl_2 . Product **151** was purified by column chromatography on silica gel using petroleum ether/diethyl ether (5:1) mixture as a white powder (0.133 g, 0.46 mmol, 91 %).



^1H and ^{13}C NMR data were in agreement with the literature⁹⁴.

^1H NMR (400 MHz, CDCl_3) 8.03 (1H, s, NH) 7.92 (1H, d, $J=8.2\text{Hz}$, Ar-H) 7.36 (1H, d, $J=2.6\text{Hz}$, Ar-H) 7.32 (1H, dd, $J=8.2, 1.4\text{Hz}$, Ar-H) 7.21-7.14 (2H, m, Ar-H) 4.46 (1H, dq, $J=10.8, 7.4\text{Hz}$, CH_2CH_3) 4.44 (1H, s, OH) 4.37 (1H, dq, $J=10.8, 7.4\text{Hz}$, CH_2CH_3) 3.74 (3H, s, NCH_3) 1.31 (3H, t, $J=7.4\text{ Hz}$, CH_2CH_3)

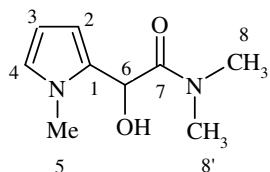
^{13}C NMR (100 MHz, CDCl_3) 169.64, 136.82, 125.31, 124.66, 123.61 (q, $J_{\text{C-F}}=284.8\text{Hz}$), 122.19, 121.26, 120.37, 111.64, 109.03, 77.07 (q, $J_{\text{C-F}}=29.3\text{Hz}$), 64.72, 14.35.

Friedel-Crafts reaction in water**General procedure**

To a flask was added sat. NaHCO₃ or 1M NaCl, subsequently glyoxamide (as a crude) and *N*-methylpyrrole were added. Reaction mixture was stirred for 20 h at RT. After that time reaction mixture was extracted with CH₂Cl₂ (6 x 10 mL), dried by MgSO₄, solvent was removed by rotary evaporation and the mixture was submitted to flash chromatography.

2-Hydroxy-*N,N*-dimethyl-2-(1'-methylpyrrol-2'-yl)acetamide (153)

The general procedure was used with starting materials of *N*-methylpyrrole (0.057 g, 0.7 mmol) and *N,N*-dimethyl glyoxamide (0.16 g, 1.4 mmol as a crude) in saturated NaHCO₃ (3 mL). Product **153** was isolated by column chromatography on silica gel using EtOAc, as a pale yellow solid (0.12 g, 0.65 mmol, 94 % yield).



¹H NMR (400 MHz, CDCl₃) 6.54 (1H, dd, *J*=3.0, 3.0Hz, (H3)) 5.95 (1H, dd, *J*=3.0, 1.6, (H4)) 5.87 (1H, dd, *J*=3.0, 1.6Hz, (H2)) 5.22 (1H, d, *J*=6.0Hz, (H6)) 4.27 (1H, d, *J*=6.0Hz, OH) 3.62 (3H, s, (H5)) 3.01 (3H, s, (H8 or 8')) 2.75 (3H, s, (H8 or 8'))

¹³C NMR (100 MHz, CDCl₃) 171.62 (C7), 129.27 (C1), 123.86 (C4), 108.45 (C3), 106.88 (C2), 64.28 (C6), 36.56 (C8 or 8'), 36.27 (C8 or 8'), 34.12 (C5).

IR (KBr) ν (cm⁻¹) 3462, 2984, 2052, 1681, 1636, 1486, 1369, 1301.

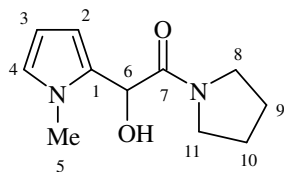
HRMS (EI, 70 eV) Calculated for 183.1128; Found 183.1130

R_f EtOAc=0.48

m.p.=64-66 °C

2-hydroxy-2-(1'-methylpyrrol-2'-yl)-1-(pyrrolidin-1-yl) ethanone (154)

The general procedure was used with starting materials of *N*-methylpyrrole (0.081 g, 1.0 mmol) and 2-oxo-2-(pyrrolidin-1-yl)acetaldehyde **134** (0.51 g, 4.0 mmol as a crude) in saturated NaHCO₃ (3 mL). Product **154** was isolated by column chromatography on silica gel using EtOAc, as a pale yellow solid (0.192 g, 0.92 mmol, 92 % yield).



^1H NMR (400 MHz, CDCl_3) 6.53 (1H, dd, $J=2.8, 2.8\text{Hz}$, (H3)) 5.99 (1H, dd, $J=2.8, 1.4\text{Hz}$, (H4)) 5.96 (2H, td, $J=2.8, 1.4\text{Hz}$, (H2)) 5.08 (1H, s, (H6)) 4.28 (1H, s, OH) 3.59 (3H, s, (H5)) 3.59-3.21 (4H, m, (H8,11)) 1.83-1.77 (4H, m, (H9,10))

^{13}C NMR (100 MHz, CDCl_3) 169.78 (C7), 128.96 (C1), 123.86 (C4), 109.05 (C3), 106.76 (C2), 65.45 (C6), 46.50 (C8 or 11), 45.84 (C8 or 11), 34.12 (C5), 25.90 (C9 or 10), 23.86 (C9 or 10).

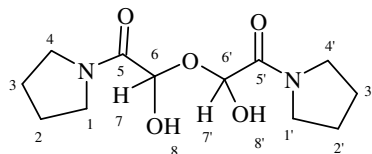
IR (KBr) ν (cm^{-1}) 3464, 2986, 2056, 1678, 1634, 1487, 1372, 1301.

HRMS (EI, 70 eV) Calculated for 209.1285; Found 209.1283

R_f EtOAc=0.45

m.p.=66-68 $^\circ\text{C}$

Product **136** was isolated as a white solid after catalytic Friedel-Crafts reactions carried with 2-oxo-2-(pyrrolidin-1-yl)acetaldehyde **134**. Proposed structure below, see page 54 for possible alternative structure.



NMR in CDCl_3

^1H NMR (400 MHz, CDCl_3) 5.51 (2H, d, $J= 9.4\text{ Hz}$, (H7,7')) 5.21 (2H, d, $J= 9.4\text{ Hz}$, (H8,8')) 3.71-3.44 (8H, m, (H1,4,1',4')) 1.98-1.94 (8H, m, (H2,3,2',3'))

^{13}C NMR (100 MHz, CDCl_3) 166.87 (C5,5'), 86.88 (C6,6'), 46.32 (C1,1' or 4,4'), 45.70 (C1,1' or 4,4'), 25.83 (C2,2' or 3,3'), 23.91 (C2,2' or 3,3').

NMR in D_2O

^1H NMR (400 MHz, D_2O) 5.37 (2H, s, (H7,7')) 3.47 (4H, t, $J= 6.8\text{ Hz}$, (H1,1' or 4,4')) 3.30 (4H, t, $J= 6.8\text{ Hz}$, (H1,1' or 4,4')) 1.87-1.724 (8H, m, (H2,3,2',3'))

^{13}C NMR (100 MHz, D_2O) 168.56 (C5,5'), 85.04 (C6,6'), 46.4 (C1,1' or 4,4'), 46.3 (C1,1' or 4,4'), 25.3 (C2,2' or 3,3'), 23.4 (C2,2' or 3,3').

IR (KBr) ν (cm^{-1}) 3484, 2981, 1676, 1158, 1125.

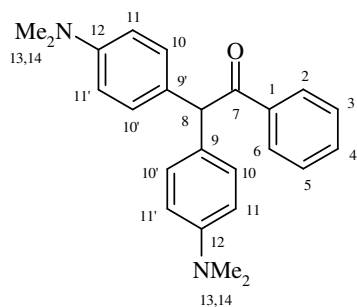
HRMS (EI, 70 eV) Calculated for 273.1445; Found 273.1458

m.p.=109-111 $^\circ\text{C}$

2,2-Bis(4-(dimethylamino)phenyl)-1-phenylethanone (156)

To a flame-dried flask catalyst $\text{Zn}(\text{OTf})_2$ (0.036g, 0.05 mmol, 20 mol%) was added and dried under *vacuum* for 4 h. Then BMIMBF_4 (5 mL) and phenylglyoxal monohydrate **155** (0.30 g, 2.0 mmol) were added under N_2 and stirred for 20 min. *N,N*-Dimethylaniline **104** (0.061 g, 0.063 mL, 0.50 mmol) was added in one portion and the reaction mixture stirred at 40 °C for 14 h. after that time the reaction mixture was filtered through a pad of silica with CH_2Cl_2 , solvent was removed in *vacuo* and the product was purified by flash chromatography on silica gel using Et_2O /petroleum ether (1:1). Product **156** was isolated as a pale green solid (0.23 mmol, 0.083 g, 93 % yield).

Experiment was repeated using the same ratio of starting materials in BDMIMBF_4 (5 mL) at 60 °C to give product **156** in 91 % isolated yield (0.081 g, 0.22 mmol).



^1H NMR (400 MHz, CDCl_3) 7.92 (2H, dd, $J=7.2,1.6\text{Hz}$, (H2,6)) 7.41-7.26 (3H, m, (H3,4,5)) 7.04 (4H, d, $J=7.8\text{Hz}$, (H10,10')) 6.60 (4H, d, $J=7.8\text{Hz}$, (H11,11')) 5.77 (1H, s, (H8)) 2.81 (12H, s, (H13,14))

^{13}C NMR (100 MHz, CDCl_3) 199.41 (C7), 149.52 (12,12'), 137.30 (C1), 132.56 (C4), 129.72 (C9,9'), 129.03 (C10,10'), 128.45 (C2,6), 127.78 (C3,5), 112.87 (C11,11'), 57.65 (C8), 40.67 (C13,14).

R_f $\text{Et}_2\text{O}/\text{PET}$ 1:1=0.5

m.p.=87-89 °C

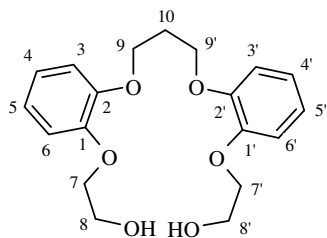
8.2 Model macrocycles and their precursors

General procedure (160-166)

A mixture of 2-(2-hydroxyethoxy)phenol **159** (10.0 mmol), alkyl dihalide (5.0 mmol) and sodium carbonate (15.0 mmol) in dry DMF (5.0 mL) was stirred for 7 h at 120 °C. After that time the reaction mixture was allowed to cool to room temperature and distilled water was added. Solid precipitated and was filtered under vacuum and washed with copious amounts of water. Crude product was recrystallized from chloroform/hexane or when necessary separated by flash chromatography.

1,3-Bis[2-(2-hydroxyethoxy)phenoxy]propane (**160**)

The general procedure was used with the starting materials 2-(2-hydroxyethoxy)phenol (10.0 mmol), and 1,3-dichloropropane (0.56 g, 5.0 mmol). Product **160** was isolated by column chromatography on silica gel using CH₂Cl₂:EtOAc (1:1) as a white solid (0.94 g, 2.7 mmol, 54 % yield).



¹H NMR (400 MHz, CDCl₃) 6.92-6.81 (8H, m, (H3-6,3'-6')) 4.23 (4H, t, *J* = 5.6 Hz, (H9,9')) 3.99 (4H, t, *J* = 4.4 Hz, (H7,7')) 3.83 (4H, t, *J* = 4.4 Hz, (H8,8')) 2.14 (2H, p, *J* = 5.6 Hz, (H10))

¹³C NMR (100 MHz, CDCl₃) 149.49 (C2,2'), 148.21 (C1,1'), 122.38 (C5,5'), 121.56 (C4,4'), 115.98 (C6,6'), 114.13 (C3,3'), 70.98 (C7,7'), 66.72 (C9,9'), 61.23 (C8,8'), 29.04 (C10).

IR (KBr) ν (cm⁻¹) 3334, 2932, 2875, 1593, 1507, 1455, 1385, 1255, 1126, 1052.

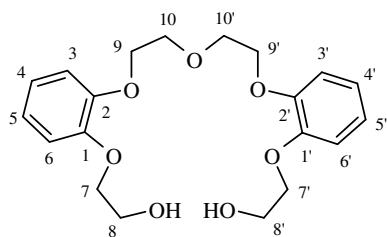
HRMS (EI, 70 eV) Calculated for C₁₉H₂₄O₆H⁺ 349.1646; Found 349.1659;

m.p. = 82-84 °C

R_f EtOAc/DCM (1:1) = 0.34

1,5-Bis[2-(2-hydroxyethoxy)phenoxy]-3-oxapentane (161)

The general procedure was used with the starting materials 2-(2-hydroxyethoxy)phenol (10.0 mmol), and 2,2'-chloroethylether (1.13 g, 0.63 mL, 5.0 mmol). Recrystallization from chloroform:hexane (3:1) gave the title product as white powder (1.63 g, 4.3 mmol, 86% yield) and (1.29 g, 3.4 mmol, 68% yield) when 2,2'-bromoethylether was used as a starting material.



^1H NMR (400 MHz, CDCl_3) 6.93-6.78 (8H, m, (H3-6,3'-6')) 4.13 (4H, t, $J= 4.4\text{Hz}$, (H9,9')) 4.01 (4H, t, $J= 4.2\text{Hz}$, (H7,7')) 3.91 (4H, t, $J= 4.4\text{Hz}$, (H10,10')) 3.84 (4H, t, $J= 4.2\text{Hz}$, (H8,8'))

^{13}C NMR (100 MHz, CDCl_3) 148.91 (C2,2'), 148.45 (C1,1'), 122.11 (C5,5'), 121.48 (C4,4'), 114.43 (C6,6'), 114.09 (C3,3'), 71.19 (C7,7'), 69.89 (C10,10'), 68.91 (9,9'), 60.98 (C8,8').

IR (KBr) ν (cm^{-1}) 3552, 3376, 3213, 2939, 1667, 1595, 1507, 1455, 1325, 1255, 1242, 1124, 1053.

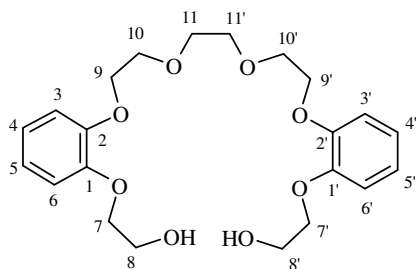
HRMS (EI, 70 eV) Calculated for $\text{C}_{20}\text{H}_{26}\text{O}_7\text{H}^+$ 379.1751; Found 379.1750;

m.p.= 92-94°C

$R_{\text{f EtOAc}} = 0.22$

1,8-Bis[2-(2-hydroxyethoxy)phenoxy]- 3,6-dioxaoctane (162)

The general procedure was used with the starting materials 2-(2-hydroxyethoxy)phenol (10.0 mmol), and 1,2-bis(2-chloroethoxy)ethane (0.93 g, 0.50 mL, 5.0 mmol). Recrystallization from chloroform:hexane (4:1) gave the title product as white powder (1.71 g, 4.05 mmol, 81 % yield) and (1.14 g, 2.7 mmol, 54 % yield) when 1,2-bis(2-iodoethoxy)ethane was used as a starting material.



^1H NMR (400 MHz, CDCl_3) 6.89-6.77 (8H, m, (H3-6,3'-6')) 4.09 (4H, t, $J=4.6\text{Hz}$, (H9,9')) 3.99 (4H, t, $J=4.4\text{Hz}$, (H7,7')) 3.81-3.78 (8H, m, overlap, (H8,8',10,10')) 3.71 (4H, s, (H11,11'))

^{13}C NMR (100 MHz, CDCl_3) 148.79 (C2,2'), 148.61 (C1,1'), 121.78 (5,5'), 121.45 (C4,4'), 114.27 (C6,6'), 113.91 (C3,3'), 71.56 (C7,7'), 70.71 (C11,11'), 69.78 (C10,10'), 68.81 (C9,9'), 61.02 (C8,8').

IR (KBr) ν (cm^{-1}) 3370, 2933, 1594, 1514, 1452, 1332, 1259, 1224, 1126, 1089, 1045.

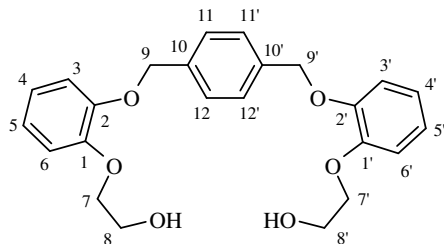
HRMS (EI, 70 eV) Calculated for $\text{C}_{22}\text{H}_{30}\text{O}_8\text{H}^+$ 423.2013; Found 423.2026;

m.p.=69-71°C

$R_{f\text{EtOAc}}$ =0.12

1,4-Bis[2-(2-hydroxyethoxy)phenoxy]-*p*-xylene (163)

The general procedure was used with the starting materials 2-(2-hydroxyethoxy)phenol (10.0 mmol), and α,α' -dibromo-*p*-xylene (1.32 g, 5.0 mmol). Recrystallization from chloroform:hexane (5:1) gave the title product as white powder (1.58 g, 3.9 mmol, 77 % yield) and (1.80 g, 4.4 mmol, 88 % yield) when α,α' -dichloro-*p*-xylene was used as a starting material.



^1H NMR (400 MHz, CDCl_3) 7.36 (4H, s, (H11,11',12,12')) 6.88-6.55 (8H, m, (H3-6,3'-6')) 5.01 (4H, s, (H9,9')) 4.00 (4H, t, $J=4.6\text{Hz}$, (H7,7')) 3.76 (4H, t, $J=4.6\text{Hz}$, (H8,8'))

^{13}C NMR (100 MHz, CDCl_3) 149.08 (C2,2'), 148.79 (C1,1'), 136.76 (C10,10'), 127.88 (C11,11',12,12'), 122.12 (C5,5'), 121.89 (C4,4'), 115.56 (C6,6'), 114.67 (C3,3'), 71.45 (C9,9'), 71.21 (C7,7'), 61.18 (C8,8').

IR (KBr) ν (cm^{-1}) 3536, 3488, 2938, 2871, 1593, 1506, 1454, 1329, 1252, 1211, 1199, 1125, 1014.

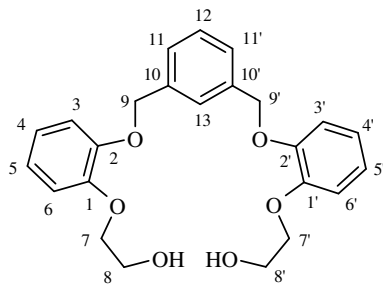
HRMS (EI, 70 eV) Calculated for $\text{C}_{24}\text{H}_{26}\text{O}_6\text{H}^+$ 411.1802; Found 411.1800;

m.p. = 104-106 °C

R_f (EtOAc/DCM 1:1) = 0.31

1,3-Bis[2-(2-hydroxyethoxy)phenoxy]-*m*-xylene (164)

The general procedure was used with the starting materials 2-(2-hydroxyethoxy)phenol (10.0 mmol), and α,α' -dibromo-*m*-xylene (1.32 g, 5.0 mmol). Recrystallization from chloroform:hexane (5:1) gave the title product as white powder (1.46 g, 3.6 mmol, 71 % yield) and (1.87 g, 4.6 mmol, 91 % yield) when α,α' -dichloro-*m*-xylene was used as a starting material.



^1H NMR (400 MHz, CDCl_3) 7.56 (1H, s, (H13)) 7.31-7.22 (3H, m, (H11,11',12)) 6.89-6.80 (8H, m, (H3-6,3'-6')) 5.02 (4H, s, (H9,9')) 3.99 (4H, t, $J=4.6\text{Hz}$, (H7,7')) 3.76 (4H, t, $J=4.6\text{Hz}$, (H8,8'))

^{13}C NMR (100 MHz, CDCl_3) 148.99 (C2,2'), 148.82 (C1,1'), 137.61 (C10,10'), 128.82 (C12), 127.17 (C11,11'), 126.78 (C13), 121.94 (C5,5'), 121.92 (C4,4'), 115.18 (C6,6'), 115.08 (C3,3'), 71.62 (C9,9'), 71.43 (C7,7'), 61.18 (C8,8')

IR (KBr) ν (cm^{-1}) 3499, 3360, 2924, 1590, 1507, 1452, 1329, 1249, 1211, 1124, 1081, 1050, 1008.

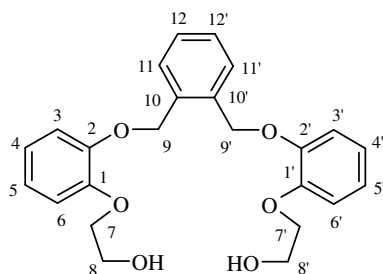
HRMS (EI, 70 eV) Calculated for $\text{C}_{24}\text{H}_{26}\text{O}_6\text{H}^+$ 411.1802; Found 411.1797;

m.p.=84-86°C

R_f (EtOAc)=0.57

1,2-Bis[2-(2-hydroxyethoxy)phenoxy]-*o*-xylene (165)

The general procedure was used with the starting materials 2-(2-hydroxyethoxy)phenol (10.0 mmol), and α,α' -dibromo-*o*-xylene (1.32 g, 5.0 mmol). Recrystallization from chloroform:hexane (5:1) gave the title product as white powder (1.56 g, 3.8 mmol, 76 % yield) and (1.60 g, 3.9 mmol 78 % yield) when α,α' -dichloro-*o*-xylene was used as a starting material.



^1H NMR (400 MHz, CDCl_3) 7.37 (2H, dd, $J=5.6, 3.6\text{Hz}$, (H12,12')) 7.25-7.21 (2H, dd, $J=5.6, 3.6\text{Hz}$, (H11,11')) 6.88-6.77 (8H, m, (H3-6,3'-6')) 5.26 (4H, s, (H9,9')) 3.96 (4H, t, $J= 4.2\text{Hz}$, (H7,7')) 3.75 (4H, t, $J= 4.2\text{Hz}$, (H8,8'))

^{13}C NMR (100 MHz, CDCl_3) 148.27 (C2,2'), 146.96 (C1,1'), 134.32 (C10,10'), 128.27 (C12,12'), 127.33 (C11,11'), 121.27 (C5,5'), 120.34 (C4,4'), 114.89 (C6,6'), 112.83 (C3,3'), 69.70 (C9,9'), 69.22 (C7,7'), 60.09 (C8,8').

IR (KBr) ν (cm^{-1}) 3267, 2901, 1590, 1505, 1395, 1323, 1256, 1126, 1040, 1000.

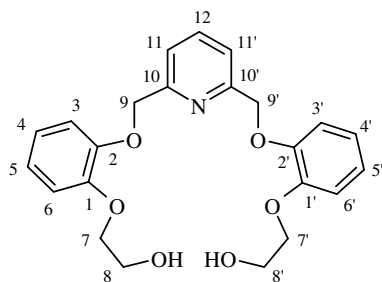
HRMS (EI, 70 eV) Calculated for $\text{C}_{24}\text{H}_{26}\text{O}_6\text{H}^+$ 411.1802; Found 411.1805;

m.p.=66-68 °C

R_f (EtOAc)=0.52

1,6-Bis[2-(2-hydroxyethoxy)phenoxy]lutidine (166)

The general procedure was used with the starting materials 2-(2-hydroxyethoxy)phenol (10.0 mmol), and 2,6-bis(chloromethyl)pyridine (0.88 g, 5.0 mmol). Recrystallization from chloroform gave the title product as white powder (1.89 g, 4.6 mmol, 92 % yield).



^1H NMR (400 MHz, CDCl_3) 7.69 (1H, t, $J=7.6\text{Hz}$, (H12)) 7.41 (2H, d, $J=7.6\text{Hz}$, (H11,11')) 6.92-6.81 (8H, m, (H3-6,3'-6')) 5.18 (4H, s, (H9,9')) 4.06 (4H, t, $J=4.4\text{Hz}$, (H7,7')) 3.85 (4H, t, $J=4.4\text{Hz}$, (H8,8'))

^{13}C NMR (100 MHz, CDCl_3) 156.68 (C10,10'), 149.18 (C2,2'), 148.45 (C1,1'), 138.07 (C12), 122.63 (C11,11'), 121.89 (C5,5'), 121.24 (C4,4'), 116.22 (C6,6'), 115.03 (C3,3'), 72.10 (C9,9'), 71.38 (C7,7'), 61.04 (C8,8').

IR (KBr) ν (cm^{-1}) 3341, 2927, 1592, 1506, 1452, 1379, 1328, 1259, 1222, 1126, 1085, 1049.

HRMS (EI, 70 eV) Calculated for $\text{C}_{23}\text{H}_{25}\text{NO}_6\text{H}^+$ 412.1755; Found 412.1743;

m.p.=101-103 $^\circ\text{C}$

R_f (EtOAc)=0.36

Macrocyclizations

General procedure 1 (169-184)

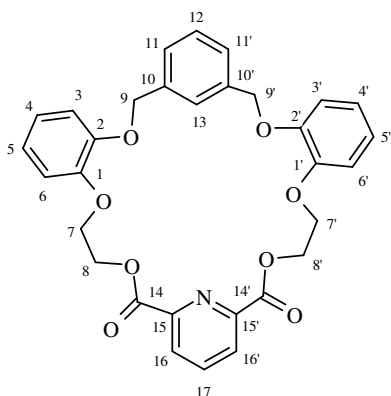
Open structure (1.0 mmol) was dissolved in dry 1,4-dioxane (80 mL) then potassium hydroxide (0.78 g, 14.0 mmol) was added and mixture was warmed up to 60 °C and stirred for 30 min. Alkyl dichloride (1.0 mmol) and potassium iodide (0.2 mmol) were added in one portion and reaction mixture was refluxed for 36 hours. After that time organic solvent was removed by rotary evaporation and distilled water (70 mL) was added to the residue. Then reaction mixture was transferred to a separation funnel and extracted with chloroform (6 x 30 mL). The organic layer was dried over MgSO₄ and filtered then solvent was evaporated to give the crude. Purification of the product was carried out by column chromatography on silica gel.

General procedure 2 (167, 168)

Open structure (1.0 mmol) was dissolved in dry dichloromethane (150 mL) then potassium carbonate (1.93 g, 14.0 mmol) was added under atmosphere of nitrogen and then acyl dichloride (1.0 mmol) was added in one portion and reaction mixture was refluxed over night. After that time reaction mixture was quenched with distilled water (70 mL) and all was transferred to a separation funnel and the organic and aqueous layers were separated. The organic layer was dried over MgSO₄, filtered then organic solvent was evaporated to give the crude. Purification of the product was carried out by column chromatography on silica gel.

2,3,6,8,11,12,18,20-tetrabenzo-19-aza-1,4,10,13,16,22-hexaoxacyclotetraeicosa-2,6,7,11,18,19-hexaene-17,21-dione (167)

The general procedure 2 was used with the starting materials **164** (0.41 g, 1.0 mmol) and 2,6-pyridine dicarbonyl dichloride (0.21 g, 1.0 mmol). Product **167** was isolated by column chromatography on silica gel using EtOAc as a white solid (0.19 g, 0.31 mmol, 31 % yield).



^1H NMR (400 MHz, CDCl_3) 7.92 (2H, d, $J=7.6\text{Hz}$, (H16,16')) 7.66 (1H, t, $J=7.6\text{Hz}$, (H17)) 7.44 (1H, s, (H13)) 7.12-7.10 (3H, m, overlap, (H11,11',12)) 6.94-6.84 (8H, m, (H3-6,3'-6')) 4.92 (4H, s, (H9,9')) 4.69 (4H, t, $J=4.4\text{Hz}$, (H8,8')) 4.37 (4H, t, $J=4.4\text{Hz}$, (H7,7'))

^{13}C NMR (100 MHz, CDCl_3) 163.17 (C14,14'), 148.45 (C2,2'), 148.42 (C15,15'), 146.89 (C1,1'), 136.71 (C17), 136.43 (C10,10'), 128.08 (C16,16'), 127.07 (C12), 126.67 (C13), 125.40 (C11,11'), 121.48 (C4,4'), 121.39 (C5,5'), 116.32 (C6,6'), 115.07 (C3,3'), 71.21 (C9,9'), 66.70 (C7,7'), 63.39 (C8,8').

IR (KBr) ν (cm^{-1}) 2942, 1743, 1588, 1506, 1450, 1378, 1291, 1256, 1125, 1081.

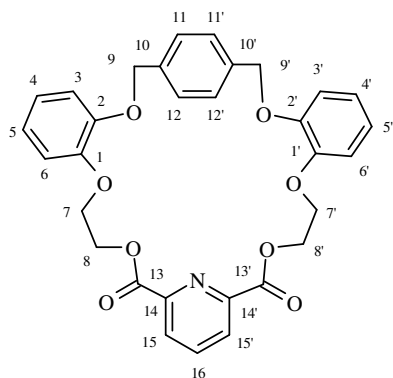
HRMS (EI, 70 eV) Calculated for $\text{C}_{31}\text{H}_{27}\text{NO}_8\text{H}^+$ 542.1809; Found 542.1791;

m.p.= 164-166 °C

R_f EtOAc= 0.66

2,3,6,9,12,13,19,21-tetrabenzo-20-aza-1,4,11,14,17,23-hexaoxacyclopentaecicosa-2,6,7,8,12,19,20-hexaene-18,22-dione (168)

The general procedure 2 was used with the starting materials **163** (0.41 g, 1.0 mmol) and 2,6-pyridine dicarbonyl dichloride (0.21 g, 1.0 mmol). Product **168** was isolated by column chromatography on silica gel using EtOAc as a white solid (0.14 g, 0.26 mmol, 26 % yield).



^1H NMR (400 MHz, DMSO) 8.18 (2H, d, $J=7.6\text{Hz}$, (H15,15')) 7.71 (1H, t, $J=7.6\text{Hz}$, (H16)) 7.16-6.92 (12H, m, overlap, (H3-6,3'-6',11,11',12,12')) 4.99 (4H, s, (H9,9')) 4.79 (4H, t, $J=4.4\text{Hz}$, (H8,8')) 4.47 (4H, t, $J=4.4\text{Hz}$, (H7,7'))

^{13}C NMR (100MHz, DMSO) 163.78 (C13,13'), 148.31 (C14,14'), 147.90 (C2,2'), 147.83 (C1,1'), 139.21 (C16), 136.40 (C10,10'), 128.19 (C15,15'), 126.89 (C11,11',12,12'), 121.60 (C4,4'), 121.34 (C5,5'), 115.20 (C6,6'), 113.89 (C3,3'), 69.70 (C9,9'), 66.17 (C7,7'), 63.58 (C8,8').

IR (KBr) ν (cm^{-1}) 2932, 1759, 1591, 1503, 1460, 1388, 1293, 1254, 1126, 1019.

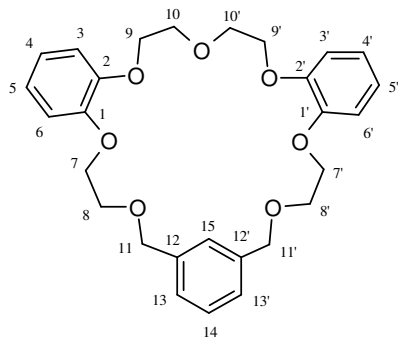
HRMS (EI, 70 eV) Calculated for $\text{C}_{31}\text{H}_{27}\text{NO}_8\text{H}^+$ 542.1809; Found 542.1810;

m.p.=185-187 °C

$R_{\text{fEtOAc}}=0.64$

2,3,11,12,18,20-tribenzo-1,4,7,10,13,16,22-hepta-oxacyclotetraeicosane-2,11,18,19-tetraene (169)

The general procedure 1 was used with the starting materials **161** (0.38 g, 1.0 mmol) and α,α' -dichloro-*m*-xylene (0.17 g, 1.0 mmol). Product **169** was isolated by column chromatography on silica gel using EtOAc/ CHCl_3 (1:1) as a white solid (0.19 g, 0.40 mmol, 40 % yield).



^1H NMR (400 MHz, CDCl_3) 7.35 (1H, s, (H15)) 7.22-7.18 (3H, m, overlap, (H13,13',14)) 6.86-6.78 (8H, m, (H3-6,3'-6')) 4.61 (4H, s, (H11,11')) 4.11 (4H, t, $J=4.6\text{Hz}$, (H9,9')) 4.08 (4H, t, $J=4.8\text{Hz}$, (H7,7')) 3.82 (4H, t, $J=4.6\text{Hz}$, (H10,10')) 3.80 (4H, t, $J=4.8\text{Hz}$, (H8,8'))

^{13}C NMR (100 MHz, CDCl_3) 149.40 (C2,2'), 149.02 (C1,1'), 138.45 (C12,12'), 128.41 (C14), 127.4 (C15), 127.11 (C13,13'), 121.89 (C4,4'), 121.60 (C5,5'), 115.87 (C6,6'), 114.42 (C3,3'), 73.46 (C11,11'), 70.29 (C8,8'), 69.72 (C9,9'), 69.30 (C7,7') 68.78 (C10,10')

IR (KBr) ν (cm^{-1}) 2930, 1594, 1505, 1449, 1357, 1256, 1123, 1041.

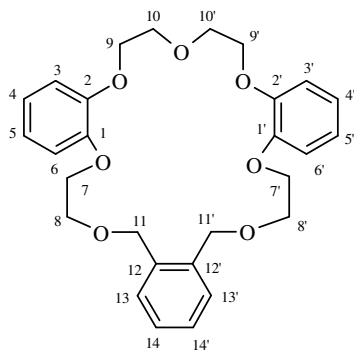
HRMS (EI, 70 eV) Calculated for $\text{C}_{28}\text{H}_{32}\text{O}_7\text{H}^+$ 481.2221; Found 481.2215;

m.p.=90-92 °C

$R_f^{\text{EtOAc/CHCl}_3}=0.81$

2,3,11,12,18,19-tribenzo-1,4,7,10,13,16,21-heptaoxacyclotricosa-2,11,18-triene (170)

The general procedure 1 was used with the starting materials **161** (0.38 g, 1.0 mmol) and α,α' -dichloro-*o*-xylene (0.17 g, 1.0 mmol). Product **170** was isolated by column chromatography on silica gel using CHCl_3 as a white solid (0.25 g, 0.50 mmol, 50 % yield).



^1H NMR (400 MHz, CDCl_3) 7.33 (2H, dd, $J=5.6, 3.2\text{Hz}$, (H14,14')) 7.22 (2H, dd, $J=5.6, 3.2\text{Hz}$, (H13,13')) 6.88-6.79 (8H, m, (H3-5,3'-6')) 4.71 (4H, s, (H11,11')) 4.13-4.08 (4H, m, overlap, (H7,7',9,9')) 3.95 (4H, t, $J=4.4\text{Hz}$, (H10,10')) 3.77 (4H, t, $J=4.6\text{Hz}$, (H8,8'))

^{13}C NMR (100 MHz, CDCl_3) 149.40 (C2,2'), 148.68 (C1,1'), 136.71 (C12,12'), 129.02 (C14,14'), 127.78 (C13,13'), 121.81 (C5,5'), 121.32 (C4,4'), 115.30 (C6,6'), 113.59 (3,3'), 71.29 (C11,11'), 70.21 (C8,8'), 69.58 (C9,9'), 68.90 (C7,7'), 68.69 (C10,10')

IR (KBr) ν (cm^{-1}) 2931, 1593, 1509, 1452, 1260, 1130, 1030.

HRMS (EI, 70 eV) Calculated for $\text{C}_{28}\text{H}_{32}\text{O}_7\text{H}^+$ 481.2221; Found 481.2240;

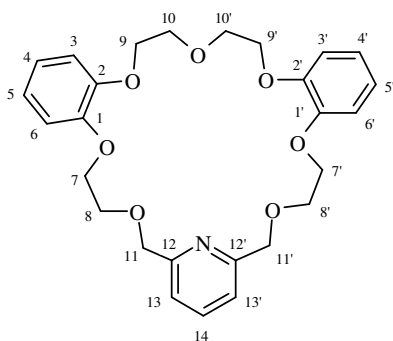
Na adduct Calculated for $\text{C}_{28}\text{H}_{32}\text{O}_7\text{Na}^+$ 503.2040; Found 503.2052;

m.p.=109-111 °C

R_f CHCl_3 =0.30

2,3,11,12,18,20-tribenzo-19-aza-1,4,7,10,13,16,22-heptaoxacyclotetra-eicosa-2,11,18,19-tetraene (171)

The general procedure 1 was used with the starting materials **161** (0.38 g, 1.0 mmol) and 2,6-*bis*(chloromethyl)pyridine (0.17 g, 1.0 mmol). Product **171** was isolated by column chromatography on silica gel using EtOAc/ CHCl_3 (3:1) as a white solid (0.21 g, 0.45 mmol, 45 % yield).



^1H NMR (400 MHz, CDCl_3) 7.67 (1H, t, $J=7.6\text{Hz}$, (H14)) 7.35 (2H, d, $J=7.6\text{Hz}$, (H13,13')) 6.85-6.81 (8H, m, (H3-6,3'-6')) 4.82 (4H, s, (H11,11')) 4.14 (4H, t, $J=4.4\text{Hz}$, (H9,9')) 4.03 (4H, t, $J=4.8\text{Hz}$, (H7,7')) 3.93 (4H, t, $J=4.4\text{Hz}$, (H10,10')) 3.83 (4H, t, $J=4.8\text{Hz}$, (H8,8'))

^{13}C NMR (100 MHz, CDCl_3) 158.08 (C12,12'), 149.17 (C2,2'), 149.04 (C1,1'), 137.41 (C14), 121.60 (C4,4'), 121.37 (C5,5'), 119.89 (C13,13'), 114.87 (C6,6'), 113.80 (C3,3'), 74.58 (C11,11'), 70.29 (C8,8'), 69.63 (C9,9'), 69.42 (C10,10'), 69.31 (C7,7').

IR (KBr) ν (cm^{-1}) 2933, 1599, 1509, 1460, 1258, 1131, 1058.

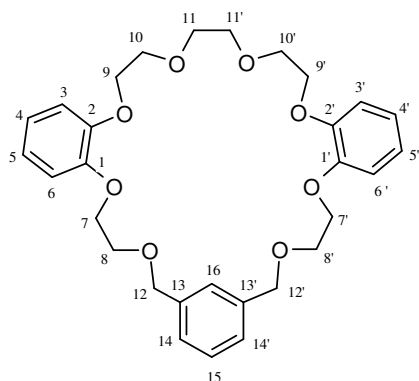
HRMS (EI, 70 eV) Calculated for $\text{C}_{27}\text{H}_{31}\text{NO}_7\text{H}^+$ 482.2173; Found 482.2169

m.p.=150-152 °C

R_f EtOAc/ CHCl_3 (3:1)=0.25

2,3,14,15,21,23-tribenzo-1,4,7,10,13,16,19,25-octaoxacyclo-heptaecosa-2,14,21,22-tetraene (172)

The general procedure 1 was used with the starting materials **162** (0.42 g, 1.0 mmol) and α,α' -dichloro-*m*-xylene (0.17 g, 1.0 mmol). Product **172** was isolated by column chromatography on silica gel using $\text{CHCl}_3/\text{EtOAc}$ (3:1) as a white solid (0.23 g, 0.43 mmol, 43 % yield).



^1H NMR (400 MHz, CDCl_3) 7.28 (1H, s, (H16)) 7.24-7.22 (3H, m, (H14,14',15)) 6.82-6.78 (8H, m, (H3-6,3'-6')) 4.60 (4H, s, (H12,12')) 4.11 (4H, t, $J=4.4\text{Hz}$, (H9,9')) 4.05 (4H, t, $J=4.8\text{Hz}$, (H7,7')) 3.79 (4H, t, $J=4.4\text{Hz}$, (H10,10')) 3.71 (4H, t, $J=4.8\text{Hz}$, (H8,8')) 3.53 (4H, s, (H11,11'))

^{13}C NMR (100 MHz, CDCl_3) 149.08 (C2,2'), 148.99 (C1,1'), 138.46 (C13,13'), 128.56 (C15), 127.32 (C16), 127.22 (C14,14'), 121.64 (C5,5'), 121.51 (C4,4'), 114.50 (C3,3',6,6')*, 73.45 (C12,12'), 70.89 (C11,11'), 69.80 (C8,8'), 69.43 (C9,9'), 69.22 (C7,7'), 68.80 (C10,10') * double intensity peak

IR (KBr) ν (cm^{-1}) 2928, 2872, 1594, 1511, 1447, 1348, 1259, 1126, 1047.

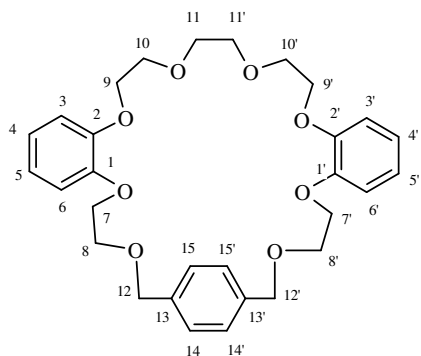
Na adduct Calculated for $\text{C}_{30}\text{H}_{36}\text{O}_8\text{Na}^+$ 547.2308; Found 547.2320;

m.p.=109-111 °C

R_f $\text{CHCl}_3/\text{EtOAc}$ (3:1)=0.51

2,3,14,15,21,24-tribenzo-1,4,7,10, 13,16,19,26-octaoxacyclooctaeca-2,14,21,22,23-tetraene (173)

The general procedure 1 was used with the starting materials **162** (0.42 g, 1.0 mmol) and α,α' -dichloro-*p*-xylene (0.17 g, 1.0 mmol). Product **173** was isolated by column chromatography on silica gel using $\text{EtOAc}/\text{CHCl}_3$ (1:1) as a white solid (0.19 g, 0.38 mmol, 38 % yield).



^1H NMR (400 MHz, CDCl_3) 7.33 (4H, s, (H14,14',15,15')) 6.88-6.77 (8H, m, (H3-6, 3'-6')) 4.62 (4H, s, (H12,12')) 4.12 (4H, t, $J=4.4\text{Hz}$, (H9,9')) 4.07 (4H, t, $J=4.8\text{Hz}$, (H7,7')) 3.79 (4H, t, $J=4.4\text{Hz}$, (H10,10')) 3.74 (4H, t, $J=4.8\text{Hz}$, (H8,8')) 3.56 (4H, s, (H11,11'))

^{13}C NMR (100 MHz, CDCl_3) 148.98 (C1,1',2,2'), 137.71 (C13,13'), 127.93 (C14,14',15,15'), 121.49 (C4,4'), 121.46 (C5,5'), 114.31 (C6,6'), 114.07 (C3,3'), 73.15 (C12,12'), 70.88 (C11,11'), 69.79 (C8,8'), 69.18 (C9,9'), 69.06 (C7,7'), 68.41 (C10,10')

IR (KBr) ν (cm^{-1}) 2928, 1595, 1507, 1454, 1334, 1259, 1125, 1048.

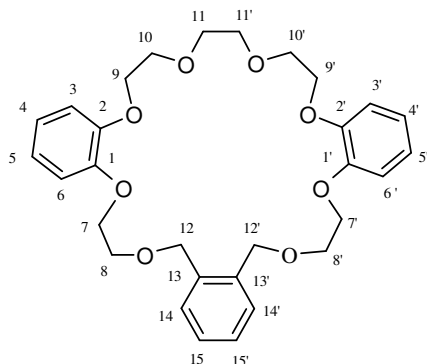
HRMS (EI, 70 eV) Calculated for $\text{C}_{30}\text{H}_{36}\text{O}_8\text{H}^+$ 525.2483; Found 525.2486;

m.p.= 104-106 °C

R_f $\text{EtOAc}/\text{CHCl}_3$ = 0.63

2,3,14,15,21,22-tribenzo-1,4,7,10,13,16,19,25-octaoxacyclohexaeicosa-2,14,21-triene (174)

The general procedure 1 was used with the starting materials **162** (0.42 g, 1.0 mmol) and α,α' -dichloro-*o*-xylene (0.17 g, 1.0 mmol). Product **174** was isolated by column chromatography on silica gel using $\text{CHCl}_3/\text{EtOAc}$ (3:1) as a white solid (0.28 g, 0.51 mmol, 51 % yield).



^1H NMR (400 MHz, CDCl_3) 7.35 (2H, dd, $J=5.6, 3.2\text{Hz}$, (H15,15')) 7.20 (2H, dd, $J=5.6, 3.2\text{Hz}$, (H14,14')) 6.81-6.76 (8H, m, (H3-6,3'-6')) 4.69 (4H, s, (H12,12')) 4.08-4.03 (8H, m, overlap, (H7,7',9,9')) 3.78-3.75 (8H, m, overlap, (H8,8',10,10')) 3.62 (4H, s, (H11,11'))

^{13}C NMR (100 MHz, CDCl_3) 147.94 (C2,2'), 147.91 (C1,1'), 135.58 (C13,13'), 127.89 (C15,15'), 126.70 (C14,14'), 120.38 (C4,4'), 120.31 (C5,5'), 113.16 (C6,6'), 113.07 (C3,3'), 70.02 (C12,12'), 69.90 (C11,11'), 68.66 (C8,8'), 68.09 (C9,9'), 67.92 (C7,7'), 67.80 (C10,10')

IR (KBr) ν (cm^{-1}) 2922, 1594, 1511, 1454, 1261, 1127, 1055.

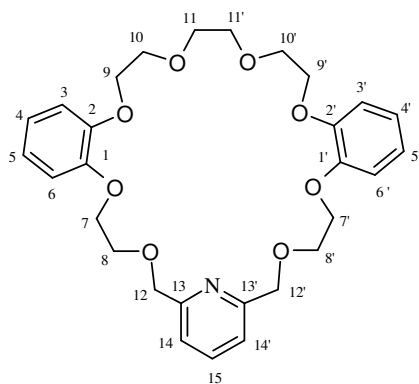
Na adduct Calculated for $\text{C}_{30}\text{H}_{36}\text{O}_8\text{Na}^+$ 547.2308; Found 547.2315;

m.p.=91-93 °C

R_f $\text{CHCl}_3/\text{EtOAc}$ (3:1)= 0.5

2,3,14,15,21,23-tribenzo-22-aza-1,4,7,10,13,16,19,25-octaoxacycloheptaecosa-2,14,21,22-tetraene (175)

The general procedure 1 was used with the starting materials **162** (0.42 g, 1.0 mmol) and 2,6-bis(chloromethyl)pyridine (0.17 g, 1.0 mmol). Product **175** was isolated by column chromatography on silica gel using $\text{EtOAc}/\text{CHCl}_3$ (3:1) as a white solid (0.20 g, 0.38 mmol, 38 % yield).



^1H NMR (400 MHz, CDCl_3) 7.89 (1H, t, $J=7.2\text{Hz}$, (H15)) 7.54 (2H, d, $J=7.2\text{Hz}$, (H14,14')) 6.88-6.80 (8H, m, (H3-6,3'-6')) 4.78 (4H, s, (H12,12')) 4.15 (4H, t, $J=4.2\text{Hz}$, (H9,9')) 4.07 (4H, t, $J=4.8\text{Hz}$, (H7,7')) 3.90 (4H, t, $J=4.2\text{Hz}$, (H10,10')) 3.76 (4H, t, $J=4.8\text{Hz}$, (H8,8')) 3.56 (4H, s, (H11,11'))

^{13}C NMR (100 MHz, CDCl_3) 157.68 (C13,13'), 148.78 (C1,1',2,2')*, 137.21 (C15), 121.40 (C4,4',5,5')*, 120.23 (C14,14'), 113.83 (C6,6'), 113.45 (C3,3'), 73.61 (C12,12'), 70.80 (C8,8'), 69.92 (C10,10'), 69.34 (C7,7'), 68.71 (C9,9'). * double intensity peak

IR (KBr) ν (cm^{-1}) 2932, 2866, 1594, 1508, 1452, 1258, 1125, 1055;

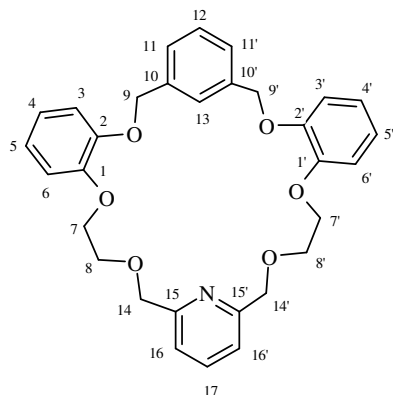
HRMS (EI, 70 eV) Calculated for $\text{C}_{29}\text{H}_{35}\text{NO}_8\text{H}^+$ 526.2435; Found 526.2432;

m.p.=144-146 °C

R_f EtOAc/ CHCl_3 (3:1)=0.19

2,3,6,8,11,12,18,20-tetrabenzo-19-aza-1,4,10,13,16,22-hexaoxacyclotetraeicosa-2,6,7,11,18,19-hexaene (176)

The general procedure 1 was used with the starting materials **164** (0.41 g, 1.0 mmol) and 2,6-bis(chloromethyl)pyridine (0.17 g, 1.0 mmol). Product **176** was isolated by column chromatography on silica gel using EtOAc/ CHCl_3 (3:1) as a white solid (0.22 g, 0.43 mmol, 43 % yield).



^1H NMR (400 MHz, CDCl_3) 7.67 (1H, t, $J=7.6\text{Hz}$, (H17)) 7.54-7.46 (6H, m, overlap, (H11,11',12,13,16,16')) 7.02-6.83 (8H, m, (H3-6,3'-6')) 4.96 (4H, s, (H9,9')) 4.63 (4H, s, (H14,14')) 4.12 (4H, t, $J=4.6\text{Hz}$, (H7,7')) 3.81 (4H, t, $J=4.6\text{Hz}$, (H8,8'))

^{13}C NMR (100 MHz, CDCl_3) 158.38 (C15,15'), 148.78 (C2,2'), 148.69 (C1,1'), 137.60 (C17), 137.14 (C10,10'), 130.03 (C12), 129.45 (C13), 121.22 (C5,5'), 120.89 (C4,4'), 119.45 (C16,16') 112.91 (C6,6'), 111.90 (C3,3'), 74.32 (C9,9'), 70.98 (14,14'), 70.43 (C8,8'), 69.83 (C7,7').

IR (KBr) ν (cm^{-1}) 2937, 1597, 1508, 1459, 1377, 1258, 1127, 1059, 1008.

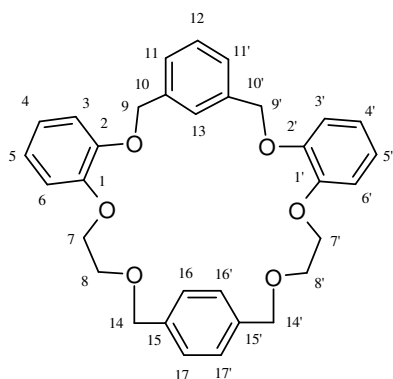
HRMS (EI, 70 eV) Calculated for $\text{C}_{31}\text{H}_{33}\text{NO}_6\text{H}^+$ 514.2224; Found 514.2224

m.p.=178-180 °C

R_f EtOAc/ CHCl_3 (3:1)=0.39

2,3,6,8,11,12,18,21-tetrabenzo-1,4,10,13,16,23-hexaoxacyclopentaeicosa-2,6,7,11,18,19,20-hexaene (177)

The general procedure 1 was used with the starting materials **164** (0.41 g, 1.0 mmol) and α,α' -dichloro-*p*-xylene (0.17 g, 1.0 mmol). Product **177** was isolated by column chromatography on silica gel using CHCl_3 as a white solid (0.22 g, 0.44 mmol, 44 % yield).



^1H NMR (400 MHz, CDCl_3) 7.37 (4H, s, (H16,16',17,17')) 7.25-7.11 (4H, m, overlap, (H11,11',12,13)) 6.86-6.82 (8H, m, (H3-6,3'-6')) 4.99 (4H, s, (H9,9')) 4.60 (4H, s, (H14,14')) 4.14 (4H, t, $J=4.2\text{Hz}$, (H7,7')) 3.83 (4H, t, $J=4.2\text{Hz}$, (H8,8'))

^{13}C NMR (100 MHz, CDCl_3) 149.37 (C2,2'), 148.71 (C1,1'), 138.45 (C15,15'), 136.78 (C10,10'), 128.71 (C12), 127.69 (C16,16',17,17')*, 126.88 (C13), 126.82 (C11,11'), 121.81 (C4,4'), 121.28 (C5,5'), 115.02 (C6,6'), 113.69 (C3,3'), 73.70 (C9,9'), 71.01 (C14,14'), 69.38 (C7,7'), 68.89 (C8,8'). *double intensity peak

IR (KBr) ν (cm^{-1}) 2922, 1592, 1505, 1455, 1374, 1254, 1122, 1008.

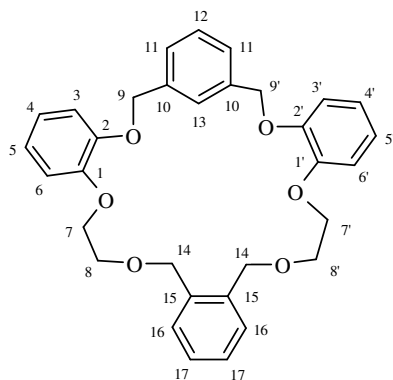
HRMS (EI, 70 eV) Calculated for $\text{C}_{32}\text{H}_{32}\text{O}_6\text{H}^+$ 513.2272; Found 513.2285;

m.p.=155-157 °C

R_f CHCl_3 =0.21

2,3,6,8,11,12,18,19-tetrabenzo-1,4,10,13,16,21-hexaoxacyclo-trieicosa-2,6,7,11,18-pentaene (178)

The general procedure 1 was used with the starting materials **164** (0.41 g, 1.0 mmol) and α,α' -dichloro-*o*-xylene (0.17 g, 1.0 mmol). Product **178** was isolated by column chromatography on silica gel using CHCl_3 as a white solid (0.16 g, 0.29 mmol, 29 % yield).



^1H NMR (400 MHz, CDCl_3) 7.67 (1H, s, (H13)) 7.27-7.23 (3H, m, (H12,11,11')) 7.21 (2H, dd, $J=5.6, 3.2\text{Hz}$, (H17,17')) 7.15 (2H, dd, $J=5.6, 3.2\text{Hz}$, (H16,16')) 6.93-6.77 (8H, m, (H3-6,3'-6')) 5.02 (4H, s, (H9,9')) 4.65 (4H, s, (H14,14')) 4.08 (4H, t, $J=4.4\text{Hz}$, (H7,7')) 3.72 (4H, t, $J=4.4\text{Hz}$, (H8,8'))

^{13}C NMR (100 MHz, CDCl_3) 149.78 (C2,2'), 149.01 (C1,1'), 138.04 (C10,10'), 136.78 (C15,15'), 129.21 (C17,17'), 128.29 (C13), 127.67 (C16,16'), 127.21 (C12), 127.09 (C11,11'), 122.20 (C4,4'), 121.37 (C5,5'), 116.61 (C6,6'), 114.33 (C3,3'), 72.19 (C9,9'), 71.42 (C14,14'), 69.01 (C7,7'), 68.72 (C8,8')

IR (KBr) ν (cm^{-1}) 2930, 1592, 1506, 1452, 1378, 1255, 1124, 1097, 1021.

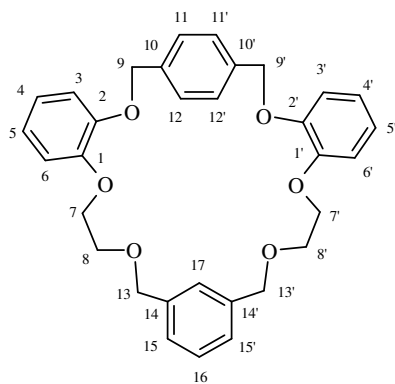
HRMS (EI, 70eV) Na^+ adduct Calculated for $\text{C}_{32}\text{H}_{32}\text{O}_6\text{Na}^+$ 535.2091; Found 535.2092;

m.p.=84-86 °C

R_f CHCl_3 =0.34

2,3,6,9,12,13,19,21-tetrabenzo-1,4,11,14,17,23-hexaoxacyclopentaeicosa-2,6,7,8,12,19,20-hexaene (179)

The general procedure 1 was used with the starting materials **163** (0.41 g, 1.0 mmol) and α,α' -dichloro-*m*-xylene (0.17 g, 1.0 mmol). Product **179** was isolated by column chromatography on silica gel using CHCl_3 as a white solid (0.22 g, 0.43 mmol, 43 % yield).



^1H NMR (400 MHz, CDCl_3) 7.37 (4H, s, (H11,11',12,12')) 7.24-7.12 (4H, m, overlap, (H15,15',16,17)) 6.93-6.84 (8H, m, (H3-6,3'-6')) 4.99 (4H, s, (H9,9')) 4.61 (4H, s, (H13,13')) 4.15 (4H, t, $J=4.4\text{Hz}$, (H7,7')) 3.84 (4H, t, $J=4.4\text{Hz}$, (H8,8'))

^{13}C NMR (100 MHz, CDCl_3) 149.38 (C2,2'), 148.72 (C1,1'), 138.47 (C10,10'), 136.78 (C14,14'), 128.60 (C16), 127.59 (C11,11',12,12')*, 126.90 (C17), 126.82 (C15,15'), 121.80 (C4,4'), 121.29 (5,5'), 115.03 (C6,6'), 113.70 (C3,3'), 73.71 (C9,9'), 71.02 (C13,13'), 69.42 (C7,7'), 68.89 (C8,8'). * double intensity peak

IR (KBr) ν (cm^{-1}) 2924, 1591, 1505, 1455, 1374, 1254, 1121, 1008.

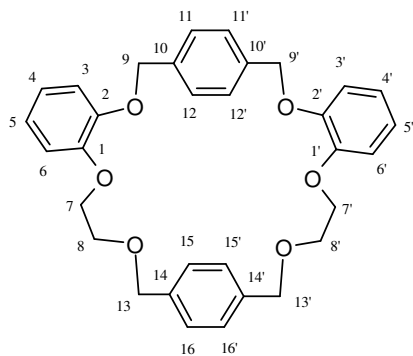
HRMS (EI, 70 eV) Calculated for $\text{C}_{32}\text{H}_{32}\text{O}_6\text{H}^+$ 513.2272; Found 513.2291;

m.p.=159-161 $^\circ\text{C}$

R_f CHCl_3 =0.26

2,3,6,9,12,13,19,22-tetrabenzo-1,4,11,14,17,24-hexaoxacyclohexaeicosa-2,6,7,8,12,19,20,21-hexaene (180)

The general procedure 1 was used with the starting materials **163** (0.41 g, 1.0 mmol) and α,α' -dichloro-*p*-xylene (0.17 g, 1.0 mmol). Product **180** was isolated by column chromatography on silica gel using CHCl_3 as a white solid (0.19 g, 0.38 mmol, 38 % yield).



^1H NMR (400 MHz, CDCl_3) 7.41 (4H, s, (H11,11',12,12')) 7.15 (4H, s, (H15,15',16,16')) 6.97-6.82 (8H, m, (H3-6,3'-6')) 5.03 (4H, s, (H9,9')) 4.59 (4H, s, (H13,13')) 4.15 (4H, t, $J=4.2\text{ Hz}$, (H7,7')) 3.79 (4H, t, $J=4.2\text{ Hz}$, (H8,8'))

^{13}C NMR (100 MHz, CDCl_3) 149.29 (C2,2'), 148.56 (C1,1'), 137.50 (C10,10'), 136.78 (C14,14'), 127.70 (C11,11',12,12')*, 127.62 (15,15',16,16')*, 121.70 (C4,4'), 121.08 (C5,5'), 114.79 (C6,6'), 113.12 (C3,3'), 73.00 (C9,9'), 71.02 (C13,13'), 68.83 (C7,7'), 68.08 (C8,8'). * double intensity peak

IR (KBr) ν (cm^{-1}) 1591, 1506, 1451, 1257, 1216, 1124, 1097, 1049, 1015.

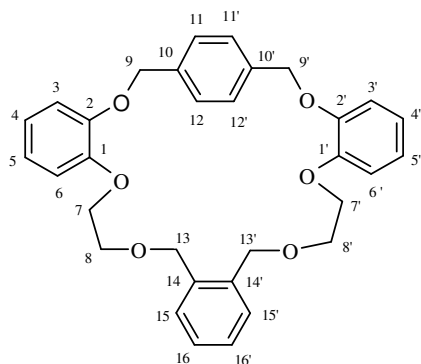
HRMS (EI, 70 eV) Calculated for $\text{C}_{32}\text{H}_{32}\text{O}_6\text{H}^+$ 513.2272; Found 513.2265;

R_f $\text{CHCl}_3=0.32$

m.p.=135-137 °C

2,3,6,9,12,13,19,20-tetrabenzo-1,4,11,14,17,22-hexaoxacyclo-tetraeicosa-2,6,7,8,12,19-hexaene (181)

The general procedure 1 was used with the starting materials **163** (0.41 g, 1.0 mmol) and α,α' -dichloro-*o*-xylene (0.17 g, 1.0 mmol). Product **181** was isolated by column chromatography on silica gel using CH_2Cl_2 as a white solid (0.26 g, 0.48 mmol, 48 % yield).



^1H NMR (400 MHz, CDCl_3) 7.41 (4H, s, (H11,11',12,12')) 7.36 (2H, dd, $J=5.6, 3.2\text{ Hz}$, (H16,16')) 7.21 (2H, dd, $J=5.6, 3.2\text{ Hz}$, (H15,15')) 6.96-6.82 (8H, m, (H3-6,3'-6')) 5.00 (4H, s, (H9,9')) 4.67 (4H, s, (H13,13')) 4.12 (4H, t, $J=4.4\text{ Hz}$, (H7,7')) 3.77 (4H, t, $J=4.4\text{ Hz}$, (H8,8'))

^{13}C NMR (100 MHz, CDCl_3) 149.49 (C2,2'), 149.05 (C1,1'), 136.85 (C10,10'), 136.44 (C14,14'), 128.95 (C16,16'), 127.79 (C15,15'), 127.43 (C11,11',12,12'), 121.83 (C4,4'), 121.59 (C5,5'), 115.19 (C6,6'), 114.52 (C3,3'), 71.21 (C9,9'), 70.99 (C13,13'), 69.32 (C7,7'), 69.05 (C8,8')

IR (KBr) ν (cm⁻¹) 2933, 1591, 1509, 1452, 1259, 1125, 1028.

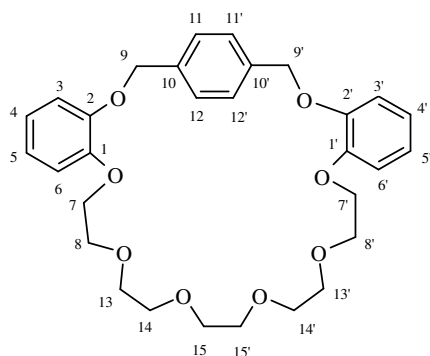
HRMS (EI, 70 eV) Na⁺ adduct Calculated for C₃₂H₃₂O₆Na⁺ 535.2091; Found 535.2079;

m.p.=175-177 °C

R_f DCM =0.44

2,3,6,9,12,13-tribenzo-1,4,11,14,17,20,23,26-octaoxacyclooctaica-2,6,7,8,12-tetraene (182)

The general procedure 1 was used with the starting materials **163** (0.41 g, 1.0 mmol) and 1,2-bis-(2-chloroethoxy)ethane (0.19 g, 0.10 mL, 1.0 mmol). Product **182** was isolated by column chromatography on silica gel using EtOAc/Et₂O (1:1) as a white solid (0.027 g, 0.05 mmol, 5 % yield).



¹H NMR (400 MHz, CDCl₃) 7.42 (4H, s, (H11,11',12,12')) 6.92-6.81 (8H, m, (H3-6, 3'-6')) 5.05 (4H, s, (H9,9')) 4.12 (4H, t, *J*=4.4Hz, (H7,7')) 3.84 (4H, t, *J*=4.4Hz, (H8,8')) 3.69 (4H, t, *J*=4.6Hz, (H13,13')) 3.54 (4H, t, *J*=4.6Hz, (H14,14')) 3.52 (4H, s, (H15,15'))

¹³C NMR (100 MHz, CDCl₃) 149.38 (C2,2'), 148.61 (C1,1'), 136.99 (C10,10'), 127.71 (C11,11',12,12')*, 121.87 (C4,4'), 121.32 (C5,5'), 115.48 (C6,6'), 113.82 (C3, 3'), 71.21 (C9,9') 71.06 (C15,15'), 70.79 (C13,13'), 70.72 (C14,14'), 69.74 (C8,8'), 69.09 (C7,7'). *double intensity peak

IR (KBr) ν (cm⁻¹) 2931, 1593, 1506, 1452, 1336, 1255, 1125, 1046.

HRMS (EI, 70 eV) Calculated for C₃₀H₃₆O₈H⁺ 525.2483; Found 525.2477;

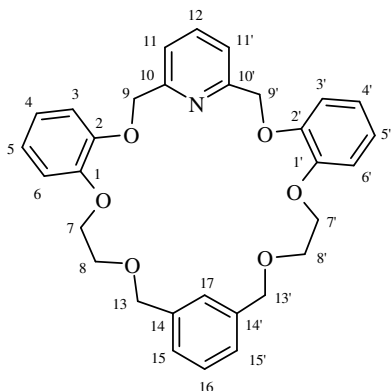
Na adduct Calculated for C₃₀H₃₆O₈Na⁺ 547.2302; Found 547.2284;

m.p.=84-86 °C

R_f EtOAc/Et₂O 1:1=0.28

2,3,6,8,11,12,18,20-tetrabenzo-7-aza-1,4,10,13,16,22-hexaoxacyclo-tetraeicosa-2,6,7,11,18,19-hexaene (183)

The general procedure 1 was used with the starting materials **166** (0.41 g, 1.0 mmol) and α,α' -dichloro-*m*-xylene (0.17 g, 1.0 mmol). Product **183** was isolated by column chromatography on silica gel using EtOAc as a white solid (0.19 g, 0.38 mmol, 38 % yield).



^1H NMR (400 MHz, CDCl_3) 7.65 (1H, t, $J=7.6\text{Hz}$, (H12)) 7.58 (1H, s, H17), 7.53-7.44 (5H, m, overlap, (H11,11',15,15',16,)) 7.02-6.83 (8H, m, (H3-6,3'-6')) 4.94 (4H, s, (H9,9')) 4.62 (4H, s, (H13,13')) 4.11 (4H, t, $J=4.4\text{Hz}$, (H7,7')) 3.81 (4H, t, $J=4.4\text{Hz}$, (H8,8'))

^{13}C NMR (100 MHz, CDCl_3) 157.57 (C10,10'), 148.78 (C2,2'), 148.71 (C1,1'), 137.06 (C14,14'), 129.98 (C15,15'), 129.65 (C11,11'), 129.51 (C12), 127.18 (C16), 121.30 (C4,4'), 121.00 (C5,5'), 119.52 (C17), 113.11 (C6,6'), 112.13 (C3,3'), 73.58 (C9,9'), 71.12 (C13,13'), 68.45 (C7,7'), 67.89 (C8,8')

IR (KBr) ν (cm^{-1}) 2937, 1596, 1509, 1459, 1377, 1258, 1127, 1056.

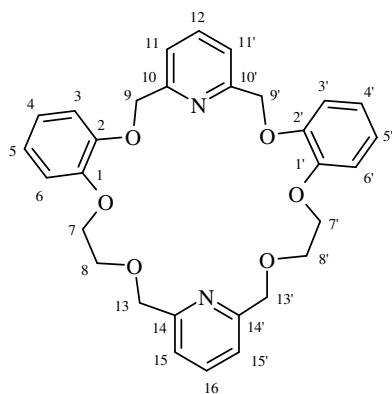
HRMS (EI, 70 eV) Calculated for $\text{C}_{31}\text{H}_{31}\text{NO}_6\text{H}^+$ 514.2224; Found 514.2222;

m.p.=166-168 °C

$R_{\text{f EtOAc}}=0.28$

2,3,6,8,11,12,18,20-tetrabenzo-7,19-diaza-1,4,10,13,16,22-hexaoxacyclo-tetraeicosa-2,6,7,11,18,19-hexaene (184)

The general procedure 1 was used with the starting materials **166** (0.41 g, 1.0 mmol) and 2,6-*bis*(chloromethyl)pyridine (0.17 g, 1.0 mmol). Product **184** was isolated by column chromatography on silica gel using EtOAc as a white solid (0.25 g, 0.49 mmol, 49 % yield).



¹H NMR (400 MHz, CDCl₃) 7.48 (2H, d, *J*=7.8Hz, (H11,11')) 7.34 (3H, m, overlap, (H12,15,15')) 7.02-6.87 (8H, m, (H3-6,3'-6')) 6.78 (1H, t, *J*=7.8Hz, (H16)) 5.07 (4H, s, (H9,9')) 4.61 (4H, s, (H13,13')) 4.17 (4H, t, *J*=4.4Hz, (H7,7')) 3.87 (4H, t, *J*= 4.4Hz, (H8,8'))

¹³C NMR (100 MHz, CDCl₃) 157.61 (C10,10'), 156.47 (C14,14'), 149.32 (C2,2'), 148.90 (C1,1'), 137.51 (C12), 137.20 (C16), 122.03 (C11,11'), 121.58 (C4,4'), 121.42 (C5,5'), 119.40 (C15,15'), 114.89 (C6,6'), 113.52 (C3,3'), 73.70 (C9,9'), 72.51 (C13,13'), 69.37 (C7,7'), 68.66 (C8,8')

IR (KBr) ν (cm⁻¹) 2920, 1594, 1507, 1456, 1362, 1259, 1125, 1053;

HRMS (EI, 70 eV) Calculated for C₃₀H₃₀N₂O₆H⁺ 514.2230; Found 514.2245;

m.p.=145-147 °C

R_f EtOAc=0.18

8.3 Morphine macrocycles and their precursors

General procedure 194, 198, 199, 200

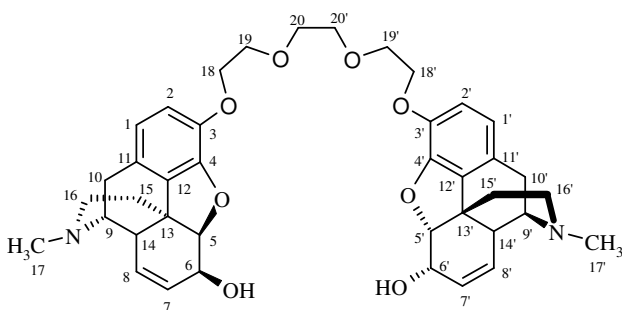
Morphine hydrochloride (0.43 g, 1.5 mmol) was suspended in absolute methanol (3 mL) and while stirring sodium methoxide (0.22 g, 4.0 mmol) as a suspension in absolute methanol (3 mL) was added dropwise over 1h. α,α' -Dibromoxylene (0.20 g, 0.75 mmol) was added and mixture was refluxed for 48 h. After that time solvent was removed by rotary evaporation and distilled water (40 mL) was added into the crude. Mixture was extracted with dichloromethane (5 x 20 mL) organic layer was dried over sodium sulphate, concentrated *in vacuo* and purified by column chromatography on silica gel and CH₂Cl₂/MeOH/NH₄OH mixture (10:1:0.01) as a mobile phase. R_f values are calculated with this solvent mixture.

General procedure 197, 201, 202

Morphine hydrochloride (0.43 g, 1.5 mmol) was suspended in dry tetrahydrofuran (3 mL) and while stirring potassium *tert*-butoxide (0.17 g, 1.5 mmol) as a suspension in tetrahydrofuran (3 mL) was added dropwise over 1h. α,α' -Dibromoxylene (0.75 mmol) was added into the mixture and was refluxed for 18 h. After that time solvent was removed by rotary evaporation and distilled water (40 mL) was added into the crude. Mixture was extracted with dichloromethane (5 x 20 mL) organic layer was dried over sodium sulphate, concentrated *in vacuo* and purified by column chromatography on silica gel and CH₂Cl₂/MeOH/NH₄OH mixture (10:1:0.01) as a mobile phase.

1,8-Bis(3-morphinyl)-3,6-dioxaoctane (194)

The general procedure was used with the starting materials morphine hydrochloride (0.43 g, 1.5 mmol), and 1,2-bis(iodoethoxyethane) (0.277 g, 0.137 mL, 0.75 mmol). Product **194** was isolated by column chromatography as white foam (0.349 g, 0.51 mmol, 68 % yield).



^1H NMR (400 MHz, CDCl_3) 6.62 (2H, d, $J=8.4\text{Hz}$, (H2,2')) 6.47 (2H, d, $J=8.4\text{Hz}$, (H1,1')) 5.62 (2H, ddd, $J=10.0, 2.8, 1.2\text{Hz}$, (H7,7')) 5.20 (2H, dt, $J=10.0, 2.6\text{Hz}$, (H8,8')) 4.81 (2H, dd, $J=6.4, 1.2\text{Hz}$, (H5,5')) 4.22-4.18 (2H, m, (H18,18')) 4.11-4.02 (4H, m, overlap, (H6,6',18,18')) 3.76 (4H, t, $J=4.8\text{Hz}$, (H19,19')) 3.69-3.61 (4H, m, (H20,20')) 3.49 (2H, s, OH) 3.35 (2H, dd, $J=6.2, 3.2\text{Hz}$, (H9,9')) 2.99 (2H, d, $J=18.8\text{Hz}$, (H10,10')) 2.68 (2H, dd, $J=3.2, 2.6\text{Hz}$, (H14,14')) 2.61 (2H, dd, $J=12.4, 4.2\text{Hz}$, (H16,16')) 2.41 (6H, s, (H17,17')) 2.39 (2H, td, $J=12.4, 3.6\text{Hz}$, (H16,16')) 2.31 (2H, dd, $J=18.8, 6.2\text{Hz}$, (H10,10')) 2.10 (2H, td, $J=12.4, 5.2\text{Hz}$, (H15,15')) 1.83 (2H, dd, $J=12.4, 4.2\text{Hz}$, (H15,15'))

^{13}C NMR (100 MHz, CDCl_3) 146.98 (C3,3'), 141.05 (C4,4'), 133.49 (C7,7'), 131.36 (C12,12'), 128.21 (C11,11'), 127.79 (C8,8'), 119.51 (C1,1'), 115.55 (C2,2'), 91.39 (C5,5'), 70.71 (C20,20'), 69.93 (C19,19'), 69.14 (C18,18'), 66.49 (C6,6'), 58.82 (C9,9'), 46.42 (C16,16'), 43.10 (C17,17'), 42.86 (C13,13'), 40.74 (C14,14'), 35.76 (C15,15'), 20.47 (C10,10').

IR (KBr disc): ν (cm^{-1}) 3389, 2925, 2779, 1504, 1451, 1259, 1120.

HRMS (EI, 70 eV) Calculated for $\text{C}_{40}\text{H}_{49}\text{N}_2\text{O}_8$ 685.3489; Found 685.3489;

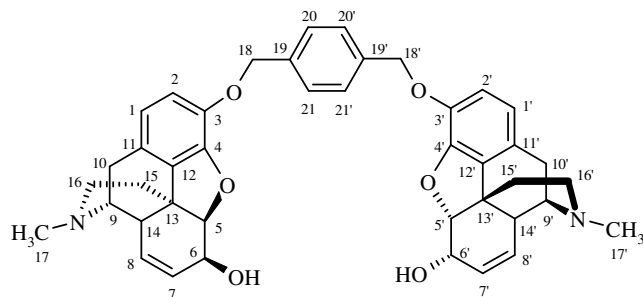
m.p.= 54-56 °C

R_f $\text{CH}_2\text{Cl}_2/\text{MeOH}/\text{NH}_4\text{OH}$ mixture (10:1:0.01) = 0.11

$[\alpha]_D^{25} = -75^\circ$ $c = (0.2, \text{CHCl}_3, 589 \text{ nm}, 20^\circ \text{C})$

1,4-Bis(3-morphinyl)-*p*-xylene (198)

The general procedure was used with the starting materials morphine hydrochloride (0.43 g, 1.5 mmol), and α,α' -dibromo-*p*-xylene (0.198 g, 0.75 mmol). Product **198** was isolated by column chromatography as a white solid (0.303 g, 0.45 mmol, 60 % yield).



^1H NMR (400 MHz, CDCl_3) 7.34 (4H, s, (H20,20',21,21')) 6.64 (2H, d, $J=8.4\text{Hz}$, (H2,2')) 6.47 (2H, d, $J=8.4\text{Hz}$, (H1,1')) 5.62 (2H, ddd $J=9.8, 2.8, 1.2\text{Hz}$, (H7,7')) 5.23 (2H, dt, $J=9.8, 2.6\text{Hz}$, (H8,8')) 5.10 (2H, d, $J=12.0\text{Hz}$, (H18,18')) 5.02 (2H, d, $J=12.0\text{Hz}$, (H18,18')) 4.82 (2H, dd, $J=6.4, 1.2\text{Hz}$, (H5,5')) 4.11 (2H, dd, $J=6.4, 2.8\text{Hz}$, (H6,6')) 3.31 (2H, dd, $J=6.0, 3.2\text{Hz}$, (H9,9')) 2.99 (2H, d, $J=18.8\text{Hz}$, (H10,10')) 2.66 (2H, dd, $J=3.2, 2.6\text{Hz}$, (H14,14')) 2.57 (2H, dd, $J=12.2, 4.0\text{Hz}$, (H16,16')) 2.38 (6H, s, (H17,17')) 2.33 (2H, td, $J=12.2, 3.2\text{Hz}$, (H16,16')) 2.27 (2H, dd, $J=18.8, 6.4\text{Hz}$, (H10,10')) 2.05 (2H, td, $J=12.2, 4.8\text{Hz}$, (H15,15')) 1.83 (2H, dd, $J=12.2, 4.0\text{Hz}$, (H15,15'))

^{13}C NMR (100 MHz, CDCl_3) 146.90 (C3,3'), 141.05 (C4,4'), 137.04 (C19,19'), 133.36 (C7,7'), 131.40 (C12,12'), 128.30 (C11,11'), 127.86 (C8,8'), 127.72 (C20,20', 21,21'), 119.67 (C1,1'), 115.71 (C2,2'), 91.34 (C5,5'), 71.47 (C18,18'), 66.44 (C6,6'), 58.83 (C9,9'), 46.43 (C16,16'), 43.10 (C17,17'), 42.90 (C13,13'), 40.74 (C14,14'), 35.76 (C15,15'), 20.50 (C10,10')

IR (KBr disc): ν (cm^{-1}) 3383, 2927, 1497, 1446, 1259, 1119.

HRMS (EI, 70 eV) Calculated for $\text{C}_{42}\text{H}_{44}\text{N}_2\text{O}_6\text{H}^+$ 673.3272; Found 673.3267;

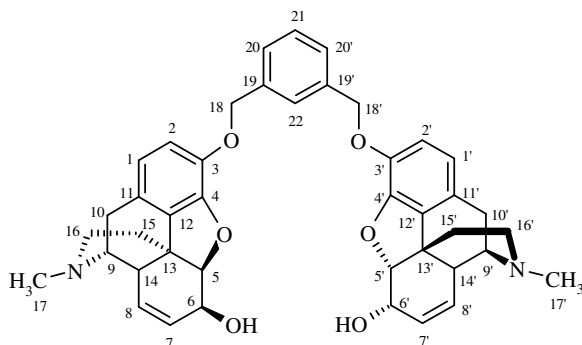
m.p.=118-120 °C

R_f $\text{CH}_2\text{Cl}_2/\text{MeOH}/\text{NH}_4\text{OH}$ mixture (10:1:0.01) =0.34

$[\alpha]_D = -140^\circ$ ($c = 0.2$, CHCl_3 , 589 nm, 20 °C)

1,3-Bis(3-morphinyl)-*m*-xylene (199)

The general procedure was used with the starting materials morphine hydrochloride (0.43 g, 1.5 mmol), and α,α' -dibromo-*m*-xylene (0.198 g, 0.75 mmol). Product **199** was isolated by column chromatography as a white solid (0.363 g, 0.54 mmol, 72 % yield).



^1H NMR (400 MHz, CDCl_3) 7.42 (1H, s, (H22)) 7.31-7.27 (3H, m, (H20,20',21)) 6.64 (2H, d, $J=8.2\text{Hz}$, (H2,2')) 6.46 (2H, d, $J=8.2\text{Hz}$, (H1,1')) 5.61 (2H, ddd, $J=10.0, 2.8, 1.2\text{Hz}$, (H7,7')) 5.22 (2H, dt, $J=10.0, 2.4\text{Hz}$, (H8,8')) 5.10 (2H, d, $J=12.0\text{Hz}$, (H18,18')) 5.01 (2H, d, $J=12.0\text{Hz}$, (H18,18')) 4.81 (2H, dd, $J=6.4, 0.8\text{Hz}$, (H5,5')) 4.10 (2H, dd, $J=6.4, 2.8\text{Hz}$, (H6,6')) 3.29 (2H, dd, $J=6.2, 3.0\text{Hz}$, (H9,9')) 2.98 (2H, d, $J=18.8\text{Hz}$, (H10,10')) 2.63 (2H, dd, $J=3.0, 2.4\text{Hz}$, (H14,14')) 2.54 (2H, dd, $J=12.2, 4.0\text{Hz}$, (H16,16')) 2.36 (6H, s, (H17,17')) 2.34 (2H, td, $J=12.2, 3.6\text{Hz}$, (H16,16')) 2.25 (2H, dd, $J=18.8, 6.2\text{Hz}$, (H10,10')) 2.01 (2H, td, $J=12.2, 5.2\text{Hz}$, (H15,15')) 1.80 (2H, dd, $J=12.2, 4.0\text{Hz}$, (H15,15'))

^{13}C NMR (100 MHz, CDCl_3) 146.99 (C3,3'), 141.08 (C4,4'), 137.66 (C19,19'), 133.36 (C7,7'), 131.38 (C12,12'), 128.70 (C21), 128.25 (C8,8'), 127.83 (C11,11'), 127.10 (C20,20'), 126.60 (C22), 119.63 (C1,1'), 115.81 (C2,2'), 91.39 (C5,5'), 71.65 (C18,18'), 66.50 (C6,6'), 58.84 (C9,9'), 46.44 (C16,16'), 43.06 (C17,17'), 42.91 (C13,13'), 40.69 (C14,14'), 35.69 (C15,15'), 20.54 (C10,10').

IR (KBr disc): ν (cm^{-1}) 3391, 2926, 1498, 1445, 1251, 1120.

HRMS (EI, 70 eV) Calculated for $\text{C}_{42}\text{H}_{44}\text{N}_2\text{O}_6\text{H}^+$ 673.3272; Found 673.3294;

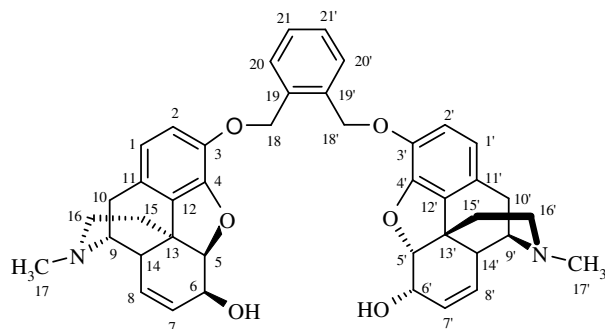
m.p.=110-112 $^\circ\text{C}$

R_f $\text{CH}_2\text{Cl}_2/\text{MeOH}/\text{NH}_4\text{OH}$ mixture (10:1:0.01) =0.31

$[\alpha]_D = -164^\circ$ ($c = 0.2$, CHCl_3 , 589 nm, 20 $^\circ\text{C}$)

1,2-Bis(3-morphinyl)-*o*-xylene (200)

The general procedure was used with the starting materials morphine hydrochloride (0.43 g, 1.5 mmol), and α,α' -dibromo-*o*-xylene (0.198 g, 0.75 mmol). Product **200** was isolated by column chromatography as a white solid (0.242 g, 0.36 mmol, 48 % yield).



^1H NMR (400 MHz, CDCl_3) 7.44 (2H, dd, $J=5.6, 3.6\text{Hz}$, (H21,21')) 7.27 (2H, dd, $J=5.6, 3.6\text{Hz}$, (H20,20')) 6.61 (2H, d, $J=8.2\text{Hz}$, (H2,2')) 6.46 (2H, d, $J=8.2\text{Hz}$, (H1,1')) 5.63 (2H, ddd, $J=9.8, 2.8, 1.0\text{Hz}$, (H7,7')) 5.27-5.06 (6H, m, overlap, (H8,8',18,18')) 4.79 (2H, dd, $J=6.4, 1.0\text{Hz}$, (H5,5')) 4.12 (2H, dd, $J=6.4, 2.8\text{Hz}$, (H6,6')) 3.27 (2H, dd, $J=6.0, 3.0\text{Hz}$, (H9,9')) 2.97 (2H, d, $J=18.6\text{Hz}$, (H10,10')) 2.61 (2H, dd, $J=3.0, 2.4\text{Hz}$, (H14,14')) 2.54 (2H, dd, $J=12.2, 4.0\text{Hz}$, (H16,16')) 2.36 (6H, s, (H17,17')) 2.33 (2H, td, $J=12.2, 3.6\text{Hz}$, (H16,16')) 2.23 (2H, dd, $J=18.6, 6.2\text{Hz}$, (H10,10')) 1.99 (2H, td, $J=12.4, 5.2\text{Hz}$, (H15,15')) 1.78 (2H, dd, $J=12.4, 4.0\text{Hz}$, (H15,15'))

^{13}C NMR (100 MHz, CDCl_3) 147.45 (C3,3'), 141.23 (C4,4'), 136.68 (C19,19'), 133.58 (C7,7'), 131.32 (C12,12'), 128.72 (C21,21'), 128.21 (C11,11'), 127.64 (C8,8'), 127.34 (C20,20'), 119.32 (C1,1'), 115.57 (C2,2'), 91.13 (C5,5'), 71.32 (C18,18'), 66.84 (C6,6'), 58.61 (C9,9'), 46.34 (C16,16'), 43.04 (C17,17'), 42.92 (C13,13'), 40.63 (C14,14'), 35.82 (C15,15'), 20.53 (C10,10').

IR (KBr disc): ν (cm^{-1}) 3343, 2924, 1502, 1449, 1276, 1121.

HRMS (EI, 70 eV) Calculated for $\text{C}_{42}\text{H}_{44}\text{N}_2\text{O}_6\text{H}^+$ 673.3272; Found 673.3269;

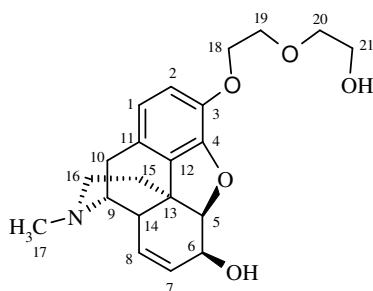
m.p.=125-127 °C

R_f $\text{CH}_2\text{Cl}_2/\text{MeOH}/\text{NH}_4\text{OH}$ mixture (10:1:0.01) =0.37

$[\alpha]_D = -121^\circ$ ($c = 0.2, \text{CHCl}_3, 589 \text{ nm}, 20^\circ \text{C}$)

2-[(3-morphinyl)ethoxy]ethanol (197)

The general procedure was used with the starting materials morphine hydrochloride (0.33 g, 1.0 mmol), and 2-bromoethyl ether (0.116 g, 0.062 mL, 0.5 mmol). Product **197** was isolated by column chromatography as yellow oil (0.052 g, 0.14 mmol, 28 % yield).



^1H NMR (400 MHz, CDCl_3) 6.61 (1H, d, $J=8.4\text{Hz}$, (H2)) 6.46 (1H, d, $J=8.4\text{Hz}$, (H1)) 5.63 (1H, ddd, $J=9.8, 2.6, 1.0\text{Hz}$, (H7)) 5.23 (1H, dt, $J=9.8, 2.6\text{Hz}$, (H8)) 4.82 (1H, dd, $J=6.4, 1.0\text{Hz}$, (H5)) 4.24-4.19 (1H, m, (H18)) 4.18-4.07 (2H, m, overlap, (H6,18)) 3.76-3.71 (4H, m, overlap, (H19,20)) 3.58 (2H, t, $J=5.6\text{Hz}$, (H21)) 3.31 (1H, dd, $J=6.2, 3.2\text{Hz}$, (H9)) 2.98 (1H, d, $J=18.6\text{Hz}$, (H10)) 2.62 (1H, dd, $J=3.2, 2.6\text{Hz}$, (H14)) 2.56 (1H, dd, $J=12.2, 3.8\text{Hz}$, (H16)) 2.39 (3H, s, (H17)) 2.37 (1H, td, $J=12.2, 3.2\text{Hz}$, (H16)) 2.27 (1H, dd, $J=18.6, 6.2\text{Hz}$, (H10)) 2.04 (1H, td, $J=12.4, 5.2\text{Hz}$, (H15)) 1.81 (1H, dd, $J=12.2, 3.8\text{Hz}$, (H15))

^{13}C NMR (100 MHz, CDCl_3) 146.89 (C3), 140.95 (C4), 133.47 (C7), 131.36 (C12), 128.19 (C11), 127.82 (C8), 119.63 (C1), 115.58 (C2), 91.38 (C5), 71.43 (C20), 69.99 (C19), 69.11 (C18), 66.41 (C6), 58.83 (C9), 46.41 (C16), 43.02 (C21), 43.02 (C17), 42.80 (C13), 40.58 (C14), 35.63 (C15), 20.50 (C10).

IR (KBr disc): ν (cm^{-1}) 3334, 2925, 2782, 1502, 1449, 1257, 1121.

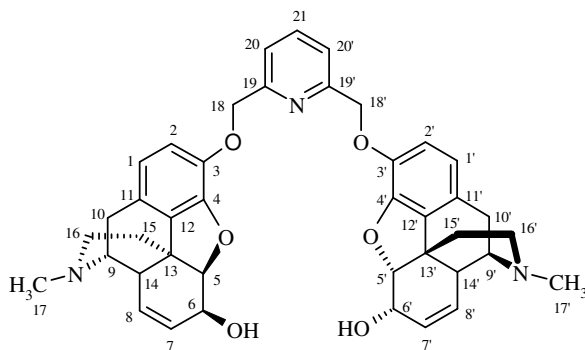
HRMS (EI, 70 eV) Calculated for $\text{C}_{21}\text{H}_{27}\text{NO}_5\text{H}^+$ 374.1962; Found 374.1978;

R_f $\text{CH}_2\text{Cl}_2/\text{MeOH}/\text{NH}_4\text{OH}$ mixture (10:1:0.01) =0.27

$[\alpha]_D = -84^\circ$ $c = (0.2, \text{CHCl}_3, 589 \text{ nm}, 20^\circ \text{C})$

2,6-Bis-(3-morphinylmethylene)lutidine (201)

The general procedure was used with the starting materials morphine hydrochloride (0.43 g, 1.5 mmol), and 2,6-bis(chloromethyl)pyridine (0.132 g, 0.75 mmol). Product **201** was isolated by column chromatography as a white solid (0.216 g, 0.32 mmol, 42 % yield).



^1H NMR (400 MHz, CDCl_3) 7.66 (1H, t, $J=7.6\text{Hz}$, (H21)) 7.40 (2H, d, $J=7.6\text{Hz}$, (H20,20')) 6.61 (2H, d, $J=8.4\text{Hz}$, (H2,2')) 6.42 (2H, d, $J=8.4\text{Hz}$, (H1,1')) 5.58 (2H, ddd, $J=9.8, 2.8, 0.8\text{Hz}$, (H7,7')) 5.38 (2H, d, $J=13.6\text{Hz}$, (H18,18')) 5.19 (2H, dt, $J=9.8, 2.4\text{Hz}$, (H8,8')) 5.14 (2H, d, $J=13.6\text{Hz}$, (H18,18')) 4.82 (2H, dd, $J=6.4, 0.8\text{Hz}$, (H5,5')) 4.12 (2H, dd, $J=6.4, 2.8\text{Hz}$, (H6,6')) 3.28 (2H, dd, $J=6.0, 3.2\text{Hz}$, (H9,9')) 2.96 (2H, d, $J=18.4\text{Hz}$, (H10,10')) 2.61 (2H, dd, $J=3.2, 2.4\text{Hz}$, (H14,14')) 2.54 (2H, dd, $J=12.4, 4.2\text{Hz}$, (H16,16')) 2.36 (3H, s, (H17,17')) 2.33 (2H, td, $J=12.4, 3.6\text{Hz}$ (H16,16')) 2.22 (2H, dd, $J=18.4, 6.0\text{Hz}$, (H10,10')) 2.03 (2H, td, $J=12.4, 5.2\text{Hz}$, (H15,15')) 1.81 (2H, dd, $J=12.4, 4.2\text{Hz}$, (H15,15'))

^{13}C NMR (100 MHz, CDCl_3) 156.01 (C19,19'), 145.78 (C3,3'), 139.32 (C4,4'), 136.69 (C21), 132.34 (C7,7'), 130.63 (C12,12'), 127.29 (C11,11'), 127.07 (C8,8'), 119.87 (C20,20'), 118.59 (C1,1'), 115.56 (C2,2'), 90.61 (C5,5'), 71.04 (C18,18'), 65.54 (C6,6'), 57.82 (C9,9'), 45.37 (C16,16'), 42.05 (C17,17'), 41.77 (C13,13'), 39.67 (C14,14'), 34.66 (C15,15'), 19.50 (C10,10').

IR (KBr disc): ν (cm^{-1}) 3341, 2927, 1503, 1452, 1259, 1126.

HRMS (EI, 70 eV) Calculated for $\text{C}_{41}\text{H}_{43}\text{N}_3\text{O}_6\text{H}^+$ 674.3225; Found 674.3245;

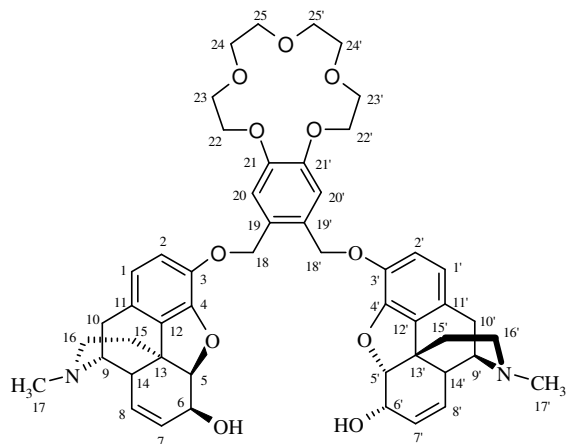
m.p.=129-131 °C

R_f $\text{CH}_2\text{Cl}_2/\text{MeOH}/\text{NH}_4\text{OH}$ mixture (10:1:0.01) =0.26

$[\alpha]_D = -167^\circ$ $c = (0.2, \text{CHCl}_3, 589 \text{ nm}, 20^\circ \text{C})$

1,2-Bis(3-morphinyl)-*o*-(1',2'-15-crown-5)xylene (202)

The general procedure was used with the starting materials morphine hydrochloride (0.33 g, 1.0 mmol), and α,α' -dibromo-1,2-(15-crown-5)xylene (0.226 g, 0.5 mmol). Product **202** was isolated by column chromatography as white foam (0.164 g, 0.19 mmol, 37 % yield).



$^1\text{H NMR}$ (400 MHz, CDCl_3) 6.85 (2H, s, (H20,20')), 6.68 (2H, d, $J=8.2\text{Hz}$, (H2,2')) 6.46 (2H, d, $J=8.2\text{Hz}$, (H1,1')) 5.62 (2H, ddd, $J=9.6, 2.0, 1.0\text{Hz}$, (H7,7')) 5.21 (2H, dt, $J=9.6, 2.8\text{Hz}$, (H8,8')) 5.17 (2H, d, $J=11.6\text{Hz}$, (H18,18')) 5.11 (2H, d, $J=11.6\text{Hz}$, (H18,18')) 4.78 (2H, dd, $J=6.4, 1.2\text{Hz}$, (H5,5')) 4.07-3.99 (6H, m, overlap, (H6,6',22,22')) 3.82 (4H, t, $J=4.4\text{Hz}$, (H23,23')) 3.69-3.61 (8H, m, (H24,24',25,25')) 3.34 (2H, dd, $J=6.0, 3.2\text{Hz}$, (H9,9')) 2.99 (2H, d, $J=18.8\text{Hz}$, (H10,10')) 2.68 (2H, dd, $J=3.2, 2.8\text{Hz}$, (H14,14')) 2.59 (2H, dd, $J=12.0, 4.2\text{Hz}$, (H16,16')) 2.41 (6H, s, (H17,17')) 2.36 (2H, td, $J=12.0, 3.2\text{Hz}$, (H16,16')) 2.30 (2H, dd, $J=18.8, 6.0\text{Hz}$, (H10,10')) 2.07 (2H, td, $J=12.0, 5.2\text{Hz}$, (H15,15')) 1.80 (2H, dd, $J=12.0, 4.2\text{Hz}$, (H15,15'))

$^{13}\text{C NMR}$ (100 MHz, CDCl_3) 148.56 (C3,3'), 147.88 (C21,21'), 140.64 (C4,4'), 133.55 (C12,12'), 131.34 (C7,7'), 128.71 (C19,19'), 128.32 (C11,11'), 127.94 (C8,8'), 119.60 (C1,1'), 117.26 (C20,20'), 115.73 (C2,2'), 91.46 (C5,5'), 70.96 (C18,18'), 70.40 (C25,25'), 70.14 (C24,24'), 69.47 (C22,22'), 69.04 (C23,23'), 66.63 (C6,6'), 58.97 (C9,9'), 46.48 (C16,16'), 42.94 (C17,17'), 42.82 (C13,13'), 40.46 (C14,14'), 35.39 (C15,15'), 20.73 (C10,10').

IR (KBr disc): ν (cm^{-1}) 3437, 2928, 2778, 1496, 1445, 1256, 1123.

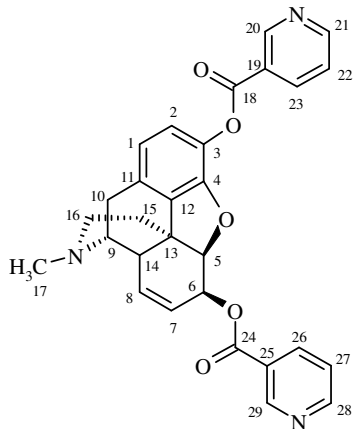
HRMS (EI, 70 eV) Calculated for $\text{C}_{50}\text{H}_{58}\text{N}_2\text{O}_{11}\text{H}^+$ 863.4113; Found 863.4117;

m.p.= 112-114°C R_f $\text{CH}_2\text{Cl}_2/\text{MeOH}/\text{NH}_4\text{OH}$ mixture (10:1:0.01) =0.34

$[\alpha]_D = -118^\circ$ $c = (0.10, \text{CHCl}_3, 589 \text{ nm}, 20^\circ\text{C})$

Morphine 3,6-dinicotinate (213)

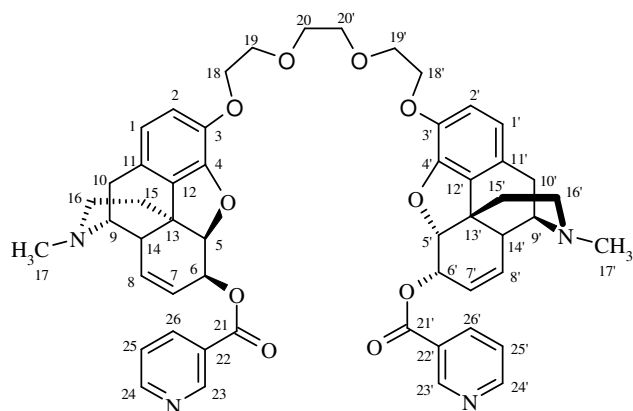
Compound was prepared according to the method reported in the literature. Recrystallization from water furnished **213** as a white crystalline product (0.59 g, 1.2 mmol, 71 % isolated yields).



^1H and ^{13}C NMR data were in agreement with the literature¹⁴⁵.

215

A mixture of nicotinic acid (0.16 g, 1.3 mmol) and thionyl chloride (0.77 g, 0.50 mL, 6.5 mmol) was refluxed for 2 hours. Excess of thionyl chloride was removed by rotary evaporation. Dry chloroform (1.5 mL) and dry pyridine (0.3 mL) were added to the residue and was refluxed for 2 h. After that time mixture was cooled down to 10 °C and **194** (0.301 g, 0.44 mmol) was added in small portions over a 30 min period of time then all was stirred at room temperature for 2 days. Chloroform was removed *in vacuo* and product was separated by column chromatography using $\text{CH}_2\text{Cl}_2/\text{MeOH}$ (3:1) as a mobile phase to give **215** as white solid (0.089 g, 0.10 mmol, 22 % yield).



^1H NMR (400 MHz, CDCl_3) 9.16 (2H, d, $J=1.8\text{Hz}$, (H23,23')) 8.70 (2H, dd, $J=4.8$, 1.8Hz , (H24,24')) 8.27 (2H, dt, $J=7.8$, 1.8Hz , (H26,26')) 7.34 (2H, dd, $J=7.8$, 4.8Hz , (H25,25')) 6.63 (2H, d, $J=8.0\text{Hz}$, (H2,2')) 6.48 (2H, d, $J=8.0\text{Hz}$, (H1,1')) 5.70 (2H, ddd, $J=10.0$, 2.0 , 0.8Hz , (H7,7')) 5.47 (2H, dt, $J=10.0$, 2.8Hz , (H8,8')) 5.40 (2H, ddd, $J=6.8$, 2.8 , 2.0Hz , (H6,6')) 5.13 (2H, dd, $J=6.8$, 0.8Hz , (H5,5')) 3.98 (4H, t, $J=5.2\text{Hz}$, (H18,18')) 3.42 (4H, t, $J=5.2\text{Hz}$, (H19,19')) 3.40 (4H, s, (H20,20')) 3.36 (2H, dd, $J=5.2$, 3.2Hz , (H9,9')) 3.00 (2H, d, $J=18.8\text{Hz}$, (H10,10')) 2.82 (2H, dd, $J=3.2$, 2.8Hz , (H14,14')) 2.59 (2H, dd, $J=12.2$, 4.0Hz , (H16,16')) 2.41 (6H, s, (H17,17')) 2.37 (2H, td, $J=12.2$, 3.6Hz , (H16,16')) 2.31 (2H, dd, $J=18.8$, 5.2Hz , (H10,10')) 2.07 (2H, td, $J=12.2$, 4.8Hz , (H15,15')) 1.83 (2H, dd, $J=12.2$, 4.0Hz , (H15,15'))

^{13}C NMR (100 MHz, CDCl_3) 163.66 (C21,21'), 152.54 (C24,24'), 150.13 (C23,23'), 145.77 (C3,3'), 140.16 (C4,4'), 136.28 (C26,26'), 129.67 (C12,12'), 128.79 (C8,8'), 127.05 (C7,7'), 126.16 (C22,22'), 124.86 (C11,11'), 122.29 (C25,25'), 118.50 (C1,1'), 115.60 (C2,2'), 86.48 (C5,5'), 69.49 (C20,20'), 68.70 (C19,19'), 68.21 (C18,18'), 67.76 (C6,6'), 58.17 (C9,9'), 45.74 (C16,16'), 41.95 (C17,17'), 41.36 (C13,13'), 39.40 (C14,14'), 34.14 (C15,15'), 19.42 (C10,10').

IR (KBr disc): ν (cm^{-1}) 2968, 2780, 2496, 1728, 1452, 1286, 1133.

HRMS (EI, 70 eV) Calculated for $\text{C}_{52}\text{H}_{54}\text{N}_4\text{O}_{10}\text{H}^+$ 895.3913; Found 895.3900;

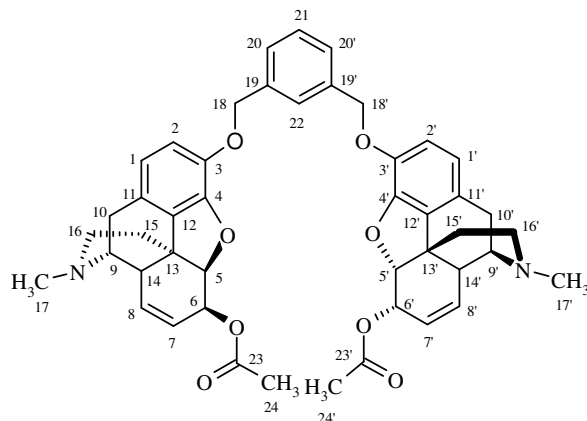
m.p.= 89-91 $^\circ\text{C}$

R_f $\text{CH}_2\text{Cl}_2/\text{MeOH}$ (3:1) = 0.53

$[\alpha]_D = -88^\circ$ $c = (0.10, \text{CHCl}_3, 589\text{ nm}, 20^\circ\text{C})$

216

Morphine macrocyclic precursor **199** (0.471 g, 0.70 mmol) and acetic anhydride (5 mL) were stirred at 60 °C overnight. Reaction mixture was quenched with distilled water (40 mL) and extracted with CH₂Cl₂ (5 x 20 mL). Organic layer was dried with Na₂SO₄, filtered, solvent was removed by rotary evaporation. Purification was performed by column chromatography on silica gel using CH₂Cl₂/MeOH (3:1). Product was isolated as brown oil (0.098 g, 0.13 mmol, 19 % yield).



¹H NMR (400 MHz, CDCl₃) 7.34 (1H, s, (H22)) 7.32-7.27 (3H, m, (H20,20',21)) 6.60 (2H, d, *J*=8.4Hz, (H2,2')) 6.43 (2H, d, *J*=8.4Hz, (H1,1')) 5.58 (2H, ddd, *J*=9.8, 2.8, 1.0Hz, (H7,7')) 5.38 (2H, dt, *J*=9.8, 2.6Hz, (H8,8')) 5.14-5.10 (2H, m, (H6,6')) 5.10-5.02 (6H, m, overlap, (H5,5',18,18')) 3.30 (2H, dd, *J*=6.0, 3.4Hz, (H9,9')) 2.98 (2H, d, *J*=18.4Hz, (H10,10')) 2.69 (2H, dd, *J*=3.4, 2.6Hz, (H14,14')) 2.54 (2H, dd, *J*=12.4, 3.8Hz, (H16,16')) 2.37 (6H, s, (H17,17')) 2.34 (2H, td, *J*=12.4, 3.6Hz, (H16,16')) 2.25 (2H, dd, *J*=18.4, 6.0Hz, (H10,10')) 2.03 (6H, s, (H24,24')) 2.01 (2H, td, *J*=12.4, 5.2Hz, (H15,15')) 1.82 (2H, dd, *J*=12.4, 3.8Hz, (H15,15'))

¹³C NMR (100 MHz, CDCl₃) 169.97 (C23,23'), 146.73 (C3,3'), 140.36 (C4,4'), 137.09 (C19,19'), 130.36 (C12,12'), 128.99 (C8,8'), 127.93 (C21), 127.81 (C7,7'), 127.12 (C11,11'), 126.50 (C20,20'), 126.18 (C22), 118.67 (C1,1'), 116.16 (C2,2'), 87.34 (C5,5'), 71.16 (C18,18'), 67.59 (C6,6'), 58.45 (C9,9'), 46.07 (C16,16'), 42.44 (C17,17'), 41.96 (C13,13'), 40.02 (C14,14'), 34.73 (C15,15'), 20.24 (C24,24'), 19.79 (C10,10').

IR (KBr disc): ν (cm⁻¹) 3391, 2926, 1726, 1501, 1448, 1254, 1121.

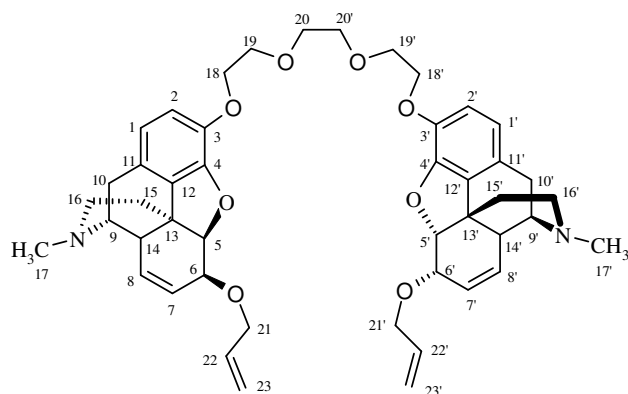
HRMS (EI, 70 eV) Calculated for C₄₆H₄₈N₂O₈H⁺ 757.3483; Found 757.3489;

m.p.= 101-103 °C R_f CH₂Cl₂/MeOH (3:1) =0.41

$[\alpha]_D = -152^\circ c = (0.2, \text{CHCl}_3, 589 \text{ nm}, 20^\circ\text{C})$

222

Dry tetrahydrofuran (10 mL) was cooled to $-20\text{ }^{\circ}\text{C}$ and excess of potassium hydride as a 36% suspension in mineral oil (3.30 g) was added under nitrogen. **194** (0.48 g, 0.70 mmol) was added into the mixture and stirred for 10 min. Allyl bromide (0.247 g, 0.178 mL, 2.1 mmol) was added in one portion and reaction was stirred at $-20\text{ }^{\circ}\text{C}$ for 4 h then overnight at RT. Absolute ethanol (80 mL) was added into the mixture to neutralize the excess of potassium hydride and solvents were removed by rotary evaporation. Distilled water (40 mL) was added to the residue and extracted with dichloromethane (5 x 20 mL) organic layer was dried with sodium sulphate. Product was purified by column chromatography on silica gel with $\text{CH}_2\text{Cl}_2/\text{MeOH}/\text{NH}_4\text{OH}$ (10:1:0.01) as eluent to give a brown oil (0.084 g, 0.11 mmol, 16 % yield)



^1H NMR (400 MHz, CDCl_3) 6.61 (2H, d, $J=8.4\text{Hz}$, (H2,2')) 6.41 (2H, d, $J=8.4\text{Hz}$, (H1,1')) 5.95 (2H, ddt, $J=16.0, 10.8, 5.6\text{Hz}$, (H22,22')) 5.65 (2H, ddd, $J=10.0, 2.8, 1.2\text{Hz}$, (H7,7')) 5.28-5.22 (4H, m, overlap, (H8,8',23,23')) 5.14 (2H, dd, $J=10.0, 1.4\text{Hz}$, (H23,23')) 4.86 (2H, dd, $J=6.4, 1.2\text{Hz}$, (H5,5')) 4.22-4.05 (8H, m, overlap, (H18,18',21,21')) 3.89 (2H, ddd, $J=6.4, 2.8, 2.4\text{Hz}$ (H6,6')) 3.73 (4H, t, $J=5.0\text{Hz}$, (H19,19')) 3.62 (4H, s, (H20,20')) 3.30 (2H, dd, $J=6.2, 3.2\text{Hz}$, (H9,9')) 2.97 (2H, d, $J=18.8\text{Hz}$, (H10,10')) 2.58 (2H, dd, $J=3.2, 2.6\text{Hz}$, (H14,14')) 2.54 (2H, dd, $J=12.2, 4.0\text{Hz}$, (H16,16')) 2.38 (6H, s, (H17,17')) 2.37-2.31 (2H, td, $J=12.2, 3.6\text{Hz}$, (H16,16')) 2.26 (2H, dd, $J=18.8, 6.2\text{Hz}$, (H10,10')) 2.00 (2H, td, $J=12.2, 4.8\text{Hz}$, (H15,15')) 1.83 (2H, dd, $J=12.2, 4.0\text{Hz}$, (H15,15'))

^{13}C NMR (100 MHz, CDCl_3) 146.78 (C3,3'), 139.89 (C4,4'), 133.82 (C12,12'), 130.09 (C7,7'), 129.93 (C11,11'), 127.56 (C8,8'), 126.42 (C22,22'), 117.94 (C1,1'), 116.11 (C2,2'), 115.81 (C23,23'), 88.53 (C5,5'), 72.29 (C6,6'), 69.65 (C20,20'), 68.92 (C21,21'), 68.88 (C19,19'), 68.41 (C18,18'), 57.95 (C9,9'), 45.52 (C16,16'),

42.12 (C17,17'), 42.04 (C13,13'), 39.96 (C14,14'), 34.81 (C15,15'), 19.52 (C10,10').

IR (KBr disc): ν (cm⁻¹) 2928, 2778, 1501, 1450, 1256, 1120.

HRMS (EI, 70 eV) Calculated for C₄₆H₅₆N₂O₈H⁺ 765.4109; Found 765.4092;

m.p.= 43-45 °C

R_f CH₂Cl₂/MeOH/NH₄OH (10:1:0.01)=0.46

[α]_D = -77° c = (0.1, CHCl₃, 589 nm, 20 °C)

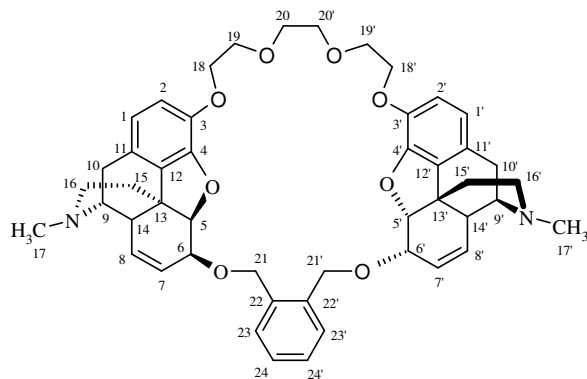
Morphine macrocycles

General procedure

Morphine macrocyclic precursor (1.0 mmol) was dissolved in dry tetrahydrofuran (80 mL) then cesium hydroxide (12.0 mmol) was added in one portion. Mixture was warmed up to 50 °C and stirred for additional 40 min. α,α' -Dichloroethylene (1.0 mmol) and KI (0.2 mmol) were added and mixture was refluxed overnight. Solvent was removed by rotary evaporation and distilled water was added (30 mL) to the crude and solid crashed out. Solid was then filtered by vacuum filtration, dried under high vacuum for 4 h and mixture was separated by column chromatography on silica gel and CH₂Cl₂/MeOH/NH₄OH mixture (10:1:0.01) as a mobile phase.

Morphine macrocycle (217)

The general procedure was used with the starting materials **194** (0.343 g, 0.50 mmol), and α,α' -dichloro-*o*-xylene (0.087 g, 0.50 mmol). Product **217** was isolated by column chromatography as a white solid (0.094 g, 0.13 mmol, 26% yield).



^1H NMR (400 MHz, CDCl_3) 7.43 (2H, dd, $J=5.6, 3.6\text{Hz}$, (H24,24')) 7.24 (2H, dd, $J=5.6, 3.6\text{Hz}$, (H23,23')) 6.58 (2H, d, $J=8.0\text{Hz}$, (H2,2')) 6.41 (2H, d, $J=8.0\text{Hz}$, (H1,1')) 5.73-5.66 (2H, m, (H7,7')) 5.25 (2H, dt, $J=9.8, 2.4\text{Hz}$, (H8,8')) 5.02 (2H, d, $J=12.0\text{Hz}$, (H21,21')) 4.88 (2H, dd, $J=6.0, 1.2\text{Hz}$, (H5,5')) 4.61 (2H, d, $J=12.0\text{Hz}$, (H21,21')) 4.12 (4H, t, $J=5.0\text{Hz}$, (H18,18')) 3.91 (2H, ddd, $J=6.0, 2.8, 2.4\text{Hz}$, (H6,6')) 3.72-3.64 (4H, m, (H19,19')) 3.56 (4H, s, (H20,20')) 3.26 (2H, dd, $J=6.0, 3.2\text{Hz}$, (H9,9')) 2.96 (2H, d, $J=18.8\text{Hz}$, (H10,10')) 2.58 (2H, dd, $J=3.2, 2.4\text{Hz}$, (H14,14')) 2.50 (2H, dd, $J=12.0, 4.0\text{Hz}$, (H16,16')) 2.34 (6H, s, (H17,17')) 2.30 (2H, td, $J=12.2, 3.2\text{Hz}$, (H16,16')) 2.24 (2H, dd, $J=18.8, 6.0\text{Hz}$, (H10,10')) 1.92 (2H, td, $J=12.2, 5.2\text{Hz}$, (H15,15')) 1.83 (2H, dd, $J=12.2, 4.0\text{Hz}$, (H15,15'))

^{13}C NMR (100 MHz, CDCl_3) 147.79 (C3,3'), 141.05 (C4,4'), 136.77 (C22,22'), 131.26 (C7,7'), 131.13 (C12,12'), 129.06 (C11,11'), 128.50 (C24,24'), 127.83 (C8,8'), 127.45 (C23,23'), 118.93 (C1,1'), 116.31 (C2,2'), 89.24 (C5,5'), 73.02 (C6,6'), 70.58 (C20,20'), 69.62 (C18,18') 69.56 (C19,19') 68.29 (C21,21'), 58.98 (C9,9'), 46.57 (C16,16'), 43.05 (C17,17'), 43.01 (C13,13'), 40.86 (C14,14'), 35.72 (C15,15'), 20.48 (C10,10').

IR (KBr disc): ν (cm^{-1}) 2923, 2782, 1509, 1459, 1258, 1127.

HRMS (EI, 70 eV) Calculated for $\text{C}_{48}\text{H}_{54}\text{N}_2\text{O}_8\text{H}^+$ 787.3953; Found 787.3934;

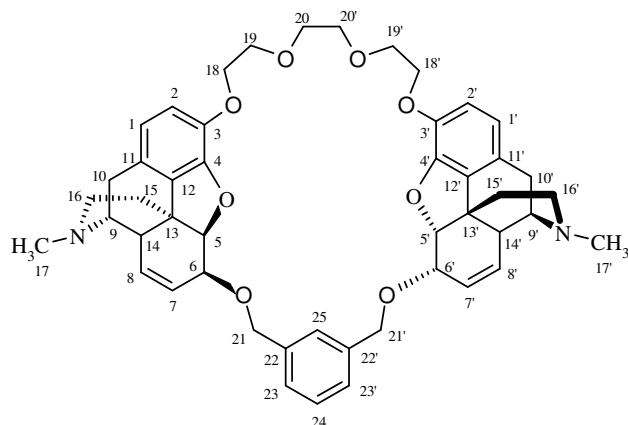
m.p.=127-129°C

R_f $\text{CH}_2\text{Cl}_2/\text{MeOH}/\text{NH}_4\text{OH}$ (10:1:0.01) = 0.29

$[\alpha]_D = -124^\circ$ $c = (0.10, \text{CHCl}_3, 589 \text{ nm}, 20^\circ\text{C})$

Morphine macrocycle (218)

The general procedure was used with the starting materials **194** (0.685 g, 1.00 mmol), and α,α' -dichloro-*m*-xylene (0.175 g, 1.00 mmol). Product **218** was isolated by column chromatography as a white solid (0.141 g, 0.18 mmol, 18 % yield).



^1H NMR (400 MHz, CDCl_3) 7.40 (1H, s, (H25)) 7.30-7.22 (3H, m, (H23,23',24)) 6.61 (2H, d, $J=8.0\text{Hz}$, (H2,2')) 6.43 (2H, d, $J=8.0\text{Hz}$, (H1,1')) 5.74-5.68 (2H, m, (H7,7')) 5.28 (2H, dt, $J=10.0, 2.6\text{Hz}$, (H8,8')) 4.99 (2H, dd, $J=6.2, 0.8\text{Hz}$, (H5,5')) 4.84 (2H, d, $J=11.6\text{Hz}$, (H21,21')) 4.55 (2H, d, $J=11.6\text{Hz}$, (H21,21')) 4.15-4.07 (4H, m, (H18,18')) 4.01 (2H, dd, $J=5.6, 2.8\text{Hz}$, (H6,6')) 3.65-3.55 (4H, m, (H19,19')) 3.42 (4H, s, (H20,20')) 3.35 (2H, dd, $J=5.8, 3.2\text{Hz}$, (H9,9')) 2.98 (2H, d, $J=18.8\text{Hz}$, (H10,10')) 2.72 (2H, dd, $J=3.2, 2.6\text{Hz}$, (H14,14')) 2.60 (2H, dd, $J=12.0, 3.6\text{Hz}$, (H16,16')) 2.41 (6H, s, (H17,17')) 2.38 (2H, td, $J=12.0, 3.6\text{Hz}$, (H16,16')) 2.31 (2H, dd, $J=18.8, 6.0\text{Hz}$, (H10,10')) 2.06 (2H, td, $J=12.4, 5.0\text{Hz}$, (H15,15')) 1.86 (2H, dd, $J=12.4, 3.6\text{Hz}$, (H15,15'))

^{13}C NMR (100 MHz, CDCl_3) 147.86 (C3,3'), 141.16 (C4,4'), 138.67 (C22,22'), 131.33 (C12,12'), 131.15 (C7,7'), 128.30 (C11,11'), 128.08 (C8,8'), 127.31 (C24), 126.50 (C23,23'), 126.24 (C25), 119.17 (C1,1'), 117.57 (C2,2'), 89.02 (C5,5'), 73.41 (C6,6'), 70.50 (C20,20'), 70.44 (C21,21'), 70.19 (C18,18'), 69.82 (C19,19') 59.20 (C9,9'), 46.69 (C16,16'), 42.95 (C17,17'), 42.75 (C13,13'), 40.56 (C14,14'), 35.50 (C15,15'), 20.61 (C10,10').

IR (KBr disc): ν (cm^{-1}) 2927, 2778, 1497, 1445, 1254, 1124.

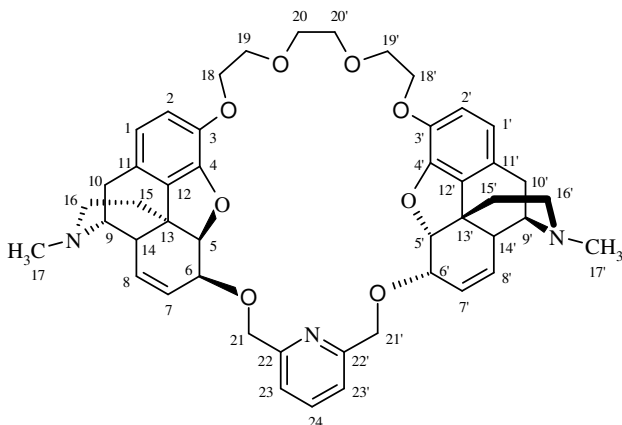
HRMS (EI, 70 eV) Calculated for $\text{C}_{48}\text{H}_{54}\text{N}_2\text{O}_8\text{H}^+$ 787.3953; Found 787.3955;

m.p.=123-125°C R_f $\text{CH}_2\text{Cl}_2/\text{MeOH}/\text{NH}_4\text{OH}$ (10:1:0.01) = 0.23

$[\alpha]_D = -133^\circ$ $c = (0.10, \text{CHCl}_3, 589 \text{ nm}, 20^\circ \text{C})$

Morphine macrocycle **219**

The general procedure was used with the starting materials **194** (0.343 g, 0.50 mmol), and 2,6-bis(chloromethyl)pyridine (0.088 g, 0.50 mmol). Product **219** was isolated by column chromatography as a white solid (0.085 g, 0.11 mmol, 21% yield).



¹H NMR (400 MHz, CDCl₃) 7.78 (1H, t, *J*=7.6Hz, (H24)) 7.56 (2H, d, *J*=7.6Hz, (H23,23')) 6.60 (2H, d, *J*=8.0Hz, (H2,2')) 6.44 (2H, d, *J*=8.0Hz, (H1,1')) 5.79-5.71 (2H, m, (H7,7')) 5.31 (2H, dt, *J*=10.0, 2.6Hz, (H8,8')) 5.02 (2H, dd, *J*=6.4, 1.0Hz, (H5,5')) 4.85 (2H, d, *J*=12.0Hz, (H21,21')) 4.67 (2H, d, *J*=12.0Hz, (H21,21')) 4.12-4.04 (6H, m, overlap (H6,6',18,18')) 3.60-3.56 (4H, m, (H19,19')) 3.38 (4H, s, (H20,20')) 3.35 (2H, dd, *J*=6.0, 3.2Hz, (H9,9')) 2.99 (2H, d, *J*=18.4Hz, (H10,10')) 2.73 (2H, dd, *J*=3.2, 2.6Hz, (H14,14')) 2.60 (2H, dd, *J*=12.0, 4.0Hz, (H16,16')) 2.41 (6H, s, (H17,17')) 2.39 (2H, td, *J*=12.0, 3.6Hz (H16,16')) 2.31 (2H, dd, *J*=18.6, 6.0Hz, (H10,10')) 2.07 (2H, td, *J*=12.0, 5.0Hz, (H15,15')) 1.83 (2H, dd, *J*=12.0, 4.0Hz, (H15,15'))

¹³C NMR (100 MHz, CDCl₃) 157.52 (C22,22'), 147.67 (C3,3'), 141.23 (C4,4'), 137.51 (C24), 131.18 (C12,12'), 130.87 (C7,7'), 128.30 (C8,8'), 127.36 (C11,11'), 120.69 (C23,23'), 119.18 (C1,1'), 117.07 (C2,2'), 89.14 (C5,5'), 73.89 (C6,6'), 71.63 (C21,21'), 70.50 (C20,20'), 70.03 (C19,19'), 69.84 (C18,18'), 59.20 (C9,9'), 46.70 (C16,16'), 43.00 (C17,17'), 42.73 (C13,13'), 40.56 (C14,14'), 35.51 (C15,15'), 20.58 (C10,10').

IR (KBr disc): ν (cm⁻¹) 2926, 2778, 1497, 1447, 1255, 1124.

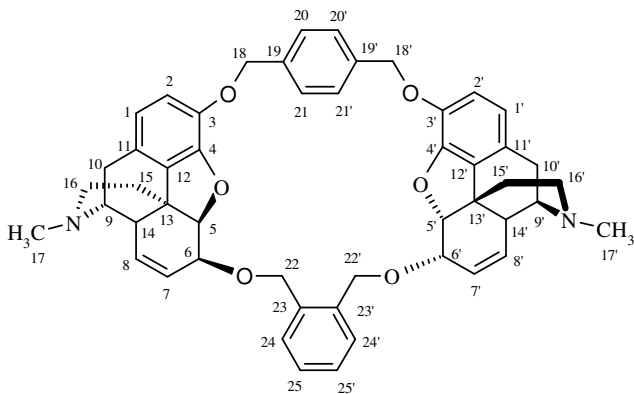
HRMS (EI, 70 eV) Calculated for C₄₇H₅₃N₃O₈H⁺ 775.3747; Found 775.3724;

m.p.=138-140 °C R_f CH₂Cl₂/MeOH/NH₄OH (10:1:0.01) = 0.18

$[\alpha]_D = -138^\circ$ $c = (0.10, \text{CHCl}_3, 589\text{nm}, 20^\circ\text{C})$

Morphine macrocycle **220**

The general procedure was used with the starting materials **198** (0.673 g, 1.00 mmol), and α,α' -dichloro-*m*-xylene (0.175 g, 1.00 mmol). Product **220** was isolated by column chromatography as a white solid (0.133 g, 0.17 mmol, 17% yield).



^1H NMR (400 MHz, CDCl_3) 7.51 (2H, dd, $J=5.6, 3.6\text{Hz}$, (H25, 25')) 7.29 (2H, dd, $J=5.6, 3.6\text{Hz}$, (H24,24')) 7.27 (4H, s, (H20,20',21,21')) 6.68 (2H, d, $J=8.0\text{Hz}$, (H2,2')) 6.39 (2H, d, $J=8.0\text{Hz}$, (H1,1')) 5.71-5.65 (2H, m, 1.0Hz , (H7,7')) 5.15 (2H, dt, $J=10.0, 2.6\text{Hz}$, (H8,8')) 5.07-4.98 (6H, m, overlap, (H18,18',22,22')) 4.91 (2H, dd, $J=6.4, 1.0\text{Hz}$, (H5,5')) 4.65 (2H, d, $J=12.0\text{Hz}$, (H22,22')) 3.85 (2H, dd, $J=6.4, 2.6\text{Hz}$, (H6,6')) 3.27 (2H, dd, $J=6.0, 3.2\text{Hz}$, (H9,9')) 2.94 (2H, d, $J=18.8\text{Hz}$, (H10,10')) 2.58-2.52 (2H, m, (H14,14')) 2.54 (2H, dd, $J=12.2, 3.6\text{Hz}$, (H16,16')) 2.36 (6H, s, (H17,17')) 2.32 (2H, td, $J=12.2, 3.8\text{Hz}$, (H16,16')) 2.24 (2H, dd, $J=18.8, 6.0\text{Hz}$, (H10,10')) 1.99 (2H, td, $J=12.2, 4.8\text{Hz}$, (H15,15')) 1.84 (2H, dd, $J=12.2, 3.8\text{Hz}$, (H15,15'))

^{13}C NMR (100 MHz, CDCl_3) 149.20 (C3,3'), 140.62 (C4,4'), 136.79 (C19,19'), 136.47 (C23,23'), 131.12 (C7,7'), 130.98 (C12,12'), 129.00 (C25,25'), 128.23 (C8,8'), 127.95 (C24,24'), 127.63 (C11,11'), 127.45 (C20,20',21,21'), 118.85 (C1,1'), 116.56 (C2,2'), 90.08 (C5,5'), 73.89 (C6,6'), 71.77 (C18,18'), 68.45 (C22,22'), 59.03 (C9,9'), 46.52 (C16,16'), 43.36 (C17,17'), 42.97 (C13,13'), 40.80 (C14,14'), 35.54 (C15,15'), 20.68 (C10,10').

IR (KBr disc): ν (cm^{-1}) 2931, 2782, 1501, 1448, 1254, 1126.

HRMS (EI, 70 eV) Calculated for $\text{C}_{50}\text{H}_{50}\text{N}_2\text{O}_6\text{H}^+$ 787.3958; Found 787.3934;

m.p.= 218-220 °C

R_f $\text{CH}_2\text{Cl}_2/\text{MeOH}/\text{NH}_4\text{OH}$ (10:1:0.01) =0.36

$[\alpha]_D = -147^\circ$ $c = (0.10, \text{CHCl}_3, 589 \text{ nm}, 20^\circ \text{C})$

Bibliography

1. Pedersen, C. J. *J. Am. Chem. Soc.*, **1967**, *89*:26, 7017.
2. Satoshi Omura, *Macrolide Antibiotics: Chemistry, Biology, and Practice*: Academic Press; **2002**: Second Ed.
3. Inai, Y.; Yabuki, M.; Kanno, T.; Akiyama, J.; Yasuda, T.; Utsumi, K. *Cell Struct. Funct.*, **1997**, *22*, 555.
4. Gisin, B. F.; Merrifield, R. B.; Tosteson, *J. Am. Chem. Soc.* **1969**, *91*, 2691.
5. Dobler, M.; Dunitz, J. D.; Kilbourn, B. T. *Helv. Chim. Acta*, **1969**, *52*, 2573.
6. Corbaz, R.; Ettliger, L.; Gaumann, E.; Keller-Schielein, W.; Kradolfer, F.; Neipp, L.; Prelog, V.; Zahner, H. *Helv. Chim. Acta*, **1955**, *38*, 1445.
7. Prestegard, J. H.; Chan, S. I. *J. Am. Chem. Soc.*, **1970**, *92*, 4440.
8. Gerlach, H.; Oertle, K.; Thalmann, A.; Servi, S. *Helv. Chim. Acta*, **1975**, *58*, 2036.
9. Schmidt, U.; Gombos, J.; Haslinger, E.; Zak, H. *Chem. Ber.*, **1976**, *109*, 2628.
10. Bartlett, P. A.; Meadows, J. D.; Ottow, E. *J. Am. Chem. Soc.*, **1984**, *106*, 5304.
11. Fleming, I.; Ghosh, S. K. *J. Chem. Soc., Perkin Trans 1*, **1998**, *17*, 2733.
12. Lee, J. Y.; Kim, B. H. *Tetrahedron*, **1996**, *52*, 571.
13. Prosser, B. L. T.; Palleroni, N. J. *Polyether Antibiotics: Naturally Occurring Acid Ionophores*, **1982**, Marcel Dekker, New York
14. Hamidinia, S. A.; Shimelis, O. I.; Tan, B., Erdahl, W. L.; Chapman, C. J.; Renkes, G. D.; Taylor, R. W.; Pfeiffer, D. R. *J. Biol. Chem.*, **2002**, *41*, 38111.
15. Pearson, R. G. *J. Am. Chem. Soc.*, **1963**, *85*, 3533.
16. Ercolani, G.; Mandolini, L.; Masci, B. *J. Am. Chem. Soc.*, **1981**, *103*, 7484.
17. Karbach, S.; Löhr, W.; Vögtle, F. *J. Chem. Res. (S)*, **1981**, 314.
18. Thompson, M. C.; Busch, D. H. *J. Am. Chem. Soc.*, **1964**, *84*, 4834.
19. Greene, R. N. *Tetrahedron Lett.*, **1972**, *18*, 1793.
20. Ercolani, G.; Mandolini, L.; Masci, B. *J. Am. Chem. Soc.*, **1983**, *105*, 6146.
21. Iluminati, G.; Mandolini, L.; Masci, B. *J. Am. Chem. Soc.*, **1983**, *105*, 555.

22. Mandolini, L.; Masci, B. *J. Am. Chem. Soc.*, **1984**, *106*, 168.
23. Helgeson, R. C.; Timko, J. M.; Moreau, P.; Peacock, S. C.; Mayer, J. M.; Cram, D. J. *J. Am. Chem. Soc.*, **1974**, *96*, 6762.
24. Cram, D. J.; Helgeson, R. C.; Koga, K.; Kyba, E. P.; Madan, K.; Sousa, L. R.; Siegel, M. G.; Moreau, P.; Gokel, G. W.; Timko, J. M.; Sogah, G. D. Y. *J. Org. Chem.*, **1978**, *43*, 2758.
25. Chao, Y.; Weisman, G. R.; Sogah, G. D. Y.; Cram, D. J. *J. Am. Chem. Soc.*, **1979**, *101*, 4948.
26. Peacock, S. C.; Cram, D. J. *J. Chem. Soc. Chem. Commun.*, **1976**, 282.
27. Lingenfelter, D. S.; Helgeson, R. C.; Cram, D. J. *J. Org. Chem.*, **1981**, *46*, 393.
28. Kakuchi, T.; Sasaki, H.; Yokota, K. *Macromol. Chem.*, **1988**, *189*, 1279.
29. Yamamoto, K.; Fukushima, H.; Okamoto, Y.; Hatada, K.; Nakazaki, M. *J. Chem. Soc. Chem. Commun.*, **1984**, 1111.
30. Stoddart, J. F. *Chem. Soc. Rev.*, **1979**, *8*, 85.
31. Girodeau, J. M.; Lehn, J. M.; Sauvage, J. P. *Angew. Chem., International Edition in English*, **1975**, *14*, 654.
32. Luk'yanenko, N. G.; Lobach, A. V.; Leus, O. N.; Titova, N. Y. *Russ. J. Org. Chem.*, **2002**, *38*, 895.
33. Hirose, K.; Fujiwara, A.; Matsunaga, K.; Aoki, N.; Tobe, Y. *Tetrahedron: Asym.*, **2003**, *14*, 555.
34. Stoddart, J. F.; Wheatley, C. M. *J. Chem. Soc. Chem. Commun.*, **1974**, 879.
35. Dale, J.; Kristiansen, P. O. *Acta. Chem. Scand.*, **1972**, *26*, 1471.
36. Hayward, R. C.; Overton, C. H.; Whitham, G. H. *J. Chem. Soc.*, **76**, *22*, 2413.
37. Yamato, K.; Bartsch, R. A.; Broker, G. A.; Rogers, R. D.; Dietz, M. L. *Tetrahedron Lett.*, **2002**, *43*, 5805.
38. Naemura, K.; Miyabe, H.; Shingai, Y. *J. Chem. Soc. Perkin Trans.*, **1991**, *1*, 957.
39. Naemura, K.; Miyabe, H.; Shingai, Y.; Tobe, Y. *J. Chem. Soc., Perkin Trans.*, **1993**, *1*, 1073.
40. Katakya, R.; Nicholson, P. E.; Parker, D. *Tetrahedron Lett.*, **1989**, *30*, 4559.
41. Kimura, K.; Kitazawa, S.; Shono, T. *Chem. Lett.*, **1984**, 639.

42. Kimura, K.; Yano, H.; Kitazawa, S.; Shono, T. *J. Chem. Perkin Trans. II*, **1986**, 1945.
43. Pfeiffer, G.; Marchi, Ch. Siv, C.; Bendayan, A.; Malouli Bibout, M. El. *Heterocyclic Commun.*, **1995**, *1*, 245.
44. Focella, A.; Bizzarro, F.; Exon, C. *Synth. Commun.*, **1991**, *21*, 2165.
45. Seibel, J.; Moraru, R.; Götze, S. *Tetrahedron*, **2005**, *61*, 7081.
46. Mach, M.; Jarosz, S.; Listkowski, A. *Carbohydr. Chem.*, **2001**, *20*, 485.
47. Jarosz, S.; Listkowski, A. *J. Carbohydr. Chem.*, **2003**, *22*, 753.
48. Jarosz, S.; Listkowski, A.; Lewandowski, B.; Ciunik, Z.; Brzuszkiewicz, A. *Tetrahedron*, **2005**, *61*, 8485.
49. Kanakamma, P. P.; Mani, N. S.; Maitra, U.; Nair, V. *J. Chem. Soc. Perkin Trans.*, **1995**, *1*, 2339.
50. Faltin, F.; Fehring, V.; Miethchen, R. *Synthesis*, **2002**, *13*, 1851.
51. Faltin, F.; Fehring, V.; Kadyrov, R.; Arrieta, A.; Schareina, T.; Selke, R.; Miethchen, R. *Synthesis*, **2001**, *4*, 638.
52. Veeneman, G. H.; van Leeuwen, S. H.; van Boom, J. H. *Tetrahedron Lett.*, **1990**, *31*, 1331.
53. Vocke, W.; Hänel, R.; Flöther, F.-U. *Chem. Tech. (Leipzig)*, **1987**, *39*, 123.
54. Turgut, Y.; Hosgören, H. *Tetrahedron: Asym.*, **2003**, *14*, 3815.
55. Togrul, M.; Demirel, N.; Kaynak, F. B.; Özbey, S.; Hosgören, H. *J. Inclusion Phenom. Macroc. Chem.*, **2004**, *50*, 165.
56. Joly, J. P.; Schröder, G. *Tetrahedron Lett.*, **1997**, *38*, 8197.
57. Zhao, H.; Hua, W. *J. Org. Chem.*, **2000**, *65*, 2933.
58. Demirel, N.; Bulut, Y. *Tetrahedron: Asymm.*, **2003**, *14*, 2633.
59. Blasius, E.; Janzen, K.-P. *Pure Appl. Chem.*, **1982**, *54*, 2115.
60. Blasius, E.; Janzen, K.-P. Klein, W.; Klotz, H.; Nguyen, V. B.; Nguyen-Tien, T.; Pfeiffer, R.; Scholten, G.; Simon, H.; Stockemer, H.; Toussaint, A. *J. Chromatogr.*, **1980**, *201*, 147.
61. Crossley, R. in *Chirality and the Biological Activity of drugs*; CRC Press: Boca Raton, **1995**.
62. Aboul-Enein, H. Y.; Seringnese, V. *Biomed. Chromatogr.*, **1997**, *757*, 225.
63. Walbroehl, Y.; Wagner, J. *J. Chromatogr.*, **1994**, *680*, 253.
64. Nishi, H.; Nakamura, K.; Nakai, H.; Sato, T. *J. Chromatogr. A*, **1997**, *757*, 225.

65. Shinbo, T.; Yamaguchi, T.; Nishimura, K.; Sugiura, M. *J. Chromatogr.*, **1987**, *405*, 145.
66. Peter, A.; Lazar, L.; Fulop, F.; Armstrong, D. W. *J. Chromatogr. A*, **2001**, *926*, 229.
67. Lee, W.; Hong, C. Y. *J. Chromatogr. A*, **2000**, *879*, 113.
68. Hyun, M. H.; Jin, J. S.; Lee, W. *J. Chromatogr. A*, **1998**, *822*, 155.
69. Machida, Y.; Nishi, H.; Nakamura, K.; Nakai, H.; Sato, T. *J. Chromatogr. A*, **1998**, *805*, 82.
70. Hyun, M. H. *J. Sep. Sci.*, **2003**, *26*, 242.
71. Liotta, C. L.; Harris, H. P. *J. Am. Chem. Soc.*, **1974**, *96*, 2250.
72. Cook, F. L.; Bowers, C. W.; Liotta, C. L. *J. Org. Chem.*, **1974**, *39*, 3416.
73. Zubrick, J. W.; Dunbar, B. I.; Durst, H. D. *Tetrahedron Lett.*, **1975**, 71.
74. Landini, D.; Maia, A. M.; Montanari, F.; Pinsi, F. M. *Gazz Chim Ital.*, **1975**, *105*, 863.
75. Landini, D.; Montanari, F. *Chem. Commun.*, **1974**, 879.
76. Herriott, A. W.; Picker, D. *J. Am. Chem. Soc.*, **1975**, *97*, 2345.
77. Sam D.J.; Simmons, H. F. *J. Am. Chem. Soc.*, **1974**, *96*, 2252.
78. Matsuda, T.; Koida, K. *Bull. Chem. Soc. Jpn.*, **1973**, *46*, 2259
79. Bartsch, R. A.; Wieggers, K. E. *Tetrahedron Lett.*, **1972**, 3819.
80. Hiraoka, M. in *Crown compounds: their characteristics and Applications*. Elsevier, Amsterdam, **1982**.
81. Sam D. J.; Simmons, H. F. *J. Am. Chem. Soc.*, **1972**, *94*, 4024.
82. Gao, J.; Martell, A. E. *Org. Biomol. Chem.*, **2003**, *1*, 2795.
83. Li, Z.-B.; Liu, T.-D.; Pu, L. *J. Org. Chem.*, **2007**, *72*, 4340.
84. Zhang, W.; Loebach, J. L.; Wilson, S. R.; Jacobsen, E. N. *J. Am. Chem. Soc.*, **1990**, *112*, 2801.
85. Irie, R.; Noda, K.; Yto, Y.; Matsumoto, N.; Katsuki, T. *Tetrahedron Lett.*, **1990**, *31*, 7345.
86. Martinez, A.; Hemmert, C.; Loup, C.; Barre, G.; Meunier, B. *J. Org. Chem.*, **2006**, *71*, 1449.
87. Cram, D. J.; Sogah, G. D. Y. *J. Chem. Soc., Chem. Commun.*, **1981**, *13*, 625.
88. Boyle, G. A.; Govender, T.; Kruger, H. G.; Maguire, G. E. M. *Tetrahedron Asym.*, **2004**, *15*, 3775.

89. Zhu, C.; Yuan, C.; Lv, Y. *Synlett*, **2006**, 8, 1221.
90. Roberts, R. M.; Khalaf A. A. *Friedel-Crafts Alkylation Chemistry. A Century of Discovery*, Marcel Dekker: New York, **1984**.
91. Olah, G.A. *Friedel-Crafts Chemistry*; Wiley-Interscience: New York, **1973**.
92. Trost, B. M.; Fleming, I. (Eds.), Pergamon: New York, **1991**; Vol.3, p 293-339.
93. Gathergood, N.; Zhuang, W.; Jørgensen, K. A. *J. Am. Chem. Soc.*, **2000**, 122, 12517.
94. Zhuang, W.; Gathergood, N.; Hazell, R. G.; Jørgensen, K. A. *J. Org. Chem. Soc.*, **2001**, 66, 1009.
95. Nakamura, K.; Tsuji, K.; Kiyoshi, K.; Nobukiyo, M.; Matsuo, M. *Chem. Pharm. Bull.*, **1993**, 41, 2050.
96. Khalaj, A.; Shadnia, H.; Sharifzadeh, M. *Pharm. Pharmacol. Commun.*, **1998**, 4, 373.
97. Aronson, J. K. *British Medical Journal*, **2000**, 320, 506.
98. Shukla, P. K.; Mishra, P. C.; Suhai, S. *Chemical Physics Letters*, **2007**, 449, 323.
99. Desaphy J. F., Pierno, S.; De Luca, A.; Didonna, P.; Camerino, D.C. *Mol. Pharmacol.*, **2003**, 63, 659.
100. Gottesman, M. M.; Fojo, T.; Bates, S. E. *Nat. Rev. Cancer.*, **2002**, 2, 48.
101. Avendaño, C.; Menéndez, J. C. *Curr. Med. Chem.*, **2002**, 9, 159.
102. Avendaño, C.; Menéndez, J. C. *Med. Res. Rev.*, **2004**, 1, 419.
103. Wang, R. B.; Kuo, C. L.; Lien, L. L.; Lien, E. J. *J. Clin. Pharm. Ther.*, **2003**, 28, 203.
104. Baer, M. R.; George, S. L.; Dodge, R. K.; O'Loughlin, K. L.; Minderman, H.; Caligiuri, M. A.; Anastasi, J.; Powell, B. L.; Kolitz, J. E.; Schiffer, C. A.; Bloomfield, C. D.; Larson, R. A. *Blood*, **2002**, 100, 1224.
105. Tsuruo, T.; Iida, H.; Tsukagoshi, S.; Sakurai, Y. *Cancer Res.*, **1981**, 41, 1967.
106. Lo, A.; Burckart, G. J. *J. Clin. Pharmacol.*, **1999**, 39, 995.
107. Friedenber, W. R.; Rue, M.; Blood, E. A.; Dalton, W. S.; Shustik, C.; Larson, R. A.; Sonneveld, P.; Greipp, P. R. *Cancer*, **2006**, 106, 830.
108. Yanagisawa, T.; Newman, A.; Coley, H.; Renshaw, J.; Pinkerton, C. R.; Pritchard Jones, K. *Br. J. Cancer*, **1999**, 80, 1190.

109. Nokihara, H.; Yano, S.; Nishioka, Y.; Hanibuchi, M.; Higasida, T.; Tsuruo, T.; Sone, S. *Jpn. J. Cancer Res.*, **2001**, *92*, 785.
110. Sorbera, L. A.; Castaner, J.; Silvestre, J. S.; Bayes, M. *Drugs Future*, **2003**, *28*, 125.
111. Friedenber, W. R.; Rue, M.; Blood, E. A.; Dalton, W. S.; Shustik, C.; Larson, R. A.; Sonneveld, P.; Greipp, P. R. *Cancer*, **2006**, *106*, 830.
112. Ueda, K.; Kamuraj, N.; Hiraij, M.; Tanigawaraj, Y.; Saeki, T.; Kioka, N.; Komano, T.; Horij, R. *J. Biol. Chem.*, **1992**, *267*, 24248.
113. Pleban, K.; Ecker, G. F. *Mini-Rev. Med. Chem.*, **2005**, *5*, 153.
114. a) Juliano, R.L.; Ling, V. *Biochim. Biophys. Acta*, **1976**, *455*, 152. b) Doyle, L. A.; Yang, W.; Abruzzo, L.V.; Krogmann, T.; Gao, Y.; Rishi, A. K.; Ross, D. D. *Proc. Natl. Acad. Sci. USA* **1998**, *95*, 15665.
115. Hyafil, F.; Vergely, C.; Du Vignaud, P.; Grand-Perret T. *Cancer Res.*, **1993**, *53*, 4595.
116. Kruijtzter, C. M. F.; Beijnen, J. H.; Rosing, H.; Schot, M.; Jewell, R. C.; Paul, E. M.; Schellens, J. H. M. *J. Clin. Oncol.*, **2002**, *20*, 2943.
117. Wang, R. B.; Kuo, C. L.; Lien, L. L.; Lien, E. J. *J. Clin. Pharm. Ther.*, **2003**, *28*, 203.
118. Klopman, G.; Shi, L. M.; Ramu, A. *Mol. Pharmacol.*, **1997**, *52*, 323.
119. Lo, A.; Burckart, G. J. *J. Clin. Pharmacol.*, **1999**, *39*, 995.
120. Driggers, E. M.; Hale, S. P.; Lee, J. Terrett, N. K. *Nature Reviews*, **2008**, *7*, 609.
121. Xu, P.; Lin, W.; Zou, X. *Synthesis*, **2002**, *8*, 1017.
122. Seebach, D.; Kalinowski, H. O.; Bastani, B.; Crass, G.; Daum, H.; Doerr, H.; Du Preez, N. P.; Ehrig, V.; Langer, W. *Helv. Chim. Acta*, **1977**, *60*, 301.
123. Modin, S. A.; Andersson, P. G. *J. Org. Chem.*, **2000**, *65*, 6736.
124. Zhuang, W.; Jørgensen, K. A. *Chem. Commun.*, **2002**, 1336.
125. Ross, J.; Xiao, J. L. *Green Chem.*, **2002**, *4*, 129.
126. Ziegler, K. Über ringschluss-reaktionen. *Ber. Dtsch. Chem. Ges.*, **1934**, *67A*, 139.
127. Sendhoff, N.; Mekelburger, H-B.; Vögtle, F. *Top. Curr. Chem.*, **1992**, *161*, 1.
128. Richardson, T. I.; Rychnovsky, S. D. *J. Am. Chem. Soc.*, **1997**, *119*, 12360.
129. Maloney, D. J.; Hecht, S. M. *Org. Lett.*, **2005**, *7*, 4297.

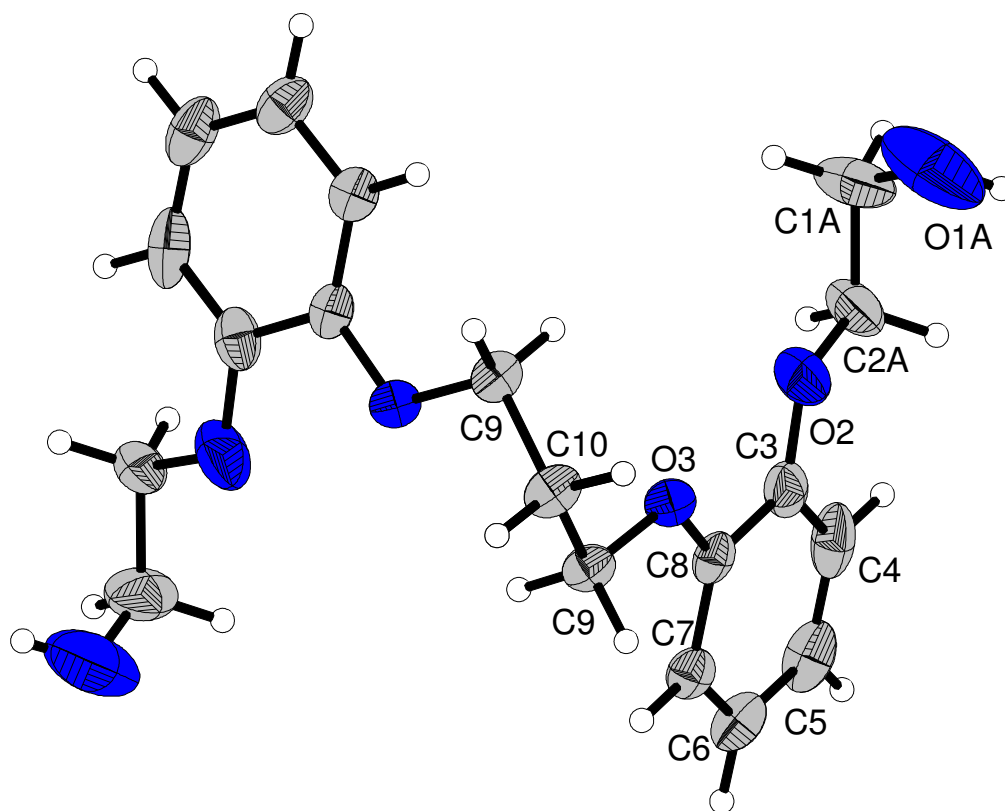
130. Morrison, R. T.; Boyd, R. T. *Organic Chemistry, Sixth Edition*, **1992**.
131. Blakemore, P. R.; White, J. D. *Chem. Commun.*, **2002**, 1159.
132. a) Sertürner, F. W. A. *Trommsdorff's J. Pharm.*, **1805**, 13, 234; b) Setürner, F. W. A. *Trommsdorff's J. Pharm.*, **1806**, 14, 47.
133. Pasternak, G. W. in *The Opiate Receptors*, ed. Humana Press, Clifton, New Jersey, **1988**.
134. MacDougall, J. M.; Zhang, X.-D.; Polgar, W. E.; Khroyan, T. V.; Toll, L.; Cashman, J. R. *Bioorg. Med. Chem.*, **2004**, 12, 5983.
135. Pasternak, G. W. *Neuropharmacology*, **2004**, 24, 312.
136. Schmidhammer, H.; Daurer, D.; Wieser, M.; Monory, K.; Borsodi, A.; Elliot, J.; Traynor, J. R. *Bioorg. Med. Chem. Lett.*, **1997**, 7, 151.
137. Surratt, C. K.; Johnson, P. S.; Moriwaki, A.; Seidleck, B. K.; Blaschak, C. J.; Wang, J. B.; Uhl, G. R. *J. Biol. Chem.*, **1994**, 269, 20539.
138. Gu, X. P.; Nishida, N.; Ikeda, I.; Okahara, M. *J. Org. Chem.* **1987**, 52, 3192.
139. a) Kosterlitz, H. W. *Nature*, **1985**, 317, 671 b) Kosterlitz, H. W. *Nature*, **1987**, 330, 606.
140. Lenz, R.; Zenk, M. H.; *Eur. J. Biochem.*, **1995**, 233, 132.
141. Taber, D. F.; Neubert, T. D.; Rheingold, A. L. *J. Am. Chem. Soc.*, **2002**, 124, 12416.
142. Bertha, C.M.; Ellis, M.; Flippen-Anderson, J. L.; Porreca, F.; Rothman, R. B.; Davis, P.; Xu, H.; Becketts, K.; Rice, K. C. *J. Med. Chem.*, **1996**, 39, 2081.
143. Frensch, K.; Vögtle, F. *Liebigs Ann. Chem.*, **1979**, 2118.
144. Lindner, W.; Raab, M.; Schaupp, K. *Arch. Pharm. (Weinheim)*, **1981**, 314, 328.
145. Hosztafi, S.; Köhegyi, I.; Simon, C.; Fürst, Z. *Arzneim.-Forsch./Drug. Res.*, **1993**, 43, 1200.
146. Kotha, S.; Lahiri, K. *Synlett*, **2007**, 18, 2767.
147. Grubbs, R. H.; Miller, S. J.; Fu, G. C. *Acc. Chem. Res.*, **1995**, 28, 446.
148. Nicolaou, K. C.; Xu, H. *Chem. Commun.*, **2006**, 600.
149. Scholl, M.; Trnka, T. M.; Morgan, J. P.; Grubbs, R. H. *Tetrahedron Lett.*, **1999**, 40, 2247.
150. Neville, G. A.; Ekiel, I.; Smith, I. C. P. *Magn. Reson. Chem.*, **1986**, 25, 31.

151. Schmidtchen, F. P.; Berger, M. *Chem. Rev.*, **1997**, *97*, 1609.
152. Marsden, B. D.; Sundstrom, M.; Knapp, S. *Expert Opinion on Drug Discovery*, **2006**, *1*, 123.
153. Alves, J. A. C.; Barkley, J. V.; Brigas, A. F.; Johnstone, R. A. W. *J. Chem. Soc., Perkin Trans.*, **1997**, *2*, 669.
154. Pauling, L. in *The Nature of the Chemical Bond*, Cornell University Press, Ithaca, **1960**, pp. 239, 255.
155. Gilli, P.; Bertolasi, V.; Ferretti, V.; Gilli, G. *J. Am. Chem. Soc.* **1994**, *116*, 909.
156. Allen, F. H.; Kennard, O.; Watson, D. G.; Brammer, L.; Orpen, A. G. *J. Chem. Soc. Perkin Trans. II*, **1987**, 1.
157. Pedersen, C. J. *Fed. Proc. Fed. Am. Soc. Expl. Biol.*, **1968**, *27*, 1305.
158. Pedersen, C. J. *Science*, **1988**, 536.
159. Nakagawa, K.; Okada, S.; Inoue, Y.; Tai, A.; Hakushi, T. *Anal. Chem.*, **1988**, *60*, 2527.
160. Kumar, S.; Bhalla, V.; Singh, H. *Bioorg. Med. Chem. Lett.*, **1995**, *5*, 1917.
161. Aguilar, J.-C.; Bernes, S.; Gomez-Tagle, P.; Bartach, R. A.; Gyves, J. J. *Chem. Cryst.*, **2006**, *36*, 473.
162. Pedersen, C. J. Frensdorff, H. K. *Angew. Chem., Int. Ed. Engl.*, **1972**, *11*, 16.
163. Zhu, C.; Yuan, C.; Lv, Y. *Synlett*, **2006**, *8*, 1221.
164. Thomas, H.; Coley, H. M.; *Cancer Control*, **2003**, *10*, 159.
165. Ferry, D. R.; Traunecker, H.; Kerr, D. J. *Eur. J. Cancer.*, **1996**, *6*, 1070.
166. Armarego, W. L. F.; Perrin, D. D. *Purification of Laboratory Chemicals*, 4th; Butterworth-Heinemann: Oxford, **2002**.

9 Appendix

9.1 Appendix A

1,3-Bis[2-(2-hydroxyethoxy)phenoxy]propane (160)

Fig. A 1 X-ray crystal structure of 1,3-Bis[2-(2-hydroxyethoxy)phenoxy]propane **160**Table A 1 Crystal data and structure refinement for **160**

Identification code	gat11	
Empirical formula	C ₁₉ H _{24.50} O _{6.25}	
Molecular formula	C ₁₉ H ₂₄ O ₆ x 0.25 (H ₂ O) ^{a)}	
Formula weight	352.89	
Temperature	100(2) K	
Wavelength	0.71073 Å	
Crystal system	Monoclinic	
Space group	C2 (#5)	
Unit cell dimensions	a = 22.897(3) Å	α = 90°.
	b = 4.9486(6) Å	β = 116.539(2)°.

	$c = 17.2590(19) \text{ \AA}$ $\gamma = 90^\circ$.
Volume	1749.5(3) \AA^3
Z	4
Density (calculated)	1.340 Mg/m ³
Absorption coefficient	0.100 mm ⁻¹
F(000)	754
Crystal size	0.80 x 0.10 x 0.10 mm ³
Theta range for data collection	1.83 to 25.99°.
Index ranges	-28<=h<=28, -6<=k<=6, -21<=l<=21
Reflections collected	7435
Independent reflections	1923 [R(int) = 0.0221]
Completeness to theta = 25.99°	99.7 %
Absorption correction	Semi-empirical from equivalents
Max. and min. transmission	0.9901 and 0.8489
Refinement method	Full-matrix least-squares on F ²
Data / restraints / parameters	1923 / 76 / 292 ^{b)}
Goodness-of-fit on F ²	1.059
Final R indices [I>2sigma(I)]	R1 = 0.0644, wR2 = 0.1637
R indices (all data)	R1 = 0.0683, wR2 = 0.1676
Largest diff. peak and hole	0.476 and -0.251 e. \AA^{-3}

^{a)} The hydrogen atoms of the water molecule could not be detected.

^{b)} DELU restraints were applied to all thermal displacement parameters. Equivalent distances in the disorder parts were restrained to be similar using SADI.

Table A 2 Bond lengths [\AA] and angles [$^\circ$] for **160**

O(1A)–C(1A)	1.466(15)	C(2B)–O(2)	1.417(10)
O(1A)–H(1A)	0.8400	C(2B)–H(2B1)	0.9900
C(1A)–C(2A)	1.485(10)	C(2B)–H(2B2)	0.9900
C(1A)–H(1A1)	0.9900	O(2)–C(3)	1.359(5)
C(1A)–H(1A2)	0.9900	C(3)–C(4)	1.393(6)
C(2A)–O(2)	1.513(9)	C(3)–C(8)	1.407(5)
C(2A)–H(2A1)	0.9900	C(4)–C(5)	1.383(6)
C(2A)–H(2A2)	0.9900	C(4)–H(4)	0.9500
O(1B)–C(1B)	1.369(15)	C(5)–C(6)	1.365(6)
O(1B)–H(1B)	0.8400	C(5)–H(5)	0.9500
C(1B)–C(2B)	1.565(15)	C(6)–C(7)	1.391(5)
C(1B)–H(1B1)	0.9900	C(6)–H(6)	0.9500
C(1B)–H(1B2)	0.9900	C(7)–C(8)	1.382(5)

Appendix

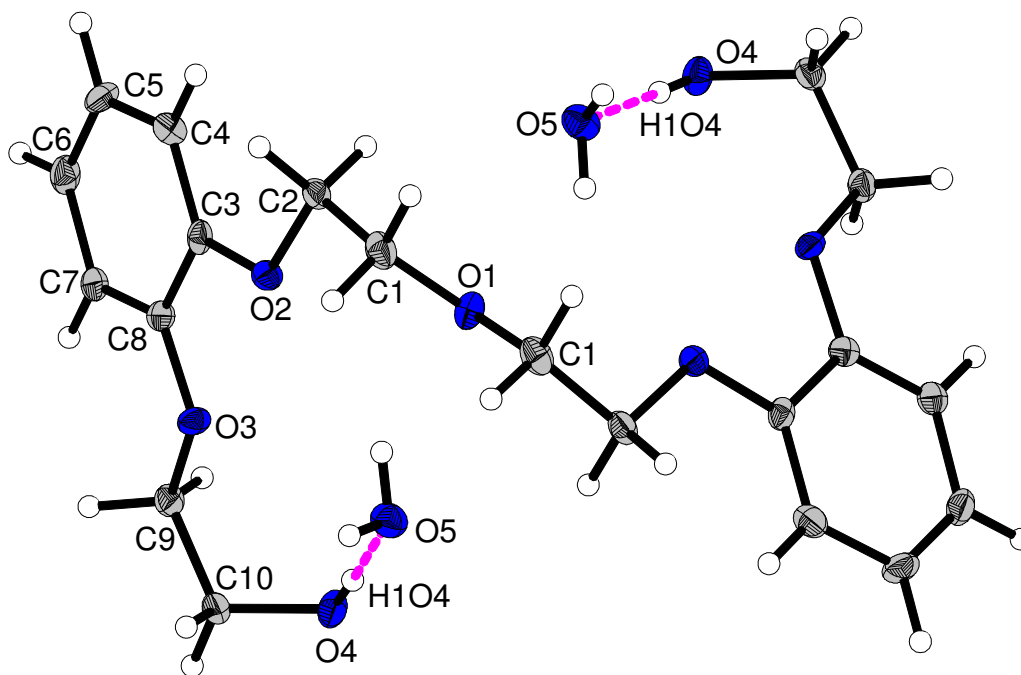
C(7)–H(7)	0.9500	C(19)–C(20)	1.513(6)
C(8)–O(3)	1.364(4)	C(19)–H(19A)	0.9900
O(3)–C(9)	1.430(4)	C(19)–H(19B)	0.9900
C(9)–C(10)	1.514(5)	C(20)–C(19)#2	1.513(6)
C(9)–H(9A)	0.9900	C(20)–H(20)	0.9900
C(9)–H(9B)	0.9900	C(20)–H(20)#2	0.9900
C(10)–C(9)#1	1.514(5)		
C(10)–H(10)	0.9900	C(1A)–O(1A)–H(1A)	109.5
C(10)–H(10)#1	0.9900	O(1A)–C(1A)–C(2A)	109.0(9)
O(4A)–C(11A)	1.362(18)	O(1A)–C(1A)–H(1A1)	109.9
O(4A)–H(4A)	0.8400	C(2A)–C(1A)–H(1A1)	109.9
C(11A)–C(12A)	1.495(16)	O(1A)–C(1A)–H(1A2)	109.9
C(11A)–H(11A)	0.9900	C(2A)–C(1A)–H(1A2)	109.9
C(11A)–H(11B)	0.9900	H(1A1)–C(1A)–H(1A2)	108.3
C(12A)–O(5)	1.479(16)	C(1A)–C(2A)–O(2)	106.5(6)
C(12A)–H(12A)	0.9900	C(1A)–C(2A)–H(2A1)	110.4
C(12A)–H(12B)	0.9900	O(2)–C(2A)–H(2A1)	110.4
O(4B)–C(11B)	1.34(2)	C(1A)–C(2A)–H(2A2)	110.4
O(4B)–H(4B)	0.8400	O(2)–C(2A)–H(2A2)	110.4
C(11B)–C(12B)	1.493(18)	H(2A1)–C(2A)–H(2A2)	108.6
C(11B)–H(11C)	0.9900	C(1B)–O(1B)–H(1B)	109.5
C(11B)–H(11D)	0.9900	O(1B)–C(1B)–C(2B)	107.3(9)
C(12B)–O(5)	1.460(13)	O(1B)–C(1B)–H(1B1)	110.3
C(12B)–H(12C)	0.9900	C(2B)–C(1B)–H(1B1)	110.3
C(12B)–H(12D)	0.9900	O(1B)–C(1B)–H(1B2)	110.3
O(5)–C(13)	1.351(5)	C(2B)–C(1B)–H(1B2)	110.3
C(13)–C(14)	1.384(6)	H(1B1)–C(1B)–H(1B2)	108.5
C(13)–C(18)	1.412(7)	O(2)–C(2B)–C(1B)	104.4(9)
C(14)–C(15)	1.344(7)	O(2)–C(2B)–H(2B1)	110.9
C(14)–H(14)	0.9500	C(1B)–C(2B)–H(2B1)	110.9
C(15)–C(16)	1.349(9)	O(2)–C(2B)–H(2B2)	110.9
C(15)–H(15)	0.9500	C(1B)–C(2B)–H(2B2)	110.9
C(16)–C(17)	1.429(8)	H(2B1)–C(2B)–H(2B2)	108.9
C(16)–H(16)	0.9500	C(3)–O(2)–C(2B)	132.3(8)
C(17)–C(18)	1.370(6)	C(3)–O(2)–C(2A)	108.7(5)
C(17)–H(17)	0.9500	C(2B)–O(2)–C(2A)	33.5(6)
C(18)–O(6)	1.366(5)	O(2)–C(3)–C(4)	125.5(4)
O(6)–C(19)	1.434(5)	O(2)–C(3)–C(8)	115.4(4)

Appendix

C(4)–C(3)–C(8)	119.1(3)	C(11A)–C(12A)–H(12B)	107.9
C(5)–C(4)–C(3)	121.2(4)	H(12A)–C(12A)–H(12B)	107.2
C(5)–C(4)–H(4)	119.4	C(11B)–O(4B)–H(4B)	109.5
C(3)–C(4)–H(4)	119.4	O(4B)–C(11B)–C(12B)	110.2(18)
C(6)–C(5)–C(4)	119.4(4)	O(4B)–C(11B)–H(11C)	109.6
C(6)–C(5)–H(5)	120.3	C(12B)–C(11B)–H(11C)	109.6
C(4)–C(5)–H(5)	120.3	O(4B)–C(11B)–H(11D)	109.6
C(5)–C(6)–C(7)	120.7(4)	C(12B)–C(11B)–H(11D)	109.6
C(5)–C(6)–H(6)	119.7	H(11C)–C(11B)–H(11D)	108.1
C(7)–C(6)–H(6)	119.7	O(5)–C(12B)–C(11B)	104.3(12)
C(8)–C(7)–C(6)	120.7(3)	O(5)–C(12B)–H(12C)	110.9
C(8)–C(7)–H(7)	119.6	C(11B)–C(12B)–H(12C)	110.9
C(6)–C(7)–H(7)	119.6	O(5)–C(12B)–H(12D)	110.9
O(3)–C(8)–C(7)	124.9(3)	C(11B)–C(12B)–H(12D)	110.9
O(3)–C(8)–C(3)	116.2(3)	H(12C)–C(12B)–H(12D)	108.9
C(7)–C(8)–C(3)	118.9(3)	C(13)–O(5)–C(12B)	119.5(7)
C(8)–O(3)–C(9)	116.7(2)	C(13)–O(5)–C(12A)	113.2(7)
O(3)–C(9)–C(10)	107.9(2)	C(12B)–O(5)–C(12A)	16.0(15)
O(3)–C(9)–H(9A)	110.1	O(5)–C(13)–C(14)	124.1(5)
C(10)–C(9)–H(9A)	110.1	O(5)–C(13)–C(18)	115.4(4)
O(3)–C(9)–H(9B)	110.1	C(14)–C(13)–C(18)	120.6(4)
C(10)–C(9)–H(9B)	110.1	C(15)–C(14)–C(13)	120.5(5)
H(9A)–C(9)–H(9B)	108.4	C(15)–C(14)–H(14)	119.8
C(9)–C(10)–C(9)#1	113.3(5)	C(13)–C(14)–H(14)	119.8
C(9)–C(10)–H(10)	108.9	C(14)–C(15)–C(16)	120.7(5)
C(9)#1–C(10)–H(10)	108.9	C(14)–C(15)–H(15)	119.6
H(10)–C(10)–H(10)#1	107.7	C(16)–C(15)–H(15)	119.6
C(11A)–O(4A)–H(4A)	109.5	C(15)–C(16)–C(17)	120.8(4)
O(4A)–C(11A)–C(12A)	108.2(15)	C(15)–C(16)–H(16)	119.6
O(4A)–C(11A)–H(11A)	110.1	C(17)–C(16)–H(16)	119.6
C(12A)–C(11A)–H(11A)	110.1	C(18)–C(17)–C(16)	119.1(5)
O(4A)–C(11A)–H(11B)	110.1	C(18)–C(17)–H(17)	120.5
C(12A)–C(11A)–H(11B)	110.1	C(16)–C(17)–H(17)	120.5
H(11A)–C(11A)–H(11B)	108.4	O(6)–C(18)–C(17)	126.0(5)
O(5)–C(12A)–C(11A)	117.5(15)	O(6)–C(18)–C(13)	115.6(4)
O(5)–C(12A)–H(12A)	107.9	C(17)–C(18)–C(13)	118.4(4)
C(11A)–C(12A)–H(12A)	107.9	C(18)–O(6)–C(19)	117.2(3)
O(5)–C(12A)–H(12B)	107.9	O(6)–C(19)–C(20)	107.6(3)

Appendix

O(6)-C(19)-H(19A)	110.2	C(19)-C(20)-C(19)#2	115.6(6)
C(20)-C(19)-H(19A)	110.2	C(19)-C(20)-H(20)	108.4
O(6)-C(19)-H(19B)	110.2	C(19)#2-C(20)-H(20)	108.4
C(20)-C(19)-H(19B)	110.2	H(20)-C(20)-H(20)#2	107.4
H(19A)-C(19)-H(19B)	108.5		

1,5-Bis[2-(2-hydroxyethoxy)phenoxy]-3-oxapentane **161**Fig. A 2 X-ray crystal structure of 1,5-Bis[2-(2-hydroxyethoxy)phenoxy]-3-oxapentane **161**Table A 3 Crystal data and structure refinement for **161**

Identification code	gat05	
Empirical formula	C ₂₀ H ₃₀ O ₉	
Molecular formula	C ₂₀ H ₂₆ O ₇ x 2 (H ₂ O)	
Formula weight	414.44	
Temperature	100(2) K	
Wavelength	0.71073 Å	
Crystal system	Monoclinic	
Space group	C2 (#5)	
Unit cell dimensions	a = 22.433(8) Å	α = 90°.
	b = 4.7894(18) Å	β = 108.808(7)°.
	c = 9.937(4) Å	γ = 90°.
Volume	1010.7(6) Å ³	
Z	2	
Density (calculated)	1.362 Mg/m ³	
Absorption coefficient	0.107 mm ⁻¹	
F(000)	444	

Crystal size	0.80 x 0.15 x 0.02 mm ³
Theta range for data collection	1.92 to 26.97°.
Index ranges	-28<=h<=28, -6<=k<=6, -12<=l<=12
Reflections collected	4116
Independent reflections	1223 [R(int) = 0.0560]
Completeness to theta = 26.97°	99.5 %
Absorption correction	Semi-empirical from equivalents
Max. and min. transmission	0.9979 and 0.8558
Refinement method	Full-matrix least-squares on F ²
Data / restraints / parameters	1223 / 3 / 139 ^{a)}
Goodness-of-fit on F ²	1.083
Final R indices [I>2sigma(I)]	R1 = 0.0457, wR2 = 0.1022
R indices (all data)	R1 = 0.0560, wR2 = 0.1054
Largest diff. peak and hole	0.261 and -0.185 e.Å ⁻³

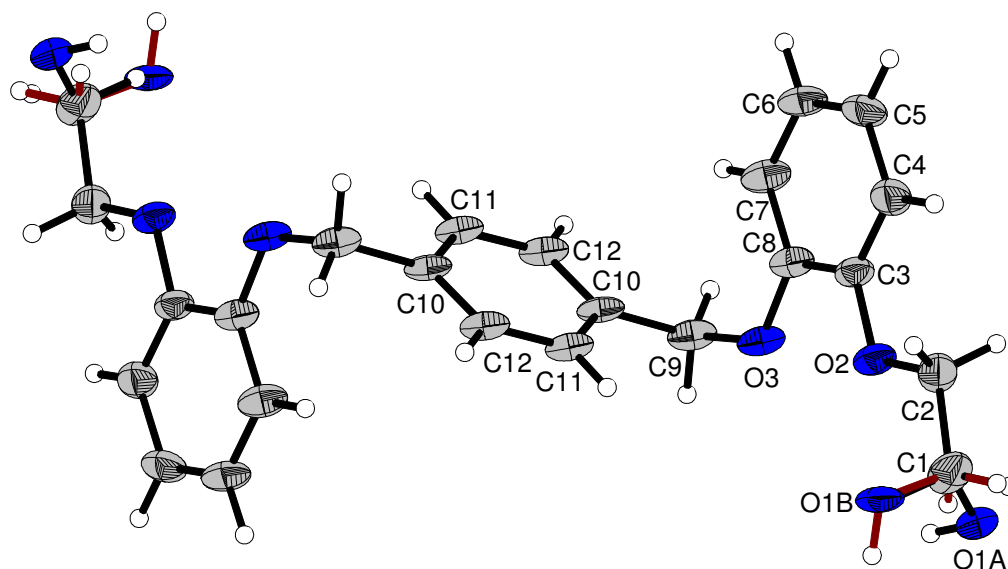
The O-H bond distances in the water molecule are restrained to be 0.84 Å.

Table A 4 Bond lengths [Å] and angles [°] for 161

O(1)-C(1)	1.430(3)	C(9)-C(10)	1.503(4)
O(1)-C(1)#1	1.430(3)	C(9)-H(9A)	0.9900
C(1)-C(2)	1.498(4)	C(9)-H(9B)	0.9900
C(1)-H(1A)	0.9900	C(10)-O(4)	1.423(3)
C(1)-H(1B)	0.9900	C(10)-H(10A)	0.9900
C(2)-O(2)	1.437(3)	C(10)-H(10B)	0.9900
C(2)-H(2A)	0.9900	O(4)-H(104)	0.8400
C(2)-H(2B)	0.9900	O(5)-H(105)	0.835(19)
O(2)-C(3)	1.375(3)	O(5)-H(205)	0.843(19)
C(3)-C(4)	1.383(4)		
C(3)-C(8)	1.406(4)	C(1)-O(1)-C(1)#1	110.1(3)
C(4)-C(5)	1.395(5)	O(1)-C(1)-C(2)	110.1(2)
C(4)-H(4)	0.9500	O(1)-C(1)-H(1A)	109.6
C(5)-C(6)	1.374(5)	C(2)-C(1)-H(1A)	109.6
C(5)-H(5)	0.9500	O(1)-C(1)-H(1B)	109.6
C(6)-C(7)	1.395(4)	C(2)-C(1)-H(1B)	109.6
C(6)-H(6)	0.9500	H(1A)-C(1)-H(1B)	108.2
C(7)-C(8)	1.384(4)	O(2)-C(2)-C(1)	108.6(2)
C(7)-H(7)	0.9500	O(2)-C(2)-H(2A)	110.0
C(8)-O(3)	1.372(3)	C(1)-C(2)-H(2A)	110.0
O(3)-C(9)	1.436(3)	O(2)-C(2)-H(2B)	110.0

Appendix

C(1)–C(2)–H(2B)	110.0	O(3)–C(8)–C(3)	115.7(2)
H(2A)–C(2)–H(2B)	108.4	C(7)–C(8)–C(3)	119.9(2)
C(3)–O(2)–C(2)	116.1(2)	C(8)–O(3)–C(9)	116.7(2)
O(2)–C(3)–C(4)	124.8(3)	O(3)–C(9)–C(10)	107.7(2)
O(2)–C(3)–C(8)	115.9(2)	O(3)–C(9)–H(9A)	110.2
C(4)–C(3)–C(8)	119.3(2)	C(10)–C(9)–H(9A)	110.2
C(3)–C(4)–C(5)	120.6(3)	O(3)–C(9)–H(9B)	110.2
C(3)–C(4)–H(4)	119.7	C(10)–C(9)–H(9B)	110.2
C(5)–C(4)–H(4)	119.7	H(9A)–C(9)–H(9B)	108.5
C(6)–C(5)–C(4)	119.9(3)	O(4)–C(10)–C(9)	113.6(2)
C(6)–C(5)–H(5)	120.0	O(4)–C(10)–H(10A)	108.8
C(4)–C(5)–H(5)	120.0	C(9)–C(10)–H(10A)	108.8
C(5)–C(6)–C(7)	120.2(3)	O(4)–C(10)–H(10B)	108.8
C(5)–C(6)–H(6)	119.9	C(9)–C(10)–H(10B)	108.8
C(7)–C(6)–H(6)	119.9	H(10A)–C(10)–H(10B)	107.7
C(8)–C(7)–C(6)	120.1(3)	C(10)–O(4)–H(10A)	109.5
C(8)–C(7)–H(7)	120.0	H(10A)–O(4)–H(10A)	97(4)
C(6)–C(7)–H(7)	120.0		
O(3)–C(8)–C(7)	124.4(2)		

1,4-Bis[2-(2-hydroxyethoxy)phenoxy]-*p*-xylene **163**Fig. A 3 X-ray crystal structure of 1,4-Bis[2-(2-hydroxyethoxy)phenoxy]-*p*-xylene **163**Table A 5 Crystal data and structure refinement for **163**

Identification code	gat12	
Empirical formula	C ₂₄ H ₂₆ O ₆	
Formula weight	410.45	
Temperature	100(2) K	
Wavelength	0.71073 Å	
Crystal system	Monoclinic	
Space group	C2/c (#15)	
Unit cell dimensions	a = 24.449(5) Å	α = 90°.
	b = 4.9250(11) Å	β = 91.677(5)°.
	c = 16.381(4) Å	γ = 90°.
Volume	1971.6(8) Å ³	
Z	4	
Density (calculated)	1.383 Mg/m ³	
Absorption coefficient	0.099 mm ⁻¹	
F(000)	872	
Crystal size	0.50 x 0.15 x 0.10 mm ³	
Theta range for data collection	1.67 to 23.00°.	
Index ranges	-26 ≤ h ≤ 26, -5 ≤ k ≤ 5, -18 ≤ l ≤ 18	
Reflections collected	5918	

Independent reflections	1371 [R(int) = 0.0570]
Completeness to theta = 23.00°	99.6 %
Absorption correction	Semi-empirical from equivalents
Max. and min. transmission	0.9902 and 0.6363
Refinement method	Full-matrix least-squares on F ²
Data / restraints / parameters	1371 / 36 / 148 ^{a)}
Goodness-of-fit on F ²	1.156
Final R indices [I > 2sigma(I)]	R1 = 0.0616, wR2 = 0.1445
R indices (all data)	R1 = 0.0680, wR2 = 0.1483
Largest diff. peak and hole	0.180 and -0.189 e.Å ⁻³

DELU restraints were applied to all thermal displacement parameters.

Table A 6 Bond lengths [Å] and angles [°] for **163**

O(1A)–C(1)	1.532(5)	C(9)–C(10)	1.503(5)
O(1A)–H(10A)	0.8400	C(9)–H(9A)	0.9900
C(1)–C(2)	1.501(5)	C(9)–H(9B)	0.9900
C(1)–H(1A)	0.9900	C(10)–C(12)#1	1.383(4)
C(1)–H(1B)	0.9900	C(10)–C(11)	1.390(4)
C(1)–H(1C)	0.9900	C(11)–C(12)	1.374(5)
C(1)–H(1D)	0.9900	C(11)–H(11)	0.9500
O(1B)–C(1)	1.352(6)	C(12)–C(10)#1	1.383(4)
O(1B)–H(10B)	0.8400	C(12)–H(12)	0.9500
C(2)–O(2)	1.426(4)		
C(2)–H(2A)	0.9900	H(10A)–O(1A)–C(1)	109.5
C(2)–H(2B)	0.9900	H(10B)–O(1B)–C(1)	109.5
O(2)–C(3)	1.374(3)	C(2)–C(1)–O(1A)	114.8(3)
C(3)–C(4)	1.373(5)	C(2)–C(1)–H(1A)	108.6
C(3)–C(8)	1.390(4)	O(1A)–C(1)–H(1A)	108.6
C(4)–C(5)	1.396(4)	C(2)–C(1)–H(1B)	108.6
C(4)–H(4)	0.9500	O(1A)–C(1)–H(1B)	108.6
C(5)–C(6)	1.355(5)	H(1A)–C(1)–H(1B)	107.5
C(5)–H(5)	0.9500	C(2)–C(1)–O(1B)	104.9(3)
C(6)–C(7)	1.387(5)	C(2)–C(1)–H(1C)	110.8
C(6)–H(6)	0.9500	O(1A)–C(1)–H(1C)	110.8
C(7)–C(8)	1.385(4)	C(2)–C(1)–H(1D)	110.8
C(7)–H(7)	0.9500	O(1A)–C(1)–H(1D)	110.8
C(8)–O(3)	1.371(4)	H(1C)–C(1)–H(1D)	108.7
O(3)–C(9)	1.427(4)	O(2)–C(2)–C(1)	107.3(3)

Appendix

O(2)-C(2)-H(2A)	110.3	C(6)-C(7)-H(7)	120.1
C(1)-C(2)-H(2A)	110.3	O(3)-C(8)-C(7)	124.9(3)
O(2)-C(2)-H(2B)	110.3	O(3)-C(8)-C(3)	115.5(2)
C(1)-C(2)-H(2B)	110.3	C(7)-C(8)-C(3)	119.6(3)
H(2A)-C(2)-H(2B)	108.5	C(8)-O(3)-C(9)	117.9(2)
C(3)-O(2)-C(2)	117.3(2)	O(3)-C(9)-C(10)	113.4(2)
C(4)-C(3)-O(2)	124.4(3)	O(3)-C(9)-H(9A)	108.9
C(4)-C(3)-C(8)	120.1(3)	C(10)-C(9)-H(9A)	108.9
O(2)-C(3)-C(8)	115.5(3)	O(3)-C(9)-H(9B)	108.9
C(3)-C(4)-C(5)	119.8(3)	C(10)-C(9)-H(9B)	108.9
C(3)-C(4)-H(4)	120.1	H(9A)-C(9)-H(9B)	107.7
C(5)-C(4)-H(4)	120.1	C(12)#1-C(10)-C(11)	117.8(3)
C(6)-C(5)-C(4)	120.2(3)	C(12)#1-C(10)-C(9)	121.3(3)
C(6)-C(5)-H(5)	119.9	C(11)-C(10)-C(9)	120.9(3)
C(4)-C(5)-H(5)	119.9	C(12)-C(11)-C(10)	120.6(3)
C(5)-C(6)-C(7)	120.6(3)	C(12)-C(11)-H(11)	119.7
C(5)-C(6)-H(6)	119.7	C(10)-C(11)-H(11)	119.7
C(7)-C(6)-H(6)	119.7	C(11)-C(12)-C(10)#1	121.5(3)
C(8)-C(7)-C(6)	119.7(3)	C(11)-C(12)-H(12)	119.2
C(8)-C(7)-H(7)	120.1	C(10)#1-C(12)-H(12)	119.2

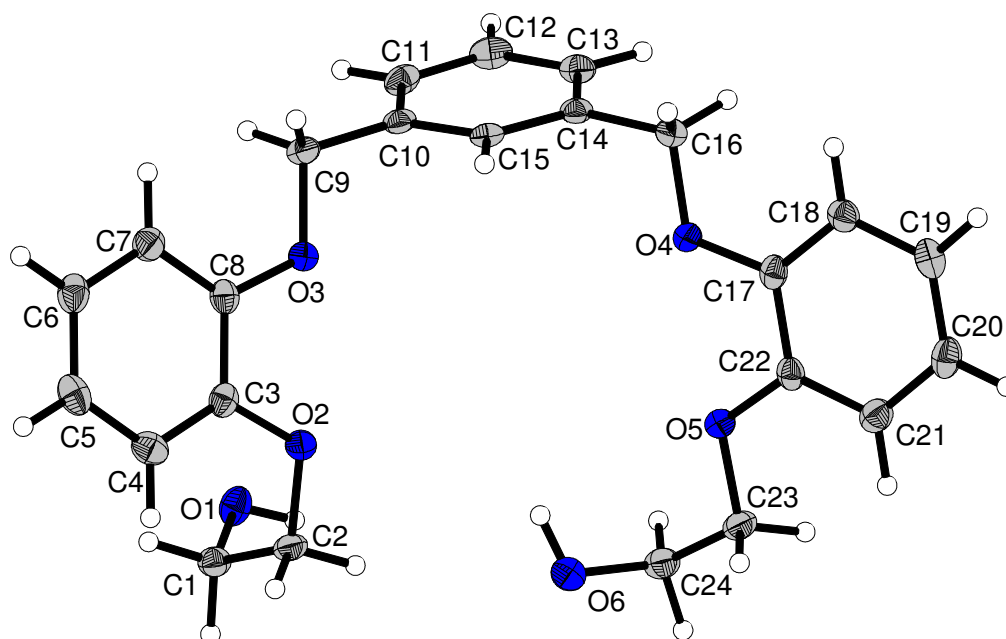
1,3-Bis[2-(2-hydroxyethoxy)phenoxy]-*m*-xylene 164Fig. A 4 X-ray crystal structure of 1,3-Bis[2-(2-hydroxyethoxy)phenoxy]-*m*-xylene 164

Table A 7 Crystal data and structure refinement for 164

Identification code	gat04
Empirical formula	C ₂₄ H ₂₆ O ₆
Formula weight	410.45
Temperature	100(2) K
Wavelength	0.71073 Å
Crystal system	Monoclinic
Space group	P2 ₁ /c (#14)
Unit cell dimensions	a = 13.4964(16) Å α = 90°. b = 7.0234(8) Å β = 104.665(2)°. c = 22.476(3) Å γ = 90°.
Volume	2061.2(4) Å ³
Z	4
Density (calculated)	1.323 Mg/m ³
Absorption coefficient	0.095 mm ⁻¹
F(000)	872
Crystal size	0.60 x 0.40 x 0.05 mm ³
Theta range for data collection	1.87 to 26.00°.

Index ranges	-16<=h<=16, -8<=k<=8, -27<=l<=27
Reflections collected	17123
Independent reflections	4056 [R(int) = 0.0359]
Completeness to theta = 26.00°	100.0 %
Absorption correction	Semi-empirical from equivalents
Max. and min. transmission	0.9953 and 0.8160
Refinement method	Full-matrix least-squares on F ²
Data / restraints / parameters	4056 / 0 / 375
Goodness-of-fit on F ²	1.018
Final R indices [I>2sigma(I)]	R1 = 0.0372, wR2 = 0.0815
R indices (all data)	R1 = 0.0490, wR2 = 0.0873
Largest diff. peak and hole	0.246 and -0.167 e.Å ⁻³

Table A 8 Bond lengths [Å] and angles [°] for **164**

O(1)–C(1)	1.4225(17)	C(10)–C(15)	1.3919(19)
O(1)–H(1O1)	0.867(19)	C(10)–C(11)	1.394(2)
C(1)–C(2)	1.505(2)	C(11)–C(12)	1.388(2)
C(1)–H(1A)	0.984(14)	C(11)–H(11)	0.960(15)
C(1)–H(1B)	1.006(15)	C(12)–C(13)	1.384(2)
C(2)–O(2)	1.4445(16)	C(12)–H(12)	0.963(17)
C(2)–H(2A)	0.977(15)	C(13)–C(14)	1.392(2)
C(2)–H(2B)	0.982(16)	C(13)–H(13)	0.996(16)
O(2)–C(3)	1.3679(16)	C(14)–C(15)	1.388(2)
C(3)–C(4)	1.381(2)	C(14)–C(16)	1.498(2)
C(3)–C(8)	1.406(2)	C(15)–H(15)	0.961(15)
C(4)–C(5)	1.396(2)	C(16)–O(4)	1.4370(16)
C(4)–H(4)	0.941(16)	C(16)–H(16A)	0.979(15)
C(5)–C(6)	1.378(2)	C(16)–H(16B)	0.980(16)
C(5)–H(5)	0.938(16)	O(4)–C(17)	1.3644(16)
C(6)–C(7)	1.392(2)	C(17)–C(18)	1.383(2)
C(6)–H(6)	0.963(15)	C(17)–C(22)	1.4113(19)
C(7)–C(8)	1.384(2)	C(18)–C(19)	1.393(2)
C(7)–H(7)	0.973(16)	C(18)–H(18)	0.942(15)
C(8)–O(3)	1.3679(17)	C(19)–C(20)	1.374(2)
O(3)–C(9)	1.4392(17)	C(19)–H(19)	0.968(16)
C(9)–C(10)	1.500(2)	C(20)–C(21)	1.396(2)
C(9)–H(9A)	0.989(15)	C(20)–H(20)	0.963(16)
C(9)–H(9B)	0.995(17)	C(21)–C(22)	1.384(2)

Appendix

C(21)–H(21)	0.963(16)	C(8)–C(7)–H(7)	120.1(9)
C(22)–O(5)	1.3687(17)	C(6)–C(7)–H(7)	119.6(9)
O(5)–C(23)	1.4338(17)	O(3)–C(8)–C(7)	125.39(13)
C(23)–C(24)	1.500(2)	O(3)–C(8)–C(3)	115.10(12)
C(23)–H(23A)	0.984(15)	C(7)–C(8)–C(3)	119.51(13)
C(23)–H(23B)	0.992(17)	C(8)–O(3)–C(9)	116.42(10)
C(24)–O(6)	1.4155(18)	O(3)–C(9)–C(10)	107.78(11)
C(24)–H(24A)	0.991(15)	O(3)–C(9)–H(9A)	109.6(9)
C(24)–H(24B)	0.999(15)	C(10)–C(9)–H(9A)	110.5(8)
O(6)–H(106)	0.88(2)	O(3)–C(9)–H(9B)	109.1(9)
		C(10)–C(9)–H(9B)	110.2(9)
C(1)–O(1)–H(101)	109.5(12)	H(9A)–C(9)–H(9B)	109.5(12)
O(1)–C(1)–C(2)	112.52(12)	C(15)–C(10)–C(11)	119.08(13)
O(1)–C(1)–H(1A)	107.2(8)	C(15)–C(10)–C(9)	120.08(13)
C(2)–C(1)–H(1A)	111.3(8)	C(11)–C(10)–C(9)	120.84(13)
O(1)–C(1)–H(1B)	110.4(9)	C(12)–C(11)–C(10)	120.64(14)
C(2)–C(1)–H(1B)	108.7(9)	C(12)–C(11)–H(11)	120.1(9)
H(1A)–C(1)–H(1B)	106.6(11)	C(10)–C(11)–H(11)	119.2(9)
O(2)–C(2)–C(1)	112.21(12)	C(13)–C(12)–C(11)	119.56(14)
O(2)–C(2)–H(2A)	103.8(9)	C(13)–C(12)–H(12)	121.1(10)
C(1)–C(2)–H(2A)	109.7(9)	C(11)–C(12)–H(12)	119.4(10)
O(2)–C(2)–H(2B)	111.4(8)	C(12)–C(13)–C(14)	120.64(14)
C(1)–C(2)–H(2B)	110.2(9)	C(12)–C(13)–H(13)	121.3(9)
H(2A)–C(2)–H(2B)	109.2(12)	C(14)–C(13)–H(13)	118.1(9)
C(3)–O(2)–C(2)	118.16(11)	C(15)–C(14)–C(13)	119.36(13)
O(2)–C(3)–C(4)	125.23(13)	C(15)–C(14)–C(16)	120.65(13)
O(2)–C(3)–C(8)	114.89(12)	C(13)–C(14)–C(16)	119.94(13)
C(4)–C(3)–C(8)	119.86(13)	C(14)–C(15)–C(10)	120.68(13)
C(3)–C(4)–C(5)	120.18(14)	C(14)–C(15)–H(15)	120.9(9)
C(3)–C(4)–H(4)	119.7(9)	C(10)–C(15)–H(15)	118.4(9)
C(5)–C(4)–H(4)	120.2(9)	O(4)–C(16)–C(14)	107.00(11)
C(6)–C(5)–C(4)	119.92(14)	O(4)–C(16)–H(16A)	107.9(9)
C(6)–C(5)–H(5)	118.9(10)	C(14)–C(16)–H(16A)	112.2(9)
C(4)–C(5)–H(5)	121.2(9)	O(4)–C(16)–H(16B)	110.8(9)
C(5)–C(6)–C(7)	120.25(14)	C(14)–C(16)–H(16B)	110.4(9)
C(5)–C(6)–H(6)	120.3(9)	H(16A)–C(16)–	108.5(12)
C(7)–C(6)–H(6)	119.4(9)	H(16B)	
C(8)–C(7)–C(6)	120.21(14)	C(17)–O(4)–C(16)	116.43(10)

Appendix

O(4)–C(17)–C(18)	125.15(13)	C(22)–O(5)–C(23)	116.25(11)
O(4)–C(17)–C(22)	115.46(12)	O(5)–C(23)–C(24)	108.46(12)
C(18)–C(17)–C(22)	119.38(13)	O(5)–C(23)–H(23A)	109.7(9)
C(17)–C(18)–C(19)	120.46(14)	C(24)–C(23)–H(23A)	110.3(9)
C(17)–C(18)–H(18)	120.2(9)	O(5)–C(23)–H(23B)	108.8(9)
C(19)–C(18)–H(18)	119.3(9)	C(24)–C(23)–H(23B)	110.8(9)
C(20)–C(19)–C(18)	120.31(14)	H(23A)–C(23)–	108.7(12)
C(20)–C(19)–H(19)	121.1(9)	H(23B)	
C(18)–C(19)–H(19)	118.6(9)	O(6)–C(24)–C(23)	113.56(13)
C(19)–C(20)–C(21)	119.86(14)	O(6)–C(24)–H(24A)	111.4(8)
C(19)–C(20)–H(20)	119.7(9)	C(23)–C(24)–H(24A)	109.7(8)
C(21)–C(20)–H(20)	120.4(9)	O(6)–C(24)–H(24B)	107.6(8)
C(22)–C(21)–C(20)	120.42(14)	C(23)–C(24)–H(24B)	107.6(9)
C(22)–C(21)–H(21)	119.4(9)	H(24A)–C(24)–	106.8(12)
C(20)–C(21)–H(21)	120.2(9)	H(24B)	
O(5)–C(22)–C(21)	124.60(13)	C(24)–O(6)–H(106)	108.0(13)
O(5)–C(22)–C(17)	115.84(12)		
C(21)–C(22)–C(17)	119.55(13)		

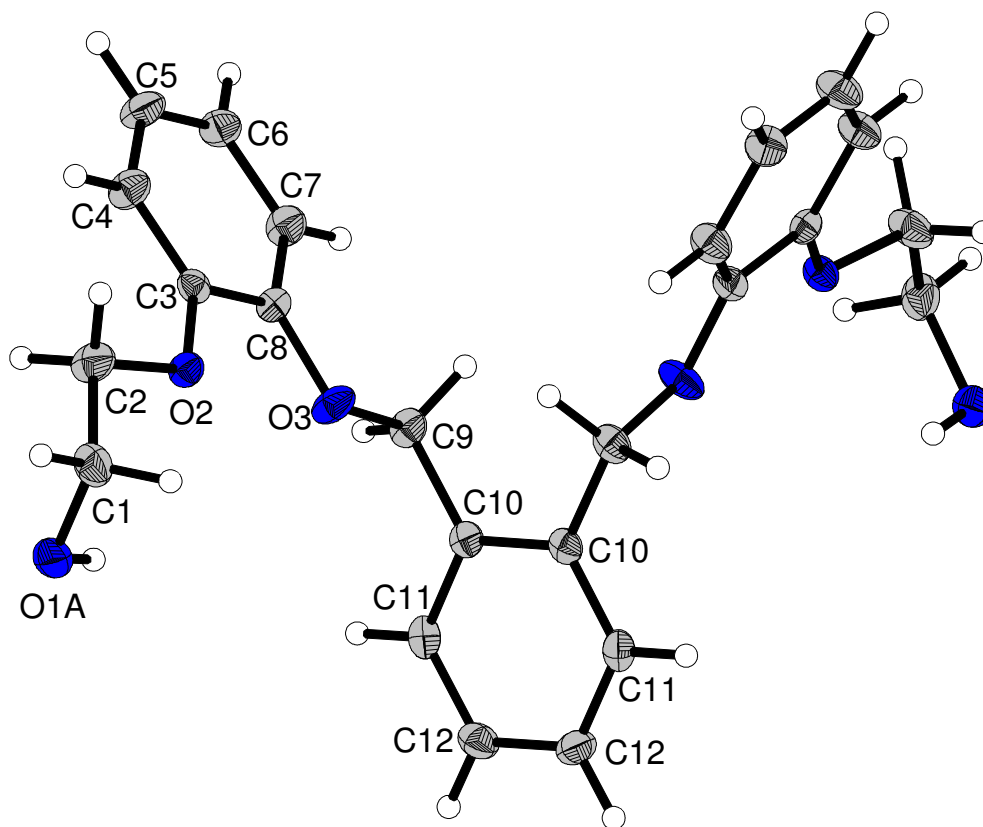
1,2-Bis[2-(2-hydroxyethoxy)phenoxy]-*o*-xylene 165Fig. A 5 X-ray crystal structure of 1,2-Bis[2-(2-hydroxyethoxy)phenoxy]-*o*-xylene 165

Table A 9 Crystal data and structure refinement for 165

Identification code	gat06	
Empirical formula	C ₂₄ H ₂₆ O ₆	
Formula weight	410.45	
Temperature	100(2) K	
Wavelength	0.71073 Å	
Crystal system	Monoclinic	
Space group	C2/c (#15)	
Unit cell dimensions	a = 26.492(4) Å	α = 90°.
	b = 9.8112(15) Å	β = 106.831(3)°.
	c = 8.4897(13) Å	γ = 90°.
Volume	2112.1(6) Å ³	
Z	4	

Density (calculated)	1.291 Mg/m ³
Absorption coefficient	0.092 mm ⁻¹
F(000)	872
Crystal size	0.60 x 0.40 x 0.01 mm ³
Theta range for data collection	1.61 to 24.73°.
Index ranges	-31<=h<=31, -11<=k<=11, -9<=l<=9
Reflections collected	7805
Independent reflections	1794 [R(int) = 0.0263]
Completeness to theta = 24.73°	99.9 %
Absorption correction	Semi-empirical from equivalents
Max. and min. transmission	0.9991 and 0.8816
Refinement method	Full-matrix least-squares on F ²
Data / restraints / parameters	1794 / 0 / 148
Goodness-of-fit on F ²	1.024
Final R indices [I>2sigma(I)]	R1 = 0.0369, wR2 = 0.0851
R indices (all data)	R1 = 0.0452, wR2 = 0.0894
Largest diff. peak and hole	0.257 and -0.163 e.Å ⁻³

Table A 10 Bond lengths [Å] and angles [°] for **165**

O(1A)–C(1)	1.505(3)	C(6)–C(7)	1.392(2)
O(1A)–H(1A)	0.8400	C(6)–H(6)	0.9500
C(1)–C(2)	1.485(2)	C(7)–C(8)	1.382(2)
C(1)–H(1A1)	0.9900	C(7)–H(7)	0.9500
C(1)–H(1A2)	0.9900	C(8)–O(3)	1.3809(17)
C(1)–H(1B1)	0.9900	O(3)–C(9)	1.4457(17)
C(1)–H(1B2)	0.9900	C(9)–C(10)	1.503(2)
O(1B)–C(1)	1.491(3)	C(9)–H(9A)	0.9900
O(1B)–H(1B)	0.8400	C(9)–H(9B)	0.9900
C(2)–O(2)	1.4289(17)	C(10)–C(11)	1.389(2)
C(2)–H(2A)	0.9900	C(10)–C(10)#1	1.405(3)
C(2)–H(2B)	0.9900	C(11)–C(12)	1.385(2)
O(2)–C(3)	1.3725(17)	C(11)–H(11)	0.9500
C(3)–C(4)	1.376(2)	C(12)–C(12)#1	1.386(3)
C(3)–C(8)	1.404(2)	C(12)–H(12)	0.9500
C(4)–C(5)	1.394(2)		
C(4)–H(4)	0.9500	C(2)–C(1)–O(1A)	103.84(14)
C(5)–C(6)	1.368(2)	C(2)–C(1)–H(1A1)	111.0
C(5)–H(5)	0.9500	O(1A)–C(1)–H(1A1)	111.0

Appendix

C(2)–C(1)–H(1A2)	111.0	C(5)–C(6)–C(7)	119.83(14)
O(1A)–C(1)–H(1A2)	111.0	C(5)–C(6)–H(6)	120.1
H(1A1)–C(1)–H(1A2)	109.0	C(7)–C(6)–H(6)	120.1
C(2)–C(1)–O(1B)	102.9(2)	C(8)–C(7)–C(6)	120.17(14)
C(2)–C(1)–H(1B1)	111.3	C(8)–C(7)–H(7)	119.9
O(1B)–C(1)–H(1B1)	111.3	C(6)–C(7)–H(7)	119.9
C(2)–C(1)–H(1B2)	111.3	O(3)–C(8)–C(7)	124.61(13)
O(1B)–C(1)–H(1B2)	111.3	O(3)–C(8)–C(3)	115.39(12)
H(1B1)–C(1)–H(1B2)	109.1	C(7)–C(8)–C(3)	119.98(13)
O(2)–C(2)–C(1)	108.83(12)	C(8)–O(3)–C(9)	115.07(11)
O(2)–C(2)–H(2A)	109.9	O(3)–C(9)–C(10)	109.02(11)
C(1)–C(2)–H(2A)	109.9	O(3)–C(9)–H(9A)	109.9
O(2)–C(2)–H(2B)	109.9	C(10)–C(9)–H(9A)	109.9
C(1)–C(2)–H(2B)	109.9	O(3)–C(9)–H(9B)	109.9
H(2A)–C(2)–H(2B)	108.3	C(10)–C(9)–H(9B)	109.9
C(3)–O(2)–C(2)	116.89(11)	H(9A)–C(9)–H(9B)	108.3
O(2)–C(3)–C(4)	124.76(13)	C(11)–C(10)–C(10)#1	119.11(8)
O(2)–C(3)–C(8)	116.02(12)	C(11)–C(10)–C(9)	119.78(13)
C(4)–C(3)–C(8)	119.22(13)	C(10)#1–C(10)–C(9)	121.07(8)
C(3)–C(4)–C(5)	120.35(14)	C(12)–C(11)–C(10)	121.23(14)
C(3)–C(4)–H(4)	119.8	C(12)–C(11)–H(11)	119.4
C(5)–C(4)–H(4)	119.8	C(10)–C(11)–H(11)	119.4
C(6)–C(5)–C(4)	120.45(14)	C(11)–C(12)–C(12)#1	119.67(9)
C(6)–C(5)–H(5)	119.8	C(11)–C(12)–H(12)	120.2
C(4)–C(5)–H(5)	119.8	C(12)#1–C(12)–H(12)	120.2

1,6-Bis[2-(2-hydroxyethoxy)phenoxy]lutidine 166

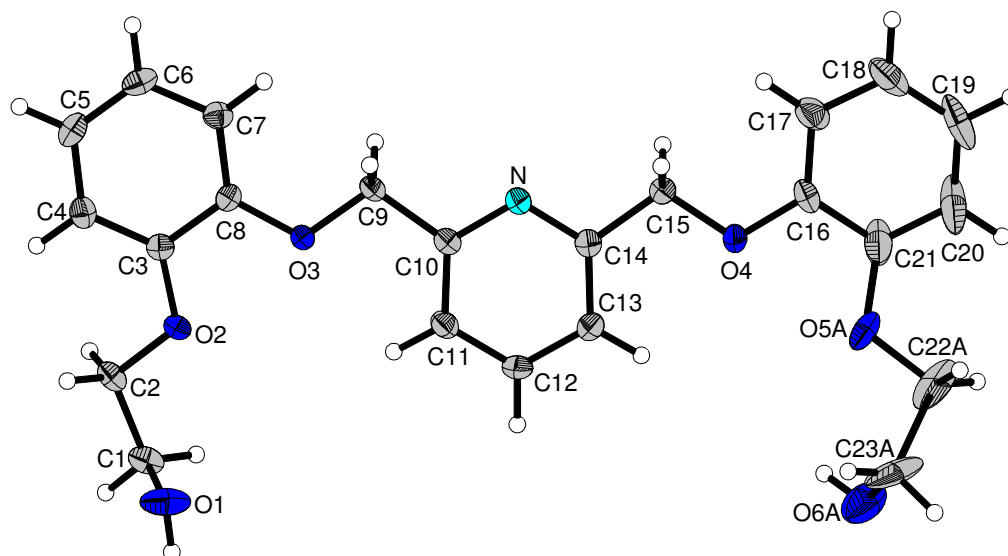


Fig. A 6 X-ray crystal structure of 1,6-Bis[2-(2-hydroxyethoxy)phenoxy]lutidine 166

Table A 11 Crystal data and structure refinement for 166

Identification code	gat14	
Empirical formula	C ₂₃ H ₂₅ N O ₆	
Formula weight	411.44	
Temperature	100(2) K	
Wavelength	0.71073 Å	
Crystal system	Monoclinic	
Space group	P2 ₁ /c (#14)	
Unit cell dimensions	a = 25.257(2) Å	α = 90°.
	b = 4.8053(5) Å	β = 108.907(2)°.
	c = 17.7782(17) Å	γ = 90°.
Volume	2041.3(3) Å ³	
Z	4	
Density (calculated)	1.339 Mg/m ³	
Absorption coefficient	0.097 mm ⁻¹	
F(000)	872	
Crystal size	0.80 x 0.10 x 0.03 mm ³	
Theta range for data collection	0.85 to 24.00°.	
Index ranges	-28 ≤ h ≤ 28, -5 ≤ k ≤ 5, -20 ≤ l ≤ 20	
Reflections collected	13847	

Independent reflections	3210 [R(int) = 0.0237]
Completeness to theta = 24.00°	100.0 %
Absorption correction	Semi-empirical from equivalents
Max. and min. transmission	0.9971 and 0.7643
Refinement method	Full-matrix least-squares on F ²
Data / restraints / parameters	3210 / 0 / 311
Goodness-of-fit on F ²	1.035
Final R indices [I > 2sigma(I)]	R1 = 0.0432, wR2 = 0.1076
R indices (all data)	R1 = 0.0500, wR2 = 0.1132
Largest diff. peak and hole	0.455 and -0.211 e.Å ⁻³

Table A 12 Bond lengths [Å] and angles [°] for **166**

O(1)–C(1)	1.418(2)	N–C(14)	1.341(2)
O(1)–H(1O1)	0.8400	C(11)–C(12)	1.379(3)
C(1)–C(2)	1.501(3)	C(11)–H(11)	0.9500
C(1)–H(1A)	0.9900	C(12)–C(13)	1.383(3)
C(1)–H(1B)	0.9900	C(12)–H(12)	0.9500
C(2)–O(2)	1.432(2)	C(13)–C(14)	1.385(2)
C(2)–H(2A)	0.9900	C(13)–H(13)	0.9500
C(2)–H(2B)	0.9900	C(14)–C(15)	1.498(2)
O(2)–C(3)	1.368(2)	C(15)–O(4)	1.418(2)
C(3)–C(4)	1.381(2)	C(15)–H(15A)	0.9900
C(3)–C(8)	1.406(2)	C(15)–H(15B)	0.9900
C(4)–C(5)	1.390(3)	O(4)–C(16)	1.373(2)
C(4)–H(4)	0.9500	C(16)–C(17)	1.373(3)
C(5)–C(6)	1.375(3)	C(16)–C(21)	1.392(3)
C(5)–H(5)	0.9500	C(17)–C(18)	1.388(3)
C(6)–C(7)	1.390(3)	C(17)–H(17)	0.9500
C(6)–H(6)	0.9500	C(18)–C(19)	1.364(4)
C(7)–C(8)	1.382(2)	C(18)–H(18)	0.9500
C(7)–H(7)	0.9500	C(19)–C(20)	1.378(4)
C(8)–O(3)	1.372(2)	C(19)–H(19)	0.9500
O(3)–C(9)	1.416(2)	C(20)–C(21)	1.377(3)
C(9)–C(10)	1.500(2)	C(20)–H(20)	0.9500
C(9)–H(9A)	0.9900	C(21)–O(5B)	1.379(4)
C(9)–H(9B)	0.9900	C(21)–O(5A)	1.462(5)
C(10)–N	1.343(2)	O(5A)–C(22A)	1.471(12)
C(10)–C(11)	1.387(2)	C(22A)–C(23A)	1.580(10)

Appendix

C(22A)–H(22A)	0.9900	C(5)–C(6)–C(7)	120.14(16)
C(22A)–H(22B)	0.9900	C(5)–C(6)–H(6)	119.9
C(23A)–O(6A)	1.406(5)	C(7)–C(6)–H(6)	119.9
C(23A)–H(23A)	0.9900	C(8)–C(7)–C(6)	120.01(16)
C(23A)–H(23B)	0.9900	C(8)–C(7)–H(7)	120.0
O(6A)–H(6A)	0.8400	C(6)–C(7)–H(7)	120.0
O(5B)–C(22B)	1.371(8)	O(3)–C(8)–C(7)	125.08(15)
C(22B)–C(23B)	1.390(15)	O(3)–C(8)–C(3)	115.00(14)
C(22B)–H(22C)	0.9900	C(7)–C(8)–C(3)	119.92(15)
C(22B)–H(22D)	0.9900	C(8)–O(3)–C(9)	116.17(12)
C(23B)–O(6B)	1.490(10)	O(3)–C(9)–C(10)	108.69(13)
C(23B)–H(23C)	0.9900	O(3)–C(9)–H(9A)	110.0
C(23B)–H(23D)	0.9900	C(10)–C(9)–H(9A)	110.0
O(6B)–H(6B)	0.8400	O(3)–C(9)–H(9B)	110.0
		C(10)–C(9)–H(9B)	110.0
C(1)–O(1)–H(1O1)	109.5	H(9A)–C(9)–H(9B)	108.3
O(1)–C(1)–C(2)	109.79(15)	N–C(10)–C(11)	122.27(16)
O(1)–C(1)–H(1A)	109.7	N–C(10)–C(9)	114.22(14)
C(2)–C(1)–H(1A)	109.7	C(11)–C(10)–C(9)	123.51(15)
O(1)–C(1)–H(1B)	109.7	C(14)–N–C(10)	118.56(14)
C(2)–C(1)–H(1B)	109.7	C(12)–C(11)–C(10)	118.50(16)
H(1A)–C(1)–H(1B)	108.2	C(12)–C(11)–H(11)	120.7
O(2)–C(2)–C(1)	107.58(15)	C(10)–C(11)–H(11)	120.7
O(2)–C(2)–H(2A)	110.2	C(11)–C(12)–C(13)	119.83(16)
C(1)–C(2)–H(2A)	110.2	C(11)–C(12)–H(12)	120.1
O(2)–C(2)–H(2B)	110.2	C(13)–C(12)–H(12)	120.1
C(1)–C(2)–H(2B)	110.2	C(12)–C(13)–C(14)	118.23(16)
H(2A)–C(2)–H(2B)	108.5	C(12)–C(13)–H(13)	120.9
C(3)–O(2)–C(2)	117.18(13)	C(14)–C(13)–H(13)	120.9
O(2)–C(3)–C(4)	125.32(15)	N–C(14)–C(13)	122.59(16)
O(2)–C(3)–C(8)	115.30(14)	N–C(14)–C(15)	113.14(14)
C(4)–C(3)–C(8)	119.38(15)	C(13)–C(14)–C(15)	124.26(15)
C(3)–C(4)–C(5)	120.29(17)	O(4)–C(15)–C(14)	110.42(13)
C(3)–C(4)–H(4)	119.9	O(4)–C(15)–H(15A)	109.6
C(5)–C(4)–H(4)	119.9	C(14)–C(15)–H(15A)	109.6
C(6)–C(5)–C(4)	120.25(17)	O(4)–C(15)–H(15B)	109.6
C(6)–C(5)–H(5)	119.9	C(14)–C(15)–H(15B)	109.6
C(4)–C(5)–H(5)	119.9	H(15A)–C(15)–H(15B)	108.1

Appendix

C(16)–O(4)–C(15)	115.19(13)	C(23A)–C(22A)–H(22A)	111.3
O(4)–C(16)–C(17)	124.84(17)	O(5A)–C(22A)–H(22B)	111.3
O(4)–C(16)–C(21)	115.91(16)	C(23A)–C(22A)–H(22B)	111.3
C(17)–C(16)–C(21)	119.25(18)	H(22A)–C(22A)–H(22B)	109.2
C(16)–C(17)–C(18)	120.2(2)	O(6A)–C(23A)–C(22A)	115.6(5)
C(16)–C(17)–H(17)	119.9	O(6A)–C(23A)–H(23A)	108.4
C(18)–C(17)–H(17)	119.9	C(22A)–C(23A)–H(23A)	108.4
C(19)–C(18)–C(17)	120.7(2)	O(6A)–C(23A)–H(23B)	108.4
C(19)–C(18)–H(18)	119.7	C(22A)–C(23A)–H(23B)	108.4
C(17)–C(18)–H(18)	119.7	H(23A)–C(23A)–H(23B)	107.4
C(18)–C(19)–C(20)	119.3(2)	C(22B)–O(5B)–C(21)	105.2(4)
C(18)–C(19)–H(19)	120.3	O(5B)–C(22B)–C(23B)	111.1(6)
C(20)–C(19)–H(19)	120.3	O(5B)–C(22B)–H(22C)	109.4
C(21)–C(20)–C(19)	120.8(2)	C(23B)–C(22B)–H(22C)	109.4
C(21)–C(20)–H(20)	119.6	O(5B)–C(22B)–H(22D)	109.4
C(19)–C(20)–H(20)	119.6	C(23B)–C(22B)–H(22D)	109.4
C(20)–C(21)–O(5B)	117.1(2)	H(22C)–C(22B)–H(22D)	108.0
C(20)–C(21)–C(16)	119.8(2)	C(22B)–C(23B)–O(6B)	112.7(6)
O(5B)–C(21)–C(16)	117.0(2)	C(22B)–C(23B)–H(23C)	109.0
C(20)–C(21)–O(5A)	124.6(3)	O(6B)–C(23B)–H(23C)	109.0
O(5B)–C(21)–O(5A)	38.63(19)	C(22B)–C(23B)–H(23D)	109.0
C(16)–C(21)–O(5A)	113.8(2)	O(6B)–C(23B)–H(23D)	109.0
C(21)–O(5A)–C(22A)	118.1(4)	H(23C)–C(23B)–H(23D)	107.8
O(5A)–C(22A)–C(23A)	102.3(6)	C(23B)–O(6B)–H(6B)	109.5
O(5A)–C(22A)–H(22A)	111.3		

**2,3,6,9,12,13,19,21-tetrabenzo-1,4,11,14,17,23-hexaoxacyclopentaecosa-
2,6,7,8,12,19,20-hexaene 179**

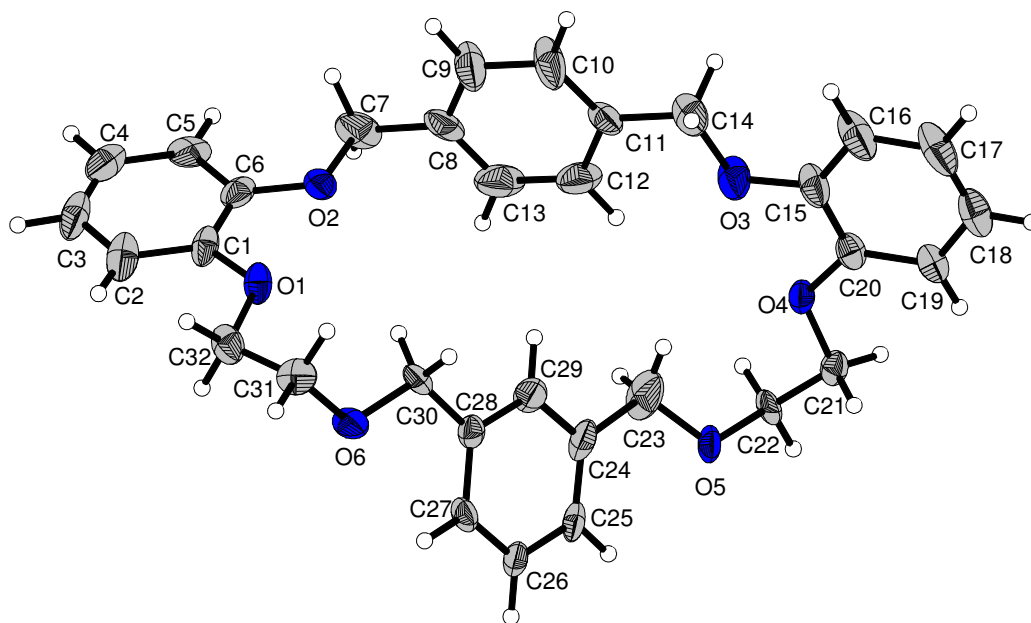


Fig. A 7 X-ray crystal structure of 2,3,6,9,12,13,19,21-tetrabenzo-1,4,11,14,17,23-hexaoxacyclopentaecosa-2,6,7,8,12,19,20-hexaene **179**

Table A 13 Crystal data and structure refinement for **179**

Identification code	gat15	
Empirical formula	C ₃₂ H ₃₂ O ₆	
Formula weight	512.58	
Temperature	100(2) K	
Wavelength	0.71073 Å	
Crystal system	Monoclinic	
Space group	P2 ₁ /n (#14)	
Unit cell dimensions	a = 4.606(3) Å	α = 90°.
	b = 17.852(10) Å	β = 93.071(11)°.
	c = 30.159(16) Å	γ = 90°.
Volume	2476(2) Å ³	
Z	4	
Density (calculated)	1.375 Mg/m ³	
Absorption coefficient	0.094 mm ⁻¹	
F(000)	1088	

Crystal size	0.50 x 0.05 x 0.05 mm ³
Theta range for data collection	1.33 to 19.00°.
Index ranges	-4<=h<=4, -16<=k<=16, -27<=l<=27
Reflections collected	6108
Independent reflections	1979 [R(int) = 0.0606]
Completeness to theta = 19.00°	99.1 %
Absorption correction	Semi-empirical from equivalents
Max. and min. transmission	0.9953 and 0.7304
Refinement method	Full-matrix least-squares on F ²
Data / restraints / parameters	1979 / 348 / 343 ^{a)}
Goodness-of-fit on F ²	1.127
Final R indices [I>2sigma(I)]	R1 = 0.0811, wR2 = 0.1776
R indices (all data)	R1 = 0.1044, wR2 = 0.1868
Largest diff. peak and hole	0.322 and -0.248 e.Å ⁻³

DELU and SIMU restraints were applied to all thermal displacement parameters.

Table A 14 Bond lengths [Å] and angles [°] for **179**

O(1)–C(1)	1.335(8)	C(10)–C(11)	1.347(10)
O(1)–C(32)	1.414(8)	C(10)–H(10)	0.9500
C(1)–C(6)	1.372(10)	C(11)–C(12)	1.370(10)
C(1)–C(2)	1.373(10)	C(11)–C(14)	1.480(10)
C(2)–C(3)	1.354(11)	C(12)–C(13)	1.369(11)
C(2)–H(2)	0.9500	C(12)–H(12)	0.9500
C(3)–C(4)	1.340(12)	C(13)–H(13)	0.9500
C(3)–H(3)	0.9500	C(14)–O(3)	1.404(8)
C(4)–C(5)	1.387(11)	C(14)–H(14A)	0.9900
C(4)–H(4)	0.9500	C(14)–H(14B)	0.9900
C(5)–C(6)	1.362(10)	O(3)–C(15)	1.359(9)
C(5)–H(5)	0.9500	C(15)–C(16)	1.351(10)
C(6)–O(2)	1.360(8)	C(15)–C(20)	1.386(10)
O(2)–C(7)	1.421(9)	C(16)–C(17)	1.362(11)
C(7)–C(8)	1.468(10)	C(16)–H(16)	0.9500
C(7)–H(7A)	0.9900	C(17)–C(18)	1.352(11)
C(7)–H(7B)	0.9900	C(17)–H(17)	0.9500
C(8)–C(9)	1.335(10)	C(18)–C(19)	1.364(10)
C(8)–C(13)	1.364(11)	C(18)–H(18)	0.9500
C(9)–C(10)	1.367(11)	C(19)–C(20)	1.378(9)
C(9)–H(9)	0.9500	C(19)–H(19)	0.9500

Appendix

C(20)–O(4)	1.342(8)	C(3)–C(2)–H(2)	119.8
O(4)–C(21)	1.421(8)	C(1)–C(2)–H(2)	119.8
C(21)–C(22)	1.479(9)	C(4)–C(3)–C(2)	122.1(9)
C(21)–H(21A)	0.9900	C(4)–C(3)–H(3)	119.0
C(21)–H(21B)	0.9900	C(2)–C(3)–H(3)	119.0
C(22)–O(5)	1.402(8)	C(3)–C(4)–C(5)	118.0(9)
C(22)–H(22A)	0.9900	C(3)–C(4)–H(4)	121.0
C(22)–H(22B)	0.9900	C(5)–C(4)–H(4)	121.0
O(5)–C(23)	1.365(8)	C(6)–C(5)–C(4)	120.9(9)
C(23)–C(24)	1.493(10)	C(6)–C(5)–H(5)	119.6
C(23)–H(23A)	0.9900	C(4)–C(5)–H(5)	119.6
C(23)–H(23B)	0.9900	O(2)–C(6)–C(5)	125.4(8)
C(24)–C(25)	1.356(10)	O(2)–C(6)–C(1)	114.5(7)
C(24)–C(29)	1.368(10)	C(5)–C(6)–C(1)	120.1(8)
C(25)–C(26)	1.382(10)	C(6)–O(2)–C(7)	117.4(6)
C(25)–H(25)	0.9500	O(2)–C(7)–C(8)	106.7(6)
C(26)–C(27)	1.362(9)	O(2)–C(7)–H(7A)	110.4
C(26)–H(26)	0.9500	C(8)–C(7)–H(7A)	110.4
C(27)–C(28)	1.372(9)	O(2)–C(7)–H(7B)	110.4
C(27)–H(27)	0.9500	C(8)–C(7)–H(7B)	110.4
C(28)–C(29)	1.381(9)	H(7A)–C(7)–H(7B)	108.6
C(28)–C(30)	1.475(9)	C(9)–C(8)–C(13)	117.4(8)
C(29)–H(29)	0.9500	C(9)–C(8)–C(7)	121.1(8)
C(30)–O(6)	1.407(7)	C(13)–C(8)–C(7)	121.5(8)
C(30)–H(30A)	0.9900	C(8)–C(9)–C(10)	120.6(8)
C(30)–H(30B)	0.9900	C(8)–C(9)–H(9)	119.7
O(6)–C(31)	1.415(8)	C(10)–C(9)–H(9)	119.7
C(31)–C(32)	1.467(10)	C(11)–C(10)–C(9)	123.3(8)
C(31)–H(31A)	0.9900	C(11)–C(10)–H(10)	118.4
C(31)–H(31B)	0.9900	C(9)–C(10)–H(10)	118.4
C(32)–H(32A)	0.9900	C(10)–C(11)–C(12)	116.3(7)
C(32)–H(32B)	0.9900	C(10)–C(11)–C(14)	121.4(7)
		C(12)–C(11)–C(14)	122.3(7)
C(1)–O(1)–C(32)	117.7(6)	C(13)–C(12)–C(11)	120.3(8)
O(1)–C(1)–C(6)	115.7(7)	C(13)–C(12)–H(12)	119.9
O(1)–C(1)–C(2)	125.7(8)	C(11)–C(12)–H(12)	119.9
C(6)–C(1)–C(2)	118.6(8)	C(8)–C(13)–C(12)	122.1(8)
C(3)–C(2)–C(1)	120.4(9)	C(8)–C(13)–H(13)	119.0

Appendix

C(12)–C(13)–H(13)	119.0	H(22A)–C(22)–H(22B)	107.8
O(3)–C(14)–C(11)	108.1(6)	C(23)–O(5)–C(22)	113.8(6)
O(3)–C(14)–H(14A)	110.1	O(5)–C(23)–C(24)	110.4(7)
C(11)–C(14)–H(14A)	110.1	O(5)–C(23)–H(23A)	109.6
O(3)–C(14)–H(14B)	110.1	C(24)–C(23)–H(23A)	109.6
C(11)–C(14)–H(14B)	110.1	O(5)–C(23)–H(23B)	109.6
H(14A)–C(14)–H(14B)	108.4	C(24)–C(23)–H(23B)	109.6
C(15)–O(3)–C(14)	117.9(6)	H(23A)–C(23)–H(23B)	108.1
C(16)–C(15)–O(3)	126.0(7)	C(25)–C(24)–C(29)	118.7(7)
C(16)–C(15)–C(20)	120.9(8)	C(25)–C(24)–C(23)	124.0(7)
O(3)–C(15)–C(20)	113.1(6)	C(29)–C(24)–C(23)	117.2(8)
C(15)–C(16)–C(17)	119.1(8)	C(24)–C(25)–C(26)	120.5(7)
C(15)–C(16)–H(16)	120.4	C(24)–C(25)–H(25)	119.7
C(17)–C(16)–H(16)	120.4	C(26)–C(25)–H(25)	119.7
C(18)–C(17)–C(16)	121.3(8)	C(27)–C(26)–C(25)	120.8(7)
C(18)–C(17)–H(17)	119.4	C(27)–C(26)–H(26)	119.6
C(16)–C(17)–H(17)	119.4	C(25)–C(26)–H(26)	119.6
C(17)–C(18)–C(19)	120.1(8)	C(26)–C(27)–C(28)	118.9(7)
C(17)–C(18)–H(18)	119.9	C(26)–C(27)–H(27)	120.5
C(19)–C(18)–H(18)	119.9	C(28)–C(27)–H(27)	120.5
C(18)–C(19)–C(20)	119.7(8)	C(27)–C(28)–C(29)	119.8(7)
C(18)–C(19)–H(19)	120.2	C(27)–C(28)–C(30)	122.1(6)
C(20)–C(19)–H(19)	120.2	C(29)–C(28)–C(30)	118.1(7)
O(4)–C(20)–C(19)	125.9(7)	C(24)–C(29)–C(28)	121.2(7)
O(4)–C(20)–C(15)	115.3(6)	C(24)–C(29)–H(29)	119.4
C(19)–C(20)–C(15)	118.8(7)	C(28)–C(29)–H(29)	119.4
C(20)–O(4)–C(21)	118.3(5)	O(6)–C(30)–C(28)	110.9(6)
O(4)–C(21)–C(22)	108.0(5)	O(6)–C(30)–H(30A)	109.5
O(4)–C(21)–H(21A)	110.1	C(28)–C(30)–H(30A)	109.5
C(22)–C(21)–H(21A)	110.1	O(6)–C(30)–H(30B)	109.5
O(4)–C(21)–H(21B)	110.1	C(28)–C(30)–H(30B)	109.5
C(22)–C(21)–H(21B)	110.1	H(30A)–C(30)–H(30B)	108.1
H(21A)–C(21)–H(21B)	108.4	C(30)–O(6)–C(31)	113.9(5)
O(5)–C(22)–C(21)	113.1(6)	O(6)–C(31)–C(32)	112.9(6)
O(5)–C(22)–H(22A)	109.0	O(6)–C(31)–H(31A)	109.0
C(21)–C(22)–H(22A)	109.0	C(32)–C(31)–H(31A)	109.0
O(5)–C(22)–H(22B)	109.0	O(6)–C(31)–H(31B)	109.0
C(21)–C(22)–H(22B)	109.0	C(32)–C(31)–H(31B)	109.0

Appendix

H(31A)–C(31)–H(31B)	107.8	O(1)–C(32)–H(32B)	110.2
O(1)–C(32)–C(31)	107.7(6)	C(31)–C(32)–H(32B)	110.2
O(1)–C(32)–H(32A)	110.2	<u>H(32A)–C(32)–H(32B)</u>	<u>108.5</u>
<u>C(31)–C(32)–H(32A)</u>	<u>110.2</u>		

2,3,6,8,11,12,18,20-tetrabenzo-7,19-diaza-1,4,10,13,16,22-hexaoxacyclo-tetraeicosa-2,6,7,11,18,19-hexaene 184

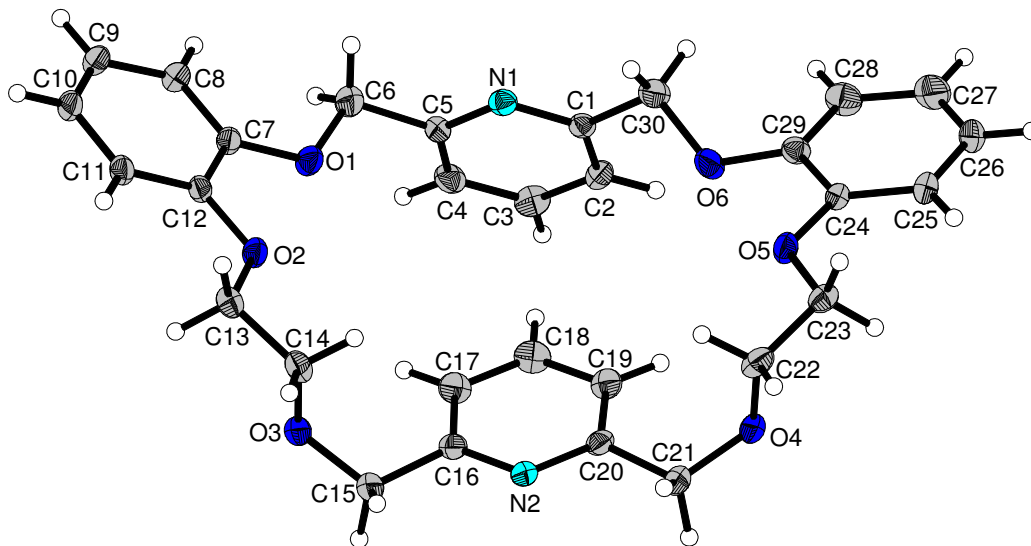


Fig. A 8 X-ray crystal structure of 2,3,6,8,11,12,18,20-tetrabenzo-7,19-diaza-1,4,10,13,16,22-hexaoxacyclo-tetraeicosa-2,6,7,11,18,19-hexaene **184**

Table A 15 Crystal data and structure refinement for **184**

Identification code	gat21	
Empirical formula	$C_{30} H_{30} N_2 O_6$	
Formula weight	514.56	
Temperature	293(2) K	
Wavelength	0.71073 Å	
Crystal system	Monoclinic	
Space group	$P2_1$ (#4)	
Unit cell dimensions	$a = 15.080(2)$ Å	$\alpha = 90^\circ$.
	$b = 5.4720(8)$ Å	$\beta = 113.695(3)^\circ$.
	$c = 17.191(2)$ Å	$\gamma = 90^\circ$.
Volume	$1299.0(3)$ Å ³	
Z	2	
Density (calculated)	1.316 Mg/m ³	
Absorption coefficient	0.092 mm ⁻¹	
F(000)	544	
Crystal size	0.50 x 0.30 x 0.20 mm ³	

Theta range for data collection	1.29 to 24.11°
Index ranges	-17<=h<=17, -6<=k<=6, -19<=l<=19
Reflections collected	9612
Independent reflections	2314 [R(int) = 0.0233]
Completeness to theta = 24.11°	99.9 %
Absorption correction	Semi-empirical from equivalents
Max. and min. transmission	0.9818 and 0.8775
Refinement method	Full-matrix least-squares on F ²
Data / restraints / parameters	2314 / 97 / 343 ^{a)}
Goodness-of-fit on F ²	1.037
Final R indices [I>2sigma(I)]	R1 = 0.0385, wR2 = 0.0973
R indices (all data)	R1 = 0.0423, wR2 = 0.1006
Largest diff. peak and hole	0.336 and -0.209 e.Å ⁻³

DELU (rigid bond) restraints were applied to all thermal displacement parameters.

Table A 16 Bond lengths [Å] and angles [°] for **184**

N(1)–C(1)	1.329(3)	C(10)–H(10)	0.9300
N(1)–C(5)	1.347(4)	C(11)–C(12)	1.378(4)
C(1)–C(2)	1.379(4)	C(11)–H(11)	0.9300
C(1)–C(30)	1.499(4)	C(12)–O(2)	1.367(3)
C(2)–C(3)	1.362(5)	O(2)–C(13)	1.425(4)
C(2)–H(2)	0.9300	C(13)–C(14)	1.482(4)
C(3)–C(4)	1.370(5)	C(13)–H(13A)	0.9700
C(3)–H(3)	0.9300	C(13)–H(13B)	0.9700
C(4)–C(5)	1.356(5)	C(14)–O(3)	1.410(4)
C(4)–H(4)	0.9300	C(14)–H(14A)	0.9700
C(5)–C(6)	1.473(4)	C(14)–H(14B)	0.9700
C(6)–O(1)	1.405(4)	O(3)–C(15)	1.422(3)
C(6)–H(6A)	0.9700	C(15)–C(16)	1.507(4)
C(6)–H(6B)	0.9700	C(15)–H(15A)	0.9700
O(1)–C(7)	1.376(3)	C(15)–H(15B)	0.9700
C(7)–C(8)	1.379(4)	C(16)–N(2)	1.336(4)
C(7)–C(12)	1.393(4)	C(16)–C(17)	1.381(5)
C(8)–C(9)	1.388(5)	N(2)–C(20)	1.337(4)
C(8)–H(8)	0.9300	C(17)–C(18)	1.362(5)
C(9)–C(10)	1.361(6)	C(17)–H(17)	0.9300
C(9)–H(9)	0.9300	C(18)–C(19)	1.372(5)
C(10)–C(11)	1.382(4)	C(18)–H(18)	0.9300

Appendix

C(19)–C(20)	1.379(4)	C(4)–C(3)–H(3)	120.4
C(19)–H(19)	0.9300	C(5)–C(4)–C(3)	118.9(3)
C(20)–C(21)	1.508(4)	C(5)–C(4)–H(4)	120.6
C(21)–O(4)	1.419(4)	C(3)–C(4)–H(4)	120.6
C(21)–H(21A)	0.9700	N(1)–C(5)–C(4)	123.0(3)
C(21)–H(21B)	0.9700	N(1)–C(5)–C(6)	118.4(4)
O(4)–C(22)	1.406(4)	C(4)–C(5)–C(6)	118.5(4)
C(22)–C(23)	1.485(4)	O(1)–C(6)–C(5)	110.5(3)
C(22)–H(22A)	0.9700	O(1)–C(6)–H(6A)	109.5
C(22)–H(22B)	0.9700	C(5)–C(6)–H(6A)	109.5
C(23)–O(5)	1.426(4)	O(1)–C(6)–H(6B)	109.5
C(23)–H(23A)	0.9700	C(5)–C(6)–H(6B)	109.5
C(23)–H(23B)	0.9700	H(6A)–C(6)–H(6B)	108.1
O(5)–C(24)	1.357(4)	C(7)–O(1)–C(6)	118.0(2)
C(24)–C(25)	1.384(4)	O(1)–C(7)–C(8)	124.3(3)
C(24)–C(29)	1.388(4)	O(1)–C(7)–C(12)	116.4(2)
C(25)–C(26)	1.374(6)	C(8)–C(7)–C(12)	119.3(3)
C(25)–H(25)	0.9300	C(7)–C(8)–C(9)	120.2(4)
C(26)–C(27)	1.348(7)	C(7)–C(8)–H(8)	119.9
C(26)–H(26)	0.9300	C(9)–C(8)–H(8)	119.9
C(27)–C(28)	1.387(6)	C(10)–C(9)–C(8)	120.3(3)
C(27)–H(27)	0.9300	C(10)–C(9)–H(9)	119.8
C(28)–C(29)	1.370(5)	C(8)–C(9)–H(9)	119.8
C(28)–H(28)	0.9300	C(9)–C(10)–C(11)	120.1(3)
C(29)–O(6)	1.360(3)	C(9)–C(10)–H(10)	120.0
O(6)–C(30)	1.417(4)	C(11)–C(10)–H(10)	120.0
C(30)–H(30A)	0.9700	C(12)–C(11)–C(10)	120.2(3)
C(30)–H(30B)	0.9700	C(12)–C(11)–H(11)	119.9
		C(10)–C(11)–H(11)	119.9
C(1)–N(1)–C(5)	117.4(3)	O(2)–C(12)–C(11)	124.7(3)
N(1)–C(1)–C(2)	122.4(3)	O(2)–C(12)–C(7)	115.4(2)
N(1)–C(1)–C(30)	116.7(3)	C(11)–C(12)–C(7)	119.9(3)
C(2)–C(1)–C(30)	120.8(3)	C(12)–O(2)–C(13)	117.8(2)
C(3)–C(2)–C(1)	119.0(3)	O(2)–C(13)–C(14)	108.1(2)
C(3)–C(2)–H(2)	120.5	O(2)–C(13)–H(13A)	110.1
C(1)–C(2)–H(2)	120.5	C(14)–C(13)–H(13A)	110.1
C(2)–C(3)–C(4)	119.2(3)	O(2)–C(13)–H(13B)	110.1
C(2)–C(3)–H(3)	120.4	C(14)–C(13)–H(13B)	110.1

Appendix

H(13A)–C(13)–H(13B)	108.4	O(4)–C(22)–H(22A)	109.8
O(3)–C(14)–C(13)	110.2(3)	C(23)–C(22)–H(22A)	109.8
O(3)–C(14)–H(14A)	109.6	O(4)–C(22)–H(22B)	109.8
C(13)–C(14)–H(14A)	109.6	C(23)–C(22)–H(22B)	109.8
O(3)–C(14)–H(14B)	109.6	H(22A)–C(22)–H(22B)	108.3
C(13)–C(14)–H(14B)	109.6	O(5)–C(23)–C(22)	107.2(3)
H(14A)–C(14)–H(14B)	108.1	O(5)–C(23)–H(23A)	110.3
C(14)–O(3)–C(15)	111.5(3)	C(22)–C(23)–H(23A)	110.3
O(3)–C(15)–C(16)	112.8(3)	O(5)–C(23)–H(23B)	110.3
O(3)–C(15)–H(15A)	109.0	C(22)–C(23)–H(23B)	110.3
C(16)–C(15)–H(15A)	109.0	H(23A)–C(23)–H(23B)	108.5
O(3)–C(15)–H(15B)	109.0	C(24)–O(5)–C(23)	118.9(2)
C(16)–C(15)–H(15B)	109.0	O(5)–C(24)–C(25)	125.3(3)
H(15A)–C(15)–H(15B)	107.8	O(5)–C(24)–C(29)	115.3(2)
N(2)–C(16)–C(17)	122.8(3)	C(25)–C(24)–C(29)	119.3(3)
N(2)–C(16)–C(15)	115.0(3)	C(26)–C(25)–C(24)	120.1(4)
C(17)–C(16)–C(15)	122.2(3)	C(26)–C(25)–H(25)	120.0
C(16)–N(2)–C(20)	117.8(3)	C(24)–C(25)–H(25)	120.0
C(18)–C(17)–C(16)	118.6(3)	C(27)–C(26)–C(25)	120.9(3)
C(18)–C(17)–H(17)	120.7	C(27)–C(26)–H(26)	119.6
C(16)–C(17)–H(17)	120.7	C(25)–C(26)–H(26)	119.6
C(17)–C(18)–C(19)	119.7(3)	C(26)–C(27)–C(28)	119.6(4)
C(17)–C(18)–H(18)	120.2	C(26)–C(27)–H(27)	120.2
C(19)–C(18)–H(18)	120.2	C(28)–C(27)–H(27)	120.2
C(18)–C(19)–C(20)	118.6(3)	C(29)–C(28)–C(27)	120.8(4)
C(18)–C(19)–H(19)	120.7	C(29)–C(28)–H(28)	119.6
C(20)–C(19)–H(19)	120.7	C(27)–C(28)–H(28)	119.6
N(2)–C(20)–C(19)	122.5(3)	O(6)–C(29)–C(28)	124.4(3)
N(2)–C(20)–C(21)	114.5(3)	O(6)–C(29)–C(24)	116.1(3)
C(19)–C(20)–C(21)	122.9(3)	C(28)–C(29)–C(24)	119.3(3)
O(4)–C(21)–C(20)	112.8(3)	C(29)–O(6)–C(30)	119.6(2)
O(4)–C(21)–H(21A)	109.0	O(6)–C(30)–C(1)	108.2(2)
C(20)–C(21)–H(21A)	109.0	O(6)–C(30)–H(30A)	110.1
O(4)–C(21)–H(21B)	109.0	C(1)–C(30)–H(30A)	110.1
C(20)–C(21)–H(21B)	109.0	O(6)–C(30)–H(30B)	110.1
H(21A)–C(21)–H(21B)	107.8	C(1)–C(30)–H(30B)	110.1
C(22)–O(4)–C(21)	113.4(3)	H(30A)–C(30)–H(30B)	108.4
O(4)–C(22)–C(23)	109.3(3)		

**2,3,6,8,11,12,18,20-tetrabenzo-19-aza-1,4,10,13,16,22-hexaoxacyclotetraeicosa-
2,6,7,11,18,19-hexaene 176**

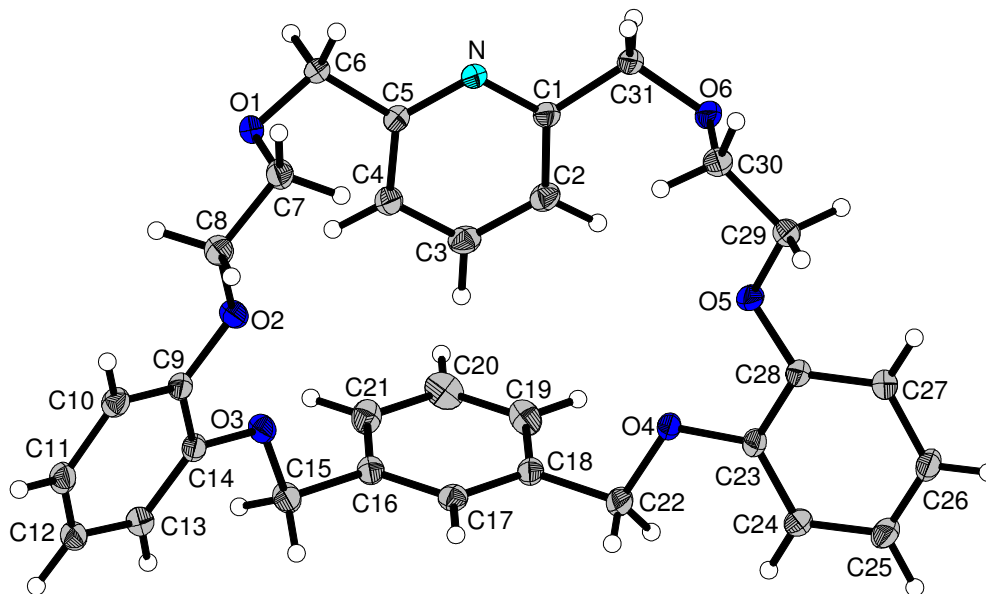


Fig. A 9 X-ray crystal structure of 2,3,6,8,11,12,18,20-tetrabenzo-19-aza-1,4,10,13,16,22-hexaoxacyclotetraeicosa-2,6,7,11,18,19-hexaene **176**

Table A 17 Crystal data and structure refinement for **176**

Identification code	gat23
Empirical formula	C ₃₁ H ₃₁ N O ₆
Formula weight	513.57
Temperature	100(2) K
Wavelength	0.71073 Å
Crystal system	Monoclinic
Space group	P2 ₁ (#4)
Unit cell dimensions	a = 14.6295(9) Å α = 90°. b = 5.2396(3) Å β = 107.767(1)°. c = 17.8162(11) Å γ = 90°.
Volume	1300.53(14) Å ³
Z	2
Density (calculated)	1.311 Mg/m ³
Absorption coefficient	0.091 mm ⁻¹
F(000)	544

Crystal size	0.5 x 0.2 x 0.2 mm ³
Theta range for data collection	1.46 to 30.52°.
Index ranges	-20<=h<=20, -7<=k<=7, -25<=l<=23
Reflections collected	15434
Independent reflections	4361 [R(int) = 0.0242]
Completeness to theta = 30.52°	99.3 %
Absorption correction	Semi-empirical from equivalents
Max. and min. transmission	0.9821 and 0.8246
Refinement method	Full-matrix least-squares on F ²
Data / restraints / parameters	4361 / 1 / 343
Goodness-of-fit on F ²	1.031
Final R indices [I>2sigma(I)]	R1 = 0.0420, wR2 = 0.1029
R indices (all data)	R1 = 0.0452, wR2 = 0.1052
Largest diff. peak and hole	0.361 and -0.216 e.Å ⁻³

Table A 18 Bond lengths [Å] and angles [°] for **176**

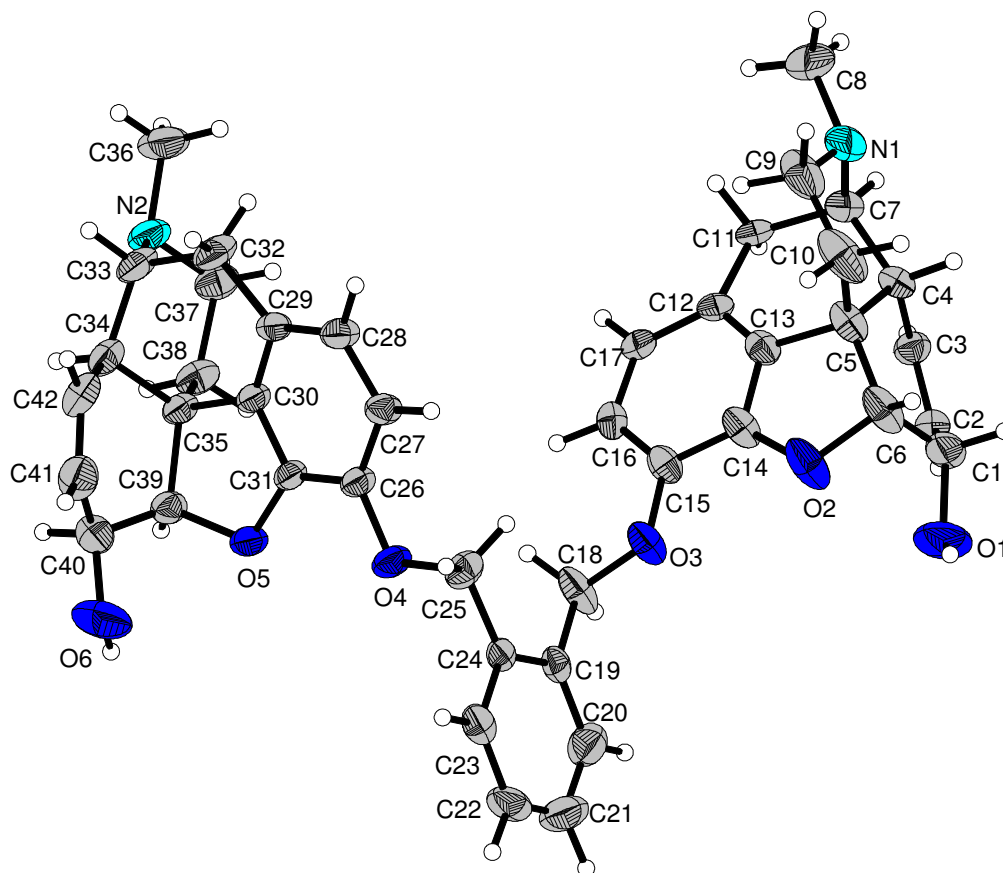
N-C(5)	1.341(2)	C(9)-C(10)	1.388(2)
N-C(1)	1.3412(19)	C(9)-C(14)	1.412(2)
C(1)-C(2)	1.392(2)	C(10)-C(11)	1.403(2)
C(1)-C(31)	1.508(2)	C(10)-H(10)	0.9500
C(2)-C(3)	1.386(2)	C(11)-C(12)	1.375(3)
C(2)-H(2)	0.9500	C(11)-H(11)	0.9500
C(3)-C(4)	1.385(2)	C(12)-C(13)	1.401(2)
C(3)-H(3)	0.9500	C(12)-H(12)	0.9500
C(4)-C(5)	1.389(2)	C(13)-C(14)	1.389(2)
C(4)-H(4)	0.9500	C(13)-H(13)	0.9500
C(5)-C(6)	1.511(2)	C(14)-O(3)	1.3689(18)
C(6)-O(1)	1.4206(18)	O(3)-C(15)	1.4390(19)
C(6)-H(6A)	0.9900	C(15)-C(16)	1.501(2)
C(6)-H(6B)	0.9900	C(15)-H(15A)	0.9900
O(1)-C(7)	1.423(2)	C(15)-H(15B)	0.9900
C(7)-C(8)	1.503(2)	C(16)-C(21)	1.388(3)
C(7)-H(7A)	0.9900	C(16)-C(17)	1.396(2)
C(7)-H(7B)	0.9900	C(17)-C(18)	1.393(2)
C(8)-O(2)	1.4331(19)	C(17)-H(17)	0.9500
C(8)-H(8A)	0.9900	C(18)-C(19)	1.392(3)
C(8)-H(8B)	0.9900	C(18)-C(22)	1.499(2)
O(2)-C(9)	1.3647(18)	C(19)-C(20)	1.378(3)

Appendix

C(19)–H(19)	0.9500	C(4)–C(3)–H(3)	120.2
C(20)–C(21)	1.390(2)	C(2)–C(3)–H(3)	120.2
C(20)–H(20)	0.9500	C(3)–C(4)–C(5)	118.11(15)
C(21)–H(21)	0.9500	C(3)–C(4)–H(4)	120.9
C(22)–O(4)	1.4310(19)	C(5)–C(4)–H(4)	120.9
C(22)–H(22A)	0.9900	N–C(5)–C(4)	123.15(14)
C(22)–H(22B)	0.9900	N–C(5)–C(6)	115.32(14)
O(4)–C(23)	1.3719(18)	C(4)–C(5)–C(6)	121.52(14)
C(23)–C(24)	1.390(2)	O(1)–C(6)–C(5)	112.37(12)
C(23)–C(28)	1.406(2)	O(1)–C(6)–H(6A)	109.1
C(24)–C(25)	1.396(2)	C(5)–C(6)–H(6A)	109.1
C(24)–H(24)	0.9500	O(1)–C(6)–H(6B)	109.1
C(25)–C(26)	1.371(3)	C(5)–C(6)–H(6B)	109.1
C(25)–H(25)	0.9500	H(6A)–C(6)–H(6B)	107.9
C(26)–C(27)	1.401(2)	C(6)–O(1)–C(7)	111.77(13)
C(26)–H(26)	0.9500	O(1)–C(7)–C(8)	108.83(14)
C(27)–C(28)	1.387(2)	O(1)–C(7)–H(7A)	109.9
C(27)–H(27)	0.9500	C(8)–C(7)–H(7A)	109.9
C(28)–O(5)	1.3678(17)	O(1)–C(7)–H(7B)	109.9
O(5)–C(29)	1.4315(19)	C(8)–C(7)–H(7B)	109.9
C(29)–C(30)	1.503(2)	H(7A)–C(7)–H(7B)	108.3
C(29)–H(29A)	0.9900	O(2)–C(8)–C(7)	107.40(13)
C(29)–H(29B)	0.9900	O(2)–C(8)–H(8A)	110.2
C(30)–O(6)	1.421(2)	C(7)–C(8)–H(8A)	110.2
C(30)–H(30A)	0.9900	O(2)–C(8)–H(8B)	110.2
C(30)–H(30B)	0.9900	C(7)–C(8)–H(8B)	110.2
O(6)–C(31)	1.4248(18)	H(8A)–C(8)–H(8B)	108.5
C(31)–H(31A)	0.9900	C(9)–O(2)–C(8)	116.03(12)
C(31)–H(31B)	0.9900	O(2)–C(9)–C(10)	124.56(15)
		O(2)–C(9)–C(14)	115.54(13)
C(5)–N–C(1)	118.05(13)	C(10)–C(9)–C(14)	119.91(14)
N–C(1)–C(2)	122.73(14)	C(9)–C(10)–C(11)	120.21(16)
N–C(1)–C(31)	114.71(13)	C(9)–C(10)–H(10)	119.9
C(2)–C(1)–C(31)	122.55(14)	C(11)–C(10)–H(10)	119.9
C(3)–C(2)–C(1)	118.35(14)	C(12)–C(11)–C(10)	119.89(15)
C(3)–C(2)–H(2)	120.8	C(12)–C(11)–H(11)	120.1
C(1)–C(2)–H(2)	120.8	C(10)–C(11)–H(11)	120.1
C(4)–C(3)–C(2)	119.60(15)	C(11)–C(12)–C(13)	120.36(15)

Appendix

C(11)–C(12)–H(12)	119.8	H(22A)–C(22)–H(22B)	108.3
C(13)–C(12)–H(12)	119.8	C(23)–O(4)–C(22)	115.90(12)
C(14)–C(13)–C(12)	120.36(16)	O(4)–C(23)–C(24)	124.50(14)
C(14)–C(13)–H(13)	119.8	O(4)–C(23)–C(28)	116.34(13)
C(12)–C(13)–H(13)	119.8	C(24)–C(23)–C(28)	119.14(14)
O(3)–C(14)–C(13)	124.90(15)	C(23)–C(24)–C(25)	120.54(16)
O(3)–C(14)–C(9)	115.90(13)	C(23)–C(24)–H(24)	119.7
C(13)–C(14)–C(9)	119.19(14)	C(25)–C(24)–H(24)	119.7
C(14)–O(3)–C(15)	116.27(12)	C(26)–C(25)–C(24)	120.40(15)
O(3)–C(15)–C(16)	108.33(12)	C(26)–C(25)–H(25)	119.8
O(3)–C(15)–H(15A)	110.0	C(24)–C(25)–H(25)	119.8
C(16)–C(15)–H(15A)	110.0	C(25)–C(26)–C(27)	119.70(15)
O(3)–C(15)–H(15B)	110.0	C(25)–C(26)–H(26)	120.1
C(16)–C(15)–H(15B)	110.0	C(27)–C(26)–H(26)	120.1
H(15A)–C(15)–H(15B)	108.4	C(28)–C(27)–C(26)	120.47(16)
C(21)–C(16)–C(17)	119.40(15)	C(28)–C(27)–H(27)	119.8
C(21)–C(16)–C(15)	119.92(15)	C(26)–C(27)–H(27)	119.8
C(17)–C(16)–C(15)	120.68(16)	O(5)–C(28)–C(27)	124.64(14)
C(18)–C(17)–C(16)	120.79(16)	O(5)–C(28)–C(23)	115.61(13)
C(18)–C(17)–H(17)	119.6	C(27)–C(28)–C(23)	119.74(14)
C(16)–C(17)–H(17)	119.6	C(28)–O(5)–C(29)	116.41(12)
C(19)–C(18)–C(17)	119.03(16)	O(5)–C(29)–C(30)	107.29(13)
C(19)–C(18)–C(22)	119.25(16)	O(5)–C(29)–H(29A)	110.3
C(17)–C(18)–C(22)	121.69(18)	C(30)–C(29)–H(29A)	110.3
C(20)–C(19)–C(18)	120.26(16)	O(5)–C(29)–H(29B)	110.3
C(20)–C(19)–H(19)	119.9	C(30)–C(29)–H(29B)	110.3
C(18)–C(19)–H(19)	119.9	H(29A)–C(29)–H(29B)	108.5
C(19)–C(20)–C(21)	120.78(18)	O(6)–C(30)–C(29)	109.29(14)
C(19)–C(20)–H(20)	119.6	O(6)–C(30)–H(30A)	109.8
C(21)–C(20)–H(20)	119.6	C(29)–C(30)–H(30A)	109.8
C(16)–C(21)–C(20)	119.73(16)	O(6)–C(30)–H(30B)	109.8
C(16)–C(21)–H(21)	120.1	C(29)–C(30)–H(30B)	109.8
C(20)–C(21)–H(21)	120.1	H(30A)–C(30)–H(30B)	108.3
O(4)–C(22)–C(18)	108.86(13)	C(30)–O(6)–C(31)	110.96(13)
O(4)–C(22)–H(22A)	109.9	O(6)–C(31)–C(1)	112.93(12)
C(18)–C(22)–H(22A)	109.9	O(6)–C(31)–H(31A)	109.0
O(4)–C(22)–H(22B)	109.9	C(1)–C(31)–H(31A)	109.0
C(18)–C(22)–H(22B)	109.9	O(6)–C(31)–H(31B)	109.0

1,2-Bis(3-morphinyl)-*o*-xylene **200**Fig. A 10 X-ray crystal structure of 1,2-Bis(3-morphinyl)-*o*-xylene **200**Table A 19 Crystal data and structure refinement for **200**

Identification code	gat22	
Empirical formula	C ₄₂ H ₄₈ N ₂ O ₈	
Molecular formula	C ₄₂ H ₄₄ N ₂ O ₆ x 2 (H ₂ O)	
Formula weight	708.82	
Temperature	100(2) K	
Wavelength	0.71073 Å	
Crystal system	Orthorhombic	
Space group	P2 ₁ 2 ₁ 2 ₁ (#19)	
Unit cell dimensions	a = 10.6944(15) Å	α = 90°.
	b = 16.220(2) Å	β = 90°.
	c = 19.964(3) Å	γ = 90°.
Volume	3463.0(9) Å ³	
Z	4	

Density (calculated)	1.360 Mg/m ³
Absorption coefficient	0.094 mm ⁻¹
F(000)	1512
Crystal size	0.50 x 0.40 x 0.03 mm ³
Theta range for data collection	1.62 to 19.91°.
Index ranges	-9<=h<=10, -13<=k<=15, -19<=l<=14
Reflections collected	11758
Independent reflections	1835 [R(int) = 0.0708]
Completeness to theta = 19.91°	99.7 %
Absorption correction	Semi-empirical from equivalents
Max. and min. transmission	0.9972 and 0.3887
Refinement method	Full-matrix least-squares on F ²
Data / restraints / parameters	1835 / 156 / 469 ^{a)}
Goodness-of-fit on F ²	1.045
Final R indices [I>2sigma(I)]	R1 = 0.0434, wR2 = 0.1113
R indices (all data)	R1 = 0.0541, wR2 = 0.1205
Largest diff. peak and hole	0.249 and -0.186 e.Å ⁻³

^{a)} DELU (rigid bond) restraints were applied to all thermal displacement parameters.

Table A 20 Bond lengths [Å] and angles [°] for **200**

O(1)–C(1)	1.426(8)	C(7)–N(1)	1.486(8)
O(1)–H(1O1)	0.8400	C(7)–C(11)	1.551(8)
C(1)–C(2)	1.477(10)	C(7)–H(7)	1.0000
C(1)–C(6)	1.516(10)	N(1)–C(9)	1.452(9)
C(1)–H(1A)	1.0000	N(1)–C(8)	1.463(9)
C(2)–C(3)	1.306(8)	C(8)–H(8A)	0.9800
C(2)–H(2)	0.9500	C(8)–H(8B)	0.9800
C(3)–C(4)	1.485(9)	C(8)–H(8C)	0.9800
C(3)–H(3)	0.9500	C(9)–C(10)	1.503(10)
C(4)–C(5)	1.531(9)	C(9)–H(9A)	0.9900
C(4)–C(7)	1.531(8)	C(9)–H(9B)	0.9900
C(4)–H(4)	1.0000	C(10)–H(10A)	0.9900
C(5)–C(13)	1.500(8)	C(10)–H(10B)	0.9900
C(5)–C(10)	1.524(9)	C(11)–C(12)	1.499(8)
C(5)–C(6)	1.558(9)	C(11)–H(11A)	0.9900
C(6)–O(2)	1.472(8)	C(11)–H(11B)	0.9900
C(6)–H(6A)	1.0000	C(12)–C(13)	1.362(8)
O(2)–C(14)	1.377(7)	C(12)–C(17)	1.381(8)

Appendix

C(13)–C(14)	1.386(8)	C(32)–C(33)	1.548(9)
C(14)–C(15)	1.366(8)	C(32)–H(32A)	0.9900
C(15)–C(16)	1.387(8)	C(32)–H(32B)	0.9900
C(15)–O(3)	1.397(7)	C(33)–N(2)	1.472(9)
O(3)–C(18)	1.435(7)	C(33)–C(34)	1.532(8)
C(16)–C(17)	1.400(8)	C(33)–H(33)	1.0000
C(16)–H(16)	0.9500	C(34)–C(42)	1.492(9)
C(17)–H(17)	0.9500	C(34)–C(35)	1.532(9)
C(18)–C(19)	1.504(8)	C(34)–H(34)	1.0000
C(18)–H(18A)	0.9900	C(35)–C(38)	1.526(9)
C(18)–H(18B)	0.9900	C(35)–C(39)	1.571(8)
C(19)–C(24)	1.376(8)	N(2)–C(37)	1.463(8)
C(19)–C(20)	1.388(9)	N(2)–C(36)	1.471(8)
C(20)–C(21)	1.375(10)	C(36)–H(36A)	0.9800
C(20)–H(20)	0.9500	C(36)–H(36B)	0.9800
C(21)–C(22)	1.361(11)	C(36)–H(36C)	0.9800
C(21)–H(21)	0.9500	C(37)–C(38)	1.531(8)
C(22)–C(23)	1.377(9)	C(37)–H(37A)	0.9900
C(22)–H(22)	0.9500	C(37)–H(37B)	0.9900
C(23)–C(24)	1.392(8)	C(38)–H(38A)	0.9900
C(23)–H(23)	0.9500	C(38)–H(38B)	0.9900
C(24)–C(25)	1.486(8)	C(39)–C(40)	1.493(9)
C(25)–O(4)	1.434(7)	C(39)–H(39)	1.0000
C(25)–H(25A)	0.9900	C(40)–O(6)	1.413(8)
C(25)–H(25B)	0.9900	C(40)–C(41)	1.476(10)
O(4)–C(26)	1.372(7)	C(40)–H(40)	1.0000
C(26)–C(27)	1.381(8)	O(6)–H(106)	0.8400
C(26)–C(31)	1.383(8)	C(41)–C(42)	1.314(9)
C(27)–C(28)	1.384(8)	C(41)–H(41)	0.9500
C(27)–H(27)	0.9500	C(42)–H(42)	0.9500
C(28)–C(29)	1.388(8)	O(7)–H(107)	0.8206
C(28)–H(28)	0.9500	O(7)–H(207)	0.8406
C(29)–C(30)	1.373(8)	O(8)–H(108)	0.8610
C(29)–C(32)	1.495(8)	O(8)–H(208)	0.8561
C(30)–C(31)	1.375(7)		
C(30)–C(35)	1.484(8)	C(1)–O(1)–H(101)	109.5
C(31)–O(5)	1.365(7)	O(1)–C(1)–C(2)	109.6(6)
O(5)–C(39)	1.465(7)	O(1)–C(1)–C(6)	110.3(6)

C(2)–C(1)–C(6)	114.2(5)	N(1)–C(8)–H(8A)	109.5
O(1)–C(1)–H(1A)	107.5	N(1)–C(8)–H(8B)	109.5
C(2)–C(1)–H(1A)	107.5	H(8A)–C(8)–H(8B)	109.5
C(6)–C(1)–H(1A)	107.5	N(1)–C(8)–H(8C)	109.5
C(3)–C(2)–C(1)	121.2(7)	H(8A)–C(8)–H(8C)	109.5
C(3)–C(2)–H(2)	119.4	H(8B)–C(8)–H(8C)	109.5
C(1)–C(2)–H(2)	119.4	N(1)–C(9)–C(10)	110.8(6)
C(2)–C(3)–C(4)	121.2(6)	N(1)–C(9)–H(9A)	109.5
C(2)–C(3)–H(3)	119.4	C(10)–C(9)–H(9A)	109.5
C(4)–C(3)–H(3)	119.4	N(1)–C(9)–H(9B)	109.5
C(3)–C(4)–C(5)	109.5(5)	C(10)–C(9)–H(9B)	109.5
C(3)–C(4)–C(7)	114.1(5)	H(9A)–C(9)–H(9B)	108.1
C(5)–C(4)–C(7)	107.7(5)	C(9)–C(10)–C(5)	111.8(6)
C(3)–C(4)–H(4)	108.5	C(9)–C(10)–H(10A)	109.3
C(5)–C(4)–H(4)	108.5	C(5)–C(10)–H(10A)	109.3
C(7)–C(4)–H(4)	108.5	C(9)–C(10)–H(10B)	109.3
C(13)–C(5)–C(10)	112.2(6)	C(5)–C(10)–H(10B)	109.3
C(13)–C(5)–C(4)	106.5(5)	H(10A)–C(10)–H(10B)	107.9
C(10)–C(5)–C(4)	108.4(5)	C(12)–C(11)–C(7)	115.0(5)
C(13)–C(5)–C(6)	100.4(5)	C(12)–C(11)–H(11A)	108.5
C(10)–C(5)–C(6)	113.3(6)	C(7)–C(11)–H(11A)	108.5
C(4)–C(5)–C(6)	115.7(6)	C(12)–C(11)–H(11B)	108.5
O(2)–C(6)–C(1)	110.5(6)	C(7)–C(11)–H(11B)	108.5
O(2)–C(6)–C(5)	106.0(5)	H(11A)–C(11)–H(11B)	107.5
C(1)–C(6)–C(5)	113.3(5)	C(13)–C(12)–C(17)	115.9(5)
O(2)–C(6)–H(6A)	109.0	C(13)–C(12)–C(11)	118.4(5)
C(1)–C(6)–H(6A)	109.0	C(17)–C(12)–C(11)	125.1(6)
C(5)–C(6)–H(6A)	109.0	C(12)–C(13)–C(14)	122.7(6)
C(14)–O(2)–C(6)	107.3(4)	C(12)–C(13)–C(5)	127.0(5)
N(1)–C(7)–C(4)	105.7(5)	C(14)–C(13)–C(5)	109.8(6)
N(1)–C(7)–C(11)	115.7(5)	C(15)–C(14)–O(2)	126.5(5)
C(4)–C(7)–C(11)	112.4(5)	C(15)–C(14)–C(13)	121.2(6)
N(1)–C(7)–H(7)	107.6	O(2)–C(14)–C(13)	112.2(5)
C(4)–C(7)–H(7)	107.6	C(14)–C(15)–C(16)	117.0(6)
C(11)–C(7)–H(7)	107.6	C(14)–C(15)–O(3)	117.6(5)
C(9)–N(1)–C(8)	111.0(6)	C(16)–C(15)–O(3)	125.4(5)
C(9)–N(1)–C(7)	112.5(5)	C(15)–O(3)–C(18)	116.3(5)
C(8)–N(1)–C(7)	111.2(6)	C(15)–C(16)–C(17)	120.6(6)

C(15)–C(16)–H(16)	119.7	C(27)–C(26)–C(31)	117.7(5)
C(17)–C(16)–H(16)	119.7	C(26)–C(27)–C(28)	120.8(6)
C(12)–C(17)–C(16)	121.9(6)	C(26)–C(27)–H(27)	119.6
C(12)–C(17)–H(17)	119.1	C(28)–C(27)–H(27)	119.6
C(16)–C(17)–H(17)	119.1	C(27)–C(28)–C(29)	121.0(6)
O(3)–C(18)–C(19)	109.2(5)	C(27)–C(28)–H(28)	119.5
O(3)–C(18)–H(18A)	109.8	C(29)–C(28)–H(28)	119.5
C(19)–C(18)–H(18A)	109.8	C(30)–C(29)–C(28)	117.4(5)
O(3)–C(18)–H(18B)	109.8	C(30)–C(29)–C(32)	117.6(5)
C(19)–C(18)–H(18B)	109.8	C(28)–C(29)–C(32)	124.1(5)
H(18A)–C(18)–H(18B)	108.3	C(29)–C(30)–C(31)	121.4(5)
C(24)–C(19)–C(20)	119.5(6)	C(29)–C(30)–C(35)	127.1(5)
C(24)–C(19)–C(18)	120.7(5)	C(31)–C(30)–C(35)	110.4(5)
C(20)–C(19)–C(18)	119.5(6)	O(5)–C(31)–C(30)	112.5(5)
C(21)–C(20)–C(19)	119.9(7)	O(5)–C(31)–C(26)	126.3(5)
C(21)–C(20)–H(20)	120.1	C(30)–C(31)–C(26)	121.0(5)
C(19)–C(20)–H(20)	120.1	C(31)–O(5)–C(39)	107.6(4)
C(22)–C(21)–C(20)	120.6(7)	C(29)–C(32)–C(33)	115.0(5)
C(22)–C(21)–H(21)	119.7	C(29)–C(32)–H(32A)	108.5
C(20)–C(21)–H(21)	119.7	C(33)–C(32)–H(32A)	108.5
C(21)–C(22)–C(23)	120.4(7)	C(29)–C(32)–H(32B)	108.5
C(21)–C(22)–H(22)	119.8	C(33)–C(32)–H(32B)	108.5
C(23)–C(22)–H(22)	119.8	H(32A)–C(32)–H(32B)	107.5
C(22)–C(23)–C(24)	119.4(6)	N(2)–C(33)–C(34)	108.4(5)
C(22)–C(23)–H(23)	120.3	N(2)–C(33)–C(32)	115.5(6)
C(24)–C(23)–H(23)	120.3	C(34)–C(33)–C(32)	112.4(5)
C(19)–C(24)–C(23)	120.1(6)	N(2)–C(33)–H(33)	106.7
C(19)–C(24)–C(25)	120.5(5)	C(34)–C(33)–H(33)	106.7
C(23)–C(24)–C(25)	119.4(5)	C(32)–C(33)–H(33)	106.7
O(4)–C(25)–C(24)	105.3(5)	C(42)–C(34)–C(35)	109.2(5)
O(4)–C(25)–H(25A)	110.7	C(42)–C(34)–C(33)	115.9(5)
C(24)–C(25)–H(25A)	110.7	C(35)–C(34)–C(33)	105.8(5)
O(4)–C(25)–H(25B)	110.7	C(42)–C(34)–H(34)	108.6
C(24)–C(25)–H(25B)	110.7	C(35)–C(34)–H(34)	108.6
H(25A)–C(25)–H(25B)	108.8	C(33)–C(34)–H(34)	108.6
C(26)–O(4)–C(25)	116.8(5)	C(30)–C(35)–C(38)	114.4(5)
O(4)–C(26)–C(27)	126.5(5)	C(30)–C(35)–C(34)	106.3(5)
O(4)–C(26)–C(31)	115.7(5)	C(38)–C(35)–C(34)	108.8(5)

Appendix

C(30)–C(35)–C(39)	100.5(5)	C(42)–C(41)–H(41)	119.5
C(38)–C(35)–C(39)	111.5(5)	C(40)–C(41)–H(41)	119.5
C(34)–C(35)–C(39)	115.2(5)	C(41)–C(42)–C(34)	119.4(7)
C(37)–N(2)–C(36)	110.6(5)	C(41)–C(42)–H(42)	120.3
C(37)–N(2)–C(33)	112.3(4)	C(34)–C(42)–H(42)	120.3
C(36)–N(2)–C(33)	113.2(5)	H(107)–O(7)–H(207)	108.5
N(2)–C(36)–H(36A)	109.5	H(108)–O(8)–H(208)	105.3
N(2)–C(36)–H(36B)	109.5		
H(36A)–C(36)–H(36B)	109.5		
N(2)–C(36)–H(36C)	109.5		
H(36A)–C(36)–H(36C)	109.5		
H(36B)–C(36)–H(36C)	109.5		
N(2)–C(37)–C(38)	109.8(5)		
N(2)–C(37)–H(37A)	109.7		
C(38)–C(37)–H(37A)	109.7		
N(2)–C(37)–H(37B)	109.7		
C(38)–C(37)–H(37B)	109.7		
H(37A)–C(37)–H(37B)	108.2		
C(35)–C(38)–C(37)	111.5(5)		
C(35)–C(38)–H(38A)	109.3		
C(37)–C(38)–H(38A)	109.3		
C(35)–C(38)–H(38B)	109.3		
C(37)–C(38)–H(38B)	109.3		
H(38A)–C(38)–H(38B)	108.0		
O(5)–C(39)–C(40)	110.5(5)		
O(5)–C(39)–C(35)	105.6(4)		
C(40)–C(39)–C(35)	112.6(5)		
O(5)–C(39)–H(39)	109.4		
C(40)–C(39)–H(39)	109.4		
C(35)–C(39)–H(39)	109.4		
O(6)–C(40)–C(41)	109.7(6)		
O(6)–C(40)–C(39)	112.5(5)		
C(41)–C(40)–C(39)	113.9(5)		
O(6)–C(40)–H(40)	106.8		
C(41)–C(40)–H(40)	106.8		
C(39)–C(40)–H(40)	106.8		
C(40)–O(6)–H(106)	109.5		
C(42)–C(41)–C(40)	121.0(7)		

9.2 Appendix B

Cells and cell culture

IC₅₀, definition:

The concentration of a drug or novel compound which causes a 50% cell kill (IC₅₀ for that drug) can be determined from a plot of the % survival (relative to the control cells) versus drug concentration using Calcsyn software.

Drug combinations terminology:

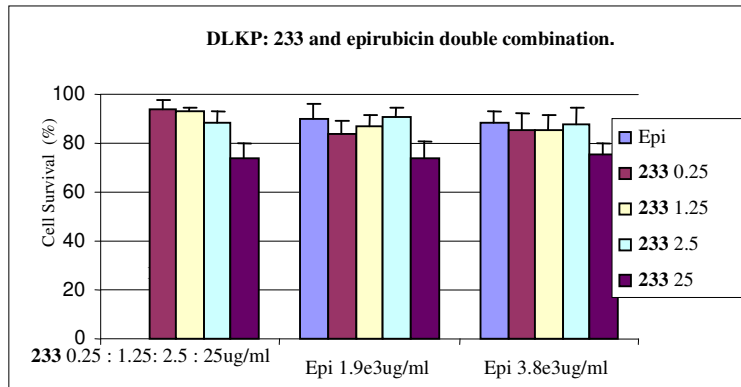
Antagonism is when the 2 or more drugs in combination act against each other therefore decreasing the effect on the cells. ($1 + 1 = -1$)

Additivity is when the total toxicity of 2 or more drugs in combination is equal to the sum of the cell kill each drug has on the cells. ($1 + 1 = 2$)

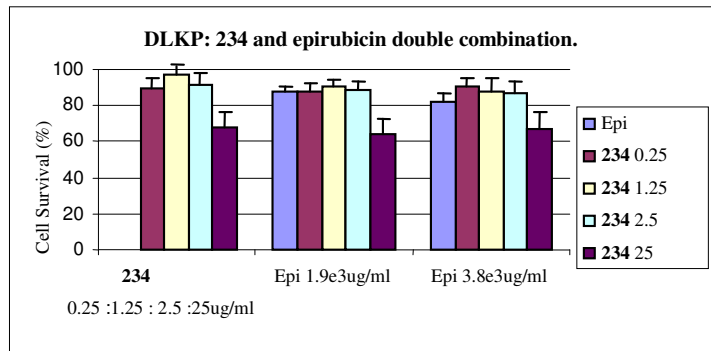
Synergy is when the total cell kill is greater than additivity. ($1 + 1 = 3$)

All cell culture work was carried out in a class II laminar airflow cabinet (Holten LaminAir). All experiments involving cytotoxic compounds were conducted in a cytogard laminar airflow cabinet (Hoolten LaminAir Maxisafe). Before and after use the laminar airflow cabinet was cleaned with 70% industrial methylated spirits (IMS). Any items brought into the cabinet were also swabbed with IMS. Only one cell line was used in the laminar airflow cabinet at a time and upon completion of work with any given cell line the laminar airflow cabinet was allowed to clear for at least 15 minutes before use. This was to eliminate any possibilities of cross-contamination between cell lines. The cabinets were cleaned fortnightly with industrial disinfectants (Virkon or TEGO). These disinfectants were alternated fortnightly. All cells were incubated at 37°C with an atmosphere of 5% CO₂. The DLKP and DLKP-A cell lines do not have CO₂ requirement. Cells were fed with fresh media or subcultured every 2-3 days in order to maintain active cell growth.

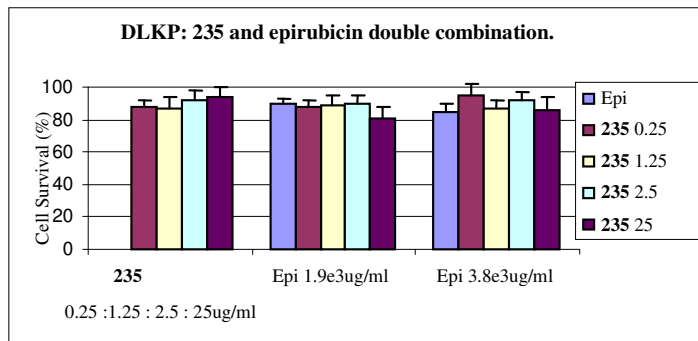
Double combinations of **233**, **234**, **235**, **236** and **4** with epirubicin in the DLKP cell line



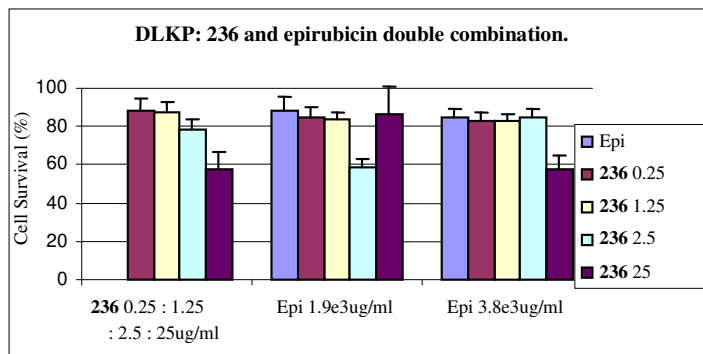
Graph B 1 Bar chart of the double combination of **233** with epirubicin in the DLKP cell line. This combination did not result in synergistic reaction.



Graph B 2 Bar chart of the double combination of **234** with epirubicin in the DLKP cell line. This combination did not result in synergistic reaction.

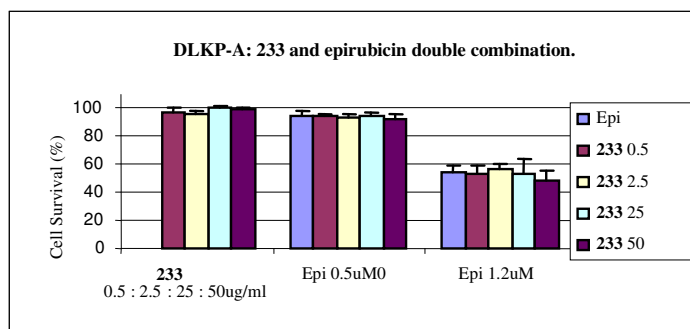


Graph B 3 Bar chart of the double combination of **235** with epirubicin in the DLKP cell line. This combination did not result in a synergistic interaction.

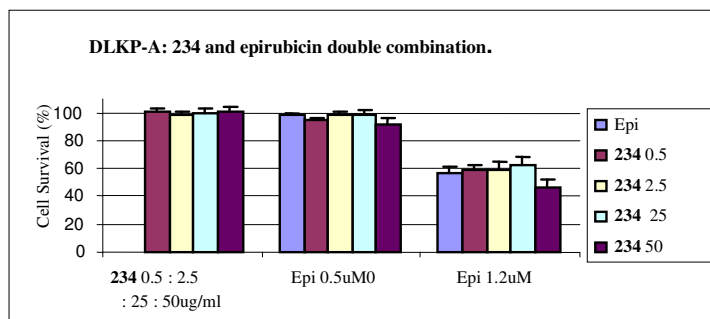


Graph B 4 Bar chart of the double combination of **236** with epirubicin in the DLKP cell line. This combination did not result in a synergistic interaction.

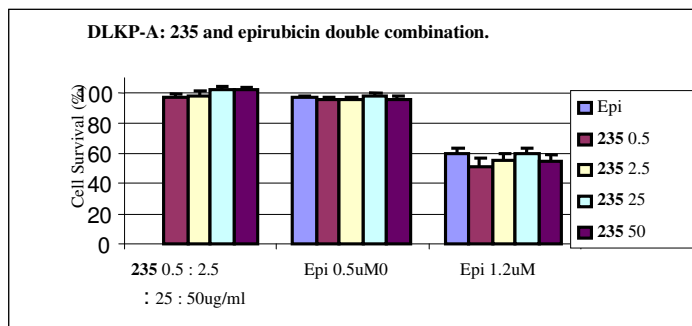
Double combinations of **233**, **234**, **235**, **236** and **4** with epirubicin in the DLKP-A cell line.



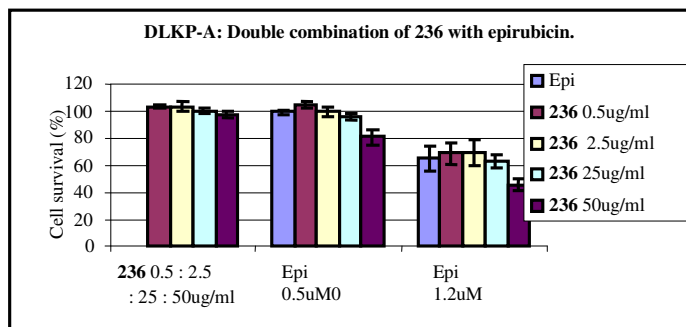
Graph B 5 Bar chart of the double combination of **233** with epirubicin on the DLKP-A cell line. The combination of this compound with epirubicin did not show any synergistic interactions in the DLKP-A cell line.



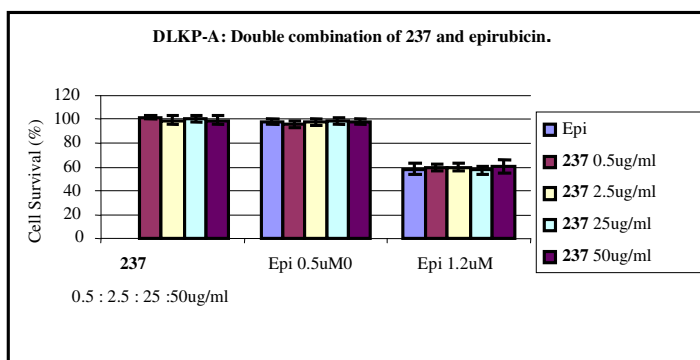
Graph B 6 Bar chart of the double combination of **234** with epirubicin in the DLKP-A cell line. This combination did not result in a synergistic reaction in the DLKP-A cell line.



Graph B 7 Bar chart of the double combination of **235** with epirubicin in the DLKP-A cell line. This combination did not result in a synergistic reaction in the DLKP-A cell line.



Graph B 8 Bar chart of the double combination of **236** with epirubicin in the DLKP-A cell line. This combination did not result in a synergistic interaction in the DLKP-A cell line.



Graph B 9 Bar chart of the double combination of **237** with epirubicin in the DLKP-A cell line. This combination did not result in a synergistic interaction in the DLK-A cell line.

9.3 List of Figures

Fig. 1.1 Valinomycin 1	2
Fig. 1.2 Nonactin 2	3
Fig. 1.3 Monensin 3	4
Fig. 1.4 Synthesis of dibenzo-18-crown-6 9	5
Fig. 1.5 Synthesis of 18-crown-6 employing potassium cations as a templating agent	6
Fig. 1.6 Structures of chiral crown ethers with binaphthyl units	7
Fig. 1.7 Structures of chiral crown ethers incorporating biphenanthryl unit	8
Fig. 1.8 Structures of macrocycles derived from D-mannitol and L-tartaric acid	8
Fig. 1.9 Synthesis of chiral macrocycles based on (<i>S</i>)-(+)-mandelic acid derivatives	9
Fig. 1.10 Chiral crown ethers containing cyclohexyl units	10
Fig. 1.11 Optically active 18-crown-6 macrocycles with chiral cyclohexane unit	11
Fig. 1.12 Chiral 14-crown-4 ether	11
Fig. 1.13 Synthesis of chiral 18-crown-6 from α -amino acids	12
Fig. 1.14 Sucrose unit	13
Fig. 1.15 Chiral macrocycles with sucrose unit	13
Fig. 1.16 Chiral crown ethers with D-glucose unit	14
Fig. 1.17 Synthesis of <i>galacto</i> -crown ethers	15
Fig. 1.18 Chiral monoaza-15-crown-5 ethers	16
Fig. 1.19 Chiral aza crown ether 67 synthesized from L-threonine	17
Fig. 1.20 Synthesis of chiral macrocycles containing pyridine moieties and chiral L-amino acids	17
Fig. 1.21 Chiral diaza 18-crown-6 derived from (<i>R</i>)-(+)-1-phenylethylamine	18
Fig. 1.22 Crown ethers incorporated on polystyrene and silica gel	20
Fig. 1.23 Structures of CSPs based on chiral crown ethers incorporating 1, 1'-binaphthyl and tartaric acid units	21
Fig. 1.24 18-crown-6 in organic synthesis	22
Fig. 1.25 Dicyclohexano-18-crown-6 in ester hydrolysis	23
Fig. 1.26 Dicyclohexano-18-crown-6 in nucleophilic substitution reaction	23
Fig. 1.27 Dibenzo-18-crown-6 in reduction reaction	24
Fig. 1.28 Dicyclohexano-18-crown-6 in elimination reaction	24
Fig. 1.29 18-crown-6 in oxidation reaction	25
Fig. 1.30 Enantioselective aldol reaction catalysed by a chiral macrocycle 90 complexed to diethyl zinc	25
Fig. 1.31 Synthesis of propargylic alcohols catalysed by a chiral macrocyclic catalyst of 94 with Me ₂ Zn	26
Fig. 1.32 Asymmetric epoxidation of alkenes with macrocyclic catalyst 95	27
Fig. 1.33 Michael addition catalyzed by a chiral crown complex of 97 with ^t BuOK	27
Fig. 1.34 Michael addition catalyzed by a chiral crown complex of 98 with ^t BuONa	28
Fig. 1.35 Enantioselective Friedel-Crafts reaction catalyzed by chiral macrocycle complex of 102 with Ti(O ^{<i>i</i>} Pr) ₄	29
Fig. 1.36 Friedel-Crafts reaction	30
Fig. 1.37 Direct preparation of phenylethanolamine library	31
Fig. 1.38 Target compounds of interest	31
Fig. 1.39 Dexverapamil 111	34
Fig. 1.40 Structure of Roll-2933 the analogue of (<i>R</i>)-verapamil	34

Fig. 1.41 Structures of tacrolimus 113 and valsopodar (PSC-833) 114 an analogue of cyclosporine A	35
Fig. 1.42 Structures of biricodar (VX-710) 115, dofequidar (MS-209) 116 and zosuquidar	35
Fig. 1.43 Structure of flupentixol 118	36
Fig. 1.44 Structures of progesterone 119, megestrol acetate 120 and mifepristone 121	36
Fig. 1.45 Structures of ethacrynic acid 122, irofulven 123 and SN-22995 124	37
Fig. 1.46 Structure of elacridar 125	37
Fig. 2.1 Synthesis of the symmetrical tartramides from diethyl-L-tartrate	39
Fig. 2.2 General synthesis of glyoxamides by periodic oxidative cleavage	40
Fig. 2.3 Catalytic Friedel-Crafts reaction of <i>N,N</i> -dimethylglyoxamide 132 with <i>N,N</i> -dimethylaniline 104	41
Fig. 2.4 Catalytic Friedel-Crafts reaction of 2-oxo-2-(pyrrolidin-1-yl)acetaldehyde 134 with <i>N,N</i> -dimethylaniline 104	42
Fig. 2.5 Side product of catalytic Friedel-Crafts reaction of 2-oxo-2-(pyrrolidin-1-yl)acetaldehyde 134 with 104	42
Fig. 2.6 Preparation of 137 and 138 from ethyl glyoxylate 105 by catalytic Friedel-Crafts reaction	44
Fig. 2.7 Preparation of 140 and 141 by catalytic Friedel-Crafts reaction	44
Fig. 2.8 Catalytic Friedel-Crafts reaction of <i>N,N</i> -dimethyl glyoxamide 132 with indole 142	45
Fig. 2.9 Friedel-Crafts reaction product of mono addition 147	46
Fig. 2.10 Catalytic Friedel-Crafts reaction of ethyl pyruvate 144 with indoles	46
Fig. 2.11 Catalytic Friedel-Crafts reaction of ethyl 3,3,3-trifluoropyruvate 139 with indoles	48
Fig. 2.12 Friedel-Crafts reaction of <i>N,N</i> -dimethyl glyoxamide 132 with indole 142	49
Fig. 2.13 Friedel-Crafts reaction of <i>N,N</i> -dimethyl glyoxamide 132 with <i>N</i> -methyl pyrrole 152	49
Fig. 2.14 Friedel-Crafts reaction of 2-oxo-2-(pyrrolidin-1-yl)acetaldehyde 134 with <i>N</i> -methyl pyrrole 152	50
Fig. 2.15 Catalytic Friedel-Crafts reaction of phenylglyoxal monohydrate 155 with <i>N,N</i> -dimethylaniline 104	51
Fig. 2.16 Catalytic Friedel-Crafts reaction of 2-oxo-2-(pyrrolidin-1-yl)acetaldehyde 134 with aromatic compounds	52
Fig. 2.17 Intermediate cations 157 and 158	53
Fig. 2.18 Dimeric form of azolidine glyoxamide	55
Fig. 3.1 Two different routes for preparation of macrocycles	56
Fig. 3.2 Synthesis of dibenzo-18-crown-6 in the presence of templating agent	57
Fig. 3.3 Synthesis of phenoxy-linked open structures	59
Fig. 3.4 Synthesis of macrocycles from phenoxy-linked precursor	60
Fig. 3.5 Macrocyclization of macrocyclic precursors 163 and 164 with 2,6-pyridine dicarbonyl dichloride	61
Fig. 3.6 Synthesis of macrocycles 169-171 with 1,5- <i>bis</i> [2-(2-hydroxyethoxy)phenoxy]-3-oxapentane unit 161	62
Fig. 3.7 Reaction scheme for preparation of 169	63
Fig. 3.8 Macrocyclic precursor 161 in the presence and absence of the template	66
Fig. 3.9 Synthesis of macrocycles from 1,8- <i>bis</i> [2-(2-hydroxyethoxy)phenoxy]-3,6-dioxaoctane 162	66
Fig. 3.10 Synthesis of macrocycles 176-178	67

Fig. 3.11 Synthesis of macrocycles 179-182	68
Fig. 3.12 Synthesis of macrocycles 183 and 184	70
Fig. 3.13 Macrocycles 170, 180, 183 synthesized with α,α' -dibromo and α,α' -dichloro-xylenes	70
Fig. 3.14 Synthesis of macrocycle 184 in one-pot approach	72
Fig. 3.15 Synthesis of macrocycle 180 in one-pot approach	72
Fig. 3.16 Attempts to synthesis of macrocycle 186	73
Fig. 3.17 Macrocycles 173 and 182	74
Fig. 3.18 ^1H NMR spectrum of 2,3,14,15,21,24-tribenzo-1,4,7,10,13,16,19,26-octaoxacycloocta-eicosa-2,14,21,22,23-tetraene, 173	75
Fig. 3.19 ^1H NMR spectrum of 2,3,6,9,12,13-tribenzo-1,4,11,14,17,20,23,26-octaoxacycloocta-eicosa-2,6,7,8,12-tetraene, 182	75
Fig. 3.20 ^{13}C NMR spectrum of 2,3,6,9,12,13-tribenzo-1,4,11,14,17,20,23,26-octaoxacycloocta-eicosa-2,6,7,8,12-tetraene, 182	77
Fig. 3.21 ^{13}C NMR spectrum of 2,3,14,15,21,24-tribenzo-1,4,7,10,13,16,19,26-octaoxacycloocta-eicosa-2,14,21,22,23-tetraene, 173	77
Fig. 3.22 Macrocycles 174	78
Fig. 3.23 The ^1H NMR spectrum of 2,3,14,15,21,22-tribenzo-1,4,7,10,13,16,19,25-octaoxa-cyclohexa-eicosa-2,14,21-triene, 174	79
Fig. 3.24 The ^{13}C NMR spectrum of 2,3,14,15,21,22-tribenzo-1,4,7,10,13,16,19,25-octaoxa-cyclohexa-eicosa-2,14,21-triene, 174	79
Fig. 3.25 Mesomeric effect, <i>ortho</i> -CH and <i>para</i> -CH	80
Fig. 3.26 Structure of 181	81
Fig. 3.27 The ^1H NMR spectrum of 2,3,6,9,12,13,19,20-tetrabenz-1,4,11,14,17,22-hexaoxa-cyclotetra-eicosa-2,6,7,8,12,19-hexaene, 181	81
Fig. 3.28 The ^{13}C NMR spectrum of 2,3,6,9,12,13,19,20-tetrabenz-1,4,11,14,17,22-hexaoxa-cyclotetra-eicosa-2,6,7,8,12,19-hexene, 181	82
Fig. 3.29 Macrocycles 171 and 172	83
Fig. 3.30 The ^1H NMR spectrum of 2,3,11,12,18,20-tribenzo-19-aza-1,4,7,10,13,16,22-heptaoxa-cyclotetra-eicosa-2,11,18,19-tetraene, 171	84
Fig. 3.31 The ^1H NMR spectrum of 2,3,14,15,21,23-tribenzo-1,4,7,10,13,16,19,25-octaoxacyclo hepta-eicosa-2,14,21,22-tetraene, 172	85
Fig. 3.32 Similar features in structures of 2-(2-hydroxyethoxy) phenol 159 and morphine 187	86
Fig. 4.1 (-)- Morphine 187	88
Fig. 4.2 Morphine derivatives codeine 188, diamorphine 189 and thebaine 190	89
Fig. 4.3 Morphine derivatives oxymorphone 191, naloxone 192 and etorphine 193	89
Fig. 4.4 n=1; 1,8-bis(3-morphinyl)-3,6-dioxaoctan, 194; n=2; 1,11-bis(3-morphinyl)-3,6,9-trioxa-undecane 195, 6-(3-morphinylmethylene)-2-pyridinylmethanol 196	91
Fig. 4.5 Precursors of morphine macrocycles	92
Fig. 4.6 Synthesis of 194, 198, 199, 200	93
Fig. 4.7 Synthesis of 197, 201 and 202	94
Fig. 4.8 Synthesis of 197	95
Fig. 4.9 Structures of morphine macrocyclic precursors 194, 198-202	96
Fig. 4.10 Synthesis of 213, 214	97
Fig. 4.11 Synthesis of 215	98
Fig. 4.12 Synthesis of 216	98
Fig. 4.13 Morphine macrocycles 217-220	99
Fig. 4.14 Synthesis of macrocycles 217, 218, 219 containing morphine units	100

Fig. 4.15 Etheral oxygens of 194 templating metal cation	100
Fig. 4.16 Synthesis of morphine macrocycle 220	101
Fig. 4.17 Synthesis of 222	104
Fig. 4.18 1 st and 2 nd Generation of Grubbs catalysts 224 and 225	105
Fig. 4.19 Attempt of ring closure by metathesis on 222	105
Fig. 4.20 Morphine macrocycle 217 and its precursor 194	108
Fig. 4.21 The ¹ H NMR spectrum of 194	108
Fig. 4.22 The ¹ H NMR spectrum of 217	109
Fig. 4.23 The ¹³ C NMR spectrum of 194	109
Fig. 4.24 The ¹³ C NMR spectrum of 217	110
Fig. 4.25 Morphine macrocycle 218	111
Fig. 4.26 The ¹ H NMR spectrum of 218	111
Fig. 4.27 The ¹³ C NMR spectrum of 218	112
Fig. 5.1 X-ray structure of 179	116
Fig. 5.2 X-ray crystal structure of 2,3,6,9,12,13,19,21-tetrabenz-1,4,11,14,17,23-hexaoxacyclopentacos-2,6,7,8,12,19,20-hexaene, 179	117
Fig. 5.3 X-ray structure of 184 visioned in Mercury 1.4.2	119
Fig. 5.4 View of the X-ray structure of 2,3,6,8,11,12,18,20-tetrabenz-7,19-diaza-1,4,10,13,16,22-hexaoxacyclo-tetraeicosa-2,6,7,11,18,19-hexaene, 184	120
Fig. 5.5 View of the X-ray crystal structure of 1,3-bis[2-(2'-hydroxyethoxy) phenoxy]propane, 160, disorder neglected for clarity	122
Fig. 5.6 X-ray crystal structure of 1,5-bis[2-(2'-hydroxyethoxy) phenoxy]-3-oxapentane, 161	123
Fig. 5.7 X-ray crystal structure and unit cell of 1,5-bis[2-(2'-hydroxyethoxy) phenoxy]-3-oxapentane, 161 depicting the hydrogen bond interactions	125
Fig. 5.8 X-ray crystal structure of 1,4-bis[2-(2'-hydroxyethoxy) phenoxy]xylene, 163	126
Fig. 5.9 X-ray crystal structure of 1,3-bis[2-(2'-hydroxyethoxy) phenoxy]xylene, 164	128
Fig. 5.10 The crystal structure of two molecules of 164 linked with intermolecular hydrogen bonds	130
Fig. 5.11 X-ray crystal structure of 1,2-bis[2-(2'-hydroxyethoxy) phenoxy]xylene 165, disorder neglected for clarity	131
Fig. 5.12 Drawing of the X-ray crystal structure of 165 depicting different 3D perspectives	132
Fig. 5.13 X-ray crystal structure of 1,6-bis[2-(2'-hydroxyethoxy) phenoxy]methylenepyridine, 166, disorder neglected for clarity	134
Fig. 5.14 Pseudocyclic structure adopted by 164 and linear arrangement of 163 in the solid state	136
Fig. 6.1 Partitioning of crown ether and potassium picrate between water and chloroform solution	137
Fig. 7.1 Structures of epirubicin 227 and taxotere 228 chemotherapeutics	162
Fig. 7.2 Macrocycles and their precursors screened for the inhibition of the P-gp	164
Fig. 7.3 Screened compounds containing ester groups	172
Fig. 7.4 Commercially available compounds screened in carcinoma assay	176
Fig. 7.5 Schematic view of screened compounds	183

9.4 List of Tables

Table 1.1 Stability constants for 1:1 18-crown-6 and its aza- and thio- analogs	5
Table 2.1 Results for the catalytic Friedel-Crafts reaction of <i>N,N</i> -dimethylglyoxamide 132 with <i>N,N</i> -dimethyl-aniline 104 under various reaction conditions	41
Table 2.2 Results for the catalytic Friedel-Crafts reaction of 2-oxo-2-(pyrrolidin-1-yl)acetaldehyde 134 with <i>N,N</i> -dimethylaniline 104 under various reaction conditions	43
Table 2.3 Results for the catalytic Friedel-Crafts reaction of <i>N,N</i> -dimethyl glyoxamide 132 with indole 142 under various reaction conditions	45
Table 2.4 Results for the catalytic Friedel-Crafts reaction of ethyl pyruvate 144 with <i>N</i> -methyl indole 145 under various reaction conditions	47
Table 2.5 Results for the catalytic Friedel-Crafts reaction of ethyl 3,3,3-trifluoropyruvate 139 with <i>N</i> -methylindole under various reaction conditions	48
Table 2.6 Results for the Friedel-Crafts reaction of <i>N,N</i> -dimethyl glyoxamide 132 with indole 142 in water solution	49
Table 2.7 Results for the Friedel-Crafts reaction of <i>N</i> -methyl pyrrole 152 with <i>N,N</i> -dimethyl glyoxamide 132	50
Table 2.8 Results for the Friedel-Crafts reaction of 2-oxo-2-(pyrrolidin-1-yl)acetaldehyde 134 with <i>N</i> -methyl pyrrole 152	50
Table 2.9 Results for the catalytic Friedel-Crafts reaction of phenylglyoxal monohydrate 155 with <i>N,N</i> -dimethylaniline 104 under various reaction conditions	51
Table 3.1 Isolated yields for phenoxy-linked open structures 160-166	59
Table 3.2 Various reaction conditions for preparation of macrocycle 169. ^a 1,4-D-Dioxane	63
Table 3.3 Solvent effect on preparation of macrocycle 169. ^a 1,4-D- 1,4 Dioxane	65
Table 3.4 Various reaction conditions for synthesis of macrocycle 180. ^a 1,4-D 1,4-dioxane	69
Table 3.5 Results of macrocyclization using alkyl chlorides <i>versus</i> bromides	71
Table 3.6 ¹ H NMR spectroscopic details for macrocycles 173 and 182	76
Table 4.1 Reaction conditions for preparation of morphine macrocycles 217-220	102
Table 4.2 Attempted preparation of morphine macrocycles from 199	102
Table 4.3 Attempted preparation of morphine macrocycles from 198	103
Table 4.4 Attempted preparation of morphine macrocycles from 200	103
Table 4.5 Attempted preparation of morphine macrocycles from 201	103
Table 4.6 Reaction conditions for preparation of 222	105
Table 5.1 Selected bond distances [Å] angles [°] for 179 with estimated standard deviations	117
Table 5.2 Selected torsion angles [°] for 179	117
Table 5.3 Dimensions of the cavity of compound 179	118
Table 5.4 Dimensions of the cavity of compound 184	120
Table 5.5 Selected bond angles [°] for 184 with estimated standard deviations	121
Table 5.6 Selected bond lengths [Å] for 184 with estimated standard deviations	121
Table 5.7 Torsion angles [°] for 184	121
Table 5.8 Selected bond lengths [Å] and angles [°] for 160	123
Table 5.9 Selected bond lengths [Å] for 161 with estimated standard deviations	124
Table 5.10 Selected bond angles [°] for 161 with estimated standard deviations	124

Table 5.11 Hydrogen bonds for 161 [\AA and $^\circ$]	125
Table 5.12 Selected bond distances [\AA] and angles [$^\circ$] for 163 with estimated standard deviations	126
Table 5.13 Dimensions of the cavity of compound 163	127
Table 5.14 Selected bond distances [\AA] bond angles [$^\circ$] and torsion angles [$^\circ$] for 164 with estimated standard deviations	128
Table 5.15 Dimensions of the cavity of compound 164	129
Table 5.16 Hydrogen bonds for 164 [\AA and $^\circ$]	129
Table 5.17 Selected bond distances [\AA] bond angles [$^\circ$] and torsion angles [$^\circ$] for 165 with estimated standard deviations	131
Table 5.18 Dimensions of the cavity of compound 165	132
Table 5.19 Selected bond distances [\AA] bond angles [$^\circ$] and torsion angles [$^\circ$] for 166 with estimated standard deviations	133
Table 5.20 Dimensions of the cavity of compound 166	134
Table 6.1 Diameter of cavity in Ångström Units	138
Table 6.2 Cations and their Diameters in Ångström Units	138
Table 6.3 Extraction results with 160	139
Table 6.4 Extraction results with 161	139
Table 6.5 Extraction results with 162	140
Table 6.6 Extraction results with 163	140
Table 6.7 Extraction results with 164	140
Table 6.8 Extraction results with 165	141
Table 6.9 Extraction results with 166	141
Table 6.10 Extraction results with 167	141
Table 6.11 Extraction results with 168	142
Table 6.12 Extraction results with 169	142
Table 6.13 Extraction results with 170	142
Table 6.14 Extraction results with 171	143
Table 6.15 Extraction results with 173	143
Table 6.16 Extraction results with 176	143
Table 6.17 Extraction results with 177	144
Table 6.18 Extraction results with 178	144
Table 6.19 Extraction results with 179	144
Table 6.20 Extraction results with 180	145
Table 6.21 Extraction results with 183	145
Table 6.22 Extraction results with 184	145
Table 6.23 Extraction results with 197	146
Table 6.24 Extraction results with 194	146
Table 6.25 Extraction results with 198	146
Table 6.26 Extraction results with 199	147
Table 6.27 Extraction results with 200	147
Table 6.28 Extraction results with 201	147
Table 6.29 Extraction results with 217	148
Table 6.30 Extraction results with 218	148
Table 6.31 Extraction results with 219	148
Table 6.32 Extraction results with 220	149
Table 6.33 Extraction results, two-phase liquid extraction: methylene chloride and water	150
Table 6.34 Extraction values of 167, 168, 169, 173, 176, 177 for Na^+ , K^+ and La^{3+}	152

Table 6.35 Extraction results for Pb ²⁺ and Cu ²⁺ with morphine 187	158
---	-----

9.5 List of Graphs

Graph 6.1 % Extraction values for macrocyclic precursors 162, 164, 165, 166	151
Graph 6.2 % Extraction values of 167, 168, 169, 173, 176, 177, 178, 180 for Na ⁺	153
Graph 6.3 % Extraction values of 162 and 194 for series of various metal cations	154
Graph 6.4 % Extraction values of 166 and 201 for series of various metal cations	155
Graph 6.5 % Extraction values of 217 for series of various metal cations	156
Graph 6.6 % Extraction values of morphine compounds for Pb ²⁺ and Cu ²⁺	157
Graph 7.1 The IC ₅₀ values of the six testable compounds on both the DLKP and DLKPA cell lines. Experiments with no errors bars were only carried out once whereas those with error bars were carried out twice.	165
Graph 7.2 Combination of 160 with epirubicin on the DLKP-A cell line	165
Graph 7.3 Combination of 165 with epirubicin on the DLKP-A cell line.	166
Graph 7.4 The double combination of 165 with epirubicin on the DLKP cell line	166
Graph 7.5 Combination of 161 with epirubicin on the DLKP-A cell line	167
Graph 7.6 Combination of 164 with epirubicin on the DLKP-A cell line	167
Graph 7.7 Combination of 166 with epirubicin on the DLKP-A cell line	168
Graph 7.8 The effect of a combination of 165 with epirubicin on the DLKP cell line	169
Graph 7.9 The effect of a combination of 165 and 5FU on the DLKP cell line	169
Graph 7.10 Effect of a combination of 165 with epirubicin on the DLKP-A cell line	170
Graph 7.11 Effect of a combination of 165 with taxotere on the DLKP-A cell line	170
Graph 7.12 Effect of a 165 with 5FU on the DLKP-A cell line	171
Graph 7.13 Effect of a combination of 229 with epirubicin on the DLKP-A cell line	172
Graph 7.14 Effect of a combination of 230 with epirubicin on the DLKP-A cell line	173
Graph 7.15 Combination of 230 with taxotere on DLKP-A cell line	173
Graph 7.16 Combination of 231 with epirubicin on the DLKP-A cell line	174
Graph 7.17 Bar chart illustrating the double combination of 231 with taxotere on the DLKP-A cell line	174
Graph 7.18 Bar chart for the combination of 238 with epirubicin in the DLKP-A cell line	176
Graph 7.19 Combination assay of 169 with epirubicin on the DLKP-A cell line	177
Graph 7.20 Combination assay of 170 with epirubicin on the DLKP-A cell line	177
Graph 7.21 Combination assay of 169 with taxotere on the DLKP-A cell line	178
Graph 7.22 Combination assay of 170 with taxotere on the DLKP-A cell line	179
Graph 7.23 Combination assay of 173 with epirubicin on the DLKP-A cell line	179
Graph 7.24 Combination assay of 173 with taxotere on the DLKP-A cell line	180
Graph 7.25 Combination assay of 178 with epirubicin on the DLKP-A cell line	180
Graph 7.26 Combination assay of 178 with taxotere on the DLKP-A cell line	181